INVESTIGATION OF FE(III)-AS(III) BEARING PHASES AND THEIR POTENTIAL FOR ARSENIC DISPOSAL

by

Faith Kokoi Opio

A thesis submitted to Robert M. Buchan Department of Mining

In conformity with the requirements for

the degree of Doctor of Philosophy

Queen's University

Kingston, Ontario, Canada

(January, 2013)

Abstract

Fe(III)-As(III) bearing precipitates have been successfully used for arsenic immobilization in copper smelter weak acid effluents. However, knowledge on their precise characteristics is very limited compared to ferric arsenate precipitates which are the preferred disposal option. As(III) is the dominant arsenic species in the weak acid effluents, and high costs are incurred in oxidizing As(III) to As(V) prior to ferric arsenate precipitation. Detailed characterization of Fe(III)-As(III) bearing residues is fundamental for accurate prediction of their long term stability. Synchrotron-based analysis of the Fe(III)-As(III) bearing precipitates from the effluent treatment plant (ETP) at Xstrata's Horne Copper Smelter in Quebec identified ferric arsenate and gypsum as the major phases, and other minor phases including zinc hydroxide and franklinite. The predominant As species was As(V) which accounted for 49 to 84% of the total As in the Horne ETP sample. The high As(V) levels detected in the Horne ETP co-precipitates may be due to the partial oxidation of As(III) during prolonged storage, prior to synchrotron analysis.

Tooeleite was investigated as an alternative potential disposal option for As(III) immobilization from copper smelter weak acid effluents. Lime neutralization of an equimolar Fe(III)-As(III) bearing weak acid solution resulted in about 85% As being removed at pH 2.7 and the formation of gypsum-bearing tooeleite at pH 2 to 3.5. At >pH 4, the rapid transformation of tooeleite occurred to form a poorly crystalline equimolar ferric arsenite which was stable at pH 6 to 10. Co-precipitation tests also showed that equimolar ferric arsenite was precipitated at pH>4. US EPA Toxicity Characteristic Leaching Procedure (TCLP) analysis indicated that both tooeleite and ferric arsenite have relatively high As solubilities. Calcination of tooeleite was explored as a method for improving the stability of tooeleite, and calcination of tooeleite in air at 600˚C produced a ferric arsenate calcine with a TCLP solubility of <5 mg/L As. The calcine

produced from the lime-precipitated tooeleite at 600 ˚C was found to contain an iron arsenate ($Fe_7As_6O_{24}$) which had a slightly higher TCLP As solubility of 13.1 mg/L. The precipitation of tooeleite from an As(III)-bearing weak acid and calcination of the resultant precipitate may offer a new process for As(III) fixation from copper smelter weak acid effluents.

Co-Authorship

Chapter 5, co-authored with Dr. H.E. Jamieson and Dr. J. Peacey, was published as a proceedings paper entitled "*Tooeleite, a new possibility for arsenic fixation: thermal decomposition and stabilization"*. The paper was published in: Proceedings of the 2nd International Seminar on Environmental Issues in the Mining Industry, November 2011, Santiago, Chile.

Acknowledgements

I would like to express special thanks to my supervisors Dr. Heather Jamieson and Dr. John Peacey for their excellent guidance, inspiration, support and great insights throughout the course of this research.

I am grateful to all past and present graduate students of Dr. Jamieson's research group for their support, advice and insightful discussions. It has been a pleasure being part of the group. Thank you to the graduate students of the mining department who have been very supportive and helpful during this research.

Thanks to Dr. Tony Lanzirotti at the NSLS and Arthur Barnes of Xstrata Process Support for their insightful advice and support during this research study. I gratefully acknowledge Alan Grant, Mauritza Bailey, and Kathy Golshani for their technical support and guidance. I am thankful to Dr. Chris Harris, Brandon Chambers, Filipe Rodrigues and Mothusi Pule for their assistance and support with part of the experimental work.

And finally, I would like to express my deep gratitude to my family for their unconditional love and support, and to my friends for their endless encouragement.

Funding for this research was provided by NSERC and Xstrata.

Table of Contents

List of Figures

List of Tables

Chapter 1

Introduction

1.1 Background

Arsenic is a common contaminant found in copper concentrates, and the removal and safe disposal of arsenic from effluent streams is a major environmental issue for the copper metallurgical industry. During the smelting of copper concentrates and roasting of high-arsenic copper concentrates, arsenic is volatilized and recovered in the wet gas cleaning section in the form of As(III) species in a weak acid solution (arsenious acid, H_3AsO_3). The removal and disposal of arsenic from weak acid and dust treatment bleed effluents poses major challenges for the copper smelters as it needs to be disposed of in an environmentally acceptable form and manner. The problem of arsenic fixation and disposal has intensified due to the steady increase in the average level of arsenic in copper concentrates, the exploitation of several high-arsenic copper deposits and the enforcement of stringent environmental regulations (Demopolous et al., 2003; Peacey et al., 2010). Various treatment and disposal practices are currently used in copper smelters for the removal of arsenic from weak acid and dust treatment bleed effluents, of which the preferred method involves lime neutralization and co-precipitation with ferric iron to form arsenical ferrihydrite (As(V)-Fh) with a Fe/As molar ratio greater than 3 (Harris, 2003; Twidwell et al., 2005; Jia and Demopoulos, 2005; Le Berre et al., 2007; Jia and Demopoulos, 2008).

At Xstrata's Horne Copper Smelter in Rouyn-Noranda, Quebec, As(III) is removed from the weak acid and dust treatment bleed effluents by lime neutralization and co-precipitation with ferric iron (Fe:As molar ratio>3) and base metals to form arsenical ferrihydrite (As(III)-Fh), base

metal hydroxides and gypsum (Godbehere et al, 1995). It is generally accepted that As(III)-Fh is formed by the adsorption of the As(III) species onto ferrihydrite (Riveros et al., 2001), and therefore are also known as Fe(III)-As(III) bearing precipitates. However, there is limited knowledge on the precise nature and characteristics of As(III)-Fh precipitates compared to As(V)-Fh (Harris and Monette, 1988; Robins et al., 1988; Krause and Ettel, 1989; Nishimura and Umetsu, 2000; Moldovan et al., 2003; Jia et al., 2003), albeit trivalent arsenic is the major arsenic species in the weak acid and dust treatment bleed solutions from copper smelters. Previous studies have focused on As(V)-Fh because it is generally assumed that As(V)-Fh is more stable than As(III)-Fh for environmental disposal (Riveros et al., 2001). The As(III)-Fh precipitates produced at the Horne Effluent Treatment Plant (Horne ETP) are co-deposited with finely ground slag mill tailings in a disposal pond at pH 8.5 – 9 (Riveros et al., 2001). However, the effect of aging on the characteristics and long term stability of the Horne ETP precipitates under actual disposal conditions is poorly understood. Detailed knowledge of the precise nature and characteristics of these precipitates (Horne ETP and disposal pond residues) is fundamental in ensuring the effective management of their disposal and accurate prediction of their long term stability.

Despite being the preferred medium for As control, the precipitation of As(V)-Fh bearing residues is associated with high consumption of ferric iron and neutralizing agent as well as the generation of large volumes of sludge with poor filtration properties resulting in high operating and disposal costs (Harris, 2003). In addition, its long term stability is of concern as it may be reduced biotically or abiotically under anoxic environments, resulting in the mobilization of arsenic (McCreadie et al., 2000; Pederson et al., 2006). Therefore, there is an incentive to develop

an alternative stable As-bearing compound with low solubility, low iron requirements, good filtration properties and a high As removal efficiency that can be utilized by the copper smelters for the removal and disposal of arsenic from weak acid effluents. Tooeleite, a ferric arsenite sulphate hydrate ($Fe_6(AsO_3)_4(SO_4)(OH)_4 \cdot 4H_2O$), has been proposed as a potential phase for the fixation of As(III) species from weak acid effluents (Nishimura and Robins, 2008). Tooeleite could be considered as the As(III) equivalent of scorodite which is regarded by copper smelters as the most suitable medium for arsenic fixation and disposal due to its low solubility in the pH range 2.8 to 5.3 (Krause and Ettel, 1989), low iron demand and high As content of 25 wt% to 30 wt% (Filippou and Demopoulos, 1997). However, the precipitation of scorodite is associated with high costs due to the use of autoclaves, although it has been found that scorodite will form at 95 ˚C under ambient pressure and supersaturation conditions (Droppert et al., 1996; Filippou and Demopoulos, 1997). Tooeleite has a high As content (25%), high As removal efficiency, a low Fe:As molar ratio of 1.2, and is stable in the pH range 2 to 3.5 (Nishimura and Robins, 2008).

1.2 Research objectives

The research objectives of this thesis were three-fold. The first objective was to characterize the mineral phases contained in the Horne ETP sludge using both conventional and synchrotron-based analytical techniques in order to understand the fundamental co-precipitation processes and mechanisms of As retention in the Fe(III)-As(III)-Zn(II)-Ca(II) system at the Horne Copper Smelter ETP.

The second objective of this research study was to characterize the sediments from the Horne Tailings Facility using both conventional and synchrotron-based analytical techniques in order to be able to predict their long term stability under actual disposal conditions. Previous

literature on As(III)-Fh transformation, as well as stability tests conducted on synthetic As(III)-Fh precipitates under simulated disposal conditions, were used to estimate the long-term stability of the Horne's As(III) bearing precipitates in its disposal pond.

The third and final objective of this research study was to investigate tooeleite as an alternative potential disposal option for the fixation of As from copper smelter weak acid effluents. This objective was achieved by investigating the precipitation of tooeleite from As(III)-bearing weak acid solutions by evaluating the effect of varying precipitation conditions (Fe:As molar ratio, pH, temperature and neutralizing agent) on the As removal efficiency, as well as precipitate characteristics and stability. Calcination was also investigated as a potential approach for enhancing the stability of tooeleite for disposal.

1.3 Thesis outline

This thesis is divided into six main chapters. Chapter 1 provides the background and rationale for undertaking the research study, the research objectives and the thesis outline. Chapter 2 provides a review of past and current research on arsenic treatment and disposal practices; adsorption of As(III) by ferrihydrite; ferrihydrite transformation; synchrotron-based analysis and tooeleite. Chapter 3 focuses on the mineralogical characterization of the Horne ETP residues using conventional and synchrotron-based techniques, and examines the effect of lime as the neutralizing agent and the role of zinc on the stability of the As(III) bearing residues. In addition, Chapter 3 investigates the effect of aging on the characteristics and stability of the Horne ETP co-precipitates by evaluating the transformation rate of As(III)-Fh under simulated disposal conditions existing at the Horne disposal pond, and discusses stability protocols and their application to the practicality of As fixation in the future. The investigation of tooeleite as an

alternative disposal option for the fixation of As from copper smelter weak acid effluents is presented in Chapter 4. Chapter 5 investigates calcination as a potential approach for enhancing the stability of tooeleite for disposal. Finally, Chapter 6 summarizes the conclusions and recommendations for further work.

Chapter 2

Literature review

2.1. Arsenic-bearing copper minerals

Arsenic is relatively abundant in the earth's crust, with an overall average concentration of 5 ppm. Elevated arsenic concentrations in the rocks and soils usually stem from either natural enrichment such as weathering processes, microbiological activity, hydrothermal processes and volcanic emissions or anthropogenic pollution via mining and smelting operations, pharmaceutical and chemical manufacturing, burning of fossil fuels and wastes, wood preservatives, pulp and paper production, cement manufacturing, and former agricultural uses of arsenic as a fungicide and pesticide (US EPA 1998; Bothe and Brown, 1999a; Karagas et al., 2001; Smedley and Kinniburg, 2002; Garelick et al., 2008).

Arsenic is widely found in various types of mineral deposits, in particular sulphide deposits associated with copper, lead, zinc, cobalt and gold. It is a constituent of over 245 minerals including elemental arsenic, arsenides, arsenates, oxides, silicates, sulphides and sulfosalts (Boyle and Jonasson, 1973; Escobar-Gonzalez and Monhemius, 1998; Mandal and Suzuki, 2002). Copper is usually associated with arsenic in the form of thioarsenate, thioarsenite or thioarsenide minerals. Of these minerals, enargite (Cu_3AsS_4) and tennantite ($Cu_{12}As_4S_{13}$) are the most common arsenic-bearing copper minerals. Other arsenic-bearing copper minerals include luzonite (Cu_3AsS_4), lautite (CuAsS), sinnerite ($Cu_6As_4S_9$), domeykite (Cu_3As) and algodonite (Cu_6As) (Filippou et al., 2007).

Enargite is a cuprous thioarsenate that is found in high sulphidation epithermal deposits, porphyry systems and high temperature carbonate-hosted deposits (Di Benedetto et al., 2011). It is frequently associated with complex copper sulphide ores and refractory gold ores (Fantauzzi et al, 2009; Riveros and Dutrizac, 2008). Tennantite is a cuprous-cupric thioarsenite that occurs in hydrothermal veins and contact-metamorphic deposits as a minor component in association with complex copper sulphide ores (Anthony et al., 1990; Smedley and Kinniburgh, 2002; Filippou et al., 2007). Both enargite and tennantite contain 48% copper and relatively high arsenic levels (enargite – 19% As; tennantite – 20% As).

The increasing global demand for copper and the depletion of low arsenic high-grade copper deposits has led to the exploitation of low-grade complex copper sulphide deposits that are associated with arsenic-bearing minerals including enargite, tennantite and arsenopyrite (Smedley and Kinniburgh, 2002; Riveros and Dutrizac, 2008). The various types of arsenic-copper bearing deposits of the world and their mineralogies are presented in Table 2.1.

Table 2.1: Arsenic-bearing copper deposits of the world (modified from Mandal and Suzuki, 2002)

Type of deposit	As mineral(s)	Average As concentration (mg kg^{-1})	Location
Enargite-bearing copper-zinc-lead	Enargite	1000 (0.1%)	United States, Argentina, Chile, Peru, Mexico, Phillippines, Spain
Enargite-bearing gold	Enargite	1000 (0.1%)	Chile, Phillipines, Bulgaria, Papua New Guinea, Peru
Arsenical pyritic copper	Arsenopyrite Tennantite	4000 (0.4%)	United States, Sweden, Germany, Japan, France

Although arsenic-bearing copper sulphide ores are of economic interest, their high arsenic content poses a major concern for copper smelters due to the potential risk of occupational exposure to gaseous arsenic emissions and the requirement to fix and dispose of arsenic as an environmentally stable residue (Piret et al.,1989; Curreli et al., 2005; Curreli et al., 2009).

2.2. Arsenic chemistry

Arsenic is a metalloid with atomic number 33 and an atomic weight of 75. It is located in group V of the periodic table with nitrogen, phosphorus, antimony and bismuth. Arsenic primarily exists in nature in two forms, organic and inorganic forms. Arsenic combines with sulphur, oxygen and chlorine to form inorganic compounds which are usually associated with other metals in igneous and sedimentary rocks. Conversely, organic compounds of arsenic including monomethylarsonic acid (MMAA) and dimethylarsinic acid (DMAA) are associated with carbon and hydrogen. Inorganic arsenic compounds are generally more toxic than the organic compounds (Hurtado-Jimenez and Gardea-Torresdey, 2006).

Arsenic can exist in several oxidation states including (-3); (-1); (0); (3) and (5). Trivalent arsenite [As(III)] and pentavalent arsenate [As(V)] are the most widespread forms of inorganic arsenic in nature (Garelick et al., 2008). Although both forms usually co-exist, As(III) is prevalent in reducing conditions while As(V) is primarily encountered in oxygenated conditions (Bang and Meng, 2004). As(III) is considered to be more mobile and 25-60 times more toxic than As(V) (Raven et al., 1998).

Redox potential (Eh) and pH control arsenic speciation and solubility. The Eh-pH diagram illustrated in Figure 2.1 facilitates the prediction of the most stable arsenic species under different conditions. In the pH range 0–14, As(III) is the prevalent form in reducing conditions in the protonation states of H_3AsO_3 and $H_2AsO_3^-$ while As(V) is dominant in oxidizing conditions in the protonated forms of H_3AsO_4, $H_2AsO_4^-$, $HAsO_4^{2-}$ and AsO_4^{3-} (Lehr and Lehr, 2000).

The aqueous solution chemistry of arsenic is important in the removal of arsenic from hydrometallurgical process solutions, which is dependent on the precipitation and adsorption processes (Robins et al., 2001). H_3AsO_3 for As(III), and $HAsO_4^{2-}$ and $H_2AsO_4^-$ for As(V) are the aqueous species that are relevant to the precipitation of arsenic compounds from hydrometallurgical process solutions.

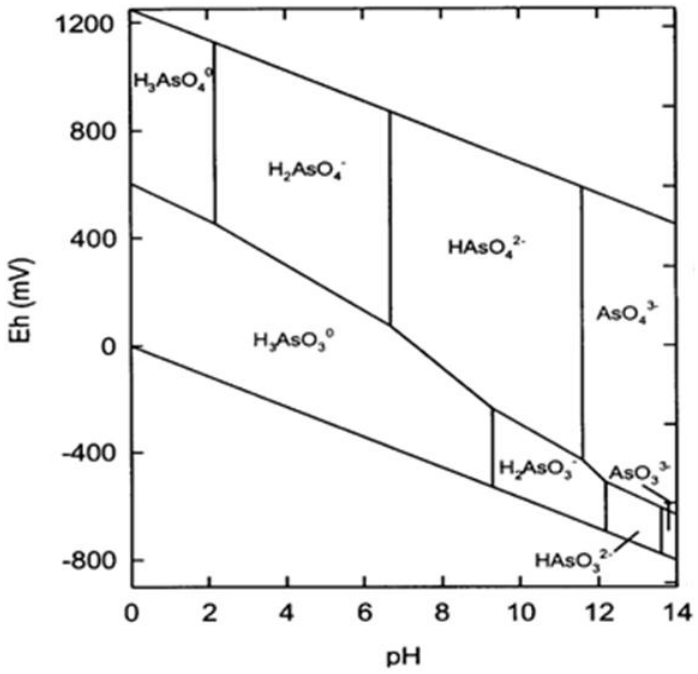

Figure 2.1: Eh-pH diagram for predominant aqueous species in the As-O_2-H_2O system at 298.15K and 1 atmosphere pressure (Pookrod et al., 2004)

2.3. Arsenic in roasting

Roasting has traditionally been used in the pretreatment of both arsenic-bearing gold and copper concentrates in order to reduce their arsenic content to low levels for subsequent extraction.

2.3.1. Roasting of arsenic-bearing gold concentrates

Many of the gold deposits that are currently being discovered and exploited are refractory in nature. The treatment of refractory gold ores using conventional cyanide leaching usually results in low gold recoveries, due to the gold being either chemically bound or encapsulated in sulphide minerals such as pyrite, pyrrhotite and arsenopyrite, and/or the presence of carbonaceous matter (Robins and Jayaweera, 1992; Fraser et al., 2003; Celep et al., 2009).

Arsenic principally exists in refractory arsenic-bearing gold ores and concentrates in the form of arsenopyrite. Refractory arsenic-bearing gold ores and concentrates require pretreatment in order to liberate the gold for subsequent recovery by conventional cyanide methods. The main pretreatment methods that are currently used include roasting, pressure oxidation and bio-oxidation (Arriagada and Osseo-Asare, 1984; Berezowsky and Weir, 1989; Marsden and House, 1992; Walker et al., 2005; Taylor, 2010). The selection of the most appropriate pretreatment process is determined by the location of the gold, the mineralogy of the gold-bearing minerals, the process economics and the ability of the process to fix arsenic into an environmentally stable residue (Filippou et al., 2007; Celep et al., 2009; Peacey et al., 2010). Roasting of refractory arsenic-bearing gold concentrates (400˚C - 700˚C) results in the volatilization of most of the arsenic as As_4O_6 (Equation 2.1), which is cooled and captured as arsenic trioxide dust in the bag-

house filters and the oxidation of the low-arsenic calcine to hematite (see Equation 2.2) (Fraser et al., 1991).

$$2FeAsS(s) + 3O_2(g) = 4FeS(s) + As_4O_6(g) \quad (2.1)$$

$$4FeS(s) + 7O_2(g) = 2Fe_2O_3(s) + 4SO_2(g) \quad (2.2)$$

2.3.2. Roasting of arsenic-bearing copper concentrates

Copper concentrates with As levels above 0.5% are pretreated by roasting so that they can be accepted as feed by the smelters (Du Pleiss et al., 2007). Partial roasting of the arsenic-bearing copper concentrates (enargite and tennantite) is conducted in a multi-hearth furnace (550˚C – 750˚C) resulting in the volatilization of arsenic sulphide and sulphur which are subsequently oxidised in excess air at 750˚C to form arsenic trioxide and sulphur dioxide. The evolved gases are cooled and the arsenic trioxide dust is captured in the bag-house filters (Bruckard et al., 2010). The partial roasting of enargite and tennantite is described by Equations 2.3-2.7 and 2.8-2.12 respectively (Filippou et al., 2007; Bruckard et al., 2010). In the presence of pyrite, enargite is converted to chalcopyrite (Equation 2.5). As indicated in Equation 2.10, chalcocite (formed from the roasting of tennantite) is converted to bornite in the presence of pyrite.

$$4Cu_3AsS_4 = Cu_{12}As_4S_{13}(s) + 3/2S_2(g) \quad (2.3)$$

$$Cu_{12}As_4S_{13}(s) = 6Cu_2S(s) + 2As_2S_3(g) + 2S_2(g) \quad (2.4)$$

$$2Cu_3AsS_4(s) + 6FeS_2(s) = 6CuFeS_2(s) + As_2S_3(g) + 5/2S_2(g) \quad (2.5)$$

$$As_2S_3(g) + 9/2O_2(g) = As_2O_3(g) + 3SO_2(g) \quad (2.6)$$

$$S_2(g) + 2O_2(g) = 2SO_2(g) \quad (2.7)$$

$$2Cu_{12}As_4S_{13}(s) = 12Cu_2S(s) + 2As_4S_4(g) + 3S_2(g) \quad (2.8)$$

$$2FeS_2(s) = FeS(s) + S_2(g) \quad (2.9)$$

$$4FeS(s) + 10Cu_2S(s) + S_2(g) = 4Cu_5FeS_4(s) \quad (2.10)$$

$$As_2S_3(g) + 9/2O_2(g) = As_2O_3(g) + 3SO_2(g) \quad (2.11)$$

$$S_2(g) + 2O_2(g) = 2SO_2(g) \quad (2.12)$$

2.3.3. Historical arsenic disposal practices

Historically, the arsenic trioxide dusts captured from the roaster off-gases were either sold as by-product or stockpiled on site. Arsenic trioxide was sold as a commercial by-product mainly for the manufacture of chromated copper arsenate (CCA) which was used as a wood preservative (Hartman, 1992). Other minor uses of arsenic trioxide included the manufacture of agricultural chemicals used as pesticides, insecticides and herbicides, glass production and medical applications (US EPA, 1998). However, the market for arsenic trioxide recently declined due to restrictions of its use owing to its highly toxic nature, and the technological development of alternative materials (Hartman, 1992). Furthermore, there were environmental concerns about long-term stockpiling of arsenic trioxide due to its relatively high solubility (Robins and Jayaweera, 1992; Filippou and Demopoulos, 1997; Riveros et al., 2001). Therefore any future roaster will be required to recover and fix its arsenic emissions in a proven environmentally acceptable form.

2.4. Arsenic in copper smelting

Copper concentrates typically contain 0.05% - 0.5% As, and about 40 million tpa of copper concentrates containing about 40,000 tpa As are currently smelted by copper smelters globally. During smelting most of the arsenic in the copper concentrates is volatilized, and oxidized to As_2O_3, and is captured in the electrostatic precipitator (ESP) dusts and the wet gas scrubbing solution (weak acid). In most smelters, most of the ESP dusts are recycled to the

smelting process for metal recovery, but a purged portion of the dust is removed to prevent build-up of impurities. As-bearing ESP dusts contain <10% As as well as other elements including copper, zinc, lead, cadmium, antimony, and bismuth, and consequently cannot be sold as a commercial product. The purged portion of the dust is leached to form an arsenic-bearing solution that is sent to the smelter's effluent treatment plant (ETP) together with an arsenic-bearing weak acid solution from the wet gas scrubbers, to form a stable residue for disposal (Piret, 1999; Riveros et al., 2001).

Due to its high toxicity, arsenic needs to be fixed and disposed of as an environmentally stable solid to prevent its release into the environment. Chronic exposure to high arsenic levels is associated with adverse health effects in humans including cancer, cardiovascular and neurological diseases (Kapaj et al., 2006). Consequently, the Canadian Metal Mining Effluent Regulations (Canadian MMER) specify that the arsenic level in discharged mine effluents should not exceed the maximum monthly mean concentration of 0.5 mg/L (Environment Canada, 1977; Metal Mining Effluent Regulations, 2002). The World Bank has an equivalent guideline of 0.5 mg/L for discharged base metal smelting effluents (World Bank, 2007).

The removal of arsenic from the weak acid and dust treatment bleed effluents poses a major concern for copper smelters due to the technical challenges and high costs encountered in fixing arsenic into an environmentally acceptable form. Consequently, most copper smelters limit their arsenic input by only treating copper concentrates with an arsenic level of less than 0.5% and typically charge a penalty of US $3/kg As if the arsenic level of the concentrates exceeds 0.2% (Peacey et al., 2010). The problem of arsenic fixation and disposal has recently intensified

due to the steady increase in the average level of arsenic in custom copper concentrates, the development of several high-arsenic copper deposits, and the enforcement of increasingly stringent environmental regulations (Demopolous et al., 2003; Peacey et al., 2010).

2.5. Arsenic treatment and disposal practices

Various treatment and disposal practices have been developed and are currently used by copper smelters for the fixation and disposal of arsenic from weak acid and dust treatment bleed effluents. These practices are summarized in Table 2.2.

Table 2.2: Treatment and disposal practices for the fixation and disposal of arsenic in copper smelters (modified from Harris, 2003)

PROCESS	As SPECIES	PRECIPITATE	DISPOSAL PRODUCT	Cu SMELTER	PRECIPITATE STABILITY (EPA TCLP)
Neutralization with lime	As(III)	Calcium arsenite and gypsum	Filter cake in lined ponds	Chuquicamata Chile	Low
	As(V)	Calcium arsenate and gypsum	Calcined cake in rotary kiln and calcine deposited in hazardous waste landfill	Caletones Chile	Low
Precipitation with sodium hydrosulphide (NaSH)	As(III)	Arsenic sulphide (>30%S)	Precipitate autoclaved with sulphur additions to As-S polymer block stored in concrete	Sagenoseki Japan	Moderate
Precipitation with ferric iron at high temperature	As(V)	Ferric arsenate and/or scorodite Fe:As=1.5 T = 90-200˚C	Tailings pond	HTPOX used in the Au industry	High
				Atmospheric precipitation (pilot stage)	-
Neutralization with ferric iron and base metals	As(III)	Arsenical ferrihydrite [As(III)-Fh] (Fe+Zn:As>4) with base metal hydroxides	Tailings pond	Horne Canada	High
Neutralization with ferric iron	As(V)	Arsenical ferrihydrite As(V)-Fh Fe:As>10	Tailings pond	Copper Cliff Canada	High US EPA Best Demonstrated Available Technology

2.5.1. Lime neutralization

The treatment of the smelter weak acid and dust treatment effluents by the addition of lime is practiced by Chilean copper smelters situated in dry regions, due to the low likelihood of lime dissolution and subsequent As release by rain (Valenzuela, 2000). At the Chuquicamata smelter in Chile, the treatment process involves lime neutralization of the As(III)-bearing weak acid effluent to form calcium arsenite (Ca-As(III)) and gypsum which are disposed of in HDPE-lined ponds. At the Caletones smelter in Chile, the As(III) species in the weak acid effluent is oxidized to As(V), and subsequently fixed by the addition of lime to produce a filter cake comprising calcium arsenate (Ca-As(V)) and gypsum. The cake is calcined in a rotary kiln and deposited in a hazardous landfill.

Atlantic Copper's smelter in Huelva, Spain has implemented its own innovative process (developed by BAMAG GmbH) for the fixation of arsenic in its weak acid effluent in order to reduce disposal volume and costs (Ante et al., 2005). The As(III)-bearing weak acid effluent is treated in three stages. In the first stage, lime is added to the weak acid effluent to precipitate pure gypsum at pH<1 and 50 - 80˚C, which is subsequently sold as a by-product. In the second stage, gypsum, calcium arsenite and heavy metal hydroxides are precipitated at pH 12, and finally in the third stage, the residual As(III) is precipitated as ferric arsenite at pH 7, which is disposed in a tailings pond (Ante et al., 2005) .

Despite being cost-effective, disposal options for arsenic immobilization from smelter weak acid effluents, both Ca-As(III) and Ca-As(V) have a moderately low As content (5-15 wt%) and low EPA Toxicity Characteristic Leaching Procedure (TCLP) stabilities (Bothe and Brown,

1999b; Zhu et al., 2005; Riveros et al., 2001; Robins et al., 2001). Swash and Monhemius (1995) evaluated the stability of synthetic Ca-As(V) residues using the USA EPA TCLP test and found the residues had high As solubilities of 1650-3600 mg/L. Furthermore, extensive research has demonstrated that both Ca-As(III) and Ca-As(V) slowly decompose when in contact with atmospheric carbon dioxide, resulting in the formation of calcium carbonate and the subsequent release of arsenic into solution (Robins, 1981, 1983 and 1988; Robins and Tazawa, 1982; Nishimura et al., 1985; Robins and Jayaweera, 1992).

Several studies have been conducted to improve the stability of Ca-As(III) and Ca-As(V). Swash and Monhemius (1995) found that Ca-As(III) and Ca-As(V) have low As solubilities in the presence of excess lime, but As dissolution increases in the long-term due to the dissolution and carbonation of lime. According to Nishimura and Tozawa (1985), the stability of Ca-As(III) and Ca-As(V) was improved by calcination with excess lime at 700˚C due to the formation of a more crystalline calcium arsenate (Equations 2.13 and 2.14). However, Stefanakis and Kontopoulos (1987) reported that the calcination of Ca-As(III) below 800˚C resulted in its incomplete transformation to a crystalline calcium arsenate.

$$Ca_3(AsO_2)_2.Ca(OH)_2(s) = Ca_3(AsO_4)_2(s)\ (crystalline) + CaO(s) + H_2O(l) \quad (2.13)$$

$$Ca(AsO_2)_2.Ca(OH)_2(s) + (n+1)Ca(OH)_2(s) + O_2(g) = Ca_3(AsO_4)_2(s)\ (crystalline) + nCaO\ (s) + (n+2)H_2O\ (l) \quad (2.14)$$

2.5.2. Neutralization with sodium hydrosulphide

The treatment of smelter weak acid and dust treatment effluents by neutralization with sodium hydrosulphide (NaSH) is practiced at the Saganoseki smelter in Japan. The arsenic

contained in the flue dusts generated at the Saganoseki smelter is leached with sulphuric acid to form a weak acid solution, which is treated by neutralization with NaSH to form arsenic sulphide (As_2S_3) (bulk density = 0.4 tonnes/m^3) (Hino et al., 1995). As_2S_3 has a high As content of 60 wt%, and is stable under acidic and reducing conditions (pH<4). It is relatively soluble in water, and liable to atmospheric and bacterial oxidation (Robins, 1988; Robins et al., 2001). Consequently, As_2S_3 produced at Saganoseki is stabilized for long term storage by being autoclaved with sulphur additions (60 wt%) at 200˚C and 1700 kPa to form an As-S polymer block (bulk density=1.3 tonne/m^3) which is stored in concrete (Hino et al., 1995; Valenzuela, 2000). This treatment practice is associated with high costs due to NaSH requirements ($500-650/ton) and the use of autoclaves (Hino et al., 1995).

2.5.3. Scorodite

High temperature pressure oxidation (HTPOX) is widely used in the gold industry for the treatment of refractory gold ores. HTPOX involves the oxidation of refractory gold ores in an autoclave at high temperatures (170˚C-200˚C) and an oxygen overpressure of 2000 kPa, resulting in the liberation of gold and the fixation of arsenic into scorodite (crystalline ferric arsenate) which is disposed into a tailings pond (Dutrizac and Jambor, 1988; Papangelakis and Demopoulos, 1990). The reaction chemistry of the HTPOX process is presented in Equations 2.15 to 2.18 (Robins and Jayaweera, 1992; Swash and Monhemius, 1994). As indicated in Equation 2.15, arsenopyrite is oxidised to form arsenic acid and ferrous sulphate. The reaction presented in Equation 2.16 occasionally occurs resulting in the formation of elemental sulphur. As illustrated in Equation 2.18, arsenic is fixed as scorodite and is stored in a lined tailings pond (Robins and Jayaweera, 1992).

$$4FeAsS(s) + 13O_2(g) + 6H_2O(l) = 4H_3AsO_4(aq) + 4FeSO_4(aq) \quad (2.15)$$

$$4FeAsS(s) + 7O_2(g) + 4H_2SO_4(aq) + 2H_2O(l) = 4H_3AsO_4(aq) + 4FeSO_4(aq) + 4S(l) \quad (2.16)$$

$$4FeSO_4(aq) + O_2(g) + 2H_2SO_4\ (aq) = 2Fe_2(SO_4)_3(aq) + 2H_2O(l) \quad (2.17)$$

$$Fe_2(SO_4)_3(aq) + 2H_3AsO_4(aq) + 2H_2O(l) = 2FeAsO_4.2H_2O(s) + 3H_2SO_4(aq) \quad (2.18)$$

Scorodite is generally regarded as the most suitable disposal option for the fixation and disposal of arsenic from weak acid effluents as it is considered to have a low As solubility, high As removal efficiency, high As content (25-30 wt%), low iron requirements (Fe:As molar ratio=1-1.5) and relatively high stability in acidic to neutral conditions (Riveros et al., 2001; Paktunc et al., 2010). In addition, scorodite has good settling and filtration properties due to its crystalline nature (Filippou and Demopoulos, 1997; Riveros et al., 2001; Demopoulos et al., 2003). However, this practice is associated with high capital costs due to the use of autoclaves (Swash and Monhemius, 1994; Filippou and Demopoulos, 1997; Demopoulos et al., 2003; Paktunc et al., 2008). Demopoulos and co-workers (Demopoulos et al., 1995; Filippou and Demopoulos, 1997; Demopoulos et al., 2003; Singhania et al., 2005, 2006) developed a new process for the fixation of arsenic from metallurgical weak acid effluents by atmospheric precipitation of scorodite at 95˚C under ambient pressure and supersaturation-controlled conditions. Despite being potentially less capital intensive than HTPOX, this treatment practice has not yet been applied commercially (Droppert et al., 1996; Filippou and Demopoulos, 1997).

Scorodite is stable under oxic conditions and in the pH range 2.8–5.3 (minimum solubility of <0.5 mg/L) (Krause and Ettel, 1989; Riveros et al., 2001; Langmuir et al., 2006; Harvey et al., 2006; Bluteau and Demopoulos, 2007). Stability studies by Swash and Monhemius (1995) and Filippou and Demopoulos (1997) have shown that scorodite has a very low US EPA

TCLP solubility (< 5 mg/L As), probably due to the fact that scorodite has its lowest solubility in the pH range 3-5 (Krause and Ettel, 1989; Riveros et al. 2001). Concerns have been expressed about the long term stability of scorodite as studies have shown that it dissolves incongruently at pH>5 to form 2-line ferrihydrite, resulting in the associated release of arsenic into solution (Krause and Ettel, 1985, 1989; Robins 1988; Welham et al., 2000; Bluteau and Demopoulos, 2007). Furthermore, scorodite may decompose under anoxic conditions or in the presence of reducing bacteria (Robins, 1981; Rochette et al., 1998; Cummings et al., 1999; Riveros et al., 2001; Papassiopi et al., 2003).

2.5.4. Arsenic removal by co-precipitation with ferric iron

Lime neutralization and co-precipitation of arsenate (As(V)) with ferric iron (Fe/As molar ratio>3) is widely used for the removal and disposal of arsenic from the smelter weak acid and dust treatment bleed effluents. Arsenic is generally present in smelter weak acid and dust treatment bleed effluents in the form of the As(III) species. Consequently, prior to the precipitation process, As(III) is generally oxidized to As(V) using various oxidants including a SO_2/O_2 mixture, O_2 or H_2O_2 which incur high costs (Riveros et al., 2001). During the precipitation process, As is fixed by the adsorption of the arsenate species (AsO_4^{3-}) by ferrihydrite to form arsenical ferrihydrite (As(V)-Fh) (Equations 2.19 and 2.20) (Robins et al, 1991; Waychunas et al., 1993; Jambor and Dutrizac, 1998; Riveros et al., 2001; Paktunc et al., 2008; Paktunc et al., 2010). Precipitation of As(V)-Fh with the addition of lime begins at pH 2-3, and the sulphate in solution reacts with the calcium to form gypsum (Swash and Monhemius, 1995; Riveros et al., 2001).

$$Fe^{3+}_{(aq)} + (3+x)\ H_2O_{(l)} = FeO(OH)(H_2O)_{1+x(s)} + 3H^{+}_{(aq)} \qquad (2.19)$$

$$FeO(OH)(H_2O)_{1+x} + AsO_4^{3-} = AsO_4^{3-}.FeO(OH)(H_2O)_{1+x\ (s)} \qquad (2.20)$$

As(V)-Fh is the preferred disposal option used by copper smelters and has been designated as the Best Demonstrated Available Technology (BDAT) by the US Environmental Protection Agency (US EPA) for the removal of arsenic from acidic mineral processing effluents (Riveros et al., 2001; Twidwell et al., 2008). Several studies have been conducted and reported in the literature on the co-precipitation of As(V)-Fh (Harris and Monette, 1988; Robins et al., 1988; Krause and Ettel, 1989; Emett and Khoe, 1993; Waychunas et al., 1993; Langmiur et al., 1999; Nishimura and Umetsu, 2000; Moldovan et al., 2003; Jia et al., 2003; Richmond et al., 2004; Twidwell et al., 2005; Langmiur et al., 2006). Robins et al. (1988), Krause et al. (1989), and Nishimura and Umetsu (2000) reported that the optimal pH range for As(V)-Fh precipitation is 3.5-5.5. According to Emett and Khoe (1994) and Khoe at al. (1994), the precipitation of As(V)-Fh from solution is effective in the pH range 4-7, but the range increases to pH 4-10 in the presence of the cations including Zn(II), Cd(II), Pb(II), Ca(II) and Mg(II). According to Jia and Demopoulos (2008), the enhanced As removal could be due to As adsorption by the co-precipitated base metal-ferric hydroxides. Swash and Monhemius (1995) observed that at very low initial Fe:As molar ratios in solution, calcium arsenate will form at pH 3-4 instead of As(V)-Fh.

Previous research has established that As(V)-Fh co-precipitates (Fe:As molar ratio>3) have a high stability, and their stability improves with increasing Fe:As molar ratio (Krause et al, 1989; Passiopi et al., 1996; Harris, 2003; Riveros et al., 2001). Krause and Ettel (1985; 1989) reported As(V)-Fh (Fe:As= 4) to have a low solubility of <0.2 mg/L at 25˚C, over the pH range 3-5. However, the long term stability of As(V)-Fh has been the subject of concern. Several theoretical studies have concluded that As(V)-Fh will decompose to goethite and finally hematite

over the long-term, thereby releasing arsenic into solution (Robins, 1983, 1990; Robins et al., 1988; Robins and Jayaweera, 1992). Furthermore, McCreadie et al. (2000) and Pederson et al. (2006) reported that As(V)-Fh may be reduced biotically or abiotically under anoxic environments, resulting in the reductive dissolution of ferrihydrite or As(V) and the mobilization of arsenic. Extensive experimental studies have demonstrated that As(V)-Fh with a high Fe:As molar ratio>3 can maintain its long term stability if stored under oxic conditions in the pH range 3-5 (Harris and Monette, 1988, 1989; Krause and Ettel, 1985, 1987, 1988, 1989; Harris and Krause, 1993; Kontopoulos et al.; 1988; Dove and Rimstidt, 1985; Nordstrom and Parks, 1987; Robins, 1987; Rimstidt and Dove, 1987; Vircikova et al., 1994, 1995, 1998). In addition, studies conducted by Harris and Monette (1989) showed that the presence of cations (Cu(II), Zn(II) and Cd(II)) increased the stability range of As(V)-Fh from pH 4-7 to pH 4-10.

At the Vale Inco Copper Cliff smelter, arsenic is removed from weak acid effluents by lime addition and co-precipitation with ferric to form As(V)-Fh (Fe:As molar ratio> 10) and gypsum. The precipitation process is carried out in a series of two autoclaves, operating at 80˚C and an oxygen overpressure of 276 kPa. Lime is added to raise the pH in the first autoclave to pH 3.3, and to pH 4 in the second autoclave, resulting in the precipitation of As(V)-Fh and gypsum. The resulting slurry is filtered, washed and repulped in water at pH 3-4, before being sent to the tailings pond for disposal with pyrrhotite-rich flotation tailings. The effluent from the disposal pond has a pH 5.5 and 0.02 mg/L As (Riveros et al., 2001). Regular monitoring of the pond has indicated that the As(V)-Fh residues have maintained their stability over twenty years (Peacey et al., 2010).

Despite being the preferred medium for As immobilization and being designated the US EPA BDAT, As(V)-Fh has a low arsenic content of 6% and its precipitation is associated with a high consumption of ferric iron and oxidizing agent resulting in high operating costs. In addition, this practice generates large volumes of sludge of poor crystallinity and filtration properties, leading to high disposal costs (Hoffmann, 1993; Filippou and Demopoulos, 1997; Riveros et al., 2001).

2.5.5. Arsenic removal by co-precipitation with ferric iron and base metals

The removal and disposal of the trivalent As species can be achieved by lime neutralization and co-precipitation with ferric iron (Fe/As>3) and base metals to form arsenical ferrihydrite (As(III)-Fh), base metal hydroxides and gypsum. The As precipitation mechanism involves the rapid neutralization of ferric iron to precipitate a poorly crystalline ferric oxyhydroxide (2-line ferrihydrite) phase (Equation 2.21). 2-line ferrihydrite (Fh) adsorbs the arsenite species (AsO_3^{3-}) to form As(III)-bearing ferrihydrite (As(III)-Fh) (Equation 2.22) (Godbehere et al., 1995; Riveros et al., 2001). This treatment process is practiced at the Horne Copper smelter. Studies by Nishimura and Umetsu (2000) demonstrated that the optimal adsorption of As(III)-Fh occurs in the pH range 8-9.

$$Fe^{3+}_{(aq)} + (3+x)\ H_2O_{(l)} = FeO(OH)(H_2O)_{1+x(s)} + 3H^+_{(aq)} \qquad (2.21)$$

$$FeO(OH)(H_2O)_{1+x(s)} + AsO_{3(aq)}^{3-} = AsO_3^{3-}.FeO(OH)(H_2O)_{1+x\ (s)} \qquad (2.22)$$

According to Nishimura and Umetsu (2000), As removal by neutralization with ferric iron is more effective if the As is present as As(V) compared to As(III). It is presumed that As(III) is more difficult to remove than As(V) as As(III) is considered to have a lower affinity for ferrihydrite than As(V) (Raven et al., 1998). Consequently, the oxidation of As(III) is deemed

necessary to increase the As removal efficiency (Lenoble et al., 2002; Bang and Meng., 2004). Moreover, since As(III) is more mobile and toxic than As(V), it is generally assumed that As(V)-Fh precipitates are more stable than As(III)-Fh for environmental disposal (Riveros et al., 2001; Das et al., 2011).

2.6. Horne copper smelter

The Horne Copper Smelter, which is located in Rouyn-Noranda, Quebec, Canada, is a custom facility that has been in operating since 1927. When the Horne Mine closed in the 1970s, it became a custom smelter treating copper concentrates from around the world and also started specializing in the treatment of complex concentrates, containing high levels of impurities such as As, Bi, Sb and Pb. The Horne Smelter has an annual production capacity of 210,000 tonnes of copper anodes and 550,000 tonnes of sulphuric acid from 800,000 tonnes of feed material (Godbehere et al., 1995). The smelter was modernized in 1981-1991, with the construction of a sulphuric acid plant to treat reactor off-gases and the addition of wet gas scrubbers to remove all impurities that were not captured in the electrostatic precipitators (ESP). The wet gas scrubbers produce a weak acid bleed solution containing arsenic and base metal impurities including Bi, Cd, Pb and Zn (Godbehere et al., 1995).

2.6.1. The Horne effluent treatment plant process

The Horne smelter has developed its own novel process for the fixation of arsenic in its smelter weak acid and dust treatment effluents using acid mine drainage from the two open pit mines, Remnor and Gallen. The removal and disposal of arsenic is achieved by lime neutralization and co-precipitation with ferric iron and base metals.

The Horne Effluent Treatment Plant (ETP) process is fully described in Godbehere et al. (1995). The As treatment process takes place in a series of two reactors. The feed into the first reactor consists of a purged portion of the ESP dusts, oxidized acid mine drainage and a weak acid solution from the wet gas scrubbers. The gases from the smelting operation are cooled, passed through the ESP to remove the entrained dust and subsequently treated to form sulphuric acid. 15-25% of the dust that is recycled to the smelter is bled from the circuit to control the build-up of impurities such as As and Cd. The recycled dust containing 2-5% arsenic, mostly in the form of As(III), is slurried in water and treated in a gravimetric separator to recover copper and precious metals. The reject fraction of the dust slurry containing 25% dissolved As and insoluble base metal arsenites and arsenates, is the first feed to the first reactor. The second feed to the first reactor consists of the weak acid (pH 1) generated from wet scrubbers, which contains 2.5 g/L As in the form of As(III) species. The third feed consists of acid mine drainage from the nearby Gallen and Remnor mine sites, which is added as an additional source of iron for the precipitation process. The acid mine drainage contains 5 g/L Fe(III), 24.5 g/L Fe(II), 2.5 g/L Zn and 4 mg/L Cd. Prior to being fed to the first vessel, the Fe(II) in the acid mine drainage (AMD) is oxidized to Fe(III) using oxygen. Lime is added to the first reactor to raise and maintain the pH to 4.5, resulting in the precipitation of arsenic from solution. The Fe:As molar ratio>3 is maintained in the reactor to ensure the precipitation of a stable precipitate.

The discharge from the first reactor is sent to the second reactor, and 5 m^3/h of acid mine drainage from the Gallen mine site is added to maintain the Fe+Zn/As molar ratio>4. Lime is added to the second reactor to raise the pH to 9.5, resulting in the precipitation of any residual

arsenic and the dissolved metals. The final discharge (40 tpd) is sent to the tailings pond, where it is co-deposited with finely ground slag mill tailings (1500 tpd). The final effluent from the tailings pond has a pH of 8.5-9 and contains <0.5 mg/L As (Riveros et al., 2001), which meets the Canadian MMER effluent discharge limits of 0.5 mg/L. Regular monitoring of the pond has indicated that the final residue has maintained its stability for over twenty years (Peacey et al., 2010).

2.6.2. The Horne ETP process chemistry

Based on the data given in Godbehere et al. (1995), the Horne ETP process chemistry is presented in Table 2.3. In the first reactor, the As-bearing weak acid (1-4 g/L) is mixed with the base metal-bearing (Zn, Cd, Cu) dust slurries and ferric-bearing AMD to give a final solution with an Fe:As molar ratio of >3. Lime is added to the solution to raise the pH to 4.5. The main reactions that occur in the first reactor include the precipitation of ~97% of the arsenic (As(III) with Fe(III), as well as gypsum, decreasing the As concentration in solution from 2500 mg/L to 50 mg/L. Previous studies by Nishimura et al. (1991) have shown that zinc arsenite begins to precipitate at pH 6, suggesting that zinc does not take part in the precipitation of As(III) as zinc arsenite in the first reactor. Copper and cadmium are typically present in minor amounts and therefore do not make a significant difference.

In the second reactor, additional ferric iron is added and the pH is raised to 9.5 with the addition of lime, resulting in the precipitation of the residual As, and the base metals (Zn, Cd and Cu) as base metal hydroxides, resulting in a final effluent discharge containing ~1 mg/L As.

Table 2.3: Horne ETP process chemistry

Mass Balance Inputs	Weak acid	Dust	Gallen (AMD)	Remnor (AMD)	Total kg/h	kmol/h	kg As/h	1st RX 97% [a]	2nd RX 3.0% [a]
t/h	70	2	30	20	120			115.00	5.00
As (g/L)	2.5	3.5%						0.05	
As (t/h)	0.175	0.07						5.75	0.08
Soluble As (t/h)	0.175	0.0175			192.5	2.57		2.57	
Insoluble As (t/h)		0.0525							
Fe (g/L)	0.004		6.5	18					0.36[b]
Fe (t/h)	0.00028		0.195	0.36	555	9.91	9.06	3.64[c]	4.66[d]
Fe^{3+}(g/L)			4	1			507.25		
Fe^{3+}(t/h)			0.12	0.02	140	2.50		5.19	55.22[e]
Zn (g/L)	0.3	10%	2.5						50.56[f]
Soluble Zn (t/h)	0.021	0.17	0.0625		253.5	3.88			61.79[g]
Insoluble Zn (g/L)		0.03							
Cd (g/L)		1%	0.004						
Soluble Cd (t/h)		0.014	0.00012		14.12	0.13			
Cu		4%							
Cu (t/h)		0.024			24	0.38			
Insoluble Cu (t/h)		0.056							
H_2SO_4 (g/L)	10.00		5.00	5.00					
H_2SO_4 (kg/h)	700.00		150.00	100.00			950.00		
$CaSO_4$. $2H_2O$ in ppt							1747.96		

(a) - % As precipitated
(b) – Gallen solution added to 2nd RX
(c) – Fe:As molar ratio in 1st RX
(d) – Fe: As molar ratio in 2nd RX (No Zn precipitated in 1st RX)
(e) – Fe+Zn+As molar ratio in 2nd RX
(f) - Zn:As molar ratio in 2nd RX
(g) - Fe+Zn+Cd+Cu: As molar ratio in 2nd RX
1st RX – first reactor & 2nd RX- second reactor

2.7. Stability of As(III)-Fh bearing residues

2.7.1. Long term stability of As(III)-Fh bearing precipitates

Due to the highly toxic nature of arsenic, the long term stability of the disposed As-bearing residues is crucial to the copper smelters. The long term stability of As-bearing residues is influenced by several factors including disposal site characteristics, climate, particle

crystallinity and size distribution, and the presence of oxygen, sulphides, bacteria and complexing agents such as chloride and organic acids (Riveros et al., 2001).

Currently, there is no definitive test to determine the long term stability of the arsenic-bearing solid residues. The stability of these residues is normally evaluated using the US EPA leachate tests, EPA Method 1311 - Toxicity Characteristic Leaching Procedure (TCLP) and EPA Method 1312 - Synthetic Precipitation Leaching Procedure (SPLP). TCLP evaluates the metal mobility in landfill whereas SPLP evaluates the potential for leaching metals into ground and surface waters (US EPA, 1992). SPLP simulates precipitation and therefore provides a more realistic assessment of metal mobility under actual field conditions (US EPA, 1994; Alforque, 1996). The TCLP test is more widely used than SPLP to evaluate the stability of As-bearing residues. Both tests are short term tests that evaluate the stability of arsenic bearing solid waste residues under specific test conditions. Both tests are suitable for providing a preliminary judgement on the environmental stability of solid waste residues. However, they are unsuitable for evaluating long term behavior as the solid waste residues may undergo chemical changes with time. Furthermore, the specific test conditions do not represent the actual disposal conditions under which the solid waste residues are stored (Riveros et al., 2001; Ghosh et al., 2004). As a consequence, these tests do not necessarily assess the long term stability of arsenic-bearing solid residues.

2.7.2. Characterization of Fe(III)-As(III) bearing residues

Despite the fact that Fe(III)-As(III) bearing residues (Fe:As molar ratio=3) have been used for the removal and safe disposal of arsenic from copper smelter acidic effluents, knowledge on their precise nature and characteristics is still limited. Furthermore, the effect of aging on the

characteristics and stability of Fe(III)-As(III) bearing precipitates under actual disposal conditions is poorly understood. In order to be able to assess the long term stability of arsenical residues and make accurate predictions about the behavior of the arsenic-bound species, detailed characterization of their mineralogical composition and arsenic speciation is fundamental (Riveros et al., 2001; Robins et al., 2001.

.

The uncertainty regarding the mineralogical composition and arsenic speciation of As bearing residues has mainly arisen from difficulties encountered in their characterization due to their poorly crystalline and heterogeneous nature. Mine wastes are known to be highly heterogeneous with respect to As-bearing minerals and compounds (Foster et al., 1998; Paktunc et al., 2003, 2004; Walker et al., 2009), therefore Fe(III)-As(III) bearing precipitates are likely to contain other As(III) phases apart from As(III)-Fh.

The recent identification of Fe(III)-As(III) bearing phases such as As(III)-rich schwertmannite and tooeleite in nature seems to suggest that these phases may also be present in the Horne ETP precipitates. In nature, both schwertmannite (iron oxyhydroxysulfate) and tooeleite (ferric arsenite sulphate hydrate) are associated with acidic, sulphate-rich waters, in particular acid mine drainage and acid rock drainage (Morin et al., 2003). Schwertmannite is formed by the oxidation of iron sulphide minerals and the direct precipitation of Fe(III) from acidic sulphate waters in the range of pH 2 to 4 (Bigham and Nordstrom, 2000). Tooeleite is a rare mineral that is formed by the metabolic activity of a bacterial strain that removes Fe(III) and As(III) from AMD water by co-precipitation in the form of As(III)-rich precipitates (Morin et al., 2003). In nature, schwertmannite and tooeleite play an important role in acting as sinks for the toxic oxyanions such as As (III) and As(V) (Morin and Calas, 2006). Schwertmannite scavenges

arsenic by adsorption onto its surface while tooeleite scavenges arsenic by incorporation into its structure (Morin et al., 2003). Carlson et al. (2002) reported that schwertmannite can adsorb up to 70 mg/g As but higher arsenic concentrations inhibit its precipitation (Carlson et al., 2002). Casiot et al. (2003, 2005) reported that tooeleite forms at higher concentrations of arsenic, when the As species is predominantly As(III). Laboratory experiments conducted by Egal et al. (2008) showed that the formation of both schwertmannite and tooeleite are dictated by the kinetics of Fe(II) oxidation, in that schwertmannite is favoured by the rapid oxidation of Fe(II) while the slow oxidation of Fe(II) leads to the formation of tooeleite.

Other Fe(III)-As(III) bearing compounds that exist in nature include karibibite ($Fe_2As_4(O,OH)_9$), schneiderhohnite ($FeFe_3As_5O_{13}$), fetiasite ($(Fe^{II},Fe^{III},Ti)_3O_2As_2O_5$). Schneiderhohnite and fetiasite contain both Fe(II) and Fe(III) (Nickel and Nichols, 1991; Graeser et al., 1994; Nelham et al., 2000).

2.8. Application of synchrotron-based analysis

Synchrotron-based analysis is a powerful analytical technique that utilizes synchrotron radiation to study the composition and the structure of materials on an atomic scale (Potts et al., 1995).

2.8.1. Introduction to synchrotron radiation

A synchrotron is a particle accelerator where high speed electrons, travelling close to the speed of light, are used to generate intense beams of light. Synchrotron radiation (or synchrotron light) is produced in storage rings under high vacuum conditions and can be generated across the range of the electromagnetic spectrum from infrared to x-rays, as illustrated in Figure 2.2.

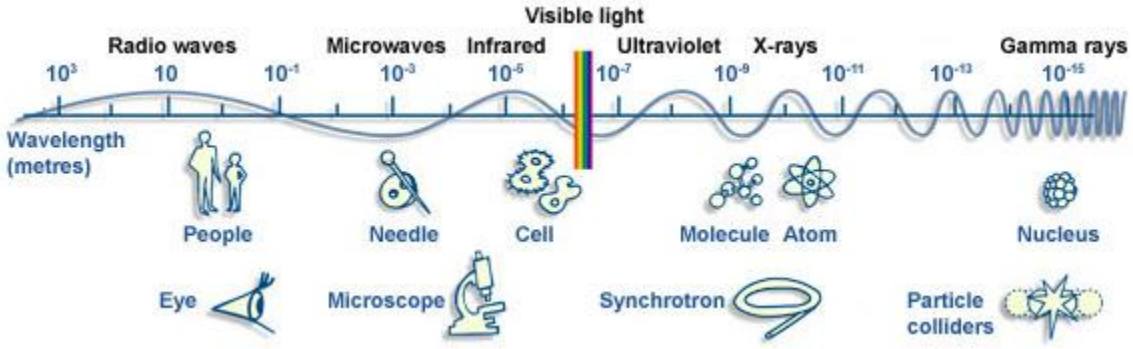

Figure 2.2: The electromagnetic spectrum (European Synchrotron Radiation Facility, 2012)

At the synchrotron facility, an electron gun is used to generate packets of high-energy electrons (Figure 2.3). The electrons are injected into a ring-shaped vacuum chamber known as the linear accelerator (LINAC), where they are accelerated to the speed of light. The electrons are further accelerated by microwaves produced in the booster ring. In addition, magnets are used to steer and focus the electrons into a fine beam. The accelerated electrons travel into the storage ring where they are deflected by bending magnets, thereby producing synchrotron light. The generated light, in the form of infrared, ultraviolet, soft x-rays and hard x-rays, is focused onto the sample at the beamlines and end stations (Potts et al., 1996; Kempson et al., 2005).

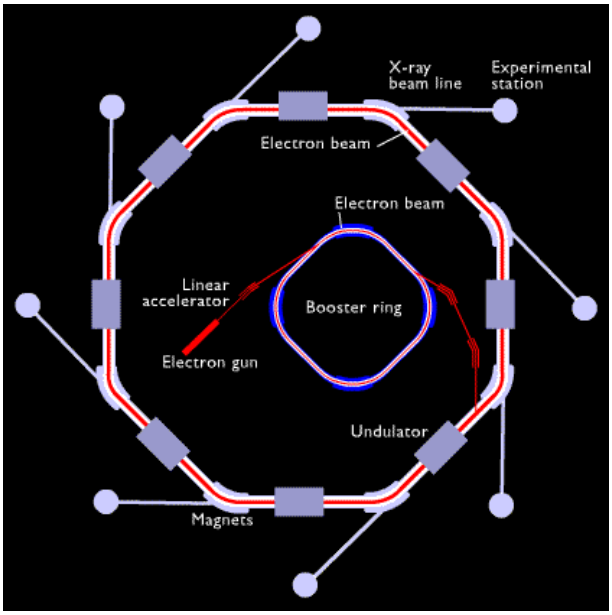

Figure 2.3: A schematic diagram of the synchrotron (Stanford Synchrotron Radiation Laboratory, 2007)

2.8.2. Application of synchrotron-based analysis

Synchrotron-based X-Ray fluorescence (XRF), X-Ray absorption near edge structure (XANES) and X-Ray diffraction (XRD) are emerging as important methods that complement characterization by conventional methods because of their elemental specificity, low detection limits and non-destructive measurement. By the employment of hard x-rays, these techniques enable the study of the elemental concentrations and distributions, chemical speciation and mineral phase identification. Synchrotron radiation microprobe techniques (μXRF, μXRD and μXANES) permit in-situ investigation and analysis of poorly crystalline and amorphous materials at a molecular level (Potts et al., 1996; Lanzirotti et al., 2010). Synchrotron-based microanalysis can be used for the extraction of other chemical and structural information of the As-bearing residues (Arai et al., 2006; Lanzirotti et al. 2010; Manceau et al., 2002; Walker et al., 2005, 2009).

Synchrotron-based μXRF is a powerful technique for the mapping of elemental composition and distribution in a matrix. μXRF is non-destructive, fast, multi-elemental, extremely sensitive, and can examine spatial heterogeneity within samples. μXRF is the only available technique for quantitative elemental mapping due to the high spatial resolution and the deep penetration of hard x-rays. μXRF has a high sensitivity and low detection limits for most elements of mineralogical interest. Elemental distribution data generated by μXRF is used as the basis for efficiently developing the μXANES and μXRD experiments. Subsequent to the generation of elemental distribution maps using μXRF, localized regions of interest in the elemental maps can be examined by μXANES and μXRD (Potts et al., 1996; Manceau et al., 2002; Jamieson and Gault, in press).

Arsenic speciation in the solid phase is difficult to determine directly using conventional methods due to the risk of modification of the arsenic species during the extraction process. Synchrotron-based μXANES is a rapid analytical technique that is capable of providing detailed accurate quantitative information about the arsenic speciation in a solid phase sample. μXANES analysis focuses on the absorption-edge region and assigns speciation identity by the comparison of unknown spectra of the samples with known spectra of model compounds to determine the ratio of valence states present (Potts et al., 1996).

Synchrotron-based μXRD enables the identification and characterization of poorly crystalline materials that are difficult to characterize using conventional techniques (Lanzirotti et al., 2010; Jamieson and Gault, in press). Synchrotron-based μXRD is ideally suitable for micro-crystalline materials due their crystallite size (less than the beam diameter) and random

orientation (Jamieson and Gault, in press). Conversely, μXRD is not suited for coarser mineral crystals as typically they will not diffract under the monochromatic X-ray beam. The increased penetration depth of the synchrotron X-ray beam means that synchrotron micro-diffraction is capable of providing high spatial resolution and facilitating in-situ investigation of mineral phases at the molecular level (Lanzirotti et al., 2010).

Synchrotron-based microanalysis has proven to be a very useful technique in several studies involving the characterization of poorly crystalline phases in arsenic-bearing residues (Cutler et al., 2001; Foster et al., 1998; Moldovan et al, 2003; Paktunc and LaFlamme, 2003; Walker et al., 2005, 2009; Andrade et al., 2010; Meunier et al., 2010; Singh et al., 2010; Corriveau et al., 2011a, 2011b; DeSisto et al., 2011; Fawcett and Jamieson, 2011; Jamieson et al., 2011). However, it must be noted that it is better to complement synchrotron-based analysis with other analytical techniques for the characterization of arsenic-bearing residues in order to gain comprehensive knowledge and understanding of their mineralogy and speciation (Jamieson and Gault, in press).

2.9. Ferrihydrite

The As immobilization mechanism during the co-precipitation of As(III)-Fh bearing residues involves the adsorption of the As(III) species by ferrihydrite. Ferrihydrite is metastable and could transform to more crystalline phases resulting in the mobilization of As. The likelihood of ferrihydrite transformation could affect the stability of the As(III)-Fh bearing residues. Consequently, knowledge about the rate of transformation of ferrihydrite in the presence of adsorbed As(III) species under simulated in-situ disposal conditions is crucial to predicting the long-term stability of As(III)-Fh residues.

2.9.1. Occurrence

Ferrihydrite is an iron oxyhydroxide that is prevalent in near-surface environments, occurring in waters, soils, sediments, mine wastes and acid mine drainage (Cornell and Schwertmann, 2003; Das et al., 2011a).

2.9.2. Characteristics

Ferrihydrite is a reddish-brown, poorly crystalline mineral. It is very finely grained and exists as spherical nano-crystals with a high specific surface area of 100-700 m^2/g (Dzombak and Morel, 1990; Jambor and Dutrizac, 1998; Cornell and Schwertmann, 2003). The nano-crystals are 2-6 nm in size, and generally stick together to form 3-10 μm aggregates (Paktunc et al., 2008). Ferrihydrite has variable chemical compositions due to its variable water content (Jambor and Dutrizac, 1998). However, the bulk chemical formula that is frequently used is $5Fe_2O_3.9H_2O$ (Schwertmann and Taylor, 1989; Das et al., 2011a).

Ferrihydrite has variable crystallinity depending on the reaction conditions. 2-line and 6-line ferrihydrite are the two common crystal forms of ferrihydrite. 2-line ferrihydrite (2-4 nm crystallite size) is formed by rapid hydrolysis at pH 7 under ambient conditions. 6-line ferrihydrite (5-6 nm crystallite size) is formed under pH 7 conditions, by slow hydrolysis under ambient temperature or rapid hydrolysis at 80˚C (Schwertmann and Cornell, 2000; Jambor and Dutrizac, 1998).

2.9.3. Characterization techniques

Characterization of ferrihydrite is very difficult due to its fine grained and poorly crystalline nature. The different analytical techniques that are used for the identification and

characterization of ferrihydrite are described by Cornell and Schwertmann (2003), and include X-ray diffraction (XRD), infrared spectroscopy (IR), Mossbauer spectroscopy (MS), Thermogravimetric and Differential Thermal analysis (TG/DTA), Scanning Electron Microscopy (SEM), Transmission Electron Microscopy (TEM) and synchrotron-based X-ray absorption fine spectroscopy. IR and Raman spectroscopy are used to obtain information about the crystal morphology and the degree of crystallinity, metal substitution and adsorbed molecules. Fourier-Transform IR provides better resolution and sensitivity as well as more rapid collection of data than IR. Under Raman spectroscopy, long exposure to the laser beam results in the transformation of ferrihydrite to hematite. MS and TG/DTA is used to identify and characterize ferrihydrite. MS provides information about the particle size, charge and coordination, and is useful in the measurement of low concentrations of ferrihydrite that cannot be detected by XRD. Synchrotron-based X-ray absorption fine spectroscopy is used to determine the speciation and structure of ferrihydrite. SEM provides information on the morphology and microtopography of ferrihydrite while TEM provides information on the structure of ferrihydrite. XRD is used to characterise the ferrihydrite, and it is the most reliable conventional technique for the identification of ferrihydrite as it is based on the long range order of atoms while the other methods, including Mossbauer spectroscopy and synchrotron-based X-ray absorption fine spectroscopy, characterize the atoms and their short range environment. Differential dissolution using Schwertmann's ammonium oxalate procedure is used for the identification of ferrihyrite as it is readily soluble in ammonium oxalate at pH 3 (Jambor and Dutrizac, 1998).

2.9.4. Adsorption of As(III) and As(V)

Ferrihydrite has a high adsorption affinity for various cations and anions, including arsenite (As(III)) and arsenate (As(V), due to its large surface area and high reactivity (Dzombak

and Morel, 1990; Jambor and Dutrizac, 1998). The absorption affinity of ferrihydrite is dependent on the degree of crystallinity, such that 2-line ferrihydrite has a greater absorption capacity than 6-line ferrihydrite (Swash and Monhemius, 1995; Cornell and Schwertmann, 2003). Previous studies have shown that ferrihydrite can adsorb and form co-precipitates with various metals, metalloids, silicates and organics but it is difficult to confirm their incorporation into the ferrihydrite structure due to its very small particle size and poor crystallinity (Schwertmann and Taylor, 1977; Dzombak and Morel, 1990; Cornell and Schwertmann, 2003; Welham, 2000).

Most adsorption studies have focused on the adsorption of As(V) by ferrihydrite but little is known about the adsorption of As(III) despite its high toxicity and environmental relevance, probably due to the fact that it is generally assumed that As(V) is more effectively adsorbed by ferrihydrite than As(III) (Raven et al., 1998). Pierce and Moore (1982) studied the adsorption of low concentrations of arsenite and arsenate (10^{-7}- 10^{-3} M) by ferrihydrite in the pH range 4-10. The authors reported that As(V) is strongly adsorbed at pH 4, while As(III) is strongly adsorbed at pH 7. Their findings were consistent with recent studies by Bang and Meng (2004) who reported that As(III) is more strongly adsorbed than As(V) at pH>8. Raven at al. (1998) studied the adsorption behavior of arsenite and arsenate on ferrihydrite under varying As concentrations (0.04-2 g/L); initial Fe:As molar ratios (0.8-29) and pH range (3-11). The authors found that As(III) adsorption was faster at relatively high pH (> 7.5) and high initial As concentrations. Conversely, As(V) adsorption was faster at low pH and low initial As concentrations. At high As concentrations, the adsorption maxima for As(V) and As(III) occurred at pH 4.6 and pH 9.2 respectively. At pH 4.6, the As(III) and As(V) adsorption maxima were 0.60 mol As/mol Fe and 0.25 mol As/mol Fe respectively. At pH 9.2, the As(III) and As(V) adsorption maxima were 0.58

mol As/mol Fe and 0.16 mol As/mol Fe. The maximum As(III) adsorption was 0.6 mole As(III)/ mole Fe at pH 9.2, which exceeds the maximum number of surface sites (~0.25 mol of sites/mol Fe) available for the adsorption of As(III) by ferrihydrite and precludes the possibility that As(III) adsorption was entirely adsorbed as a monomeric species. Consequently, the authors proposed that the high retention of As(III) was due to the transformation of ferrihydrite to ferric arsenite. The findings of the study by Raven et al. (1998) demonstrated that, contrary to general views, As(III) is adsorbed more extensively than As(V) by ferrihydrite at high pH (>7.5) and high As concentrations, and should be retained more effectively at pH 9 than As(V).

2.9.5. Ferrihydrite transformation

Ferrihydrite (2-line) ($K_{sp} = 10^{-39}$) is metastable under oxic conditions, and can gradually undergo transformation to form more stable, crystalline phases, including goethite ($K_{sp} = 10^{-41}$) and/or hematite ($K_{sp} = 10^{-43}$) (Jambor and Dutrizac, 1998; Cornell and Schwertmann, 2003; Schwertmann et al., 2004; Cudennec and Lecerf, 2006). At ambient temperature, ferrihydrite will transform to hematite under neutral conditions (pH 7-8), and to goethite under acidic (pH 2-5) and highly alkaline (pH 10-14) conditions (Cudennec et al., 2006). Conversely, under high temperatures (50-100˚C), ferrihydrite will transform to hematite under all pH conditions (Das et al, 2011b). The transformation of ferrihydrite results in a decrease in its surface area thereby reducing its adsorptive capacity, leading to the release of the adsorbed species (Dzombak and Morel, 1990; Jambor and Dutrizac, 1998; Cudennec and Lecerf, 2006; Schwertmann et al., 2004; Schwertmann and Murad, 1983; Johnston and Lewis, 1983; Cornell at el., 1987; Das et al., 2011a). The rate of ferrihydrite transformation is dependent on time, pH, temperature and the presence of sorbed species (Johnston and Lewis, 1983; Schwertmann and Murad, 1983; Jambor

and Dutrizac, 1998; Cornell and Schwertmann, 2003; Cudennec and Lecerf, 2006; Das et al., 2011a).

Several studies have reported that the presence of various adsorbed species including metals, phosphate, silicate, arsenate, sulphate, and organics can retard the rate of transformation of ferrihydrite to more crystalline phases (Paige et al., 1996; Paige et al, 1997; Jambor and Dutrizac, 1998; Cornell and Schwertmann, 2003; Twidwell et al., 2005; Robins et al., 2005; Hohn, 2005; Jia et al., 2006; Dutrizac and Jambor, 2007; Twidwell and Leondard, 2008; Jia and Demopoulos, 2008). Most studies have focused on the effect of adsorbed As(V) species on the transformation rate of ferrihydrite compared with the As(III) species (Paige et al., 1996; Paige et al, 1997; Jia et al., 2006). Paige et al. (1996; 1997) reported that absorbed As(V) decreases the rate of transformation of ferrihydrite under highly acidic (pH 1.3 at 25˚C) and alkaline (pH 12 at 70˚C) conditions. Paige et al. (1996) found that, at pH 12 and 70˚C, 50% of pure ferrihydrite transformed to goethite and hematite within 8 hours while, in the presence of 1 mol% As(V), 2.5% of the ferrihydrite is converted. Jia et al. (2006) reported that under alkaline conditions (pH 8 and 25˚C) and varying As/Fe molar ratios (0.500, 0.250, 0.125), ferrihydrite maintained its stability for a period of 2 weeks. Das et al. (2011b) studied the effect of adsorbed As(V) (As:Fe molar ratios 0.01-0.5) on the transformation of ferrihydrite under highly alkaline conditions (pH 10) and reported that ferrihydrite contained in As(V)-Fh bearing precipitates with As/Fe molar ratios ≥0.0184 would remain stable for over 10,000 years in a disposal pond at above pH 8 and under low temperature conditions (~1˚C) typical of Canadian locations. Field studies from the Sain-Yrieux gold mining district in France indicated that As(V)-Fh has maintained its stability over centuries with no transformation to goethite or hematite (Das et al., 2011b). No similar

studies have been undertaken to evaluate the effect of adsorbed As(III) on the transformation of ferrihydrite.

2.9.6. As immobilization in the environment

Ferrihydrite is frequently found as precipitates formed from mine drainages, soil solutions and lake waters. The widespread occurrence of ferrihydrite in the environment indicates the rate of ferrihydrite transformation to goethite and hematite is slow (Cornell and Schwertmann, 2003). Due to its large surface area and strong adsorptive capacity, ferrihydrite plays an important role in the sequestration of arsenic in the environment (Martinez and McBride, 1998; Das et al., 2010 and references therein). Arsenic immobilization by ferrihydrite occurs widely in nature, and is a major mechanism for regulating the natural attenuation of As pollution in soil, groundwater and sediments (Bowell, 1994; Sherman and Randall, 2003). The mobility of arsenic in natural aquatic and soil environments is controlled by the adsorption/desorption and co-precipitation with ferrihydrite (Moldovan et al., 2003; Raven et al., 1998). Immobilization of arsenic in the environment occurs through precipitation of low-solubility salts and the adsorption/co-precipitation on soils and sediments (Pierce and Moore, 1982). The mobility of arsenic is controlled by the concentrations of soluble As and ferrihydrite, its speciation, redox, pH and presence of bacteria (Morin et al., 2003). In natural systems, As(V) is more strongly adsorbed than As(III). At concentrations found in natural systems, the optimum pH for the As(V) adsorption is pH 4-7, and for As(III) adsorption is pH 7-10 (Frost and Griffin, 1977; Pierce and Moore, 1980, 1982).

2.9.7. Characterization of environmental As-bearing residues

Detailed characterization of environmental As-bearing residues is fundamental in providing a better understanding of As mobility and geochemical controls thereby improving the management of these As-bearing residues. Various methods are used in the characterization of environmental As(III)-Fh and As(V)-Fh bearing residues. XRD analysis is used to characterize As-bearing mineralogical phases. Scanning electron microscope-energy dispersive spectroscopy (SEM-EDS) and electron microprobe analysis (EMPA) is used in defining the association of arsenic with other elements. SEM also provides information on the morphology and microtopography of the arsenic-bearing residues. Synchrotron-based analysis is used in the characterization of As-bearing phases, and provides information on the association of arsenic with other elements, mineralogical composition and the As speciation. Sequential chemical extractions are used to establish the association of arsenic with various mineral phases contained in the arsenic-bearing residues.

2.10. Alternative As bearing disposal options

Despite being widely used for arsenic control at copper smelters, the precipitation of ferric arsenate precipitates is associated with high operating costs and disposal costs (Hoffmann, 1993; Riveros et al., 2001). Therefore, there is an incentive to develop an alternative stable As bearing compound with low solubility, low iron and neutralizing agent requirements, a high As removal efficiency and good filtration properties that can be utilized by the metallurgical industry for the removal and disposal of arsenic from weak acid effluents.

A ferric arsenite sulphate hydrate, known in nature as tooeleite ($Fe_6(AsO_3)_4(SO_4)(OH)_4 \bullet 4H_2O$) has recently been proposed as a potential phase for stabilising

As(III) species in acidic effluents due to its high As removal efficiency, high arsenic content (25 wt%) and low Fe:As weight ratio (1.2) (Nishimura and Robins, 2008). Tooeleite could be considered as the As(III) equivalent of scorodite as both compounds have similar characteristics and are stable in acidic media.

2.11. Tooeleite

2.11.1. Occurrence

The mineral tooeleite was first identified underground at the US Mine near Gold Hill, in Tooele County, Utah in 1964. In 1984, abundant masses of tooeleite were found on the waste dumps of the U.S. mine in the presence of assemblages consisting of pyrite, arsenopyrite, scorodite and jarosite, with the replacement minerals in thermally metamorphosed limestone (Cesbron and Williams, 1992). Recently, nanocrystalline tooeleite has been identified in certain AMD deposits and its formation related to the metabolic activity of a bacterial strain that removes Fe(III) and As(III) from AMD water by co-precipitation in the form of As(III)-rich precipitates (Morin et al., 2007; Morin et al., 2009). Walker et al. (2009) and DeSisto et al. (2011) have identified tooeleite in the pH-neutral tailings of former As-bearing gold mines in Nova Scotia.

2.11.2. Characteristics

The physical characteristics and chemistry of tooeleite were first described by Cesbron and Williams (1992). Cesbron and Williams claimed tooeleite to be an As(V) mineral with an orthorhombic structure. The chemical formula $Fe_8(AsO_4,(SO_4)_6(OH)_6 \cdot 5H_2O$ was proposed, which implied an Fe/As ratio of 1.33. Subsequent to their comprehensive study, the new mineral tooeleite had its name approved by the “Commission on New Minerals and New Mineral Names” and an X-ray diffraction pattern based on its orthorhombic structure was accepted by the JCPDS

(International Centre for Diffraction Data). Nishimura and Robins (2008) conducted electron microprobe analysis on a sample from US Mine waste dumps at Gold Hill and found that silicon influenced the analytical accuracy of the microprobe experiments performed by Cesbron and Williams.

However, a XANES investigation conducted by Morin et al (2003) indicated that arsenic species found in tooeleite is As(III). Morin et al (2007) recently determined that tooeleite is an As(III) mineral with a monoclinic structure. In their study, the crystal structure of a sample from the US Mine waste dumps in Tooele County was determined using a combination of high resolution synchrotron XRD and refined Rietveld techniques. Tooeleite was proposed to have the chemical formula $Fe_6(AsO_3)_4(SO_4)(OH)_4 \cdot 4H_2O$ which corresponds to an Fe/As ratio of 1.5. Nishimura and Robins (2008) recently synthesized tooeleite and confirmed that it is actually an As(III) compound, with the chemical structure $6Fe_2O_3.5As_2O_3.2SO_3.12H_2O$ and Fe/As ratio of 1.2. The free energy of formation of tooeleite has recently been studied by Huang et al., (2008) using results from Nishimura and Robins (2008) stepwise titration experiments with NaOH at 25˚C. Huang et al., (2008) reported an estimated free energy of formation of tooeleite to be 1240.903±1.407 kcal/mole, according to the chemical formula suggested by Morin et al., (2003).

2.11.3. Tooeleite synthesis

The synthesis of nano-crystalline tooeleite from sulphate-based Fe(III)-As(III) weak acid solutions has been investigated by Nishimura and Robins (2008). The XRD and TGA techniques were employed to identify the nature of the precipitated materials. XRD analysis of the precipitates indicated that their XRD pattern was similar to that reported by Cesbron and Williams (1992) for tooeleite. TG-DTA analysis of the precipitates led the researchers to suggest

that the thermal decomposition of ferric arsenite sulphate hydrate in the temperature range 23 – 1400˚C results in the release of H_2O, SO_3 and As_2O_5 and finally in the formation of the Fe_2O_3. A stepwise titration of an acidic Fe(III)-As(III) solution with NaOH at 25˚C resulted in the precipitation of tooeleite in the pH range 2-3.5 and its transformation to FeOOH(As) (arsenical ferrihydrite) above pH 3.5. Despite these results, Nishimura and Robins (2008) proposed that tooeleite could be a potential disposal option for removing arsenic from copper smelter weak acid effluents since tooeleite found in the waste dumps at the former US mine in Tooele County has retained its stability under severe weathering conditions over time.

2.12. Summary

As(III)-Fh bearing precipitates have been successfully used at Xstrata's Horne Copper Smelter for the fixation and disposal of As from its weak acid effluents. However, knowledge of their precise nature and characteristics is limited. In addition, the effect of aging on the characteristics and stability of As(III)-Fh bearing precipitates under actual disposal conditions is poorly understood. Detailed characterization of their mineralogical composition and arsenic speciation is fundamental to enable the assessment of their long term stability and the accurate prediction about the behavior of the arsenic-bound species. The uncertainty regarding the mineralogical composition and arsenic speciation of As(III)-Fh bearing residues has mainly arisen from difficulties encountered in their characterization due to their poorly crystalline and heterogeneous nature. Detailed characterization studies using synchrotron-based microanalysis are required to provide a better understanding of the As retention mechanism in the Horne ETP precipitates.

The mechanism of As immobilization during the co-precipitation of As(III)-Fh bearing residues involves the adsorption of the As(III) species by ferrihydrite. However, ferrihydrite is known to be metastable and could transform into more crystalline phases resulting in the mobilization of As. The likelihood of ferrihydrite transformation could have a detrimental effect on the stability of the As(III)-Fh bearing residues, leading to As mobilization. Consequently, knowledge about the rate of transformation of ferrihydrite in the presence of adsorbed As(III) species under in-situ disposal conditions is crucial to making accurate predictions about the long-term stability of As(III)-Fh residues. Based on the literature review, no studies have been conducted on the As(III)-Fh transformation rates under simulated in-situ disposal conditions.

Despite being the most widely used disposal option for the removal of As from copper smelter weak acid effluents, the precipitation of As(V)-Fh bearing precipitates is associated with high operating costs and disposal costs (Hoffmann, 1993; Riveros et al., 2001). Therefore, there is an incentive to develop an alternative cost-effective, environmentally stable Fe(III)-As(III) compound that can be utilized by copper smelters for the removal and disposal of arsenic from their weak acid effluents. A ferric arsenite sulphate hydrate, known in nature as tooeleite ($Fe_6(AsO_3)_4(SO_4)(OH)_4 \bullet 4H_2O$) has recently been proposed as a potential phase for stabilizing As(III) species in acidic effluents due to its high As removal efficiency, high arsenic content (25 wt%) , low Fe:As molar ratio (1.2) and is stable in the pH range 2 to 3.5 (Nishimura and Robins, 2008). Recently, Nishimura and Robins (2008) investigated the synthesis of nano-crystalline tooeleite from sulphate-based Fe(III)-As(III) bearing weak acid solutions and conducted preliminary characterization tests (XRD, SEM, TG/DTA) on the synthetic precipitates. However, their study did not evaluate the stability of the synthetic tooeleite precipitates. Further research

regarding the detailed characterization and stability of synthetic tooeleite precipitates is required to validate the potential application of tooeleite as a disposal option.

Chapter 3

Mineralogical characterization of the Horne Effluent Treatment Plant As(III)-bearing precipitates

3.1. Introduction

At Xstrata's Horne Copper Smelter in Rouyn-Noranda, Quebec, arsenic is effectively removed from the weak acid and dust treatment bleed effluents to low levels (<0.5 ppm) by lime neutralization and co-precipitation with ferric iron (Fe:As molar ratio>3) and base metals. According to Godbehere et al (1995), arsenical ferrihydrite (As(III)-Fh), base metal hydroxides and gypsum are formed during this treatment process . However, little is known about the precise characteristics of As(III)-Fh precipitates compared to As(V)-Fh (Harris and Monette, 1988; Robins et al., 1988; Krause and Ettel, 1989; Nishimura and Umetsu, 2000; Moldovan et al., 2003; Jia et al., 2003). As(V)-Fh is generally the preferred disposal option used by copper smelters for the removal of As from their weak acid effluents, albeit trivalent arsenic is the major arsenic species in the effluents. The reason may be that it is generally assumed that arsenic removal by lime neutralization and co-precipitation with ferric iron is more effective if the arsenic is present as As(V) (Nishimura and Umetsu, 2000; Riveros et al., 2001; Twidwell and McCloskey, 2011). Consequently, previous research has principally focused on the precipitation mechanism, stability, mineralogy and arsenic speciation of As(V)-Fh (Harris and Monette, 1988; Robins et al., 1988; Krause and Ettel, 1989; Emett and Khoe, 1993; Waychunas et al., 1993; Langmiur et al., 1999; Nishimura and Umetsu, 2000; Moldovan et al., 2003; Jia et al., 2003; Richmond et al., 2004; Twidwell et al., 2005; Langmiur et al., 2006). Therefore, the focus of this study is to

understand the fundamental co-precipitation processes and the mechanism of arsenic retention in this Fe(III)-As(III)-Zn(II)-Ca(II) system by identifying and characterizing the mineral phases contained in the Horne Effluent Treatment Plant (Horne ETP) sludge.

According to Nishimura and Umetsu (2000), optimal adsorption of As(III) on ferrihydrite is favourable at pH 8-9 relative to lower pH values. These findings are consistent with studies by Raven et al. (1998) and Dixit et al. (2003). However, conflicting views have arisen as to whether the speciation of the adsorbed As(III) is maintained during its adsorption on ferrihydrite. Robins et al. (2001) proposed that, during the adsorption of As(III) on ferrihydrite, As(III) oxidation may occur in the ferrihydrite structure resulting in the reduction of Fe(III) to Fe(II). However, Greenleaf et al. (2003) reported that As(III) oxidation adsorbed on ferrihydrite did not occur in continuously stirred batch reactors, even though it is thermodynamically possible. Oscarton et al. (1981) and Jang and Dempsey (2008) observed that the oxidation of adsorbed As(III) on ferrihydrite did not occur at low Fe/As molar ratios (<10). A recent study by Zhao et al. (2011) has shown that the gradual oxidation of As(III) adsorbed on ferrihydrite occurs at relatively high Fe:As molar ratios (>10) and longer reaction times (>24 hours) under ambient conditions at pH 4 and 7 . The authors concluded that As(III) adsorbed on ferrihydrite was oxidized to As(V) in the presence of oxygen, with ferrihydrite acting as a catalyst although Fe(II) was not detected during the oxidation reaction.

At the Horne ETP, the acid mine drainage from the Gallen and Remnor mine sites which is added as an additional source of ferric iron for the precipitation process also contains zinc. According to Godbehere et al. (1995), the presence of zinc enhances the retention of arsenic and

stability of the Horne precipitates. However, the role of zinc on the precipitation mechanism and retention of As(III) in the Horne ETP process is still not well understood.

The Horne ETP co-precipitates are co-deposited with finely ground slag tailings in a tailings facility at pH 8.5-9.5, and the final effluent from the facility contains <0.5 mg/L As (Godbehere et al., 1995; Riveros et al., 2001). Although the disposed As(III)-Fh bearing co-precipitates have maintained their stability for several years, the reason for their high stability is not evident. Furthermore, knowledge on the effect of aging on their characteristics under actual disposal conditions is poorly understood.

The general view is that the mechanism of As fixation by Fe(III)-As(III) co-precipitation with lime is by surface adsorption of the As(III) species onto ferrihydrite (Robins et al., 1988; Riveros et al., 2001; Moldovan et al., 2005). However, the long term stability of ferrihydrite is a matter of concern. Ferrihydrite is a poorly ordered iron oxyhydroxide that is known to be metastable and can gradually transform to goethite and hematite under oxic conditions (Schwertmann and Murad, 1983; Jambor and Dutrizac, 1998; Cornell and Schwertmann, 2003; Schwertmann et al., 2004; Cudennec and Lecerf, 2006). The rate of transformation of ferrihydrite is dependent on pH, temperature and time (Johnston and Lewis, 1983; Schwertmann and Murad, 1983; Jambor and Dutrizac, 1998; Cornell and Schwertmann, 2003; Cudennec and Lecerf, 2006). Under ambient conditions, ferrihydrite will transform to goethite in the pH ranges of 2-5 and 10-14 (Schwertmann and Murad, 1983; Cudennec et al., 2006). The transformation of ferrihydrite to hematite is favoured at pH 7-8 under ambient temperature (Schwertmann and Murad, 1983). Conversely, at high temperatures (50-100˚C), ferrihydrite will transform to hematite under all pH conditions (Das et al, 2011b). Goethite is formed by the dissolution of ferrihydrite, followed by

reprecipitation (Cornell and Schwertmann, 1996). Hematite is principally formed by internal dehydration and atomic rearrangement of ferrihydrite (Cornell and Schwertmann, 1996). Recently, Das et al. (2011a) investigated the transformation of 2-line ferrihydrite to goethite and hematite under varying pH (2, 7 and 10) and temperature (25, 50, 75 and 100˚C) conditions. Their studies demonstrated that the transformation rate of ferrihydrite was enhanced with increasing pH and temperature. At pH 10, the rate of transformation of ferrihydrite increased fivefold from 25˚C to 100˚C. Based on first order rate reactions, the authors concluded that pure ferrihydrite under in-situ conditions of pH 10 and 1˚C will transform to goethite or hematite (10% conversion after 3 years and 100% conversion after 90 years), suggesting that ferrihydrite will not maintain its long-term stability under such conditions.

Ferrihydrite has a high adsorption affinity for various ions including copper, nickel, zinc, cobalt, phosphate, silicate, arsenite, arsenate, sulphate, and organics, due to its high surface area and acts a sink for these ions (Dzombak and Morel, 1990; Jambor and Dutrizac, 1998; Cudennec and Lecerf, 2006; Schwertmann et al., 2004; Schwertmann and Murad, 1983; Johnston and Lewis, 1983; Cornell at el., 1987). The transformation of ferrihydrite to secondary Fe-bearing crystalline phases leads to a decrease in its surface area, thereby reducing its adsorptive capacity and promoting the desorption of the adsorbed ions from the solid phase. Several studies have shown that the presence of the adsorbed species can significantly inhibit the transformation of ferrihydrite to goethite or hematite (Cornell et al., 1987; Paige et al., 1996; Paige et al, 1997; Jambor and Dutrizac, 1998; Schwertmann and Cornell, 2003; Twidwell et al., 2005; Robins et al., 2005; Hohn, 2005; Jia et al., 2006; Dutrizac and Jambor, 2007; Twidwell and Leondard, 2008; Jia and Demopoulos, 2008). With regard to the adsorption of arsenic on ferrihydrite, many studies have investigated the effect of adsorbed As(V) on the transformation rate of ferrihydrite (Paige et

al., 1996; Paige et al, 1997; Jia et al., 2006; Das et al., 2011b). No similar studies have been undertaken to evaluate the effect of adsorbed As(III) on the transformation of ferrihydrite. A good understanding of the transformation rate of ferrihydrite in the presence of adsorbed As(III) is very important for predicting the behavior and long-term stability of As(III)-bearing ferrihydrite (As(III)-Fh) residues under actual disposal conditions.

The main objectives of this study were to: (i) identify the mineralogical composition and arsenic speciation of the Horne ETP residues precipitated from iron-rich (Fe:As molar ratio >3) weak acid effluents using synchrotron-based spectroscopic techniques; (ii) to investigate the effect of lime as a base and the role of zinc on the stability of As(III)-Fh; (iii) to evaluate the role of precipitation and adsorption in the Fe(III)-As(III) co-precipitation process and (iv) to investigate the effect of aging on the characteristics and stability of the Horne ETP co-precipitates by evaluating the transformation rate of ferrihydrite in the presence of adsorbed As(III) under simulated relatively alkaline in-situ conditions (pH 9) existing at the Horne Tailings Facility.

3.2. Materials and methods

3.2.1. Reagents

All the chemical reagents were of analytical grade and are listed in Table 3.1.

Table 3.1: List of chemical reagents used in the experiments

Reagent	Chemical formula	Provider
Ferric sulphate pentahydrate	$Fe_2(SO_4)_3.5H_2O$	Alfa Aesar
Zinc sulphate heptahydrate	$ZnSO_4.7H_2O$	Fischer Scientific
Arsenic trioxide	As_2O_3	Alfa Aesar
Arsenic pentoxide	As_2O_5	Alfa Aesar
Sodium hydroxide	NaOH	Fischer Scientific
Calcium hydroxide	$Ca(OH)_2$	Aldrich
Glacial (acetic acid)	CH_3CH_2OOH	Fischer Scientific
Hydrochloric acid	HCl	Fischer Scientific
Nitric acid	HNO_3	Fischer Scientific
Sulphuric acid	H_2SO_4	Fischer Scientific
Potassium chloride	KCl	Fischer Scientific
Sodium Phosphate Dibasic Anhydrous	Na_2HPO_4	Fischer Scientific
Acetone (ACS grade)	$(CH_3)_2CO$	Fischer Scientific
Boron nitride	BN	Fischer Scientific

3.2.2. Sample preparation

A fresh sample (~15 kg) of sludge was obtained from second reactor (pH 9) of the Horne Effluent Treatment Plant (Horne ETP) at Xstrata's Horne Copper Smelter in Quebec. The As speciation in the effluent was not measured at the time of sampling. Aliquots of the sample were vacuum-filtered using a 0.45µm membrane filter and the filtered solids were dried in air under ambient conditions.

3.2.3. Chemical analysis

Quantitative analysis of the elemental composition of the air-dried samples from the Horne ETP was determined using aqua regia digestion (3:1 HCl:HNO_3), followed by Inductively

Coupled Plasma-Optical Emissions Spectroscopy (ICP-OES). A sample of 0.5 g was dissolved in 40 ml of aqua regia and the suspension was heated for 30 minutes on a heating plate at 250˚C. Distilled water was added to adjust the final volume to 50 ml and the solution was returned to the heating plate to boil. The final solution was filtered into a volumetric flask and distilled water was added to adjust to the final volume of 100 ml. Representative data of the samples was achieved by analyzing two aliquot samples of both the ETP sludge to ensure sample homogeneity.

3.2.4. XRD analysis

X-Ray Diffraction (XRD) analysis was employed to identify the mineralogical composition of the Horne precipitates. XRD analysis was performed on a Phillips X'Pert Pro MPD diffractometer fitted with an X'Celerator high speed strip detector (X-ray source: Cu Kα radiation (Ni filtered) and operating conditions: 45 KV, 40 MA, angle between 3˚- 80˚ 2θ, step size of 0.02˚, counting time of 10 seconds at each step). PanAnalytical HighScore software was used for the identification of phases. To further investigate the mineralogy, a dried sample of the Horne precipitates (1 g) was shaken for 1 hour with 600 ml of distilled water at 200 rpm at room temperature with the aim of dissolving the gypsum (Pantuzzo et al., 2010). The suspension was vacuum-filtered using a 0.45 µm membrane filter and the filtered solids were air-dried under ambient conditions and analyzed using XRD.

3.2.5. Synchrotron-based analysis

Synchrotron-based analysis was performed using the hard X-ray micro-probe, X26A at the National Synchrotron Light Source (NSLS), Brookhaven National Laboratory. Synchrotron-based analysis was conducted using a wide (unfocused) beam (10 µm in diameter) and a micro (focused) beam (5 µm V x 9 µm H). In both cases, micro-X-Ray Fluorescence (µXRF), micro-X-

Ray diffraction (μXRD) and arsenic K-edge micro-X-Ray Absorption Near Edge Structure (μXANES) analyses were conducted on samples from the Horne ETP. μXRF, μXRD and μXANES analyses provided information on the elemental distribution, mineralogy and arsenic speciation respectively. The analytical setup and procedure that were used are fully described in Walker et al. (2005).

3.2.5.1. Sample preparation

Both powder samples and polished thin sections of the Horne precipitates were prepared for analysis. Aliquots of the Horne ETP sludge were vacuum-filtered using a 0.45 μm membrane filter. A portion of the filtered solids were dried under nitrogen gas, in a glove bag under ambient conditions, in order to maintain an unaltered speciation of the As(III) species in the samples. The rest of the filtered solids were dried in air under ambient conditions. Samples of the Horne precipitates that were dried under nitrogen gas were homogenized in a mortar and pestle before being mounted on Kapton® tape supported across a 35mm cardboard slide. The same procedure was repeated for the Horne ETP samples that were air-dried.

Polished thin sections were prepared at Vancouver Petrographics from the air-dried samples, by grinding and polishing using oil and sealtronic epoxy to a thickness of 30-50 μm and mounted on a glass slide. The thin sections were examined under a petrographic microscope to select and photograph targets (grains) for analysis under the synchrotron beam. The targets were identified, selected and photographed under transmitted and reflected light at various magnifications. Following the selection of targets, the thin section was removed from the glass slide using acetone (ACS grade). The removal procedure involved the immersion of the glass slide in an acetone bath until the thin section was detached from the slide. The detached section

was transferred onto Kapton® tape and placed in a 35mm cardboard slide-holder for micro-analysis.

3.2.5.2. µXRF, µXRD and µXANES analyses

The mounted polished thin sections and powder samples were placed in a sample holder oriented at 45˚ to the incident beam in the horizontal plane, and analyzed using a 350 µm collimated monochromatic beam generated from a Si(111) channel-cut monochromator. The monochromatic beam was focused by a pair of Rh-coated Kirkpatrick-Baez mirrors to produce both an unfocused and a focused beam.

3.2.5.3. Unfocused beam analyses

Unfocused beam analyses were conducted on the powder samples and polished thin sections to enable the analysis of both individual grains (grain size 30 – 100 µm) and a mixture of grains to provide an overview of the elemental distribution within individual grains as well as to enable a comparison of the elemental distribution between a mixture of grains.

µXRF analyses using the unfocused beam were conducted on the mounted thin sections to provide an overview of the elemental distribution. During the mapping analysis by µXRF, the energy of the incident radiation was monochromized using a Si(111) crystal and elemental maps were collected on various selected target areas in the thin section for the following elements of interest: As, Fe, Zn, Ca and Cu. The elemental maps were used to select regions to be analyzed using the focused beam. The regions were selected using elemental correlations of As with Fe, Zn and Ca. µXRD and µXANES analyses were conducted on the selected regions with high or intermediate As counts.

μXRD analysis was conducted to determine the mineralogical composition. A Bruker SMART 1500 CCD diffractometer with a fibreoptic taper, in a high resolution mode at 1024 x 1024 pixels was used to collect the 2D μXRD data in transmission mode. The incident X-Ray beam was tuned to 17.749 keV and the μXRD patterns were obtained using an exposure time of 60 seconds per sample, regulated with a timed beam shutter. The dectector was calibrated using corundum [α-Al_2O_3] and Ag behenate [$CH_3(CH_2)_{20}COOAg$] diffraction standards. μXRD analysis was conducted on Kapton as well as Kapton and epoxy, and used in the data treatment procedure.

μXANES analysis was conducted to investigate the speciation of arsenic on selected regions in the powder samples and thin sections (previously selected using the μXRF elemental maps). The μXANES spectra were recorded in fluorescence mode, by using a Si(Li) detector to scan through the As K-edge (11.867 keV). The analysis was conducted by scanning across the absorption edge region (11.80 to 11.88 keV) in three segments. The first segment, the pre-edge region (11.80 to 11.85 keV), had a step size of 5 eV and dwell time of 2 seconds. The second segment, the edge region (11.85 to 11.88 keV), had a step size of 0.4 eV and dwell time of 4 seconds. The third segment, the post-edge region, had a step size of 1 eV and dwell time of 3 seconds. Since photo-oxidation of As(III) and photo-reduction of As(V) under the X-ray beam has been observed in previous studies by Morin et al. (2008) and Arai et al. (2003) respectively, two consecutive scans of μXANES spectra were repeatedly collected on a specific spot on the powder samples.

Arsenic standards (arsenopyrite, arsenolite and scorodite), covering the oxidation states -1, +3, and +5 respectively, were analyzed and used for fitting the μXANES spectra of the powder and thin section samples (Table 3.2). The standards were prepared by being ground with boron nitride (99.9%, 1 μm) and HPLC grade ethanol in a mortar and pestle. Boron nitride was added to the pure samples of the standards and powder samples to dilute their arsenic content to ~4 wt% As in order to control self-absorption effects during analysis (Walker et al., 2005).

Table 3.2: Standards for μXANES analysis (Walker et al., 2005)

Standards	Chemical formula	Source	Oxidation state	Edge position (keV)
Scorodite	$FeAsO_4.2H_2O$	Laurium, Greece[†]	+5	11.8739
Arsenolite	As_2O_3	J.T. Baker reagent	+3	11.8700
Arsenopyrite	FeAsS	Mina La Bufa[†]	-1	11.8670

[†] Miller Museum reference, Department of Geology and Geological Engineering, Queen's University

3.2.5.4. Focused beam analyses

Focused beam analyses were conducted on the powder samples and the thin sections. Regions of interest on the thin sections that were previously selected using the wide beam XRF analysis were analyzed by μXRF. μXRF fluorescence maps were collected for As, Fe, Zn, and Ca, and these maps were used to select spots to be analyzed by μXRD and μXANES. The spots were selected using elemental correlations of As with Fe, Zn, and Ca, at high and intermediate intensities of As in order to identify the major As-host phases, and their respective As oxidation states. Paired correlations were determined by the intensity of each element at each pixel at high and intermediate As-rich spots. μXRD and μXANES were conducted on the powder samples as well as selected spots on the thin sections.

3.2.5.5. Potential limitations

The Horne ETP sludge was stored in a bucket with headspace under ambient conditions. The sludge was aged for a few months before samples were filtered and dried for the preparation of powder samples and a thin section for synchrotron microanalysis. Consequently, it is possible that partial oxidation of the Horne ETP sludge may have occurred during storage prior to synchrotron microanalysis.

Prior to the preparation of the powder samples and thin sections, the Horne ETP wet samples were dried under nitrogen to ensure that the As speciation is maintained. In addition, some of the wet samples were air-dried to evaluate if drying under air had any effect on the As speciation. The thin section was prepared under ambient conditions and oil was used for the grinding and polishing stages to prevent the dissolution of soluble phases. μXANES analysis was repeatedly conducted on the same spot (2 scans for 15 minutes each) in a powder sample to determine if any change in the As speciation occurred under the X-ray beam.

3.2.5.6. Data treatment

The μXRF elemental maps, comprising the relative elemental photon intensities (counts per sec), were plotted using the X26A_Plot program. The photon intensities of each element were proportional to its respective concentration. Fit2D software (Hammersley, 1998) was used to process the XRD data and convert the 2D images to 1D diffraction patterns (2θ vs. intensity patterns). The PanAnalytical X'Pert HighScore software package was used for phase identification by comparison with the reference diffraction patterns in an ICDD Powder Diffraction File 2010 database. The ATHENA software program (version 0.8.056) was used to process and analyze the μXANES spectra of the powder samples, thin section and the standards

(Ravel and Neville, 2005). Pre-edge background subtraction and μXANES normalization were initially performed on the μXANES spectra. Subsequently, linear combination fitting analysis was used to fit the combination of the three standards (arsenopyrite, arsenolite and scorodite) to the unknown spectra of the powder samples and thin section. This approach enabled the determination of the relative proportions of the oxidation states present in the selected regions and spots of the powder samples and thin sections.

3.2.6. Phosphate leaching protocol

A phosphate leaching protocol was applied to quantify the relative contribution of adsorption and precipitation during the Fe(III)-As(III) co-precipitation process at the Horne ETP. Co-precipitation describes the removal of As by neutralization of acidic As-bearing ferric solutions while adsorption is the removal of As from acidic As-bearing solutions using pre-synthesized ferrihydrite. Furthermore, compared to adsorbed As on ferrihydrite, the co-precipitated species have a larger proportion of sites for bidentate arsenate bonding due to the disruption of the polymerization of ferrihydrite offering an enlarged final ferrihydrite surface area for bonding (Waychunas et al., 1993). The procedure described by Pantuzzo et al. (2008) was slightly modified and was performed with a sample of the Horne precipitates. The analysis was performed using a 0.1 M Na_2HPO_4/HNO_3 (pH 5) solution through three consecutive steps and carried out in duplicate. 0.5 g of the precipitates was mixed with 50 ml of the 0.1 M Na_2HPO_4/HNO_3 (pH 5) in an Erlenmeyer flask. The flask was placed on a hot plate and continuously stirred using a magnetic stirrer bar (200 rpm) at 70˚C for 1 hour. After 1 hour, an aliquot of 10 ml was drawn and the suspension was vacuum filtered using a 0.45 μm membrane filter. Two more aliquots were taken after 2 and 3 hours respectively. The total As and Fe concentrations in the filtrate were determined using ICP-OES.

3.2.7. Role of lime and zinc on As(III) removal efficiency and stability

3.2.7.1. Batch co-precipitation experiments

Synthetic co-precipitates were prepared from Fe(III)-As(III)-Zn(II) and Fe(III)-As(V)-Zn(II) solutions under the conditions presented in Table 3.3. Both Fe(III)-As(III)-Zn(II) and Fe(III)-As(V)-Zn(II) solutions had an initial Fe:As molar ratio of 4 and Zn:As molar ratio of 1. The 0.4 M Fe(III) and 0.1 M Zn(II) stock solutions were prepared by dissolving ferric sulphate pentahydrate ($Fe_2(SO_4)_3.5H_2O$) and zinc sulphate heptahydrate ($ZnSO_4.7H_2O$) in distilled water. The 0.1 M As(III) was prepared by dissolving As_2O_3 in 0.2 M H_2SO_4 at 90˚C. The 0.1 M As(V) stock solution was prepared by dissolving As_2O_5 in 0.2 M H_2SO_4. The pH of the Fe(III)-As(III)-Zn(II) solution was initially adjusted to pH 4.5 using 2 M NaOH and continuously stirred on a stir plate for 1 hour at room temperature . After 1 hour, an aliquot of 50 ml was removed for analysis. Then the pH of the slurry was adjusted to pH 9 using NaOH and continuously stirred for 1 hour. The slurries (at pH 4.5 and pH 9) were vacuum-filtered using a 0.45 µm membrane filter and the filtrates were analyzed for As, Fe and Zn using ICP-OES. The solids were washed with distilled water and dried under ambient conditions. The precipitation procedure was repeated using a solution mixture of 0.4 M Fe(III) ($Fe_2(SO_4)_3.5H_2O$), 0.1 M Zn(II) ($ZnSO_4.7H_2O$) and 0.1 M As(V) (As_2O_5) using 2 M $Ca(OH)_2$ as the base, under similar conditions as listed in Table 3.3.

Table 3.3: Batch co-precipitation of synthetic precipitates under ambient conditions

Parameters	Conditions
Fe:As mole ratio	4
Zn:As mole ratio	1
pH	4.5, 9
Base	NaOH; $Ca(OH)_2$
Reaction time	1 hour
Stirring rate	350 rpm
Experimental temperature	25˚C

3.2.7.2. Stability experiments

In order to assess their stability, the synthetic co-precipitates were subjected to short term leaching tests including the standard US EPA Method 3111 (Toxicity Characteristic Leaching Procedure – TCLP test) (US EPA, 1992) and pH 9 leachate test. The TCLP test was conducted to determine the hazardous nature of the synthetic precipitates. The test was performed using an extraction fluid of pH 4.93 ± 0.05. The leachant was prepared by adding 5.7 ml of glacial acetic acid (CH_3CH_2OOH) and 64.3 ml of 1 M NaOH to 500 ml of distilled water, followed by bringing the mixture up to 1000 ml with distilled water. The leaching test was conducted by placing 0.5 g of each co-precipitate with the extraction fluid (solid: liquid ratio of 1:20) in a 250 ml Erlenmeyer flask. The flasks were continuously shaken in an orbital shaker at 200 rpm for 18 ± 2 hours under ambient conditions. On completion of the leaching test, the suspensions were vacuum-filtered using 0.45 µm membrane filters. The pH of the leachates was measured before being analyzed for Fe, As and Zn using ICP-OES.

The pH 9 leachate test was performed to simulate the behavior of the synthetic precipitates under relatively alkaline disposal conditions. The pH 9 leachant was prepared by the addition of 1 M NaOH to distilled water until the target pH 9 was attained. Consistent with the TCLP protocol, 0.5 g of each co-precipitate was mixed with the leachant (solid: liquid ratio of 1:20) in a 250 ml Erlenmeyer flask. The flasks were placed in the shaker and continuously agitated (200 rpm) for 18 ± 2 hours under ambient conditions. On completion of the leaching test, the suspensions were vacuum-filtered using 0.45 µm membrane filters and the pH of the leachates was measured before being analysed for Fe, As and Zn using ICP-OES.

3.2.8. Transformation of ferrihydrite

3.2.8.1. Precipitation tests

Synthetic co-precipitates were prepared from Fe(III)-As(III) and Fe(III)-As(III)-Zn(II) solutions under the conditions presented in Table 3.4. The Fe(III)-As(III)-Zn(II) solution had an initial Fe:As molar ratio of 4 and Zn:As molar ratio of 1 while Fe(III)-As(III) solution had an initial Fe:As molar ratio of 4. The 0.4 M Fe(III) and 0.1 M Zn(II) stock solutions were prepared by dissolving ferric sulphate pentahydrate ($Fe_2(SO_4)_3.5H_2O$) and zinc sulphate heptahydrate ($ZnSO_4.7H_2O$) in distilled water respectively. The 0.1 M As(III) was prepared by dissolving As_2O_3 in 0.2 M H_2SO_4 at 90˚C.

The pH of Fe(III)-As(III)-Zn(II) solution was adjusted to pH 9 using 2 M NaOH and continuously stirred on a stir plate for 1 hour at ambient temperature. After 1 hour, an aliquot of 35 ml was removed and vacuum-filtered using a 0.45 µm membrane filter. The filtrates were analyzed for As, Fe and Zn using Inductively Coupled Plasma Optical Emission Spectroscopy (ICP-OES). The solids were washed with distilled water and dried under ambient conditions. The same procedure was repeated using the Fe(III)-As(III) solution. The remainder of the Fe(III)-As(III)-Zn(II) and Fe(III)-As(III) slurries were divided into two batches, and placed in 250 ml Erlenmeyer flasks, to be retained for the time-series transformation tests.

Table 3.4: Batch co-precipitation of synthetic precipitates under ambient conditions

Key parameters	Conditions
Fe:As mole ratio	4
Zn:As mole ratio	1
pH	9
Base	2 M NaOH
Reaction time	1 hour
Stirring rate	350 rpm
Temperature	25˚C

3.2.8.2. Transformation experiments

Time-series transformation experiments were carried out as described by Das et al. (2011b), using slurries of the Horne ETP and synthetic co-precipitates, at 25˚C and 60˚C under pH 9 conditions. The experiments were performed at 25˚C to evaluate the kinetics of ferrihydrite transformation and at 60˚C to accelerate the transformation rate of ferrihydrite as well as facilitate the formation of more crystalline phases that can be easily identified using the conventional XRD analysis. A pH of 9 was chosen to simulate the in situ disposal conditions in the Horne Tailings pond. The Horne ETP slurry (200 ml) was transferred to a 250 ml Erlenmeyer flask and an initial aliquot of 35 ml was taken out for analysis. The flasks containing the Horne ETP, As(III)-Fh-Zn and As(III)-Fh slurries were placed in a shaker, and shaken at 200 rpm for 14 days at room temperature. Additional flasks containing 200 ml of the Horne ETP, As(III)-Fh-Zn and As(III)-Fh slurries were placed in an incubator shaker, and shaken at 200 rpm and 60˚C for 14 days. The pH of the slurries (at 25˚C and 60˚C) was regularly monitored and maintained at pH 9 by daily additions of 0.1 M NaOH. Aliquots of 35 ml were taken from each flask on specific days for analysis (1, 2, 4, 7 and 14 days). All samples were vacuum-filtered using 0.45 µm membrane filters and the filtrates were collected for ICP-OES analysis of As, Fe and Zn. The solid samples were dried in air under ambient conditions. The kinetics of ferrihydrite transformation to crystalline phases was evaluated by the application of an extraction protocol that selectively dissolved ferrihydrite. Aliquots of the solid samples collected on day 14 were subjected to a 30 minute extraction using 0.4 M HCl solution at a solid:solution ratio of 0.1 g of solid per 100 ml to remove any untransformed ferrihydrite (Cornell and Schneider, 1989; Paige et al., 1996). The concentrations of Fe, As and Zn in the extractant solutions were measured using ICP-OES. Quantitative analysis of Fe, As and Zn in the solid samples collected on days 0 and 14 was

performed using aqua-regia digestion (3:1 HCl:HNO_3), followed by ICP-OES. 0.5 g of the solids was digested on a hot plate with 40 ml of aqua-regia. The suspension was heated until 20 ml of the acid remained and then distilled water was added to adjust the final volume to 50 ml. The solution was returned to the hot plate to boil. The solution was filtered into a 100 ml volumetric flask and distilled water was added to adjust to the final volume.

The solids were analyzed using conventional X-Ray Diffraction (XRD) analysis. XRD analysis was conducted in order to characterize the bulk mineralogy of the aged synthetic and Horne co-precipitates. XRD analyses were performed on a Phillips X'Pert Pro MPD diffractometer fitted with an X'Celerator high speed strip detector (X-ray source: Cu Kα radiation (Ni filtered) and operating conditions: 45 KV, 40 MA, angle between 3˚- 80˚ 2θ, step size of 0.02˚, counting time of 10 seconds per step). The PanAnalytical X'Pert HighScore software package was used for phase identification, using the ICDD Powder Diffraction File 2010 database. Further analysis was performed on the As(III)-Fh-Zn and As(III)-Fh co-precipitates using a longer counting time of 60 seconds per step to try and identify the poorly crystalline phases.

3.3. Results and discussion

3.3.1. Chemical analysis

The chemical composition of the Horne precipitates is presented in Table 3.5. The Fe:As and Zn:As molar ratios of the precipitates were 3.48 and 1.11 respectively. These results are consistent with previous studies by Godbehere et al. (1995) who reported that the Fe:As molar ratio >3 and Fe+Zn:As molar ratio > 4. The high quantities of calcium and sulphur are consistent with the presence of gypsum.

Table 3.5: Elemental composition of the Horne ETP precipitates

	Chemical composition (weight%)						Fe:As	(Fe+Zn):As
Sample	Fe	As	Zn	Cd	Ca	S	molar ratio	molar ratio
H003	6.40	2.46	2.38	0.38	13.70	12.84	3.48	4.59

3.3.2. XRD analysis

XRD analysis of the unwashed Horne precipitates indicated the presence of gypsum ($CaSO_4$. $2H_2O$), while the XRD pattern of the washed Horne precipitates showed low intensity peaks which were assigned to gypsum, and the presence of a poorly crystalline phase (Figure 3.1). The presence of gypsum in the washed precipitates suggests that minor quantities of gypsum remained in the sample after washing. XRD analysis showed no evidence of any As-bearing or Zn-bearing phases even though the Horne precipitates contain relatively high quantities of As (2.46 wt%) and Zn (2.38 wt%).

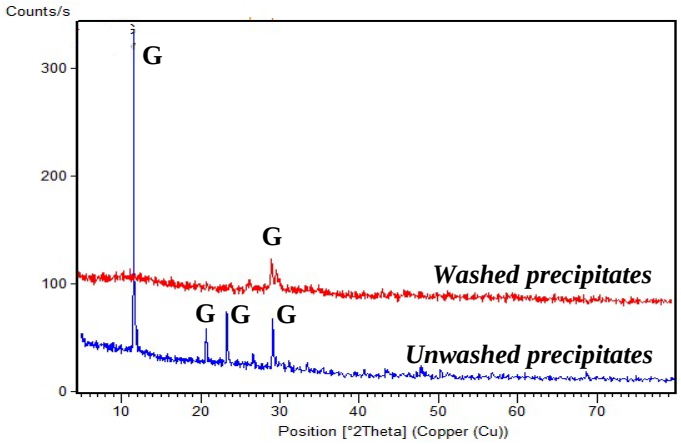

Figure 3.1: XRD pattern of the Horne ETP precipitates

3.3.3. Synchrotron-based analysis

Synchrotron-based analyses (µXRF, µXRD and µXANES) were conducted on powder samples and thin sections of the Horne ETP precipitates and the analyses were conducted on selected regions of low thickness and low As concentration to minimize self-absorption effects which would cause anomalies in the µXANES data by inducing the broadening of the peaks (Walker et al., 2005).

3.3.3.1. µXRF analysis (thin section)

µXRF analysis using an unfocused monochromatic beam was used to determine the localization of arsenic in selected regions of the thin section. Elemental distribution maps of an area 8 x 8 mm and pixel size 0.1 x 0.1 mm for As, Fe, Zn and Ca that were obtained by µXRF analysis of the thin section are presented in Figure 3.2. The intensities for each element are scaled by assigning light colours to the pixel with the highest intensities and dark colours to the pixel with the lowest intensities. The pixel intensities are scaled accordingly on a relative linear scale, located on the right of the maps, according to the elemental counts. The elemental maps

indicated that the distribution of arsenic is heterogeneous, and all the elements showed a clear and similar distribution pattern across the area of the thin section. The circled regions are high As hot spots (region 1- high As; region 2 – high As/Fe; region 3 – high As/Zn; region 4 – high As/Ca; region 5 – As/Fe/Zn) that were selected for synchrotron-based μXRD and μXANES analysis for the determination of the mineral phases and As oxidation state respectively. The dark region is an area of void region stemming from the lifting of the thin section from the silica glass slide.

Elemental correlation plots for As and Fe, Zn and Ca illustrated in Figure 3.3 provided an interpretation of the relationship between As and each of the three elements Fe, Zn and Ca. For each pixel, the corresponding value from each two-elemental map is plotted in a correlation plot where the x and y axes represent the counts for the two different elements. The plots show that there is a positive linear correlation between As and the three elements Fe, Zn and Ca, suggesting a mixture of phases are present at each pixel. The Ca/As correlation is probably due to the presence of gypsum and an As-bearing phase at every pixel. Similarly, the As/Zn correlation could signify the occurrence of Zn and As bearing phases at every pixel. The Zn/Fe positive correlation suggests that Zn may be associated with a Fe-bearing phase.

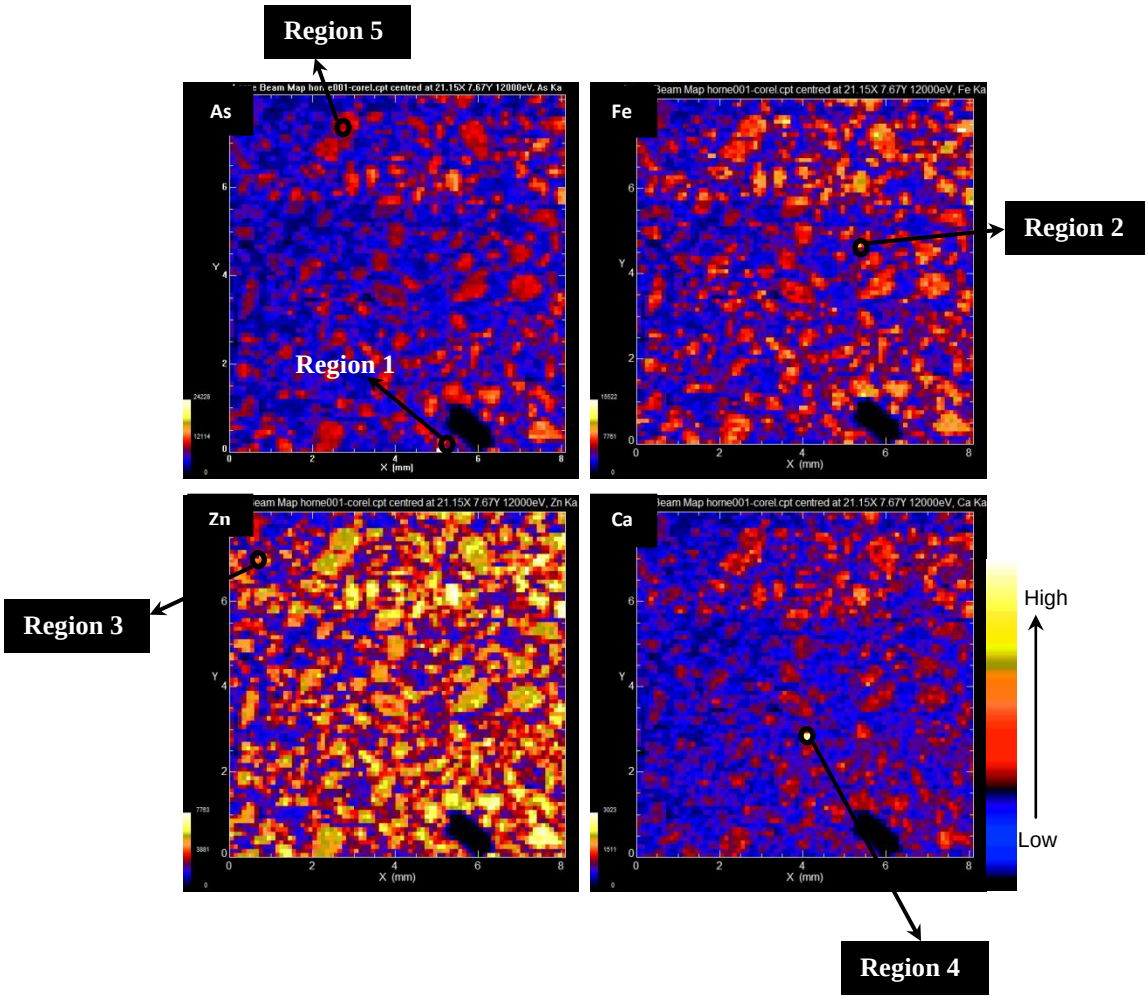

Figure 3.2: Unfocused beam µXRF elemental distribution maps (~8 x 8 mm and pixel size 0.1 x 0.1 mm) for As, Fe, Zn and Ca

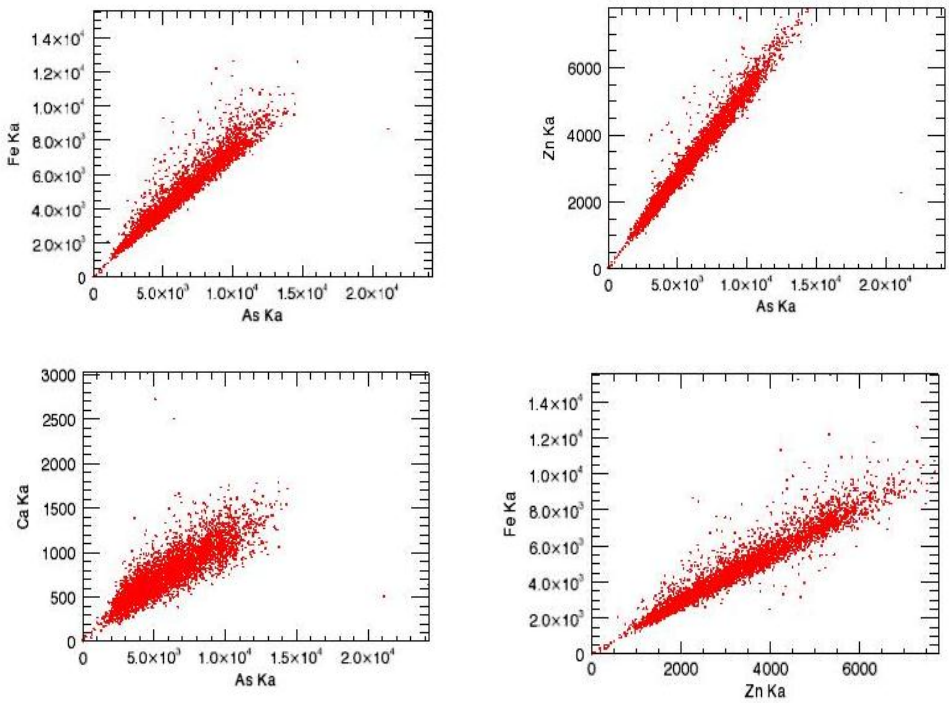

Figure 3.3: Correlation plots between: (a) As/Fe (b) As/Zn (c) As/Ca (d) Zn/Fe, based on data taken from two elemental maps where the x and y axes represent the counts for the two different elements

3.3.3.2. µXRD analysis (thin section)

The 2-D µXRD images and integrated µXRD patterns for regions 1 (High As), 2 (High As/Fe), 3 (High As/Zn), 4 (High As/Ca) and 5 (High As/Fe/Zn) are presented in Figure 3.4 and Figure 3.5. The mineral phases that were identified are presented in Table 3.6. The 2-D bulk µXRD images indicate the degree of crystallinity of the phases at the various selected regions, with the smooth rings signifying the presence of very fine crystallites (nanocrystallites) and the spotty rings denoting the presence of microcrystallites. The broad rings indicate the presence of amorphous phases (Walker et al., 2009). Gypsum was identified in all the regions, which is consistent with the conventional XRD results discussed in Section 3.3.2. The bright spots and

spotty rings in the 2-D μXRD images patterns suggest that the gypsum exists as discrete coarse crystallites. A closer examination of the integrated μXRD patterns in Regions 1, 2, 4 and 5 revealed the presence of two broad peaks with d-spacings of 2.9 Å (consistent with the broad diffraction ring observed in the 2-D μXRD image) and 1.6 Å, indicating the presence of an amorphous phase, ferric arsenate, which is in agreement with previous ferric arsenate characterization studies by several researchers (Rancourt et al., 2001; Carlson et al., 2002; Jia et al., 2006; Le Berre et al., 2007; Paktunc et al., 2008; Walker et al., 2009). This observation is consistent with the μXANES analysis results which indicated the presence of principally As(V). The broad peak observed at 4.5 Å is due to beam intensity responding to the volume of epoxy present in the sample (Walker et al., 2009). Zinc hydroxide was identified in Region 3 (high As/Zn) and Region 5 (high As/Fe/Zn), suggesting that zinc is precipitated as a hydroxide during the Horne ETP process.

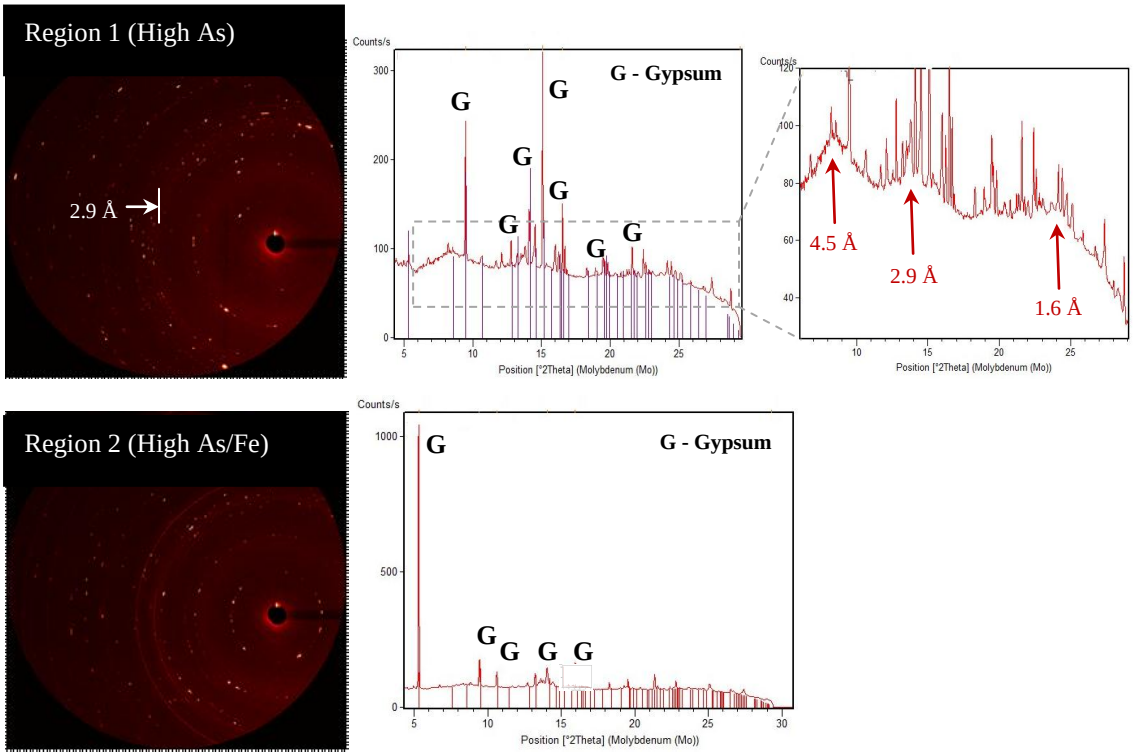

Figure 3.4: 2D μXRD images and integrated μXRD patterns for regions 1 (High As) and 2 (High As/Fe)

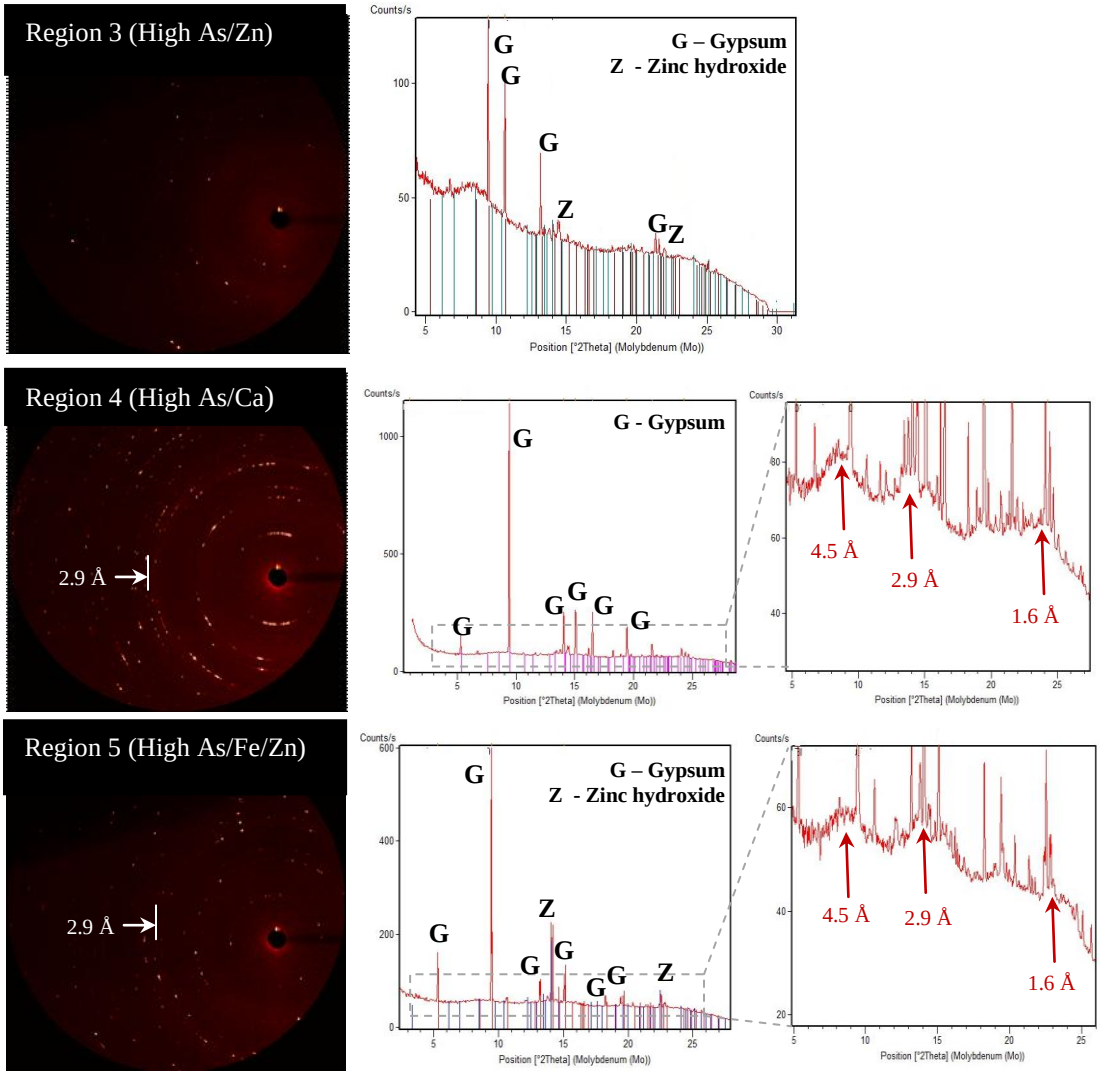

Figure 3.5: 2D μXRD images and integrated μXRD patterns for regions 3 (High As/Zn), 4 (High As/Ca) and 5 (High As/Fe/Zn)

Table 3.6: Mineral phases identified by XRD using the unfocused beam

Region	Mineral phases
1 (High As)	Gypsum (ICDD 21-816) Ferric arsenate
2 (High As/Fe)	Gypsum (ICDD 21-0816)
3 (High As/Zn)	Gypsum (ICDD 21-0816) Zinc hydroxide (ICDD 41-1359)
4 (High As/Ca)	Gypsum (ICDD 21-0816) Ferric arsenate
5 (High As/Fe/Zn)	Gypsum (ICDD 21-0816) Zinc hydroxide (ICDD 41-1359) Ferric arsenate

3.3.3.3. µXANES analysis (powder samples and thin section)

Arsenic K-edge µXANES were collected on the powder samples and the thin section using an unfocused beam. The µXANES spectra of the selected regions in the powder samples and the thin section were fitted with the spectra of standards using linear combination fitting. Fitted model spectra of less than 5% were considered negligible as they did not improve the fits (Walker et al., 2005). Analysis of the µXANES spectra of all the selected regions using linear combination fitting indicated the presence of mixed oxidation states (As(III) and As(V)), with As(V) being the predominant As species. The fitted µXANES spectra of the powder samples (dried under nitrogen and air respectively) are presented in Figure 3.6 and Figure 3.7. The fitted spectra of the powder samples dried in nitrogen and air indicate the presence of mixed oxidation states. A comparison of the two spectra suggests that potential oxidation of the As(III) species in the air-dried Horne ETP powder sample was negligible. Two repeated scans (duration =15 minutes each) conducted on the same spot in a Horne ETP powder sample (dried under nitrogen) indicated that X-Ray beam-induced photo-oxidation or photo-reduction did not occur during the analysis (Figure 3.8). µXANES spectra of As hot spots in the thin section (As/Ca; As/Fe; As/Zn; As/Fe/Zn spots) are presented in Figure 3.9. µXANES analysis was not conducted on Region 1

(high As) due to potential occurrence of self-absorption. The As(V) content found in the As hot spots varied over the range 62 – 72%, suggesting that it is present in variable proportions. The presence of the As(III) species suggests that it is probably bound to ferrihydrite, although this phase was not identified by μXRD analysis. Godbehere et. al. (1995) reported that As(III) is the dominant form of As in the Horne ETP sludge but he did not specify his characterization procedure. It is questionable if the oxidation of the As(III) species occurred during the Horne ETP precipitation process. Although the oxidation of As(III) to As(V) is thermodynamically possible, it is not known to occur in oxic conditions without the addition of a catalyst. Furthermore, it has previously been reported in a number of studies that As(III) oxidation by ferrihydrite does not occur in batch reactors under ambient conditions, and this is attributed to the fact that As(III) species does not encounter a large number of Fe(III) sites while being continuously stirred in a batch reactor system to cause its oxidation (Oscarson et al., 1981; Manning et al., 1998; Greenleaf et al., 2003). Other studies have reported that As(III) oxidation on ferrihydrite occurs at high Fe:As molar ratios (>10) and longer reaction times (>24 hours) (Oscarton et al., 1981; Jang and Dempsey, 2008; Zhao et al., 2011). According to a study by Zhao et al. (2011), the oxidation of As(III) adsorbed on ferrihydrite occurred at very high Fe:As molar ratios (50-200) in the presence of oxygen with ferrihydrite acting as the catalyst. Morin et al. (2008) reported that As(III) adsorbed on ferrihydrite can be oxidized under oxic conditions in the presence of sunlight. Consequently, it is probable that the high As(V) levels detected in the Horne ETP co-precipitates were possibly due to the partial oxidation of the Horne ETP sludge during storage, prior to characterization studies. Partial oxidation may also have occurred due to microbial oxidation under natural setting. Ona-Nguema et al. (2009) reported no oxidation of As(III) adsorbed on lepidocrocite without bacteria in the system. Further analysis of the As speciation of the effluent

before neutralization, as well as the As speciation of the precipitates at the time of sampling is required before it can be concluded that partial oxidation occurred in the sludge during storage.

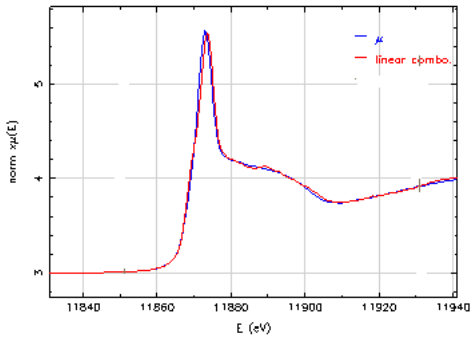

Fitted Spectrum = Horne ETP sample dried in N_2

As^{1-}= 0.00%
As^{3+}= 24.9%
As^{5+}= 75.6%

Figure 3.6: Results of the best linear combination fits for *μ*XANES spectra of the standards to the spectra of the Horne ETP powder samples (dried in nitrogen)

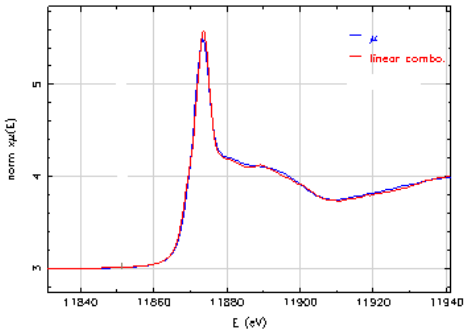

Fitted spectrum – Horne ETP sample dried in air

As^{1-} = 4.8%
As^{3+} = 14.1%
As^{5+} = 81.1%

Figure 3.7: Results of the best linear combination fits for the XANES spectra of the standards to the spectra of the Horne ETP powder samples (dried in air)

(a)

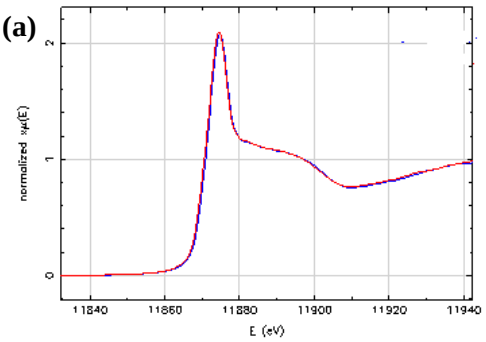

A direct overlay of two repeated scans

(b)

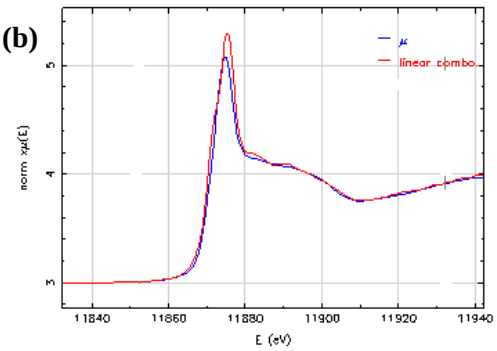

Fitted spectra of scan 1

As^{1-} = 5.6%
As^{3+} = 45.4%
As^{5+} = 49%

(c)

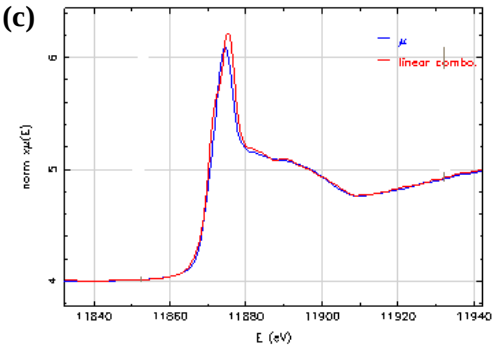

Fitted spectra of scan 2

As^{1-} = 5%
As^{3+} = 40%
As^{5+} = 55%

Figure 3.8: (a) A direct overlay of two repeated scans (scan 1 and 2) on the same spot in a Horne ETP powder sample and the results of the best linear combination fits for *μ*XANES spectra of the standards to the spectra of the repeated scans: (b) scan 1 and (c) scan 2

(a)

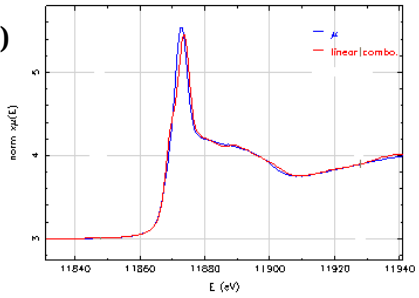

Fitted spectrum – High As/Ca region

As^{1-} = 0%
As^{3+} = 32%
As^{5+} = 68%

(b)

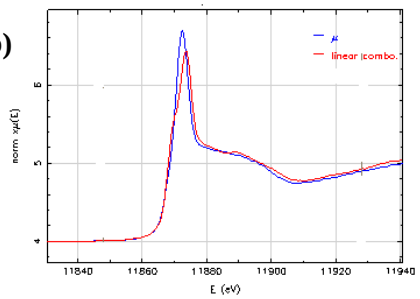

Fitted spectrum - High As/Zn region

As^{1-} = 0%
As^{3+} = 38%
As^{5+} = 62%

(c)

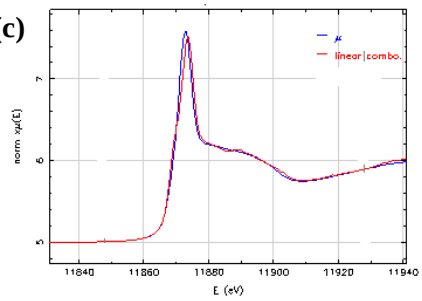

Fitted spectrum - High As/Fe region

As^{-1} = 0%
As^{3+} = 28%
As^{5+} = 72%

(d)

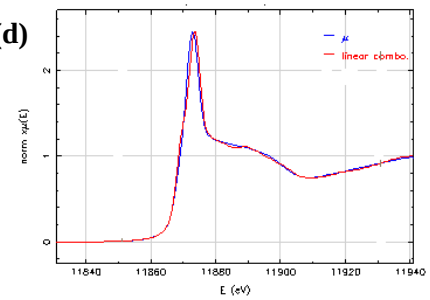

Fitted spectrum – High As/Fe/Zn region

As^{1-} = 2%
As^{3+} = 28%
As^{5+} = 70%

Figure 3.9: Results of the linear combination fits for *μ*XANES spectra of the standards to the spectra of regions: (a) Region 2 (As/Fe); (b) Region 3 (As/Zn) (c) Region 4 (As/Ca) and (d) Region 5 (As/Fe/Zn) in the Horne thin section

3.3.3.4. µXRF analysis (thin section)

µXRF analysis was conducted on Region 2 (high As/Fe spot selected from the elemental maps in Figure 3.2) using a focused beam. The elemental distribution maps of an area 0.4 mm x 0.4 mm and pixel size 10 µm x 10 µm for As, Fe, Zn and Ca that were obtained by µXRF analysis of Region 2 are presented in Figure 3.10. In addition, a red-green-blue (RGB) map which is an overlay of As, Fe and Zn distributions is shown in Figure 3.10. The purple area in the RGB represents the spatial overlapping of As and Fe. The peach/light brown areas represent the spatial overlapping of As, Fe and Zn. The dark (black) areas represent areas with no sample. The relative concentrations of the elements are represented by the scale bar. Map A represents the overlay of the As, Fe and Zn elemental maps with red, green and blue representing relative As Ka, Zn Ka and Fe Ka fluorescence intensities respectively.

The correlation plots for As/Fe; As/Zn; As/Ca and Fe/Zn are presented in Figure 3.11. The correlation plots indicate a positive linear correlation between As and the two elements, Fe and Zn. There is a positive linear correlation between Fe and Zn. No correlation is observed between As and Ca, suggesting that As and Ca are not chemically associated as a single phase. The regions (Spot 1 – High As/Fe [with moderately high Zn levels] and Spot 2 – High As/Zn) correspond to regions of interest that were selected for µXRD and µXANES analysis.

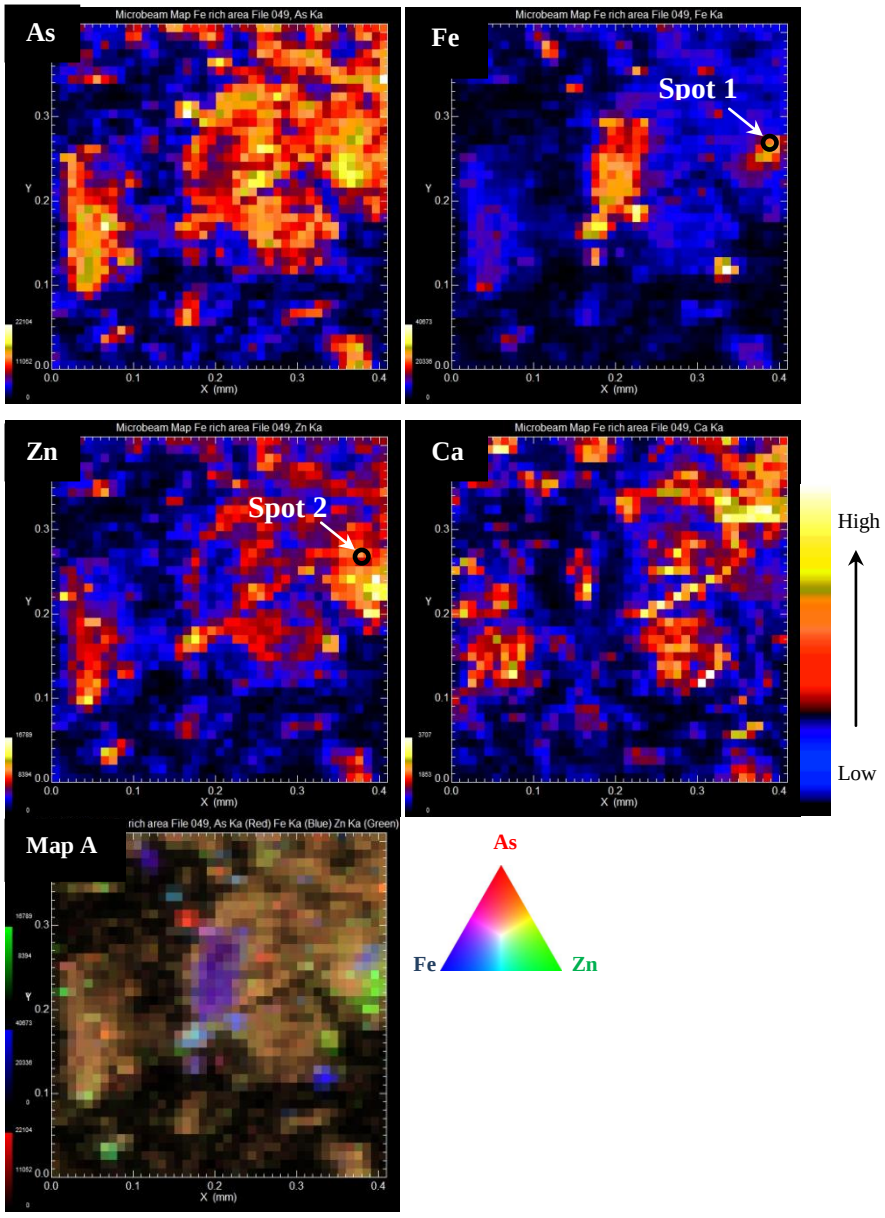

Figure 3.10: µXRF elemental distribution maps (~0.4 x 0.4 mm and pixel size 10 x 10 µm) of Region 2 (High As/Fe spot) for As, Fe, Zn and Ca. Map A represents an overlay of the As, Fe and Zn elemental maps with red, green and blue representing relative As Ka, Zn Ka and Fe Ka fluorescence intensities respectively.

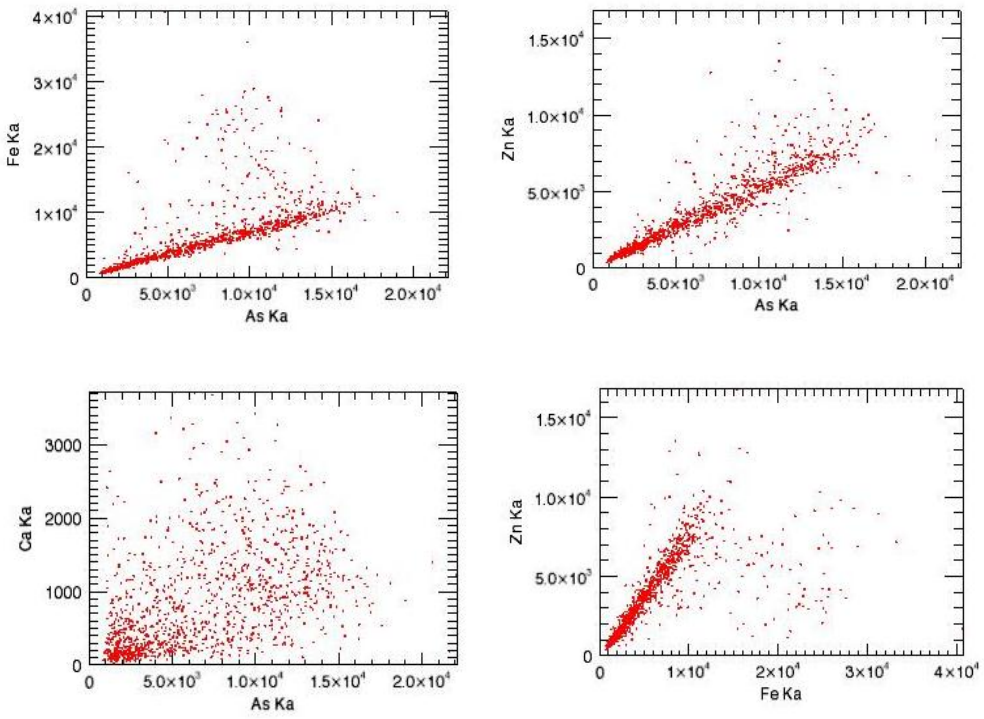

Figure 3.11: Correlation plots between: (a) As/Fe; (b) As/Zn; (c) As/Ca and (d) Fe/Zn, based on data taken from two elemental maps where the x and y axes represent the counts for the two different elements

3.3.3.5. µXRD analysis (thin section)

The 2D µXRD images and integrated µXRD patterns for spots 1 (High As/Fe) and 2 (High As/Zn) are presented in Figure 3.12. The mineral phases that were identified are presented in Table 3.7. µXRD analysis of spot 1 (high As/Fe) and spot 2 (high As/Zn) identified franklinite as the crystalline phase that is present at these high As hot spots. On close examination, the integrated µXRD patterns confirmed the presence of 2 broad peaks at d-spacings of 2.9 Å and 1.6 Å, which was identified as amorphous ferric arsenate (Rancourt et al., 2001; Carlson et al., 2002; Jia et al., 2006; Le Berre et al., 2007; Paktunc et al., 2008; Walker et al., 2009)..

Franklinite, $ZnFe_2O_4$, is a spinel that normally forms at high temperatures but has been reported to form from the dissolution of a ferrihydrite in a Zn^{2+} bearing solution. Sadiq et al. (1991) proposed that in soils, Zn^{2+} is quickly adsorbed by the hydrated iron oxide (ferrihydrite), and slowly diffuses into the hydrated layer of iron oxides. Once the concentrations of the diffused Zn^{2+} reach solubility limits, the Zn^{2+} reacts chemically with the hydrated iron oxide to form a zinc-ferrite compound, franklinite. Reddy et al. (1988) studied the solubility relationships of zinc associated with acid mine drainage and based on their results, the authors suggested that zinc solubility in acid mine drainage under aerobic unsaturated conditions may be controlled by franklinite ($ZnFe_2O_4$) solid phase. Therefore, based on the µXRD analytical studies and previous studies by Sadiq et al. (1991) it could be proposed that during the co-precipitation process, Zn is co-precipitated as zinc-ferric hydroxide (Zn adsorbed onto ferrihydrite), but some of the Zn^{2+} cations slowly diffuse into the ferrihydrite structure and chemically react with ferrihydrite to form franklinite. The µXRD results suggest that further analysis using Zn K-edge µXANES is needed to identify the presence of the zinc-ferric hydroxide phase. Franklinite was detected in both the high As/Fe and As/Zn spots, which indicates that it is present in regions of high Fe and Zn concentrations. These findings suggest that the Horne precipitates may contain low levels of franklinite as it was identified by synchrotron-based µXRD analysis using the focused X-ray beam, but not under the unfocused beam. It is also possible that franklinite could be detrital from the AMD used in the precipitation process, and so further analysis is required to determine the occurrence of franklinite in the overall sample.

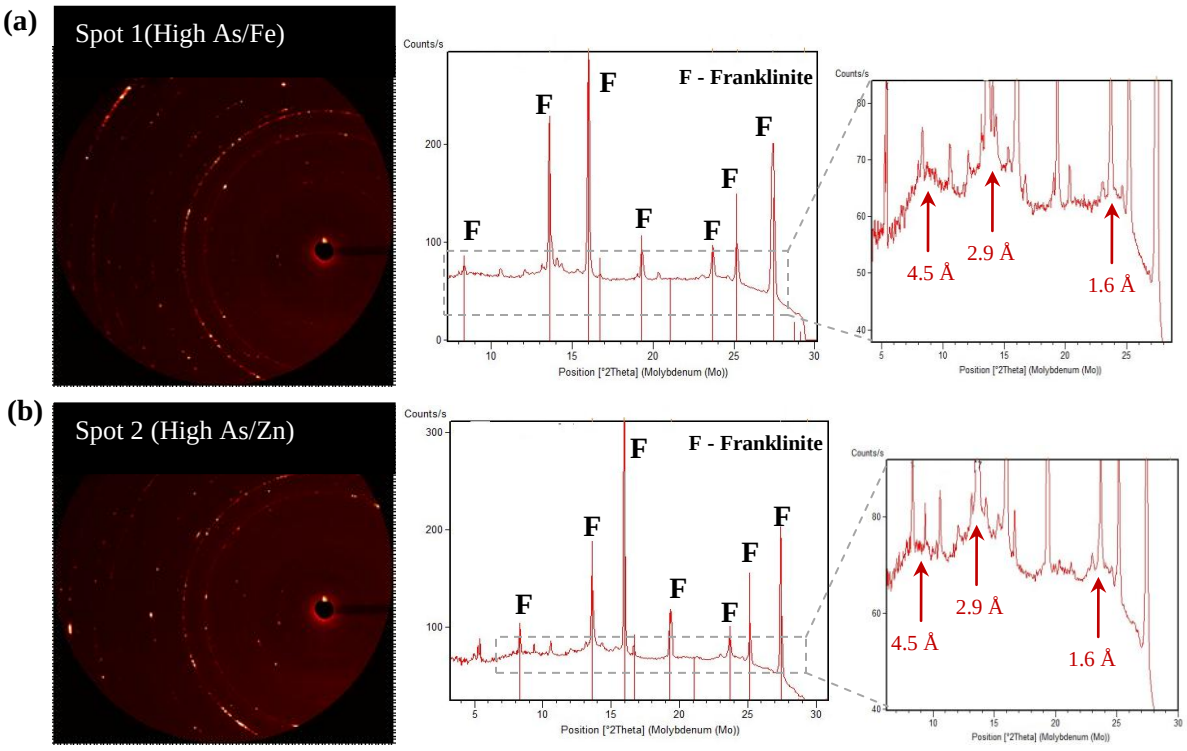

Figure 3.12: 2D µXRD images and integrated µXRD patterns of the As hot spots: (a) spot 1 (As/Fe) and spot 2 (As/Zn) located in region 2 of the thin section

Table 3.7: Mineral phases identified by µXRD

Spot	Mineral phases
1 (high As/Fe)	Franklinite (ICDD 70-6393) Ferric arsenate
2 (high As/Zn)	Franklinite (ICDD 70-6393) Ferric arsenate

3.3.3.6. µXANES analysis (thin section)

Arsenic K-edge µXANES were collected on As hot spots (As/Fe and As/Zn spots) in the thin section. The µXANES spectra of the standards were fitted with the spectra of the selected As hot spots (high As/Fe and As/Zn spots) using linear combination fitting. The fitted µXANES spectra of the As/Fe and As/Zn spots are presented in Figure 3.13. Analysis of the µXANES

spectra using linear combination fitting indicated the presence of mixed oxidation states, with As(V) being the predominant species. The presence of the As(III) species suggests that it is probably bound to ferrihydrite, although this was not identified by µXRD analysis.

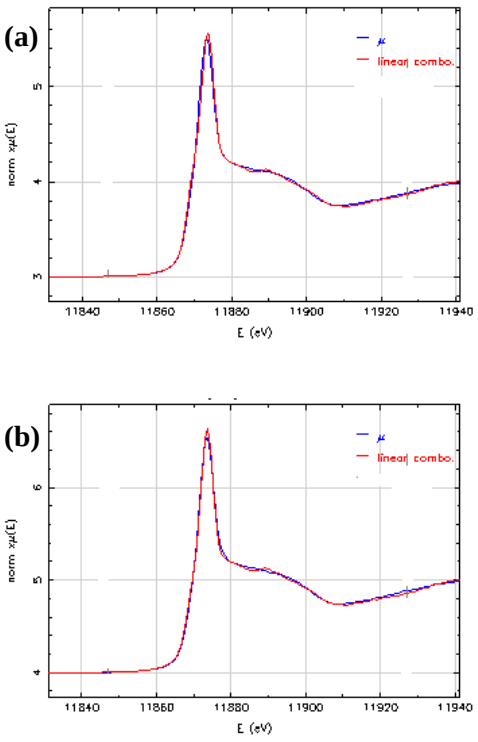

Fitted spectrum – High As/Fe spot

As^{1-} = 1%
As^{3+} = 21%
As^{5+} = 79%

Fitted spectrum – High As/Zn spot

As^{1-} = 4%
As^{3+} = 12%
As^{5+} = 84%

Figure 3.13: Linear combination fits for spectra of the standards fitted to the spectra of the As hot spots: (a) spot 1 (As/Fe) and (b) spot 2 (As/Zn) located in Region 2 (high As/Fe) of the thin section

3.3.4. Estimation of adsorption versus precipitation

A phosphate leaching protocol was applied to an air-dried sample of Horne precipitates to determine the mechanism of As immobilization in the Horne ETP precipitation process. The As and Fe extraction yields are shown in Table 3.8. The extracted As from the Horne precipitates is 2.61% of the total As (total As in the precipitates), which indicates that the co-precipitation mechanism predominates over the surface complexation (adsorption) mechanism. These results

suggest that the Horne precipitates consist of predominantly a co-precipitated arsenic-bearing ferrihydrite phase with negligible adsorbed As(III) or As(V) species. The extraction tests were conducted through three consecutive steps, and in duplicate to counteract the effects of As re-adsorption and redistribution (Goh and Lim, 2005). The absence of soluble Fe indicates that the arsenic-bearing ferrihydrite phase was not leached.

Table 3.8: Extracted As(%) and Fe(%) in relation to total As and Fe in the Horne precipitates

Sample	% As Ext.	% Fe Ext.
Horne precipitates (Fe:As>3)	2.61 ±0.87	0.08 ± 0.38

3.3.5. Effect of lime as base and zinc on the As removal efficiency

The final concentrations of Fe, Zn and As of the Fe(III)-As(III)-Zn(II) and Fe(III)-As(V)-Zn(II) systems using NaOH and lime as bases are presented in Table 3.9. The residual As concentrations in solution decreased to <5 mg/L for both the Fe(III)-As(III)-Zn(II) and Fe(III)-As(V)-Zn(II) systems at pH 9 and using NaOH and lime as bases. Co-precipitation with lime as neutralizing agent yielded lower residual As concentrations in solution than with NaOH. Lime increases the As removal efficiency for both As(III) and As(V) bearing systems probably due to the adsorption of Ca(II) by ferrihydrite reduced the negatively charged surface, and favouring the adsorption of the anionic As species (Dzombak and Morel, 1990; Wilkie and Hering, 1996; Jambor and Dutrizac, 1998; Jia and Demopoulos, 2008).

Zinc was previously deemed to contribute to the retention of arsenic in the Horne ETP process (Godbehere et al., 1995). However, studies by Nishimura et al. (1991) have shown that zinc arsenite begins to precipitate at pH 6, suggesting that zinc does not take part in the fixation

of As(III) in the Horne ETP process.. The results in Table 3.10b indicate that most of the Zn is precipitated out of solution at pH 9 in the presence of excess ferric iron. Therefore, it is probable that Zn plays an important role in the co-precipitation process in both the Fe(III)-As(III) and Fe(III)-As(V) systems by acting as a buffer and enhancing the stability of the ferrihydrite contained in the co-precipitates by retarding its rate of transformation (Jambor and Dutrizac, 1998).

Table 3.9: Final concentrations of Fe, As and Zn in the filtrates at (a) pH 4.5 and (b) pH 9

(a)

Sample	[Fe] mg/L pH 4.5	[As] mg/L pH 4.5	[Zn] mg/L pH 4.5
Fe(III)-As(III)-Zn(II) Fe:As= 4; Zn:As=1 [NaOH]	2.37 ± 0.89	109.23 ± 12.63	1679.66 ± 35.59
Fe(III)-As(III)-Zn(II) Fe:As= 4; Zn:As=1 [$Ca(OH)_2$]	<DL‡	64.83 ± 7.03	1613.33 ± 56.88

‡DL denotes below detection limit. †Fe(III)-As(III)-Zn(II) [$Ca(OH)_2$] system simulates the Horne ETP process at pH 4.5

(b)

Sample	[Fe] mg/L pH 9	[As] mg/L pH 9	[Zn] mg/L pH 9
Fe(III)-As(III)-Zn(II) Fe:As= 4; Zn:As=1 [NaOH]	1.11 ± 0.37	1.68 ± 0.50	0.14 ± 0.18
Fe(III)-As(III)-Zn(II) Fe:As= 4; Zn:As=1 [$Ca(OH)_2$]	0.55 ± 0.18	1.13 ± 0.16	0.13 ± 0.28
Fe(III)-As(V)-Zn(II) Fe:As= 4; Zn:As=1 [NaOH]	0.36	4.53	0.10
Fe(III)-As(V)-Zn(II) Fe:As= 4; Zn:As=1 [$Ca(OH)_2$]	0.14	1.47	<DL‡

‡DL denotes below detection limit. †Fe(III)-As(III)-Zn(II) [$Ca(OH)_2$] system simulates the Horne ETP process at pH 9

3.3.6. Short term stability tests

The results of the TCLP and the pH 9 leachate tests are presented in Tables 3.10 and 3.11. Figure 3.14 shows the As concentrations and final pH of the leachates of the synthetic co-

precipitates. Under the TCLP conditions, the As(V)-bearing co-precipitates are more stable than the As(III)-bearing co-precipitates. The most stable co-precipitate was As(V)-Fh-Zn4, which yielded an arsenic leachability of 5.94 mg/L. Its high stability is attributed to the fact that the lowest solubility for As(V)-Fh lies in the pH range 3-5 (Krause and Ettel, 1989; Riveros et al., 2000). The $Ca(OH)_2$ neutralized co-precipitates (As(III)-Fh-Zn2 and As(V)-Fh-Zn4) exhibited lower TCLP As leachability levels compared to those of the NaOH neutralized co-precipitates, suggesting that the use of lime as base enhanced their stability, possibly due to the adsorption of Ca(II) by ferrihydrite reduced the negatively charged surface, and favouring the adsorption and retention of the anionic As species (Harris and Monette, 1988; Dzombak and Morel, 1990; Emett and Khoe, 1993; Harris and Krause, 1993; Wilkie and Hering, 1996; Jambor and Dutrizac, 1998; Jia and Demopoulos, 2008).

The dissolution of As in the As(III)-Fh-Zn1 and As(III)-Fh-Zn2 co-precipitates suggests that the As(III)-Fh bearing precipitates are unstable under pH 5 conditions. The TCLP leachates of the As(III) and As(V)-bearing co-precipitates are all above the TCLP threshold limit of 5 mg/L for As, indicating that all the co-precipitates would need to be disposed of as hazardous waste. The final pH of the TCLP leachates ranged from 6.38 – 6.96.

Under pH 9 leachate conditions, As(III)-Fh-Zn2 was the most stable co-precipitate with an As leachability of 7.51 mg/L. As(V)-Fh-Zn3 had significantly higher As release compared to As(III)-Fh-Zn1. The lower As mobilization of the $Ca(OH)_2$ neutralized co-precipitates (As(III)-Fh-Zn2 and As(V)-Fh-Zn4) compared to the NaOH neutralized co-precipitates (As(III)-Fh-Zn1 and As(V)-Fh-Zn3) suggests that they are more stable under in the presence of calcium. This observation was attributed to the presence of gypsum, which enhances As retention capacity on

ferrihydrite. The final pH of the pH 9 leachates ranged from 7.44 to 8.34. The TCLP and pH 9 leachate test results indicate that As(III)-Fh-Zn2 is more stable under high pH conditions.

Table 3.10: As concentrations in the TCLP (pH 5) leachates

Sample ID	Sample	As (mg/L)
As(III)-Fh-Zn1	Fe(III)-As(III); Fe:As= 4; Zn:As=1 [NaOH]	20.80 ± 6.04
As(III)-Fh-Zn2†	Fe(III)-As(III); Fe:As= 4; Zn:As=1 [$Ca(OH)_2$]	12.00 ± 3.91
As(V)-Fh-Zn3	Fe(III)-As(V); Fe:As= 4; Zn:As=1 [NaOH]	11.00 ± 2.90
As(V)-Fh-Zn4	Fe(III)-As(V); Fe:As= 4; Zn:As=1 [$Ca(OH)_2$]	5.94 ± 1.60

†As(III)-Fh-Zn2 simulates the Horne co-precipitates

Table 3.11: As concentrations in the pH 9 leachates

Sample ID	Sample	As (mg/L)
As(III)-Fh-Zn1	Fe(III)-As(III); Fe:As= 4; Zn:As=1 [NaOH]	16.30 ± 3.5
As(III)-Fh-Zn2†	Fe(III)-As(III); Fe:As= 4; Zn:As=1 [$Ca(OH)_2$]	7.51 ± 1.62
As(V)-Fh-Zn3	Fe(III)-As(V); Fe:As= 4; Zn:As=1 [NaOH]	90.10 ± 14.23
As(V)-Fh-Zn4	Fe(III)-As(V); Fe:As= 4; Zn:As=1 [$Ca(OH)_2$]	8.64 ± 2.46

†As(III)-Fh-Zn2 simulates the Horne co-precipitates

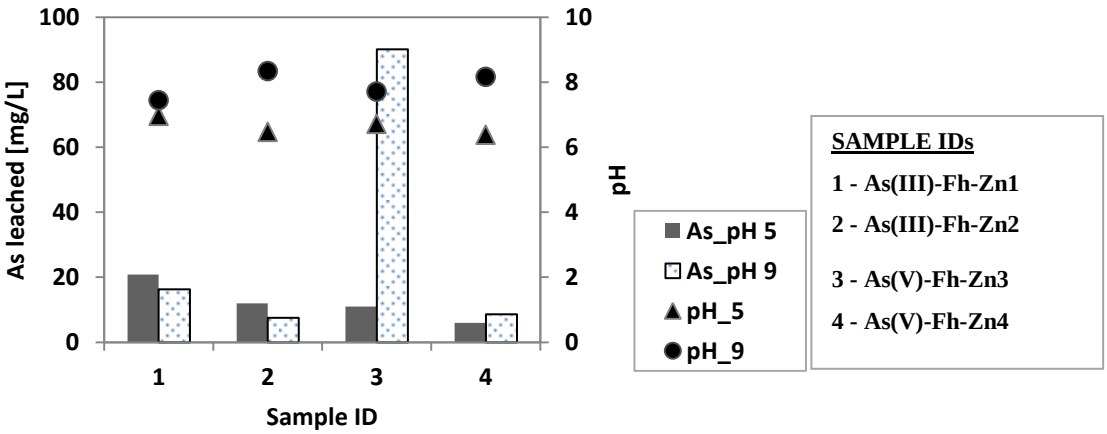

Figure 3.14: Comparison of the As concentrations and the final pH of the TCLP (pH 5) and pH 9 leachates for As(III)-Fh-Zn1; As(III)-Fh-Zn2; As(V)-Fh-Zn3 and As(V)-Fh-Zn4

3.3.7. Ferrihydrite transformation

3.3.7.1. Phase characterization

The bulk XRD patterns of the co-precipitates before and after the time series transformation tests are presented in Figure 3.15. The XRD patterns at day 0 represent the samples that were removed before the transformation tests were performed. XRD analysis of the aged Horne ETP and synthetic co-precipitates (As(III)-Fh and As(III)-Fh-Zn) showed no evidence of any crystalline Fe-bearing phases (goethite or hematite), indicating that the transformation of the precipitate assumed to be amorphous ferrihydrite was negligible during aging for 14 days at 25˚C and 60˚C. Gypsum was the only phase identified in the aged Horne ETP co-precipitates. The absence of goethite and hematite in the Horne ETP co-precipitates suggests that the presence of adsorbed As(III) and Zn(II) act to inhibit ferrihydrite transformation. The presence of adsorbed arsenite and zinc is known to have an inhibitory effect on the transformation of ferrihydrite to more crystalline phases (Cornell, 1988; Martinez and McBride, 1998).

The aged As(III)-Fh and As(III)-Fh-Zn co-precipitates exhibited similar broad and diffuse spectra, indicating the presence of a poorly crystalline mineral phase. However, the poorly crystalline nature of the phases contained in the As(III)-Fh and As(III)-Fh-Zn co-precipitates made definitive identification difficult. Further investigation that was performed using longer analytical count times produced XRD patterns with two broad peaks at the 2θ positions of ~34˚ and ~61˚, corresponding to the characteristic peaks of 2-line ferrihydrite (Jia et al., 2006) (see Figure 3.16). The absence of goethite and hematite suggests that the presence of adsorbed As(III) inhibited the transformation of ferrihydrite in As(III)-Fh-Zn and As(III)-Fh co-precipitates.

Furthermore, the presence of Zn(II) may have contributed to the retardation of ferrihydrite transformation in As(III)-Fh-Zn (Cornell, 1988; Martinez and McBride, 1998).

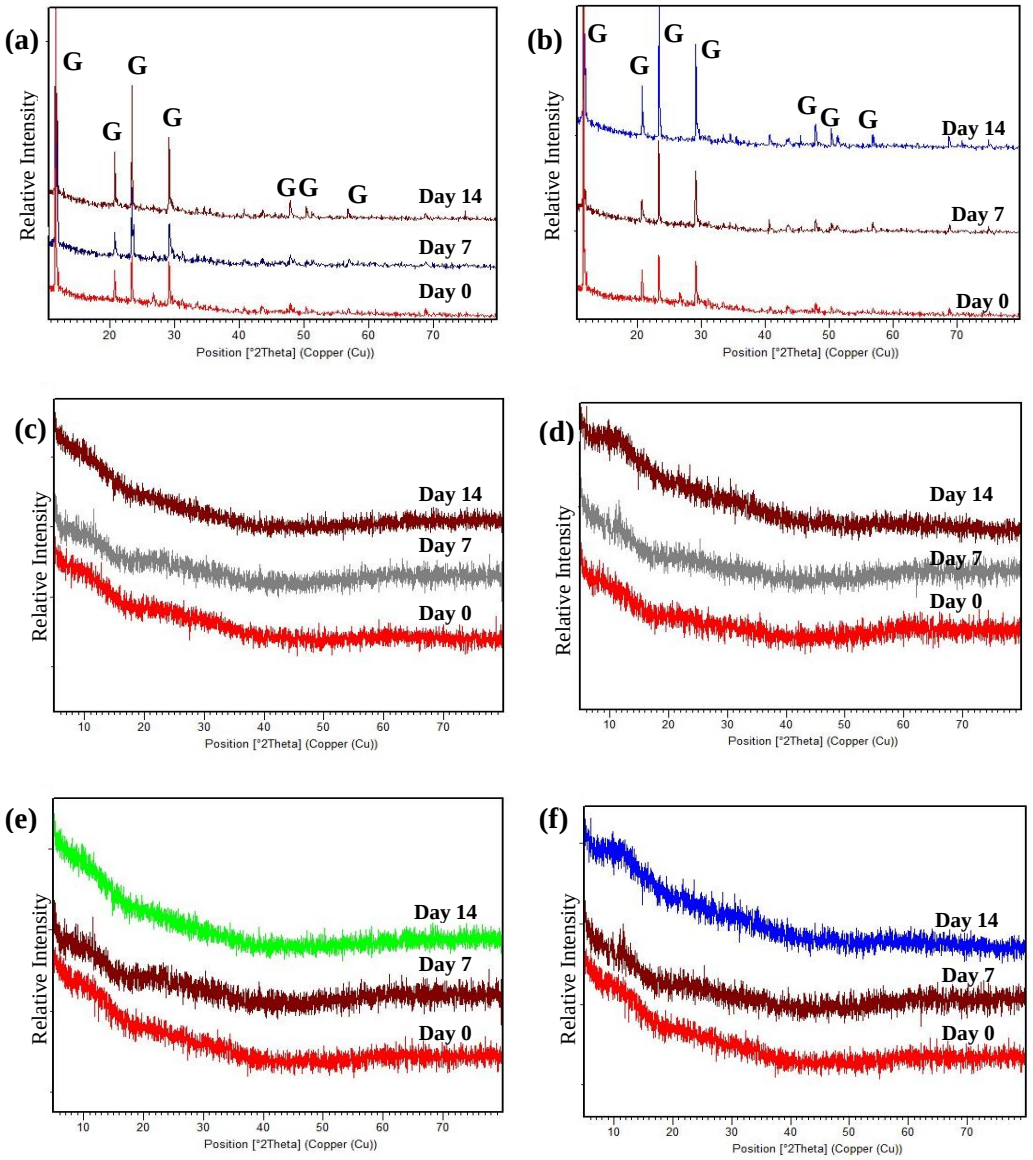

Figure 3.15: Time series transformation phases of the co-precipitates aged for 0, 7 and 14 days at pH 9 (a) Horne ETP at 25˚C (b) Horne ETP at 60˚C (c) As(III)-Fh-Zn at 25˚C (d) As(III)-Fh-Zn at 60˚C (e) As(III)-Fh at 25˚C (f) As(III)-Fh at 60˚C. G denotes the gypsum peaks.

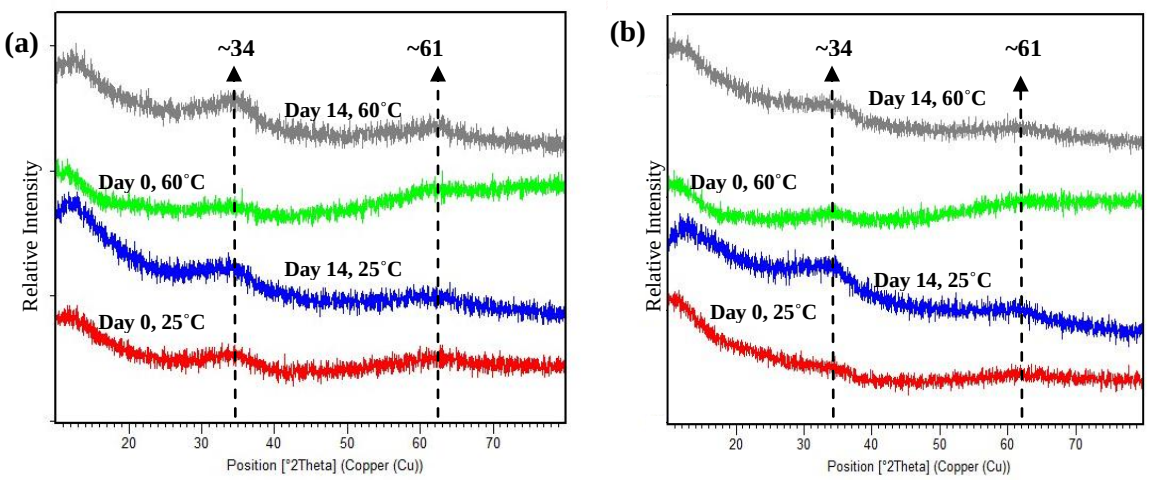

Figure 3.16: Time series transformation phases of the co-precipitates aged for 0, 7, and 14 days at pH 9 (a) As(III)-Fh-Zn (b) As(III)-Fh, using longer count times during XRD analysis

3.3.7.2. Ferrihydrite transformation kinetics

Table 3.12 summarizes the residual concentrations of Fe, As and Zn in the filtrates following the time-series transformation tests conducted over a period of 14 days at pH 9 and fixed temperatures of 25˚C and 60˚C. Compared to As(III)-Fh-Zn co-precipitates, As solubility was generally lower for the Horne ETP co-precipitates, which could be due to the presence of gypsum. Accordingly, the presence of As(III), Zn(II) and gypsum in the Horne ETP co-precipitates appear to strongly inhibit the transformation rate of ferrihydrite, which is consistent with the results obtained from XRD analysis. Similarly, As was released from the As(III)-Fh-Zn co-precipitates to a lesser extent than from the As(III)-Fh co-precipitates, suggesting that the presence of Zn(II) had a retarding effect on the transformation of ferrihydrite. For both As(III)-Fh and As(III)-Fh-Zn, co-precipitates, incongruent release of As and Fe occurred at 25˚C and 60˚C, and gradually increased with aging. This observation is probably attributable to the onset of

ferrihydrite transformation to hematite, even though no Fe-bearing crystalline phases were identified by XRD analysis. The higher As release, observed at 60˚C compared to that of 25˚C, suggests that the transformation rate of ferrihydrite is enhanced with increasing temperature. The Zn concentrations in the filtrates of the Horne ETP and As(III)-Fh-Zn co-precipitates generally remain constant throughout the aging tests. However, the Fe concentrations of the filtrates for all the As(III)-Fh and As(III)-Fh-Zn co-precipitates suddenly increase following 14 days of aging at 60˚C due to the dissolution of ferrihydrite. The transformation kinetics of ferrihydrite in the aged solid samples to crystalline phases were monitored by a selective extraction protocol, using 0.4 M HCl solution. The application of the selective protocol on the solid samples aged for 14 days resulted in the complete dissolution of the solids, which indicated that transformation of ferrihydrite to crystalline phases did not occur.

Table 3.12: The concentrations of Fe, As and Zn in the filtrates of time-series transformation tests conducted at 25˚C and 60˚C

Sample	Temperature	Time (days)	Fe (mg/L)	As (mg/L)	Zn (mg/L)
Horne [As(III)-Fh-Zn] [$Ca(OH)_2$ as base] Fe:As = 3.98‡ Zn:As= 0.64‡	25˚C	0	0.12	3.57	0.26
		1	0.17	0.44	0.61
		7	0.27	0.08	0.56
		14	0.31	0.54	0.45
	60˚C	0	0.12	3.57	0.26
		1	0.17	0.00	0.25
		7	0.07	0.00	0.33
		14	0.45	0.05	0.28
As(III)-Fh-Zn [NaOH as base] Fe:As = 3.69‡ Zn:As = 0.47‡	25˚C	0	0.14	1.07	0.26
		1	0.29	1.54	0.44
		7	0.04	1.67	0.40
		14	0.10	2.07	0.32
	60˚C	0	0.14	1.07	0.26
		1	0.18	3.14	0.46
		7	0.52	6.88	0.29
		14	1.33	11.6	0.67
As(III)-Fh [NaOH as base)] Fe:As=3.49‡	25˚C	0	0.13	5.72	
		1	0.26	2.37	
		7	0.25	3.45	
		14	0.23	3.14	
	60˚C	0	0.13	5.72	
		1	0.19	4.62	
		7	0.80	9.63	
		14	1.45	15.9	

‡ Fe:As denotes Fe/As molar ratio and ‡Zn:As denotes Zn:As molar ratio.

Paige et al. (1996) measured the transformation of ferrihydrite using a diagnostic leaching method and his findings revealed that As dissolution was a function of ferrihydrite transformation at As:Fe molar ratio >1. These tests were conducted at higher Fe:As molar ratios of 3 to 4 and the As dissolution was found to be a function of ferrihydrite transformation. Consequently, As dissolution can also be used to estimate the stability of the co-precipitates.

The transformation kinetics of ferrihydrite in the co-precipitates at 25˚C and 60˚C under pH 9 conditions was quantified using the first-order reaction equation (Equation 3.1):

$$[A]_t = [A]_0 e^{-kt} \quad \textbf{(3.1)}$$

where $[A]_t$ is % ferrihydrite remaining at time t; $[A]_0$ is the initial % ferrihydrite (100%); k= rate constant (h^{-1}); t = time (h). The first-order transformation rate constants of ferrihydrite in the presence of adsorbed As(III) were determined using equation 3.1 and are presented in Table 3.14. The data in Table 3.13 indicates that the rate constant (k) values for ferrihydrite transformation increase markedly with increasing temperature. Comparison of the reaction rate constants of the Horne ETP and As(III)-Fh-Zn suggests that gypsum has an inhibiting effect on the transformation of ferrihydrite.

Table 3.13: First-order reaction rate constants for ferrihydrite transformation at 25˚C and 60˚C for As(III)-Fh, As(III)-Fh-Zn and Horne co-precipitates

Sample	k_{60}	k_{25}
As(III)-Fh (Fe:As = 3.49‡)	6.37E-05	9.13E-07
As(III)-Fh-Zn (Fe:As = 3.69‡)	7.27E-05	6.19E-07
Horne (Fe:As = 3.98‡)	1.50E-06	9.33E-06

‡ Fe:As denotes Fe/As molar ratio

According to the results in Table 3.13, the transformation rate of ferrihydrite is dependent on temperature, which indicates that the adsorption reactions for the adsorption of As(III) by ferrihydrite are temperature dependent (Moore and Pearson, 1981). The temperature dependence of the rate is given by the Arrhenius equation (Equation 3.2):

$$\boldsymbol{k = Ae\text{^}(E_a/RT)} \qquad \textbf{(3.2)}$$

where k is the rate constant, A is the pre-exponential factor (frequency factor), Ea is the Arrhenius activation energy at pH 9, R is the universal gas constant and T is the absolute temperature. By substitution and rearrangement:

$$\boldsymbol{\ln(k_{10}/k_{60}) = E_a/R[1/T_{60} - 1/T_{10}]} \qquad \textbf{(3.3)}$$

The activation energy (Ea) of As(III)-Fh at pH 9 was derived using the data in Table 3.14 and it was found to be 110 kJ/mol, similar to findings by Das et al. (2011b). The Horne tailings are stored in in-situ relatively alkaline (pH 9), oxic conditions at 10˚C. Based on these storage conditions, the reaction rate constant (k_{10}) for the transformation rate of ferrihydrite in the co-precipitates (As(III)-Fh, As(III)-Fh-Zn and Horne) at pH 9 and 10˚C was determined using Equation 3.3 and is presented in Table 3.14. Using Equation 3.1, the predicted times required for the transformation of 10%, 50%, and 99% ferrihydrite contained in the co-precipitates, under such conditions was determined and are illustrated in Table 3.14 and Figure 3.17. Based on the data presented in Table 3.14, it is speculated that the in-situ transformation rate of ferrihydrite in the Horne co-precipitates will be extremely slow under disposal conditions of pH 9 and 10˚C, and the co-precipitates will remain stable for thousands of years. The inhibited rate of ferrihydrite

transformation is probably due to the presence of adsorbed As(III) (Fe:As=3.5) and Zn(II). In addition, the transformation tests suggest that the stability of the Horne co-precipitates could also be attributed to the dilution of the As-bearing residues with high quantities of gypsum and zinc hydroxide and their additional buffering effect. Th Horne co-precipitates contains other contaminants such as copper and cadmium, which are typically present in minor amounts and therefore does not make a significant difference.

Table 3.14: First-order reaction rate constants for ferrihydrite transformation at 10˚C and 60˚C at pH 9, for As(III)-Fh, As(III)-Fh-Zn and Horne co-precipitates

Sample	Rate constants (hr^{-1})		Duration of ferrihydrite transformation (years)		
	k_{60}	k_{10}	10%	50%	99.9%
As(III)-Fh (Fe:As = 3.49‡)	6.37E-05	5.00E-07	24	158	1052
As(III)-Fh-Zn (Fe:As = 3.69‡)	7.27E-05	5.69E-07	21	139	924
Horne (Fe:As = 3.98‡)	1.50E-06	1.18E-08	1021	6719	44639

‡ Fe:As denotes Fe/As molar ratio

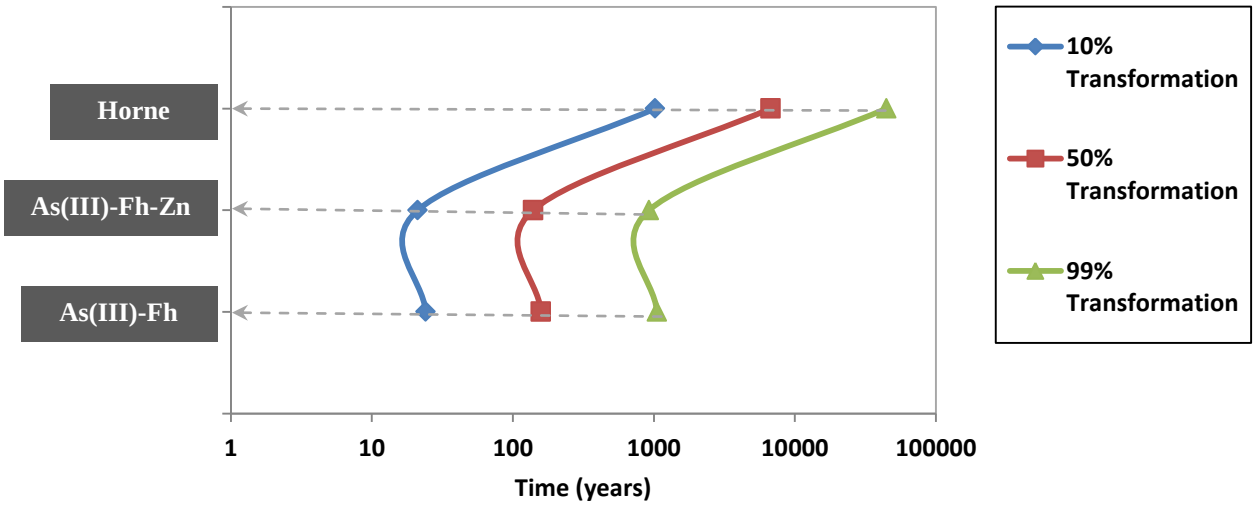

Figure 3.17: Predicted times for the 10, 50 and 99% transformation of ferrihydrite contained in the Horne, As(III)-Fh-Zn and As(III)-Fh co-precipitates at pH 9 and 10˚C

Warner and Rowson (2007) investigated the characteristics of aged sediments from the JEB Uranium Tailings Management Facility at Areva's McClean Lake Operation in the Athabas ca Basin of northern Saskatchewan using synchrotron-based μXANES analysis. Their studies indicated that in the sediments that had aged for a 4-year period, the As(III) and As(-1) species had decreased from 31% to 9% and 8% to 0% respectively, while the As(V) had increased from 66% to 91% (Figure 3.18). Extrapolation of the As(III) and As(V) lines in Figure 3.18 to zero sediment age indicates that the residues potentially contained ~70 - 80% As(III) and ~20 - 30% As(V) species. Their results suggest that under the prevailing redox conditions in the tailings pond, As(III) is being oxidized to As(V). However, the authors did not explain the oxidation mechanism of the As(III) species.

The JEB ETP process is quite similar to the Horne ETP process in that its weak acid effluent contains both As(III) (67%) and As(V) (33%) species, which are both immobilized by the addition of Fe(III) (Fe:As molar ratio≥3) and neutralization using lime to pH 4 (99% As precipitated), and subsequently to pH 7-8 where the residual As is reduced to <1 mg/L (Mahoney et al., 2005; Mahoney et al., 2007). Therefore, it is postulated that under actual disposal conditions, the As(III) species contained in the nanocrystalline Horne ETP co-precipitates is gradually oxidized to As(V) by Fe(III) over time, and concurrently Fe(III) is reduced to Fe(II) resulting in the formation of Fe(II)-Fe(III)-As(V) phase which is also stable at pH 9. However, it must be noted that the process chemistry of the Horne ETP and JEB ETP and their respective co-contaminants are may be very different, and consequently further work is required to investigate if the gradual oxidation of the As(III) species in Horne ETP co-precipitates by excess Fe(III) to form a Fe(II)-Fe(III)-As(V) phase takes place.

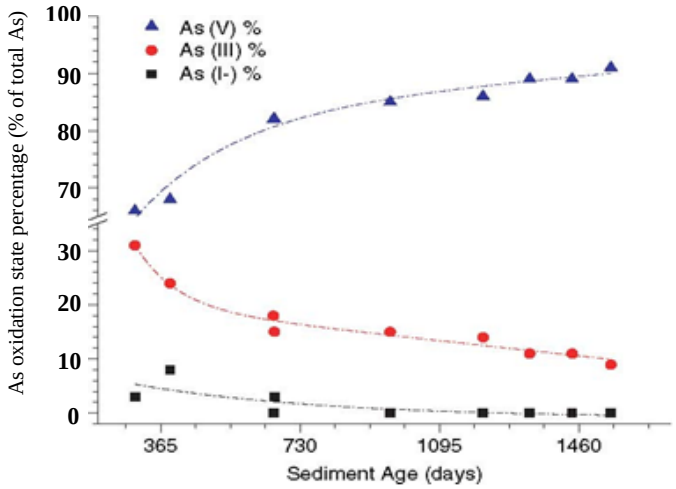

Figure 3.18: Relative As oxidation state plotted against the tailings sediment age (Warner and Rowson, 2007)

3.5. Conclusions

This study focused on the mineralogical characterization of the Horne precipitates in order to understand the mechanism of arsenic retention during the Horne ETP precipitation process. In addition, the long term stability of the Horne ETP co-precipitates was investigated by determining the transformation rate of ferrihydrite in the presence of adsorbed As(III) under relatively alkaline disposal conditions (pH 9), with the aim of understanding the effect of aging on the characteristics and stability of the Horne co-precipitates under actual in-situ disposal conditions.

Conventional XRD analysis demonstrated that the Horne ETP precipitates contained gypsum, but showed no evidence of any As-bearing phases probably due to their poorly crystalline nature. Synchrotron-based μXRD analysis identified ferric arsenate (HFA), gypsum, zinc hydroxide and franklinite as the major phases in the Horne ETP precipitates. Synchrotron-based μXANES spectra indicated a mixture of As(III) and As(V) in the Horne ETP precipitates, with As(V) being the predominant species. These results are inconsistent with previous studies by Godbehere et al. (1995). These authors reported that As(III) was the major species present in the Horne precipitates, but did not publish their characterization studies. It is possible that the higher As(V) levels could have resulted from partial oxidation of the Horne ETP sludge during storage, prior to characterization studies. The As(III) species identified by μXANES analysis is probably associated with ferrihydrite, but an As(III)-bearing ferrihydrite phase (arsenical ferrihydrite) was not identified by μXRD analysis. The application of a phosphate leaching protocol supported that the mechanism of arsenic fixation at the Horne ETP was predominantly by co-precipitation.

Characterization of the aged co-precipitates obtained from the time-series transformation experiments showed no evidence of any crystalline Fe-bearing phases, indicating that the transformation of ferrihydrite was negligible after 14 days of aging. Gypsum was the only phase identified in the aged Horne solid samples. The absence of goethite and hematite in the aged Horne solid samples suggests that the transformation of ferrihydrite was inhibited by the presence of adsorbed As(III) and Zn(II). The bulk XRD patterns of the synthetic As(III)-Fh and As(III)-Fh-Zn solid samples, after 14 days of aging, revealed broad and diffuse patterns, indicating the presence of a poorly crystalline mineral phase. Further investigation using longer analytical count times indicated the presence of 2-line ferrihydrite.

Kinetic measurements indicated that the transformation of ferrihydrite increased markedly with increasing temperature and decreasing Fe:As molar ratio. Based on first order rate reactions, it was predicted that the ferrihydrite contained in the Horne ETP co-precipitates currently disposed of in the in-situ conditions of pH 9 and 10˚C, will remain stable for thousands of years (10% conversion after 1021 years; 50% conversion after 6719 years; and 99% conversion after 44,640 years) due to the presence of adsorbed As(III) as well as other adsorbed cations including Zn(II). Furthermore, zinc hydroxide and gypsum stabilize ferrihydrite by buffering its transformation. Characterization studies of the aged sediments from the JEB tailings facility (Northern Saskatchewan) by Warner and Rowson (2007) have shown that As(III) is oxidized to As(V) under the prevailing anoxic conditions in the tailings pond. Their findings suggest that the As(III) species may undergo gradual oxidation, it is postulated that under actual disposal conditions, the As(III) species contained the nanocrystalline Horne ETP co-precipitates is gradually oxidized to As(V) by excess Fe(III) over time, and concurrently Fe(III) is reduced to

Fe(II) resulting in the formation of an Fe(II)-Fe(III)-As(V) phase which is also stable at pH 9. However, it must be noted that the process chemistry of the Horne ETP and JEB ETP and their respective co-contaminants are may be very different, and consequently further work is required to investigate if the gradual oxidation of the As(III) species in Horne ETP co-precipitates by excess Fe(III) to form a Fe(II)-Fe(III)-As(V) phase takes place.

The removal of arsenic from the weak acid and dust treatment bleed effluents poses a major concern for copper smelters due to the technical challenges and high costs encountered in fixing arsenic into an environmentally acceptable form. Any new roaster or smelter will need to consider a suitable disposal option for the fixation of arsenic from its weak acid effluents into an environmentally acceptable form. The treatment of the weak acid effluents at copper smelters involves the formation of high As-bearing residues that need to be disposed of as hazardous waste regardless of their stability as measured by TCLP or other testing protocols. Based on this view, the best treatment practice is one that minimizes the volume of the high As-bearing residues for disposal rather than the option with the highest stability. From an economic point of view, the cost of As fixation is equivalent to the total cost of As precipitation and the disposal of the As precipitate as a hazardous waste. Selecting the best disposal method of As precipitation and disposal is a very complex decision that is very site-specific. Although stability protocols are useful as a preliminary test for the evaluation of the short term stability of the wastes under specific test conditions, future smelters and roasters will select their disposal options based on the precipitation and disposal costs, and not on the stability of the residue in relation to the applied stability protocol.

Chapter 4

Tooeleite precipitation and transformation

4.1. Introduction

Arsenic is a major contaminant in effluents resulting from the roasting and smelting of arsenic-bearing copper concentrates. Due to its high toxicity, arsenic needs to be removed and disposed of in an environmentally acceptable manner. Various treatment practices are used by copper smelters for the removal and disposal of arsenic from weak acid effluents, of which the most widely used method involves co-precipitation with ferric iron (Fe:As molar ratio> 3) and lime neutralization to form arsenical ferrihydrite [As(V)-bearing ferrihydrite: As(V)-Fh] (Harris, 2003). Furthermore, As(V)-Fh has been designated as the Best Demonstrated Available Technology (BDAT) by the US Environmental Protection Agency (US EPA) for the removal of arsenic from acidic mineral processing effluents (Riveros et al., 2001; Twidwell et al., 2008). However, this treatment option is associated with the generation of high volumes of sludge, high iron demand, low As content (6 wt%) and the need to oxidize the As(III) species to As(V) prior to precipitation. In addition, the long term stability of As(V)-Fh has been the subject of concern due to the likelihood that the ferrihydrite contained in the As(V)-Fh will transform to goethite and finally hematite thereby releasing arsenic into solution (Robins, 1983; Robins et al., 1988; Robins and Jayaweera, 1992). In addition, As(V)-Fh may be reduced under anoxic environments resulting in the reductive dissolution of ferrihydrite or As(V) and the mobilization of arsenic (McCreadie et al., 2000; Pederson et al., 2006).

Scorodite ($FeAsO_4.2H_2O$) is generally regarded as the most suitable disposal option for the fixation of As due to its high arsenic removal efficiency, high arsenic content (30 wt%), low iron requirements (Fe:As molar ratio =1), and low solubility in the pH range 2.8 to 5.3. In addition, scorodite has good settling and filtration properties due to its crystalline nature (Filippou and Demopoulos, 1997; Riveros et al., 2001; Demopoulos et al., 2003). However, this disposal option is associated with high capital costs due to the use of autoclaves (170-200 ˚C and O_2 overpressure = 2000 kPa), and has a limited stability range (pH 2.8 to 5.3) (Krause and Ettel, 1989; Swash and Monhemius, 1994; Filippou and Demopoulos, 1997; Riveros et al., 2001; Demopoulos et al., 2003; Paktunc et al., 2008). Demopoulos and co-workers (Demopoulos 1996; Demopoulos et al., 1994; Demopoulos et al., 1995; Droppert et al., 1996; Filippou and Demopoulos, 1997; Demopoulos et al., 2003) developed a new process for the fixation of arsenic from metallurgical weak acid effluents by atmospheric precipitation of scorodite at 95˚C under ambient pressure and supersaturation-controlled conditions. This process is associated with lower capital costs than High Temperature Pressure Oxidation (HTPOX) and is independent of process scale but has not yet been applied commercially (Droppert et al., 1996; Filippou and Demopoulos, 1997). In addition, scorodite may decompose under anoxic conditions, by CO_2 carbonation or in the presence of reducing bacteria (Robins, 1981; Rochette et al., 1988; Cummings et al., 1999; Riveros et al., 2001; Papassiopi et al., 2003). Therefore, there is an incentive to investigate an alternative disposal option with low solubility, low iron requirements, high arsenic removal efficiency and good filtration properties that can be utilized by copper smelters for the removal and disposal of arsenic from weak acid effluents.

Tooeleite, a ferric arsenite sulphate hydrate ($6Fe_2O_3.5As_2O_3.2SO_3.12H_2O$), has been proposed as a potential disposal option for removal and immobilization of the As(III) species from weak acid effluents (Nishimura and Robins, 2008). Tooeleite could be considered as the As(III) equivalent of scorodite which is regarded by industry as the most suitable medium for arsenic disposal. Tooeleite has a high arsenic content (25 wt%), high arsenic removal efficiency, a low iron demand (Fe:As molar ratio =1.2) and precipitates easily under ambient conditions (Nishimura and Robins, 2008). Furthermore, natural tooeleite found in the waste dumps of a former As-bearing gold mine (US Mine) at Gold Hill, Tooele County, Utah has retained its stability despite undergoing severe weathering conditions over time, probably due to its crystalline nature. Despite being proposed as a potential disposal option, very little information is available on tooeleite (Cesbron and Williams, 1992; Nishimura and Robins, 2008). The physical characteristics and chemistry of tooeleite were first described by Cesbron and Williams (1992), who proposed that tooeleite was an As(V) mineral with the chemical formula $Fe_8(AsO_4,(SO_4)_6(OH)_6 \cdot 5H_2O$ and an Fe/As ratio of 1.33. μXANES investigation of sediments from the acid mine drainage of the former Carnoules Mine in France conducted by Morin et al (2003) indicated that As species found in tooeleite is As(III). Morin et al (2007) determined that tooeleite has a monoclinic crystal structure, via the characterization of a natural sample from the US Mine waste dumps in Tooele County using a combination of high resolution synchrotron XRD and refined Rietveld techniques. The authors proposed tooeleite to have the chemical formula, $Fe_6(AsO_3)_4(SO_4)(OH)_4 \cdot 4H_2O$ and an Fe:As ratio of 1.5. Huang et al., (2008) reported an estimated free energy of formation of tooeleite to be -1240.903±1.407 kcal/mole, according to the chemical formula suggested by Morin et al. (2003). Recently, Nishimura and Robins (2008) investigated the synthesis of nano-crystalline tooeleite from sulphate-based Fe(III)-As(III)

bearing weak acid solutions. Bulk XRD and TGA techniques were employed to characterize the nature of the synthetic precipitates. XRD analysis of the precipitates indicated that their XRD spectra were similar to that reported by Cesbron and Williams (1992) for tooeleite. Their characterization studies confirmed that tooeleite is an As(III) compound, with the chemical structure $6Fe_2O_3.5As_2O_3.2SO_3.12H_2O$ and an Fe/As ratio of 1.2. The authors reported that synthetic tooeleite is stable between pH 2 to 3.5, and will transform to arsenical ferrihydrite (As(III)-Fh) above pH 3.5. However, their study did not evaluate the stability of tooeleite. Since tooeleite is stable in the pH range 2 to 3.5, it would need to be deposited in a lined pond with ongoing monitoring and maintenance of acid conditions. Tooeleite has been identified in the tailings of two former As-bearing gold mines (Montague and Oldham) in Nova Scotia (Walker et al., 2009; DeSisto et al., 2011).

It is widely regarded that As-bearing residues with a high degree of crystallinity are generally stable and have a low As solubility. High temperature precipitation has been used for the formation of more crystalline As-bearing phases and previous studies have shown that high temperature precipitation generally results in the formation of As-bearing residues with higher crystallinity and lower solubility compared to those obtained at ambient temperature (Ugarte and Monhemius, 1992; Monhemius and Swash, 1999; Singhania et al., 2005).

The main objective of this study was to investigate tooeleite as a potential phase that can be utilized for the removal and immobilization of arsenic from copper smelter weak acid effluents by: (i) investigating the precipitation of tooeleite from Fe(III)-As(III) bearing weak acid solutions under the following varying parameters: Fe:As ratio; pH; temperature and neutralizing agent (ii)

characterizing the synthetic tooeleite precipitates produced under different precipitation conditions using conventional and synchrotron-based analysis (iii) determining the stability of the synthetic tooeleite precipitates produced under different precipitation conditions using the US EPA Toxicity Characteristic Leaching Procedure (Method 1311) and long term leaching tests and (iv) investigating the high temperature precipitation of tooeleite at 60˚C and 95˚C using sodium hydroxide and lime as the neutralizing agents.

4.2. Materials and methods

4.2.1. Batch co-precipitation

Tooeleite was synthesized using the procedure that is described by Nishimura and Robins (2008). The synthesis of tooeleite precipitates was conducted using analytical reagent grade chemicals and the experimental conditions summarized in Table 4.1. An As(III) stock solution was prepared by the dissolution of As_2O_3 in 0.1 M H_2SO_4 at 90 ˚C. 0.1 M Fe(III) was prepared by dissolving $Fe_2(SO_4)_3.5H_2O$ in distilled water. The pH was adjusted by the addition of 2 M NaOH to the target pH value (1.7; 1.9; 2; 2.3; 2.5; 2.7; 3; 4; 6; 8; 10 respectively), while being continuously agitated. The pH was monitored and maintained at the desired target pH value for 1 hour. An aliquot of 30 ml was removed after 1 hour and vacuum-filtered using 0.45 µm membrane filter paper. The filter cake was washed with distilled water and then dried under ambient conditions. The filtrates were analyzed for As and Fe concentration using ICP-OES. Tooeleite was synthesized using the same procedure with $Ca(OH)_2$ as the neutralizing agent since lime is the preferred base used for the neutralization and removal of arsenic from copper smelter weak acid effluents due to its relatively low cost (Jia and Demopoulos, 2008).

Table 4.1: Experimental conditions for the synthesis of tooeleite under ambient conditions

Parameters	Process conditions
Fe(III)/As(III) molar ratio	1.0
Initial pH	1.5
Final pH	1.7; 1.9; 2; 2.3; 2.5; 2.7; 3; 4; 6; 8; 10
Experimental temperature	25˚C
Neutralizing agent	2 M NaOH; 2 M $Ca(OH)_2$
Stirring rate (rpm)	350
Reaction time (hours)	1

4.2.2. Effect of Fe:As ratio

Similar experiments were conducted (as described in Section 4.2.1.) using solutions with initial Fe(III):As (III) molar ratios (Fe:As) of 1.0, 1.5 and 2.0. The experimental conditions are summarized in Table 4.2. Solution samples were taken at target pH values ranging from 1.7 to 10 after 1 hour of agitation, and then vacuum-filtered using 0.45 µm membrane filter paper. The filter cake was washed with distilled water and pH 3.6 acidified water (acidified using H_2SO_4) and dried under ambient conditions. The As and Fe concentrations in the filtrates were determined using ICP-OES. The experiments were replicated twice.

Table 4.2: Experimental conditions for the synthesis of tooeleite under ambient conditions

Parameters	Conditions
Fe(III)/As(III) molar ratio	1.0;1.5; 2.0
Initial pH	1.5
Final pH	1.7; 1.9; 2; 2.3; 2.5; 2.7; 3; 4; 6; 8; 10
Experimental temperature	25˚C
Neutralizing agent	2 M NaOH; 2 M $Ca(OH)_2$
Stirring rate (rpm)	350
Reaction time (hrs)	1

4.2.3. Mineralogical analysis

The tooeleite and gypsum-bearing tooeleite precipitates were subjected to powder X-Ray Diffraction (XRD) analysis using a Phillips X'Pert Pro MPD diffractometer fitted with an X'Celerator high speed strip detector (X-ray source: Cu Kα radiation (Ni filtered) and Operating conditions: 45 KV, 40 MA, 3˚- 80˚ 2θ). PanAnalytical HighScore software was used for the identification of phases. The particle-size, morphology and elemental composition of the tooeleite and gypsum-bearing precipitates were determined by scanning electron microscopy (SEM) and energy dispersive x-ray spectroscopy (EDS) using a MLA Quanta 650 FEG-ESEM machine.

4.2.4. Synchrotron-based analysis

Synchrotron-based analysis was conducted using the hard X-ray microprobe, X26A, at the National Synchrotron Light Source (NSLS), Brookhaven National Laboratory, Upton, New York. Micro-X-Ray Fluorescence (μXRF), micro-X-Ray diffraction (μXRD), and arsenic K-edge micro-X-Ray Absorption Near Edge Structure (μXANES) analyses were conducted on the tooeleite and gypsum-bearing tooeleite samples using a focused beam (5 μm x 9 μm in diameter). Synchrotron-based μXRF, μXRD and XANES analyses provided information on the elemental distribution, mineralogy and arsenic speciation respectively. The analytical setup and procedures that were used are fully described in Walker et al. (2005).

4.2.4.1. Sample preparation

Both powder samples and polished thin sections were made from tooeleite and gypsum-bearing tooeleite precipitates. The thin sections were made using tooeleite precipitates that were synthesized from solutions of initial Fe:As molar of 1 at pH 2.5 and 4 using NaOH as base, and gypsum-bearing precipitates that were formed at pH 2.5 using $Ca(OH)_2$ as base. The powder samples were made using tooeleite precipitates that were synthesized from solutions of initial Fe:As molar of 1 at pH 4, 6 and 10 using NaOH as the base, and gypsum-bearing precipitates that were formed at pH 4, 6, 8 and 10 using $Ca(OH)_2$ as the base. Powder samples of the tooeleite precipitates were homogenized in a mortar and pestle before being thinly spread between two strips of Kapton® tape and mounted in a 35 mm cardboard frame for analysis. The same procedure was repeated for the gypsum-bearing tooeleite precipitates. Polished thin sections were made by fixing tooeleite and gypsum-bearing tooeleite precipitates in low temperature epoxy, and grinding and polishing using oil to a thickness of 30-50 μm, and then the samples were mounted on a glass slide. The thin sections were examined using scanning electron microscopy (SEM) and

Energy Dispersive X-Ray spectroscopy (EDS) using a MLA Quanta 650 FEG-ESEM machine, in order to select targets (grains) for analysis under the synchrotron beam. Subsequent to the selection of targets, the thin sections were removed from the glass slide using acetone (ACS grade). The removal procedure involved the immersion of the glass slide in an acetone bath until the thin section was detached from the slide. The detached section was transferred onto Kapton® tape and placed in a 35 mm cardboard frame for micro-analysis.

4.2.4.2. μXRF, μXRD and μXANES analyses

The mounted polished thin sections and powder samples were analyzed using a 350 μm collimated monochromatic beam (wavelength = 0. 7193 Å) generated from a Si(111) channel-cut monochromator. The monochromatic beam was focused using a pair of Rh-coated Kirkpatrick-Baez mirrors.

μXRF analysis was conducted on the polished thin sections using the fly-scan mapping technique to enable large areas to be analyzed in a short period of time, with the aim of providing an overview of the elemental distribution in selected regions of the thin section. The mapping analysis was carried out on various selected targets in the thin section (previously selected using SEM). μXRF maps were collected for the following elements of interest: As, Fe, and Ca. The information from these elemental maps was used to select regions to be analyzed using the focused beam. The regions of interest were selected using elemental correlations of As with Fe and Ca, at high and intermediate counts of As, with the aim of characterizing the phases and their As speciation using μXRD and μXANES. μXRD and μXANES analyses were performed on selected regions in the powder samples and thin sections (previously selected using the XRF elemental maps).

A Bruker SMART 1500 CCD diffractometer with a fibre optic taper, in a high resolution mode at 1024 x 1024 pixels was used to collect the XRD patterns in transmission mode. The incident X-Ray beam was tuned to 17.749 keV and the μXRD patterns were obtained using an exposure time of 60 seconds, regulated with a timed beam shutter. μXRD data was collected on the diffraction standards, silver behenate ($CH_3(CH_2)_{20}COOAg$) and corundum (α-Al_2O_3) as well as Kapton and epoxy to be used in the data treatment procedure.

The μXANES spectra was collected in fluorescence mode, by using a Si(Li) detector to scan through the As K-edge (11.867 keV). The analysis was conducted by scanning across the absorption edge region (11.8 to 11.88 keV) in three segments. The first segment, the pre-edge region (11.8 – 11.85 keV), had a step size of 5 eV and dwell time of 2 seconds. The second segment, the edge region (11.85 – 11.88 keV), had a step size of 0.4 eV and dwell time of 4 seconds. The third segment, the post-edge region, had a step size of 1 eV and dwell time of 3 seconds. μXANES analysis was conducted on arsenic standards (arsenopyrite (FeAsS), arsenolite (As_2O_3) and scorodite ($FeAsO_4.2H_2O$)), covering the range of oxidation states -1, +3, and +5 respectively, to be used in quantitative fitting of the powder sample and thin section spectra. The standards were prepared by grinding with boron nitride (99.9%, 1 μm) and HPLC grade ethanol in a mortar and pestle. Boron nitride was added to the pure samples of the standards and the tooeleite powder samples to dilute their arsenic content to 4 wt% As, with the aim of decreasing self-absorption effects (Walker et al., 2005).

4.2.4.3. Data treatment

Fit2D software (Hammersley, 1998) was used to integrate the XRD data of the powder samples and thin sections. Silver behenate and α-Al_2O_3 were used as diffraction standards to

calibrate the camera distance and x-ray wavelength. Subsequent to the calibration, Kapton tape and epoxy were subtracted from the thin section data to produce 2D images which were processed to 1D diffraction patterns. The PanAnalytical X'Pert HighScore software was used to identify the mineral phases by comparison of the 1D diffraction patterns with the reference diffraction patterns in ICDD Powder Diffraction File 2010 database. The ATHENA software program (version 0.8.056) was used to treat the μXANES spectra of the powder samples, thin sections and the standards (Ravel et al., 2005). μXANES spectra of the standards, powder samples and thin sections were initially background subtracted and normalized. Subsequently, linear combination fitting analysis was used to fit the summed proportions of the spectra of the three standards (arsenopyrite, arsenolite and scorodite) to the unknown spectra collected from the selected regions using the unfocused beam and from spots using the focused beam. This approach enabled the determination of the relative proportions of the standards present in the selected regions and spots of the powder samples and thin sections.

4.2.4.4. Fe K-egde μXANES analysis

Fe K-egde μXANES analysis was conducted to identify and quantify the Fe-bearing phases in the tooeleite and gypsum-bearing precipitates formed at pH 2.7 (initial Fe:As molar ratio=1) under various temperatures (25˚C, 60˚C and 95˚C) using NaOH and $Ca(OH)_2$ respectively. μXANES spectra were collected on beamline X27A (equipped with a Si(311) monochromator; λ = 1.7437 Angstroms) at the National Synchrotron Light Source at the Brookhaven National Laboratory, Upton, New York. Fe-bearing reference standards (tooeleite ($Fe_6(AsO_3)_4(SO_4)(OH)_4 \cdot 4H_2O$) and 2-line ferrihydrite ($Fe(OH)_3$)) were synthesized and their identity confirmed by powder XRD. Powder samples of tooeleite, gypsum-bearing tooeleite and the synthetic Fe-bearing reference standards were prepared by being ground with boron nitride

(99.9%, 1 µm) in a mortar and pestle, before being thinly spread between two strips of Kapton® tape and mounted in a 35 mm cardboard frame for analysis. The samples and standards were diluted, by the addition of boron nitride to 5 wt% Fe, to minimize self-absorption effects. The µXANES spectra for the samples and standards were collected under ambient temperature in the transmission mode. The internal energy calibration of the monochromator was carried out using the first inflection point (7112 eV) of an iron foil. The analysis was conducted by scanning across the absorption edge region (7020 to 7320 eV) in five segments (Table 4.3). The Fe µXANES data was processed using the ATHENA software program (version 0.8.056) (Ravel et al., 2005). Linear combination fitting analysis was used to fit the summed proportions of the spectra of the standards to the unknown spectra collected from tooeleite and gypsum-bearing powder samples.

Table 4.3: Experimental conditions for Fe K-edge µXANES analysis

Region #	Start position (eV)	End position (eV)	Step size (eV)	Dwell time (seconds)
0	7020.0	7105	5.0	2
1	7105.1	7118	0.2	2
2	7118.2	7160	0.4	2
3	7161.0	7220	1.0	2
4	7225.0	7320	5.0	2

4.2.5. Sulphate analysis

A sulphate analysis of tooeleite precipitates was performed on precipitates formed at pH values of 2.7, 4, 6 and 10 from the NaOH neutralized system of initial Fe(III):As(III) molar ratio of 1, with the aim of evaluating if the sulphate content of the precipitates decreased with increasing pH due to the transformation of tooeleite to FeOOH(As) (Nishimura and Robins, 2008). Samples (0.2 g) of the precipitates formed at pH 2.7, 4, 6, 8 were mixed with 40 ml of 2 M HCl, and boiled at 90˚C until the solids dissolved. The solutions were analyzed using HPLC. Arsenical ferrihydrite (As(III)-Fh) was co-precipitated from a solution of initial Fe(III):As(III)

molar ratio of 4, at pH 4.5 using NaOH. For comparison, the As(III)-Fh precipitates were subjected to the sulphate analysis test to confirm if Fe(III)-As(III) bearing residues have low sulphate content irrespective of initial Fe:As concentrations.

4.2.6. Tooeleite precipitation at elevated temperature

The kinetics of tooeleite precipitation was studied in order to determine the time required to achieve equilibrium. The kinetics experiments were conducted in a 2000 ml glass vessel using the experimental conditions that are summarized in Table 4.4. An As(III) stock solution was prepared by the dissolution of As_2O_3 in 0.1 M H_2SO_4 at 90 ˚C. A 0.1 M Fe(III) stock solution was prepared by dissolving $Fe_2(SO_4)_3.5H_2O$ in distilled water. The Fe(III)-As(III) solution pH was adjusted by the addition of 2 M NaOH to the target pH value (pH 2, 2.2 and 2.5 respectively), while being continuously stirred. The pH was monitored and maintained at the desired target pH value for 1 hour. Aliquots of 50 ml were removed at various intervals (1, 3, 6, 9, and 24 hours) and vacuum-filtered using 0.45 µm membrane filter paper. The filter cake was washed with distilled water and pH 3.6 acidified water (acidified using H_2SO_4) to ensure the removal of any residual As(III)-bearing acidic solution. The filter cake was then dried under ambient conditions. The filtrates were analyzed for As and Fe concentration using ICP-OES. The precipitation experiment was repeated at 60˚C and 95˚C. Gypsum-bearing tooeleite was synthesized at 25˚C, 60˚C and 95˚C using the same procedure and with $Ca(OH)_2$ as the neutralizing agent.

Table 4.4: Experimental conditions for tooeleite precipitation

Parameters	Conditions
Fe(III)/As(III) molar ratio	1; 1.5; 2
Initial pH	1.5
Experimental temperature	25˚C; 60˚C; 95˚C
Stirring rate	350 rpm
Reaction time	1 hour
Neutralizing agent	2 M NaOH; 2 M $Ca(OH)_2$
Final pH values	2; 2.2; 2.5
Time intervals for aliquot removal (hours)	1, 3, 6, 9, 24

4.2.7 Stability experiments

4.2.7.1. Short term stability tests

The stability of the tooeleite and gypsum-bearing tooeleite precipitates was evaluated using a modified US EPA Method 3111 Toxicity Characteristic Leaching Procedure (TCLP) (US EPA, 1992). The TCLP test was modified from the original method described by the US EPA (US EPA, 1992) in that an Orbit Environ Shaker operated at 200 rpm was used instead of an end-over-end agitation device operated at 30 ± 2 rpm. The TCLP test was conducted to determine the short term stability and hazardous nature of the tooeleite and gypsum-bearing tooeleite precipitates (precipitated at pH 2.5, 2.7, 3, 4, 6, 8, and 10). The test was performed using an extraction fluid of pH 4.93 ± 0.05. The extraction fluid was prepared by adding 5.7 ml of acetic acid (CH_3CH_2OOH) and 64.3 ml of 1 M NaOH to 500 ml of distilled water, followed by adding distilled water to the mixture resulting in a final volume of 1000 ml. The leaching test was conducted by mixing 0.5 g of the precipitates with the extraction fluid (solid: liquid ratio of 1:20) in 250 ml Erlenmeyer flasks. The flasks were continuously shaken in a shaker (200 rpm) under ambient conditions for 18 ± 2 hours. On completion of the leaching test, the suspensions were vacuum-filtered using 0.45 µm membrane filters. The pH of the leachates was measured and they

were preserved by the addition of reagent grade nitric acid, before being analyzed for As and Fe using ICP-OES. The experiments were replicated twice.

4.2.7.2 Long term stability tests

The long term leaching tests were performed to evaluate the long term stability of tooeleite and gypsum-bearing tooeleite precipitates (precipitated at pH 2.7) under various pH regimes (pH 4, 5, 7, and 9) at 25˚C, with the aim of simulating the behavior of the precipitates under different pH in situ disposal conditions. The tests were also conducted under similar pH conditions (5, 7 and 9) at 60˚C to determine the effect of accelerated aging on the stability of the precipitates. Accelerated aging at 60˚C simulated the behavior of the precipitates for longer times under different pH regimes at ambient conditions. The duration of the leaching tests was ~30 weeks and the experimental conditions are summarized in Table 4.5.

The extraction fluids of desired pH (4, 5, 7 and 9) were prepared by the addition of 1 M HNO_3 or 1 M NaOH to 1 L of distilled water. The leaching tests were performed by mixing 2.5 g of the precipitates with each of the extraction fluids (4, 5, 7 and 9) in 250 ml Erlenmeyer flasks (solid:liquid ratio of 1:20). The flasks were placed in an orbital shaker and continuously agitated (200 rpm) at room temperature. Additional experiments were conducted at 60˚C using 2.5 g of the precipitates and extraction fluids of pH 5, 7 and 9 (solid:liquid ratio of 1:20). The Erlenmeyer flasks containing the mixtures were placed in a benchtop incubator shaker and continuously agitated at 60˚C and 200 rpm. Aliquots of 13 ml were periodically withdrawn from the flasks at various time intervals, and were vacuum-filtered using 0.45 µm membrane filters. The pH of the leachates was measured before being analyzed for As and Fe using ICP-OES. The solids were

returned to the flasks and the flasks were refilled to their initial volume by the addition of 13 ml of the extraction fluid. The pH of the suspensions was adjusted to the desired value by the addition of either 1 M NaOH or 1 M HNO_3 before returning the flasks to the shakers. The pH and the volume of the suspensions were monitored daily, and maintained by the addition of the extraction fluid and either 1 M NaOH or 1 M HNO_3. On completion of leaching tests (at 25˚C and 60˚C), the suspensions were vacuum-filtered using 0.45 μm membrane filters. The solids were washed with distilled water and dried at room temperature. The solids were subjected to XRD analysis using a Phillips X'Pert Pro MPD diffractometer fitted with an X'Celerator high speed strip detector (X-ray source: Cu Kα radiation (Ni filtered) and Operating conditions: 45 KV, 40 MA, 3˚- 80˚ 2θ, step size of 0.02˚, counting time of 10 seconds at each step). The pH of the leachates was measured before being analyzed for As and Fe using ICP-OES.

Table 4.5: Experimental conditions for the long-term leaching tests

Leaching Tests	Precipitates	Extraction fluid pH	Time intervals for aliquot removal (days)
Ambient temperature (25˚C)	Tooeleite Gypsum-bearing tooeleite	4, 5, 7, 9	1, 3, 6, 8, 13, 24, 44, 64, 78, 121, 207
60˚C	Tooeleite Gypsum-bearing tooeleite	5, 7, 9	7, 15, 36, 69, 195

4.2.8. High temperature precipitation

The high temperature precipitation tests were conducted in a 2 L glass vessel, using 0.1 M Fe(III) and 0.1 M As(III) stock solutions. The As(III) stock solution was prepared by the dissolution of As_2O_3 in 0.1 M H_2SO_4 at 90 ˚C. 0.1 M Fe(III) was prepared by dissolving

$Fe_2(SO_4)_3.5H_2O$ in distilled water. The solution mixture was heated to the desired temperature (60˚C and 95˚C), and then the pH was adjusted by the addition of 2 M NaOH to pH 1.7, while being continuously stirred at 350 rpm. The pH was monitored and maintained at pH 1.7 for 1 hour. An aliquot of 50 ml was removed after 1 hour and vacuum-filtered using 0.45 µm membrane filter papers. The pH was then sequentially adjusted to pH 2, 2.5, 2.7, 3, 4, 6, 8, 10 and maintained at each of the specific pH values for 1 hour, before taking a 50ml aliquot for filtration. The filtrates were retained for the analysis of As and Fe using ICP-OES. The filter cakes were washed with distilled water and pH 3.6 acidified distilled water (acidified using 0.2M H_2SO_4), and then dried under ambient conditions. Similar experiments were conducted at 95˚C using NaOH as the base, and again at 60˚C and 95˚C using 2 M $Ca(OH)_2$ as the base. The experiments were replicated twice.

4.2.8.1. Characterization techniques

The high temperature tooeleite and gypsum-bearing tooeleite precipitates were subjected to powder X-Ray Diffraction (XRD) analysis using a Phillips X'Pert Pro MPD diffractometer fitted with an X'Celerator high speed strip detector (X-ray source: Cu Kα radiation (Ni filtered) and Operating conditions: 45 KV, 40 MA, 3˚- 80˚ 2θ, step size of 0.02˚, counting time of 10 seconds at each step). PanAnalytical HighScore software was used for the identification of phases. The particle-size, morphology and general elemental composition of the high temperature tooeleite and gypsum-bearing precipitates were evaluated by scanning electron microscopy (SEM) and energy dispersive x-ray spectroscopy (EDS) was performed using a MLA Quanta 650 FEG-ESEM machine.

4.2.8.2. Stability experiments

A modified US EPA TCLP test was conducted as described in Section 4.2.7.1. to determine the stability of the high temperature tooeleite and gypsum-bearing tooeleite precipitates. The TCLP test was modified from the original method described by the US EPA (US EPA, 1992) in that an Orbit Environ Shaker operated at 200 rpm was used instead of an end-over-end agitation device operated at 30 ± 2 rpm.

4.3. Results and discussion

4.3.1. Effect of Fe:As molar ratio and neutralizing agent

These experiments were conducted to investigate the role of initial Fe:As molar ratio and the neutralizing agent on the arsenic removal efficiency under ambient conditions. Figure 4.1 shows the residual arsenic concentration and arsenic removal efficiency in solution as a function of pH subsequent to the neutralization of Fe(III)-As(III) solutions (initial Fe:As molar ratio = 1.0, 1.5, and 2.0; equilibration time = 1 hour) using NaOH. At all pH levels, the effectiveness of arsenic removal was enhanced with increasing Fe:As molar ratio probably due to the fact that additional ferrihydrite was available to adsorb more As(III) out of solution. The As and Fe uptake from solution increased with increasing pH, and the maximum As removal was achieved in the pH range 6 to 8 (> 97%) for all the systems (Fe:As=1.0, 1.5 and 2.0). This is consistent with previous studies that have reported that optimal adsorption of As(III) by ferrihydrite is favoured at higher pH values of pH 6 to 9.4 (Ferguson and Anderson, 1972; Pierce and Moore, 1982; Manning and Goldberg 1997; Raven et al., 1998; Sun and Doner 1998; Jain and Loeppert 2000; Nishimura and Umetsu, 2000; Dixit et al., 2003). Raven et al. (1998) hypothesized that the adsorption of As(III) by ferrihydrite is better than that of As(V) at higher pH regimes due to the surface charges of the adsorbent. At higher pH, the surface charge of the arsenite anion (H_3AsO_3) is neutral compared to the arsenate anion ($HAsO_4^{2-}$) which is negative, thereby having a higher adsorption affinity for ferrihydrite. For the Fe:As=1 system, As was released back into solution at pH 10 probably due to the instability of the As-bearing phase under pH 10 conditions. However, this was not the case for the Fe:As=1.5 and Fe:As=2 systems where As was retained in the precipitated solids, probably due to the presence of excess Fe, which was available to adsorb any As that was released due to the dissolution of As-bearing phase (formed in the pH range 6 to 8).

Figure 4.2 shows the residual arsenic concentration in solution and arsenic removal efficiency as a function of pH during the neutralization of Fe(III)-As(III) solutions (initial Fe:As molar ratio = 1.0, 1.5, and 2.0; equilibration time = 1 hour) using $Ca(OH)_2$. The use of $Ca(OH)_2$ as base enhanced the As uptake of the three systems (Fe:As=1.0, 1.5 and 2.0) compared to that of the NaOH neutralized systems. Lime neutralization of the three systems (Fe:As=1.0, 1.5 and 2.0) resulted in more than 90% As removal from solution at pH >3. The role of lime in the increased As uptake by ferrihydrite could be attributed to the participation of calcium ions in the adsorption of As(III) due to the relatively high adsorption affinity of ferrihydrite for calcium ions (Dzombak and Morel, 1990; Wilkie and Hering, 1996; Jambor and Dutrizac, 1998; Jia and Demopoulos, 2008). Wilkie and Hering (1996) proposed that the adsorption of calcium ions by ferrihydrite causes a positively charged surface which promotes the adsorption of anionic species such as the arsenite anion.

During the experiments, precipitation was observed to occur as soon as the base was added to the solution. For the Fe:As=1 system, a bright yellow-orange precipitate (later determined by XRD to be tooeleite), was observed to settle in increasing quantities in the pH range 2 to 4 (Figure 4.3a). In the pH range 6 to 10, the precipitates changed colour to a pale yellow-brownish hue (Figure 4.3a). The sudden change in the colour of the formed precipitates in the pH range 4 to 6 could be due to either tooeleite transforming to another As-bearing phase or a much higher proportion of ferrihydrite precipitating at pH 6 relative to tooeleite. According to Nishimura and Robins (2008), tooeleite formation is favoured in the pH range 2 - 3.5, and is likely to partially transform to FeOOH(As) (arsenic-bearing ferrihydrite) at pH >3.5. In addition, the brownish tint of the precipitates formed at pH >3.5 increased with increasing Fe:As molar

ratio, probably due to the formation of larger quantities of ferrihydrite from the excess Fe present in solution (Appendix A.1).

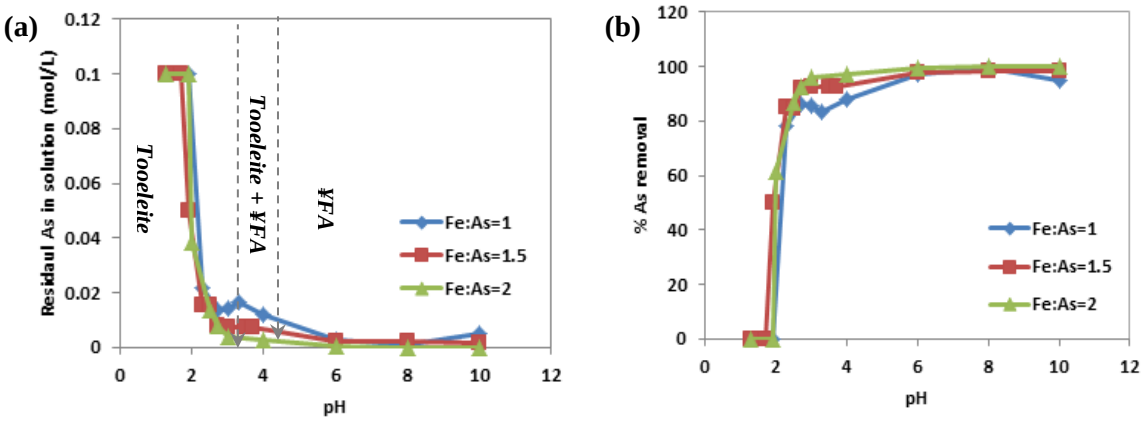

Figure 4.1: (a) Residual As concentration in solution and (b) As removal efficiency as a function of pH for Fe(III)-As(III) precipitation systems (Fe:As molar ratio = 1, 1.5 and 2; 25˚C) neutralized by NaOH. ¥FA denotes As-bearing ferrihydrite

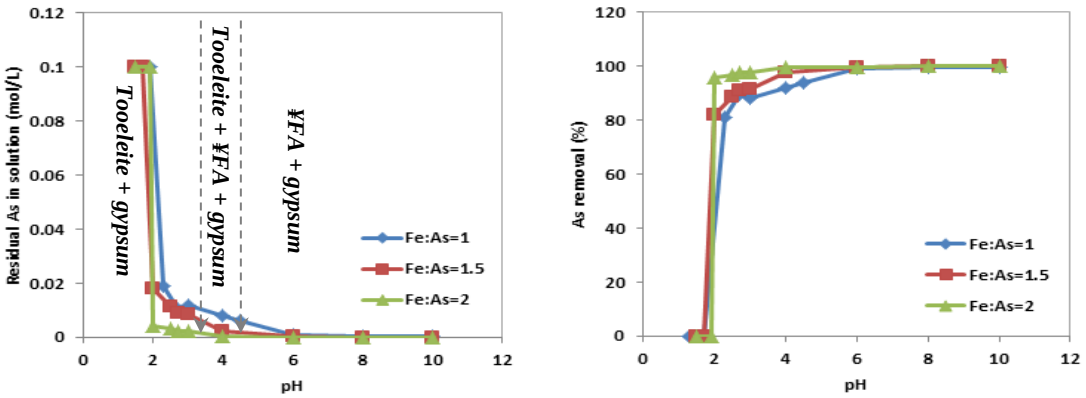

Figure 4.2: Residual As concentration in solution and (b) As removal efficiency as a function of pH for Fe(III)-As(III) precipitation systems (Fe:As molar ratio= 1, 1.5 and 2; 25˚C) neutralized by $Ca(OH)_2$. ¥FA denotes As-bearing ferrihydrite

Figure 4.3b illustrates the As:Fe molar ratio of the precipitates and As equilibrium concentration as a function of pH for Fe(III)-As(III) systems (Fe/As = 1.0, 1.5, and 2.0) neutralized by NaOH. The As:Fe molar ratio of the precipitates is observed to be dependent on the initial Fe:As molar ratio of the solution and pH. For the Fe:As=1.0 system, the As:Fe molar

ratio of the precipitates at pH 2 is 0.90 probably due to the initial precipitation of tooeleite. In the pH range 2 to 3, the molar ratio of the precipitates decreases from 0.90 to 0.83 mole As/mole Fe, probably due to the increased precipitation of tooeleite. In the pH range 3 to 6, the As:Fe molar ratio of the precipitates gradually increases from 0.83 to 0.97, possibly due to the transformation of tooeleite to an equimolar As-bearing phase (Fe:As molar ratio=1.0) or the presence of a mixture of As-bearing species (As-bearing ferrihydrite and arsenolite) in the precipitates. The As:Fe molar ratio peaks at 0.99 at pH 8, and then decreases to 0.95 at pH 10. Raven et al. (1998) investigated As(III) adsorption on ferrihydrite and found that, at high initial As(III) concentrations (13 mol As/kg ferrihydrite), the adsorption density for As(III) was 0.6 mole As/mole Fe. The authors proposed that ferrihydrite had transformed to a ferric arsenite phase as the high As retention exceeded the maximum number of surface sites available on ferrihydrite for the adsorption of As(III) (0.25 mol of sites per mol of Fe). Consequently, these findings suggest that a ferric arsenite phase may be present in the precipitates formed from the system of initial Fe:As molar ratios of 1.0 above pH 4 due to their high As:Fe molar ratio of ~1.

Nishimura and Umetsu (2000) had previously shown that co-precipitation of As(III) with ferric iron achieved the lowest solubility of As from 0.005 M solutions at pH 8 but the As:Fe molar ratio of the precipitates was observed to be only about 0.74, assuming no Fe was left in solution (Figure 4.4a). In their experiments at 0.1 M As(III):Fe(III), the authors observed that the precipitation of a yellow precipitate occurred at >pH 2, that would later be identified as tooeleite and these experiments only went up to pH<5 (Figure 4.4b). The authors did not explain why As(III) solubility continued to decrease even though all the Fe was precipitated at pH 3.2. Precipitates with lower As:Fe molar ratio were obtained for the Fe:As=1.5 and Fe:As=2.0

systems (Figure 4.3b). It was noted that the As:Fe molar ratio of the precipitates did not decrease at pH 10 for the Fe:As=1.5 and Fe:As=2.0 systems, probably due to the excess ferric iron that was present in solution. Furthermore, the presence of excess ferric iron in solution resulted in the formation of precipitates with lower As/Fe molar ratios for the Fe:As=1.5 and Fe:As=2.0 systems compared to that of the Fe:As=1.0 system and probably indicates the presence of a mixture of ferrihydrite and FeOOH(As) (As-bearing ferrihydrite).

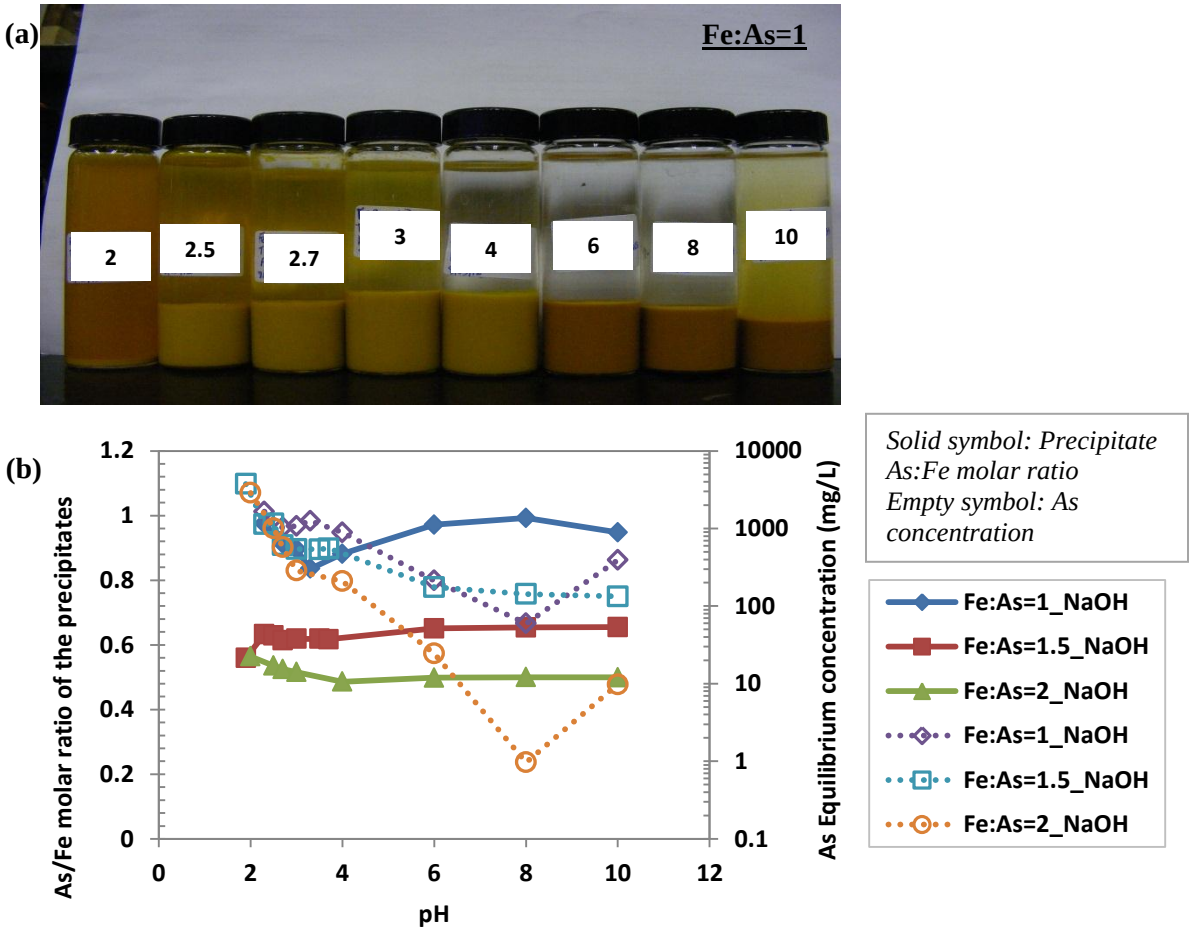

Figure 4.3: (a) Co-precipitates formed at various pH levels (pH 2.5, 2.7, 3, 4, 6, 8, 10) from an Fe(III)-As(III) system (Fe:As=1) neutralized by NaOH and (b) As:Fe molar ratio of the precipitates and As equilibrium concentration as function of pH at 25˚C and Fe:As=1, 1.5 and 2 (equilibration time = 1 hour)

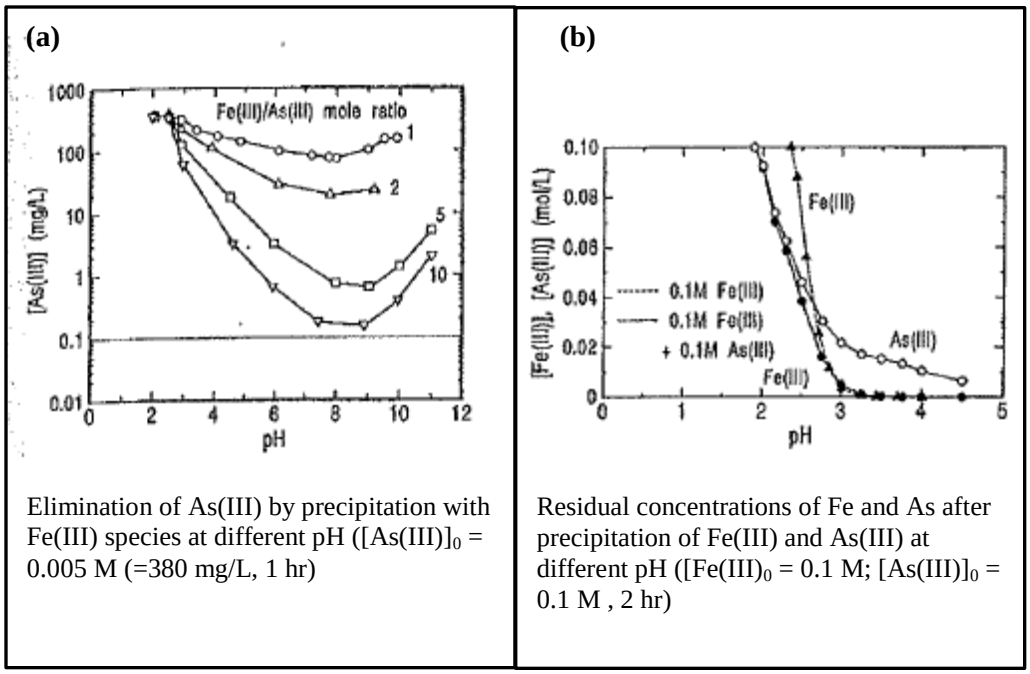

Elimination of As(III) by precipitation with Fe(III) species at different pH ($[As(III)]_0$ = 0.005 M (=380 mg/L, 1 hr)

Residual concentrations of Fe and As after precipitation of Fe(III) and As(III) at different pH ($[Fe(III)_0$ = 0.1 M; $[As(III)]_0$ = 0.1 M , 2 hr)

Figure 4.4: Elimination of As(III) from aqueous solution during co-precipitation with Fe(III) (Nishimura and Umetsu, 2000)

Figure 4.5a illustrates the colour change of the precipitates with increasing pH. Figure 4.5b illustrates the As:Fe molar ratio of the precipitates and As equilibrium concentration as a function of pH for Fe(III)-As(III) systems (Fe/As = 1.0, 1.5, and 2.0) neutralized by $Ca(OH)_2$. For the Fe:As=1.0 system, the As/Fe molar ratio of the precipitates decreases from 0.95 to 0.88 until pH 3, and then gradually increases to 0.99 at pH 8.

Unlike the NaOH neutralized system, the As:Fe molar ratio of the precipitates is maintained at 0.99 at pH 10, suggesting that the presence of gypsum increases the stability of the As-bearing phase under highly alkaline conditions of pH 10. The presence of excess ferric iron in

solution resulted in lower precipitate As:Fe molar ratio for solutions with the initial Fe:As=1.5 and Fe:As=2.0 compared to that of the Fe:As=1.0 system.

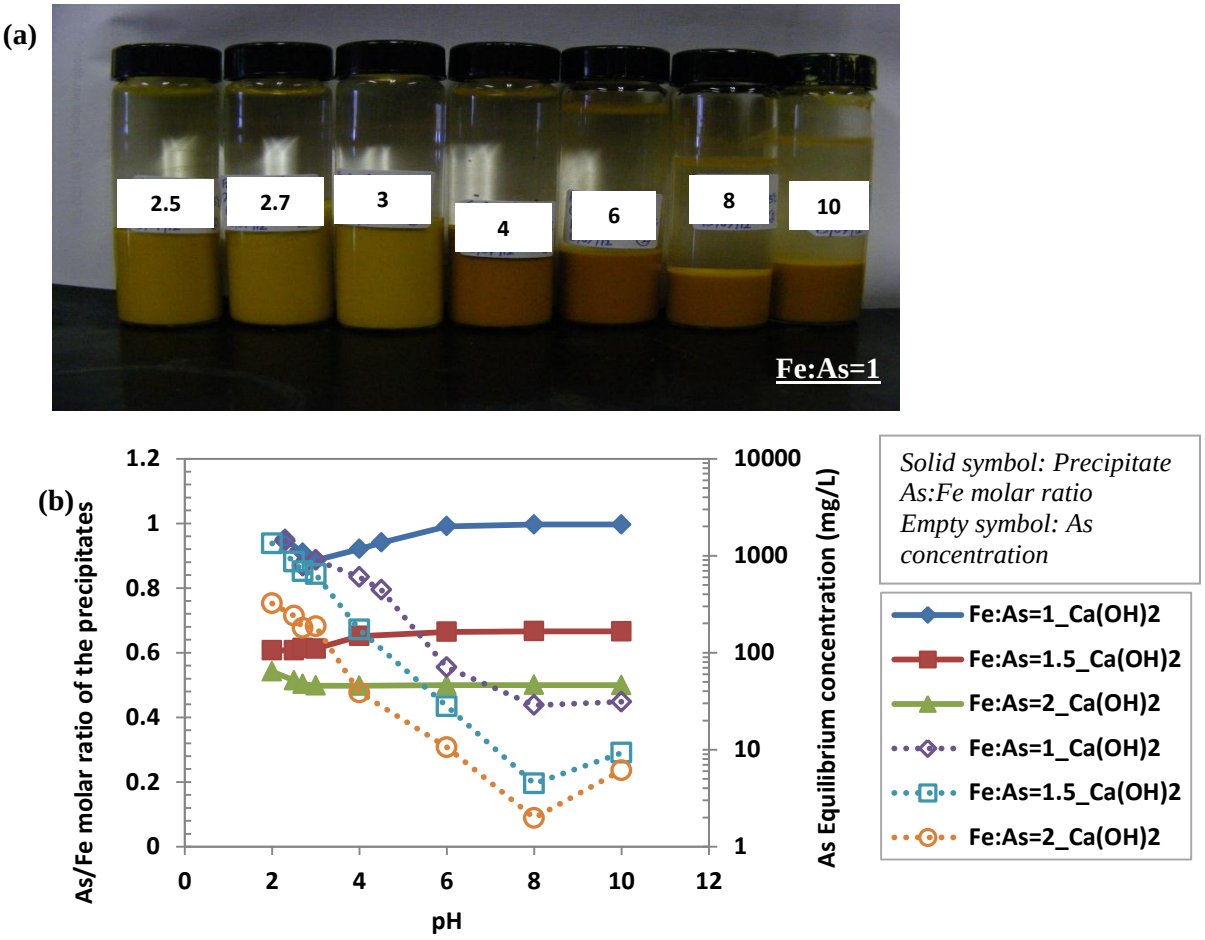

Figure 4.5 (a) Co-precipitates formed at various pH levels (pH 2.5, 2.7, 3, 4, 6, 8, 10) from an Fe(III)-As(III) system (Fe:As=1) neutralized by $Ca(OH)_2$ and (b) As:Fe molar ratio of the precipitates and As equilibrium concentration as a function of pH at 25˚C and Fe:As=1, 1.5 and 2

4.3.2. Phase characterization

4.3.2.1. XRD analysis

XRD analytical results of the precipitates formed from Fe(III)-As(III) solutions (Fe:As molar ratio = 1.0; 1.5; 2.0) using NaOH and $Ca(OH)_2$ as the bases are presented in Table 4.6. XRD analysis of the precipitates formed from the Fe:As = 1.0 system in the pH range 2 to 4 using NaOH as the base indicated the presence of tooeleite. A poorly crystalline phase was identified in the precipitates formed in the pH range 6 to 10. Nishimura and Robins (2008) reported that tooeleite is stable in the pH range 2 to 3.5, and hypothesized that it is likely to transform to FeOOH(As) at >pH 3.5. Similar XRD results were obtained for the precipitates formed from systems with initial Fe:As molar ratios of 1.5 and 2.0.

XRD analysis of the precipitates formed from the Fe:As = 1.0 system in the pH range 2 to 4 using $Ca(OH)_2$ as the base indicated the presence of tooeleite and gypsum. Gypsum was the only phase identified in the precipitates formed in the pH range 6 to 10. Similar results were obtained for the precipitates formed from solutions with initial Fe:As molar ratios of 1.5 and 2.0. XRD analysis of the solids formed at higher pH levels of 8 and 10 in the three systems (Fe:As = 1.0, 1.5 and 2.0) did not indicate the presence of calcium arsenite, even though a sudden increase in As removal was observed in this pH range during the precipitation process. As noted in Figures 4.3 and 4.5, the same increase in the precipitate As:Fe molar ratio occurred in both the NaOH and $Ca(OH)_2$ neutralized systems. Wilkie et al. (1996) proposed that the adsorption of Ca(II) by ferrihydrite resulted in a positively charged surface which enhanced the adsorption of the anionic As species. The absence of calcium arsenite suggests that calcium ions promoted the adsorption of As(III) by ferrihydrite by participating in the As(III) adsorption since ferrihydrite has a

relatively high affinity for calcium ions (Dzombak and Morel, 1990; Wilkie and Hering, 1996; Jambor and Dutrizac, 1998). However, it is possible that the formation of calcium arsenite precipitates occurs in regions of high lime concentrations at local levels in the Fe(III)-As(III) bearing solution during the precipitation process.

Table 4.6: Mineral phases identified by bulk XRD analysis of the precipitates formed from Fe(III)-As(III) solutions of initial Fe:As molar ratio of 1, 1.5, and 2 under ambient conditions using NaOH and $Ca(OH)_2$ as bases

Samples	Precipitation pH range	Mineral phases
Initial Fe:As molar ratio =1.0, 1.5 and 2.0 (NaOH)	2 - 4	Tooeleite
	6 - 10	Poorly crystalline As-bearing phase
Initial Fe:As molar ratio =1.0, 1.5 and 2.0 ($Ca(OH)_2$)	2 - 4	Tooeleite and Gypsum
	6 - 10	Gypsum

4.3.2.2. SEM analysis

Figure 4.6 and Figure 4.7 present the SEM images and EDX spectra of the tooeleite precipitates formed from an Fe:As=1 system at pH 2.5 and 4 respectively, using NaOH as the base. Figure 4.8 presents the SEM images and EDX spectra of the gypsum-bearing tooeleite precipitates formed in the Fe:As=1 system at pH 2.5 using $Ca(OH)_2$ as the base. The EDX spectra, (a), (b), (c), (d), (e), and (f) correspond to the respective elemental analyses of spots marked a, b, c, d, e and f in the SEM images. The SEM images in Figure 4.6 indicate that the pH 2.5 tooeleite precipitates consist of grains (>50 μm) with a smooth texture and white patches on the surface. The SEM images of the pH 4 tooeleite precipitates in Figure 4.7 indicate the surface of the grain has converted to a hairy-like texture. The higher magnification SEM image (5 μm)

indicates that the surface of the grain consists of regions of smooth and hairy-like textures. The EDX spectra of smooth and hairy textures indicate the presence of principally Fe/As/O/S at spot c and Fe/As/O at spot d respectively. Consequently, the hairy texture is deemed to indicate the initial gradual transformation of tooeleite. The SEM images of the pH 2.5 gypsum-bearing tooeleite precipitates indicate the presence of clusters of needle-shaped gypsum crystals with layers of As-bearing solids deposited on their surfaces (Figure 4.8). The EDX analyses indicate that the As-bearing solids consist of an association of Fe/As/S/O and are therefore deemed to be tooeleite precipitates.

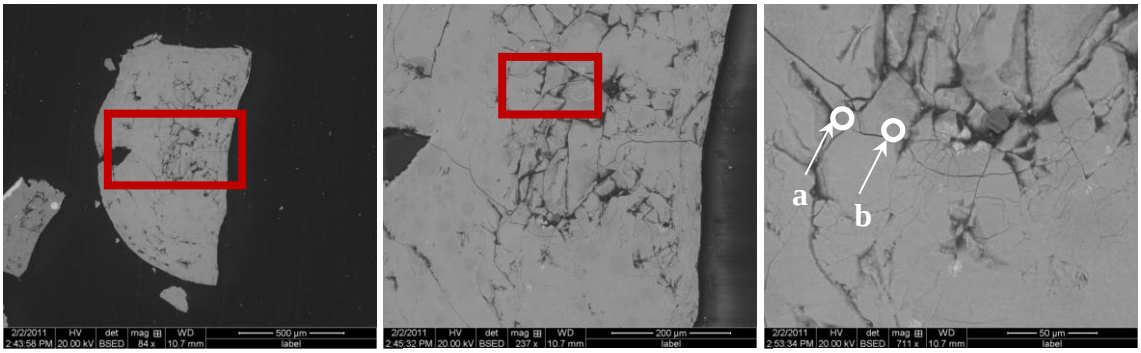

[scale bar = 500 µm] [scale bar = 200 µm] [scale bar = 50 µm]

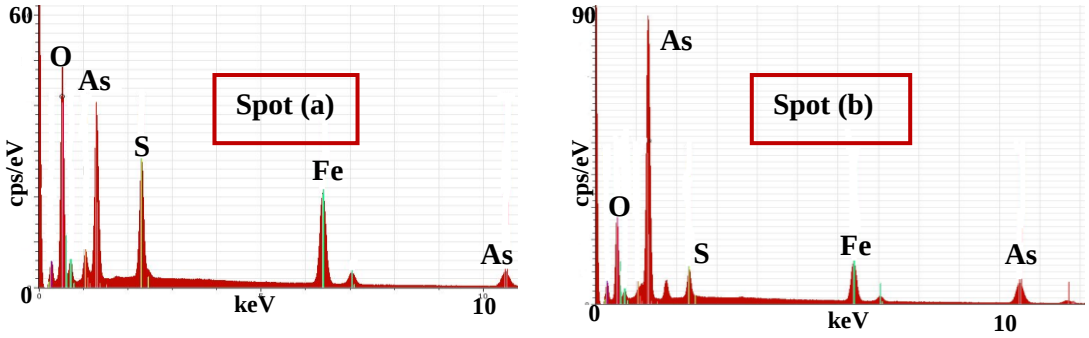

Figure 4.6: SEM images and EDX spectra of tooeleite precipitates formed from an Fe:As=1 system at pH 2.5 using NaOH as the base

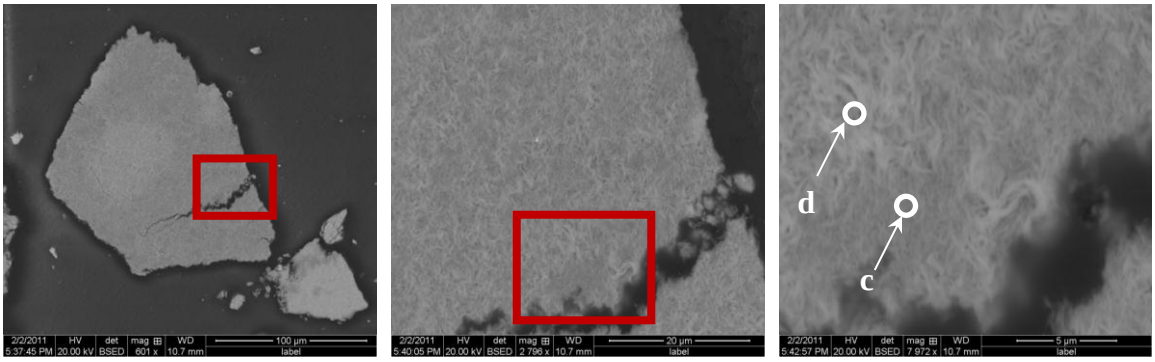

[scale bar = 100 µm] [scale bar = 20 µm] [scale bar = 5 µm]

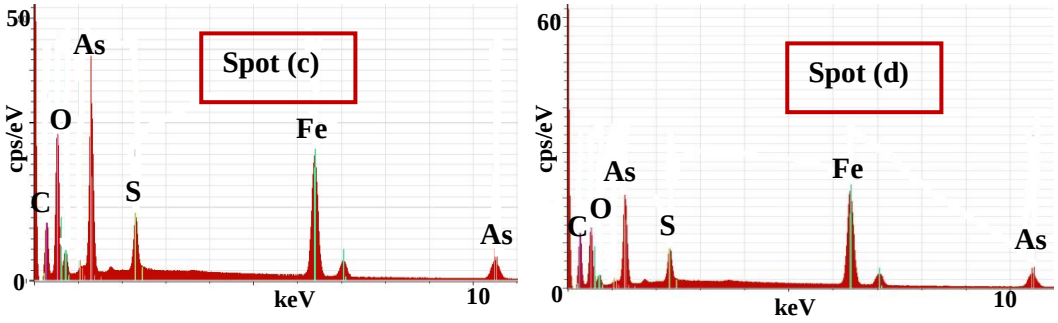

Figure 4.7: SEM images and EDX spectra of tooeleite precipitates formed from an Fe:As=1 system at pH 4 using NaOH as the base

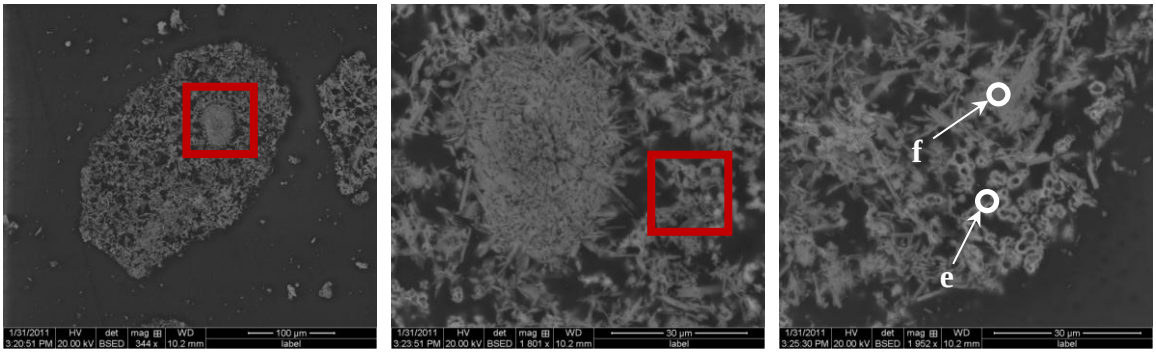

[scale bar = 100 µm] **[scale bar = 30 µm]** **[scale bar = 30 µm]**

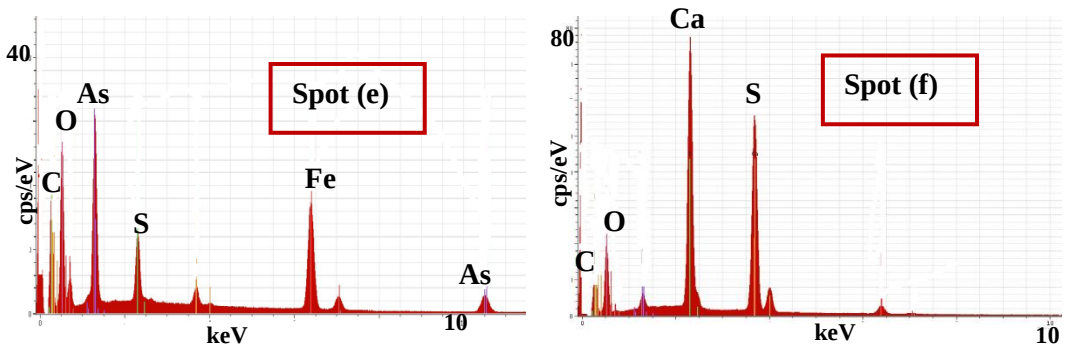

Figure 4.8: SEM images and EDX spectra of gypsum-bearing tooeleite precipitates formed from an Fe:As=1 system at pH 2.5 using $Ca(OH)_2$ as the base

4.3.2.3. Synchrotron analysis

4.3.2.3.1. µXRF, µXRD and µXANES analyses (thin sections)

The µXRF elemental distribution map (~4.5mm x 7 mm) of As and Fe in a thin section of tooeleite precipitates formed at pH 2.5 (Fe:As = 1.0) using NaOH as the base is presented in Figure 4.9a. The map represents an overlay of the As and Fe elemental maps with red and blue representing relative As Ka and Fe Ka fluorescence intensities respectively. The circled regions 1 and 2 indicate the As hot spots where µXRD analyses was conducted. The dark region is an area of void solid stemming from the loss of sample during the lifting of the thin section from the glass

slide. The elemental map indicates that the distribution of As and Fe is heterogeneous across the mapped area of the thin section.

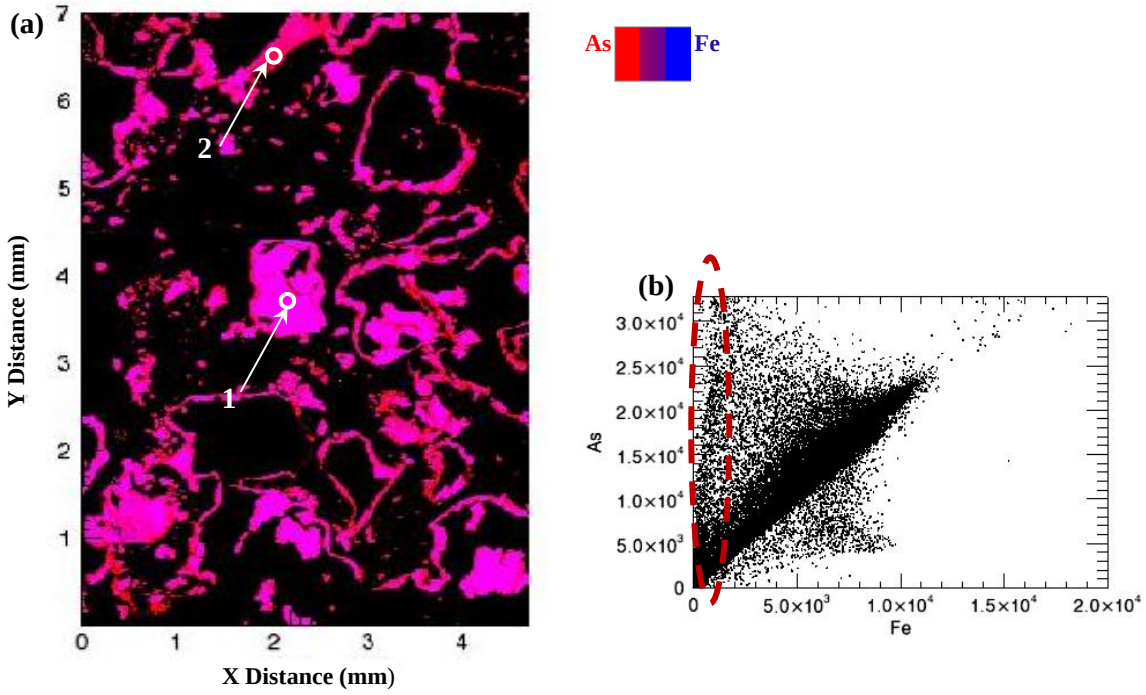

Figure 4.9: (a) µXRF elemental distribution map (~4.5 x 7 mm) of a thin section of tooeleite precipitates formed at pH 2.5 (Fe:As=1) using NaOH as the base. (b) A correlation plot of As and Fe

An elemental correlation plot of As and Fe is illustrated in Figure 4.9b. For each pixel, the corresponding value from the two-elemental map is plotted in a correlation plot where the x and y axes represent the two different elements. A positive correlation was observed between As and Fe indicating the presence of predominantly an As/Fe bearing phase. The circled region in Figure 4.9b indicates evidence of the presence of a high As phase with negligible amounts of Fe. The 2D µXRD images and integrated µXRD patterns for regions 1and 2 are presented in Figure 4.10. Tooeleite was identified in regions 1 and 2. The 2D µXRD pattern of region 1 consists of smooth rings indicating the presence of predominantly very fine crystallites (nanocrystallites) of

tooeleite (Walker et al., 2009). Arsenolite was identified in region 2, and the spotty rings in the 2-D µXRD image indicate that arsenolite exists as discrete coarse crystals. Arsenolite probably formed as a result of high concentrations of As and a shortage of Fe at initial Fe:As=1.0.

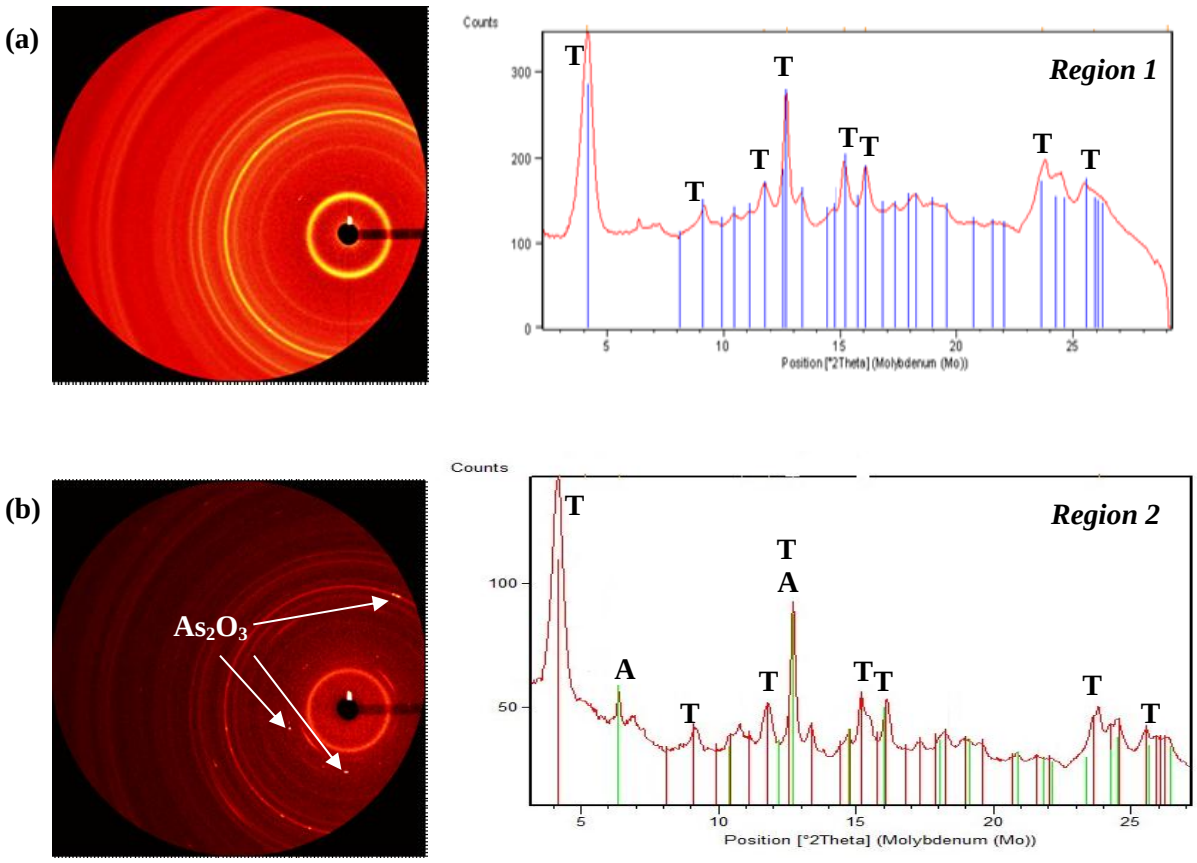

Figure 4.10: 2D µXRD images and integrated µXRD patterns of regions (a) 1 and (b) 2. The peaks labeled T and A represent tooeleite and arsenolite respectively

The µXRF elemental distribution map (4 mm x 3 mm) of As and Fe in a thin section of tooeleite precipitates formed from a NaOH neutralized system (Fe:As = 1.0) at pH 4 is presented in Figure 4.11a. The map represents an overlay of the As and Fe elemental maps with red and blue representing relative As Ka and Fe Ka fluorescence intensities respectively. The circled

regions 1 and 2 indicate the As hot spots where μXRD analyses was conducted. The darker regions on the grains indicate areas with the hairy texture, where the initial dissolution of tooeleite is possibly occurring. An elemental correlation plot of As and Fe is illustrated in Figure 4.11b. The plot shows that there is a strong positive linear correlation between As and Fe, indicating the presence of an Fe/As bearing phase.

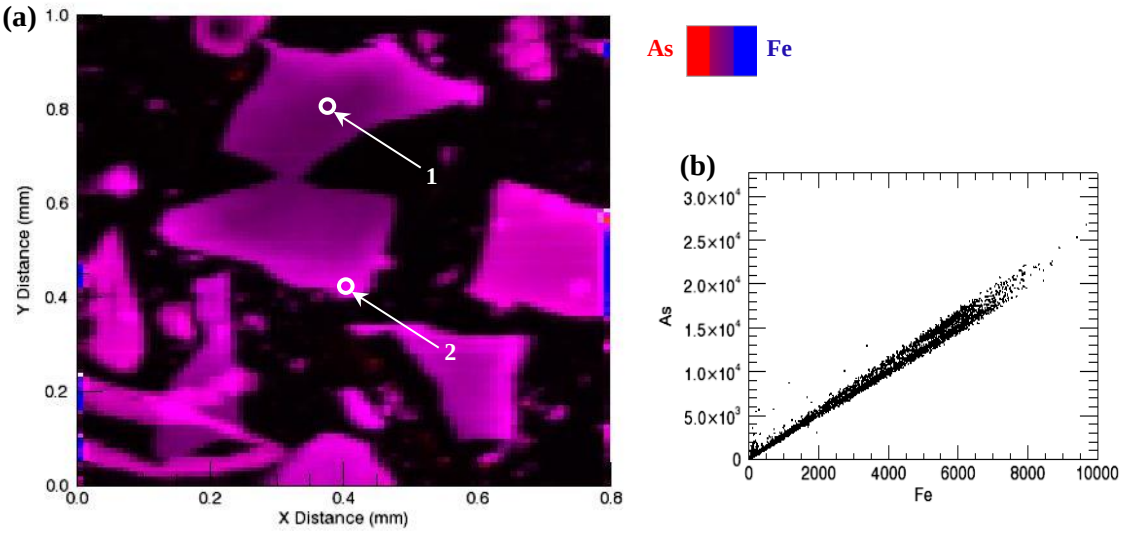

Figure 4.11: (a) μXRF elemental distribution maps (~0.8 x 1 mm) of a thin section of tooeleite precipitates formed at pH 4 (Fe:As=1) using NaOH as the base and (b) a correlation plot of As and Fe

The 2D μXRD images and integrated μXRD patterns for regions 1 and 2 are presented in Figure 4.12. The 2D μXRD images of regions 1 and 2 consist of smooth rings indicating the presence of predominantly nanocrystallites. The integrated μXRD patterns indicated the presence of tooeleite in both regions. Previous studies have hypothesised that tooeleite is more likely to dissolve incongruently at pH >3.5 to form FeOOH(As) (Nishimura and Robins, 2008). However, the FeOOH(As) phase was not identified by μXRD analysis. However, comparison of the peak intensities of the patterns in Figure 4.10 and Figure 4.12 for both regions 1 and 2 indicate that the

intensity of the tooeleite peaks obtained from the pH 4 precipitates are lower than those of the pH 2.5 precipitates, suggesting the presence of lower concentrations of tooeleite in the pH 4 precipitates probably due to its partial transformation (Nishimura and Robins, 2008).

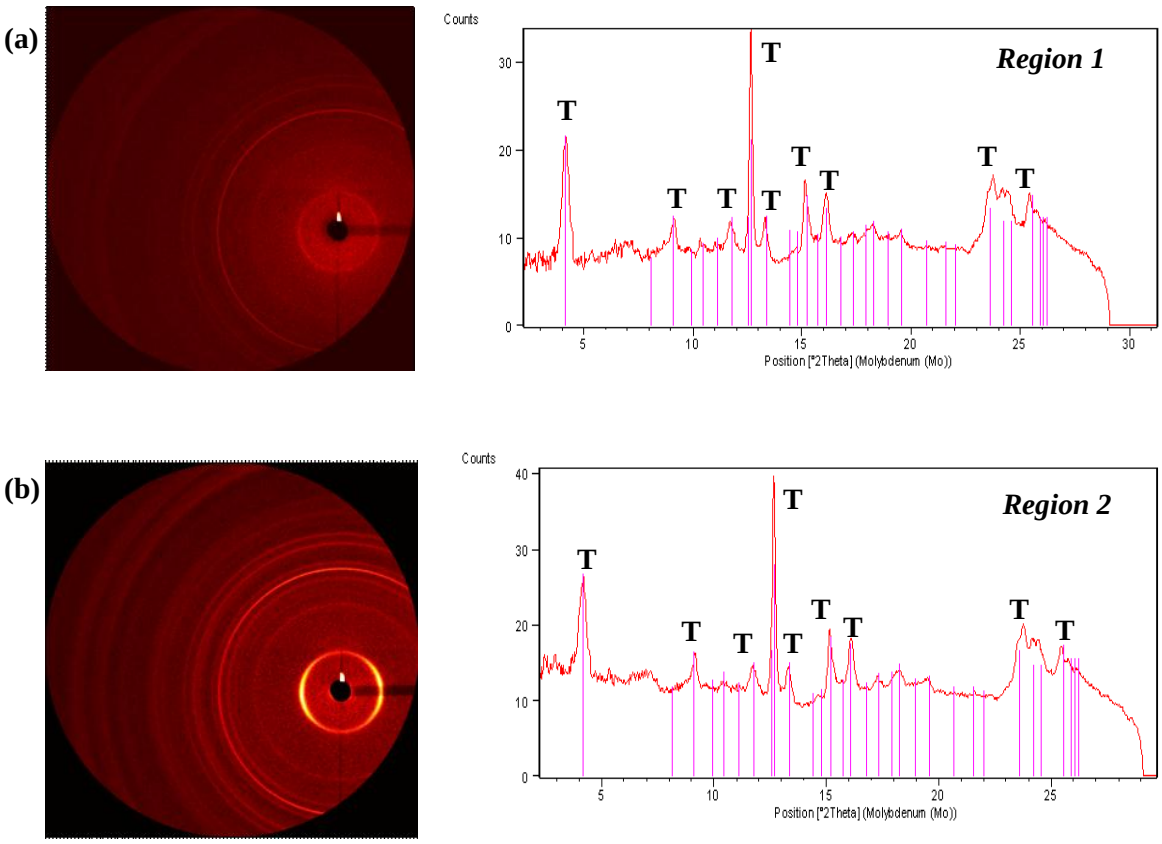

Figure 4.12: 2D µXRD images and integrated µXRD patterns of regions (a) 1 and (b) 2. The peaks labeled T represent tooeleite

The elemental distribution map (1 mm x 2 mm) of As, Fe and Ca that was obtained by µXRF analysis of the thin section consisting of precipitates formed from a $Ca(OH)_2$ neutralized system (Fe:As=1.0) at pH 2.5 is presented in Figure 4.13a. The composite map represents the overlay of the As, Fe and Ca elemental maps with red, green and blue representing relative As Ka, Ca Ka and Fe Ka fluorescence intensities respectively. The circled regions 1 and 2 indicate

the As hot spots where µXRD analyses was conducted. The dark region is an area of void solid stemming from the lifting of the thin section from the glass slide.

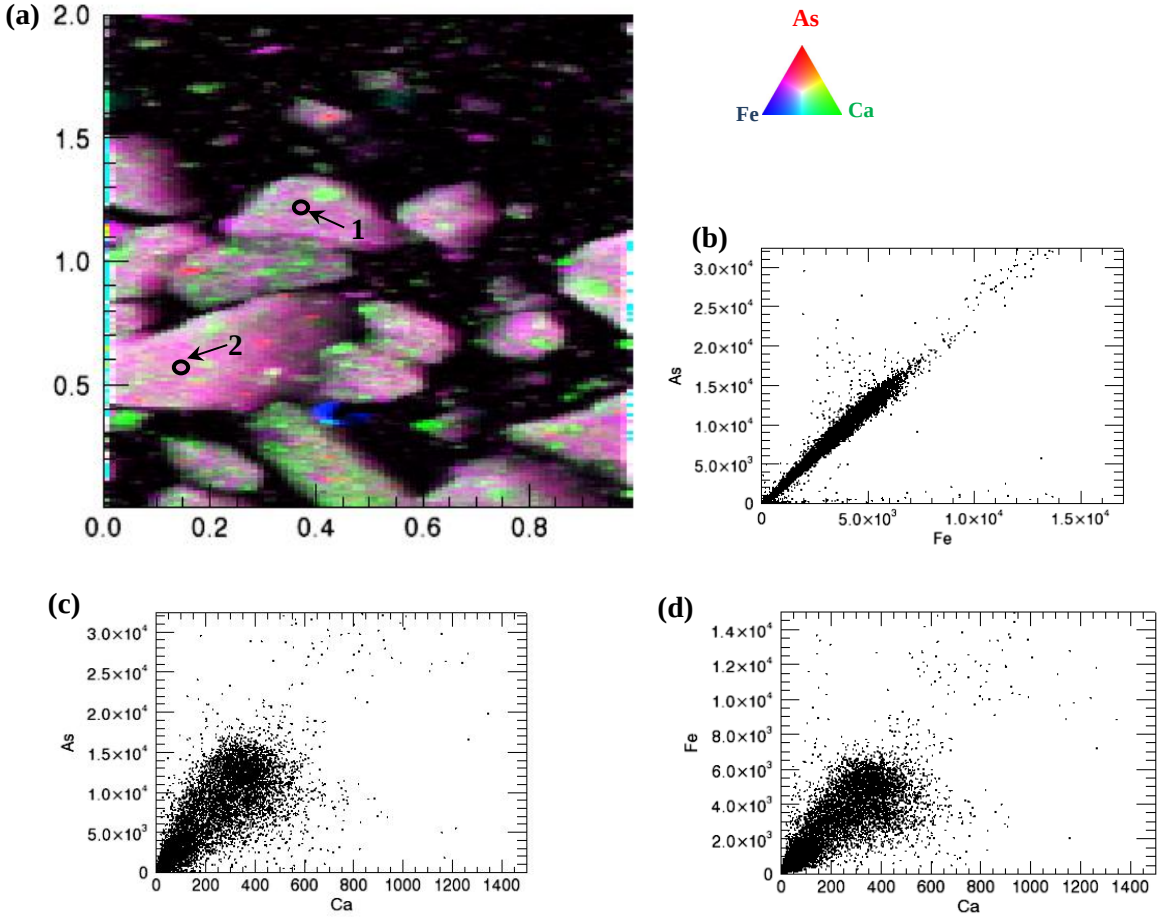

Figure 4.13: (a) µXRF elemental distribution maps (~1 x 2mm) of a thin section of tooeleite precipitates formed at pH 2.5 from an initial solution of Fe:As=1 and using $Ca(OH)_2$ as the base. Correlations plots of (b) As/Fe (c) As/Ca and (d) Fe/Ca

Elemental correlation plots of As/Fe, As/Ca and Fe/Ca are illustrated in Figures 4.13b, 4.13c and 4.13d. For each pixel, the corresponding value from the two-elemental map is plotted in a correlation plot where the x and y axes represent the two different elements. The plots show that there is a positive linear correlation between As and Fe. The Ca/As correlation is probably

due to the presence of gypsum and an As-bearing phase at every pixel. The 2D μXRD images and integrated μXRD patterns for regions 1 and 2 are presented in Figure 4.14. The integrated μXRD patterns of regions 1 and 2 indicated the presence of tooeleite and gypsum, which is in good agreement with the bulk XRD results. In addition, bassinite (calcium sulphate hemihydrate, $CaSO_4.0.5H_2O$) was also identified by μXRD analysis indicating it was present at the micro-scale level. Bassinite may have formed during the preparation of the thin section.

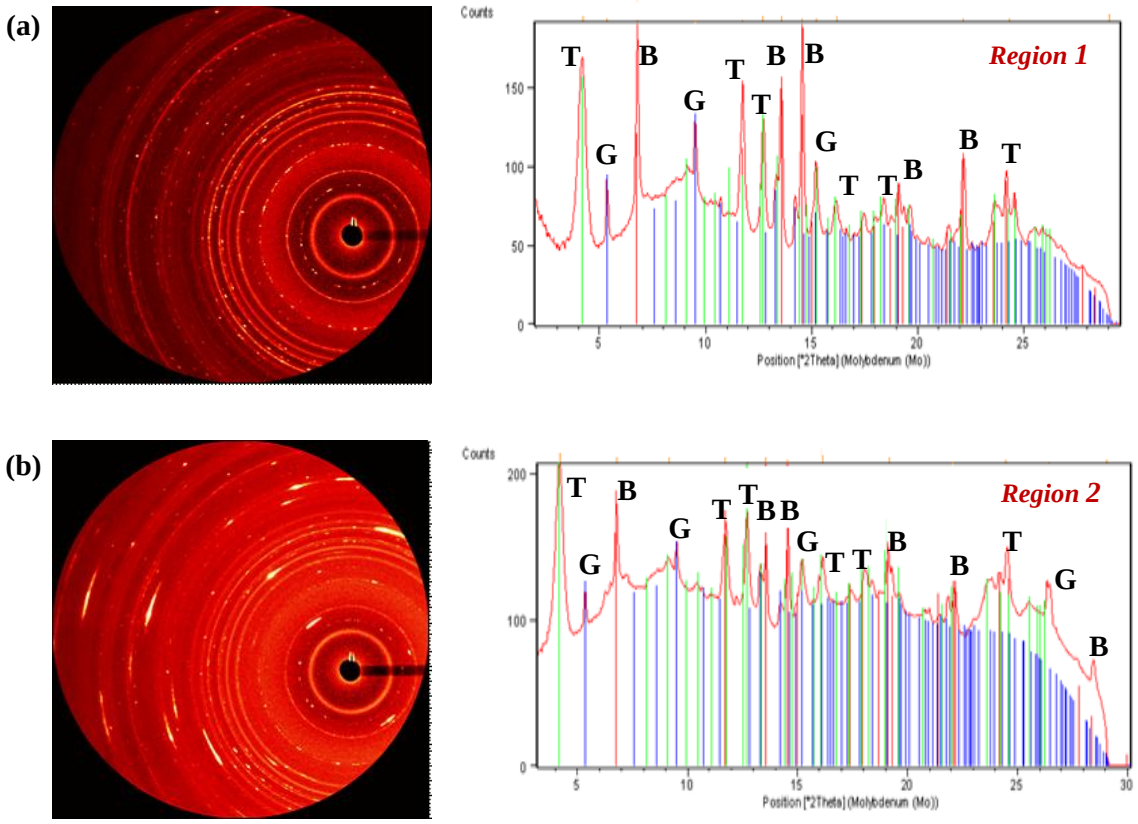

Figure 4.14: 2D μXRD images and integrated μXRD patterns of (a) Region 1 and (b) Region 2. The peaks labeled B, G and T represent bassinite, gypsum and tooeleite respectively

The normalized As K-edge μXANES spectra of the standards (arsenopyrite (-1), arsenolite (+3) and scorodite (+5)) and the thin sections (NFA125, NFA14 and CFA125) are

presented in Figure 4.15. NFA125 and NFA14 are the thin sections comprised of tooeleite precipitates formed at pH 2.5 and pH 4 from NaOH neutralized systems (Fe:As=1.0) respectively. CFA125 is the thin section comprised of gypsum-bearing tooeleite precipitates formed at pH 2.5 from $Ca(OH)_2$ neutralized systems (Fe:As=1.0). The μXANES spectra of the selected regions (region 1) in the thin sections were fitted with the spectra of standards using linear combination fitting and the results are summarized in Table 4.7. Fitted model spectra of less than 5% were considered negligible as they did not improve the fits (Walker et al., 2005). Analysis of the μXANES spectra using linear combination fitting indicated that As is predominantly present in both tooeleite and gypsum-bearing precipitates as As(III).

Table 4.7: Linear combination fitting (LCF) results determined using the As K-edge μXANES spectra of arsenopyrite, arsenolite and scorodite

Samples	LCF results
NFA125	93% As(III) ; 7% As(V)
CFA125	94% As(III); 6% As(V)
NFA14	100% As(III)

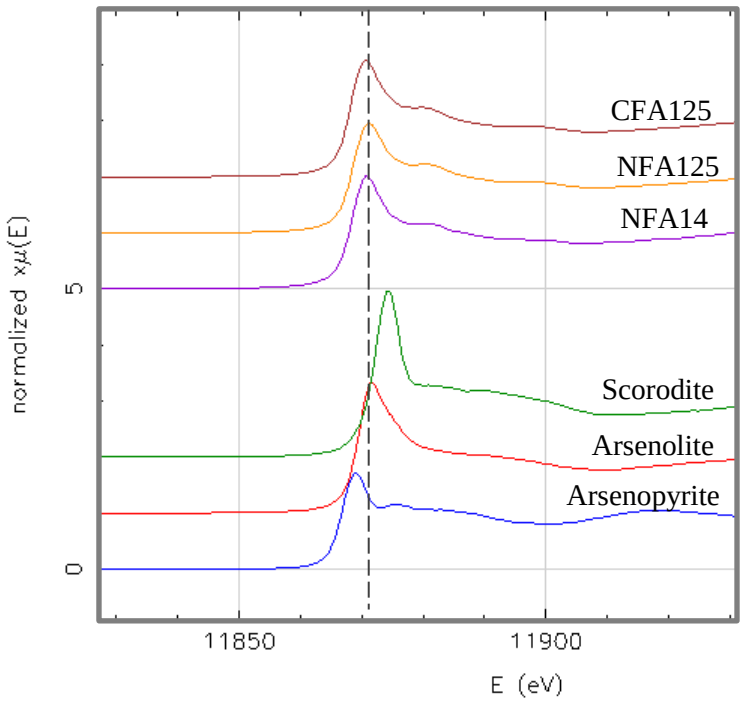

Figure 4.15: As K-edge μXANES spectra of selected spots (Region 1) on the tooeleite (NFA125 and NFA14) and gypsum-bearing tooeleite (CFA125) thin sections

4.3.2.3.2. μXRD analysis (powder samples)

μXRD analysis was conducted on powder samples of the precipitates formed from solutions of Fe:As molar ratio of 1 at pH 6 to 10, using NaOH and $Ca(OH)_2$ as the bases. The 2-D μXRD images and integrated μXRD patterns of the precipitates formed from the NaOH neutralized system at pH 6 and 10 are presented in Figure 4.16a and 4.16b respectively. The integrated μXRD patterns confirmed the presence of 2 broad peaks at d-spacings of ~0.29 nm and ~0.17 nm. This μXRD pattern is similar to that of 2-line ferrihydrite which has its major peaks located at ~2.56 nm and ~0.15 nm (Jambor and Dutrizac, 1998). The integrated μXRD pattern presented in Figure 4.16a is similar to the XRD pattern of As(III)-rich stromatolite sediments (Figure 4.17) obtained by Morin et al. (2003) in their study of tooeleite and mixed As(III)/V-

Fe(III) gels in the Carnoules acid mine drainage (AMD) in France. These results suggest that tooeleite is formed in the pH range 2 to 3, and subsequently begins to transform above ~pH 3 (Fe:As=1.0) to form an equimolar ferric arsenite, which is most stable at pH 8 (Equation 4.1).

$$\mathbf{6Fe_2O_3.5As_2O_3.2SO_3.12H_2O_{(s)} = 10FeAsO_3.xH2O_{(s)} + 2FeOOH_{(s)} + H_2SO_{4\ (aq)}} \qquad \mathbf{(4.1)}$$

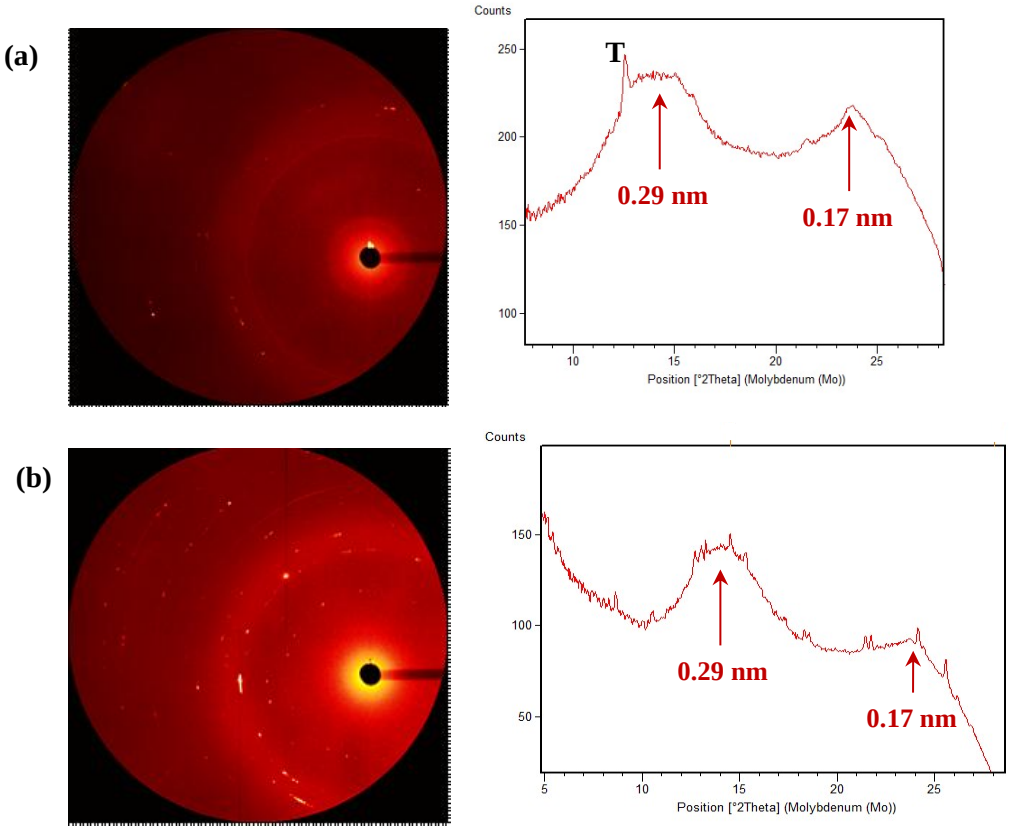

Figure 4.16: 2D µXRD images and integrated µXRD patterns for the powder samples containing tooeleite precipitates formed from solutions of initial Fe:As=1 at (a) pH 6 (b) pH 10 at 25˚C using NaOH as the base. The peak labeled T represents tooeleite.

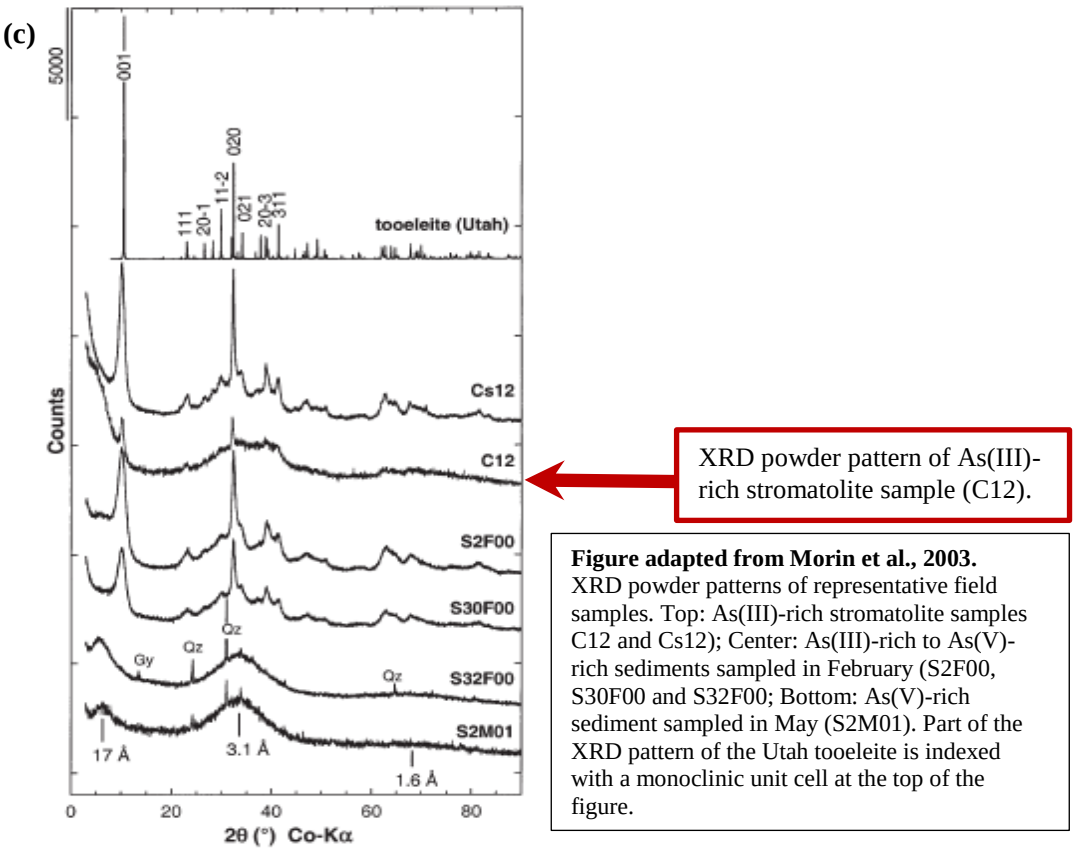

Figure 4.17: XRD powder pattern of As(III)-rich stromatolite sample (C12) from Carnoules AMD, France.

The 2D µXRD images and integrated µXRD patterns of the precipitates formed at pH 6, 8 and 10 using $Ca(OH)_2$ as the base are presented in Figure 4.18. Gypsum and tooeleite were identified in the pH 4 precipitates. Gypsum was identified as the only crystalline phase in the pH 6, 8 and 10 precipitates, but closer examination of the XRD patterns indicated the presence of 2 broad peaks at d-spacings of ~0.29 nm and ~0.17 nm (Figures 4.18b, 4.18c and 4.18d), which is similar to the µXRD results noted for the precipitates formed at pH 6 and 10 using NaOH as the base. These broad peaks are presumed to indicate the presence of an amorphous ferric arsenite phase formed from the transformation of tooeleite.

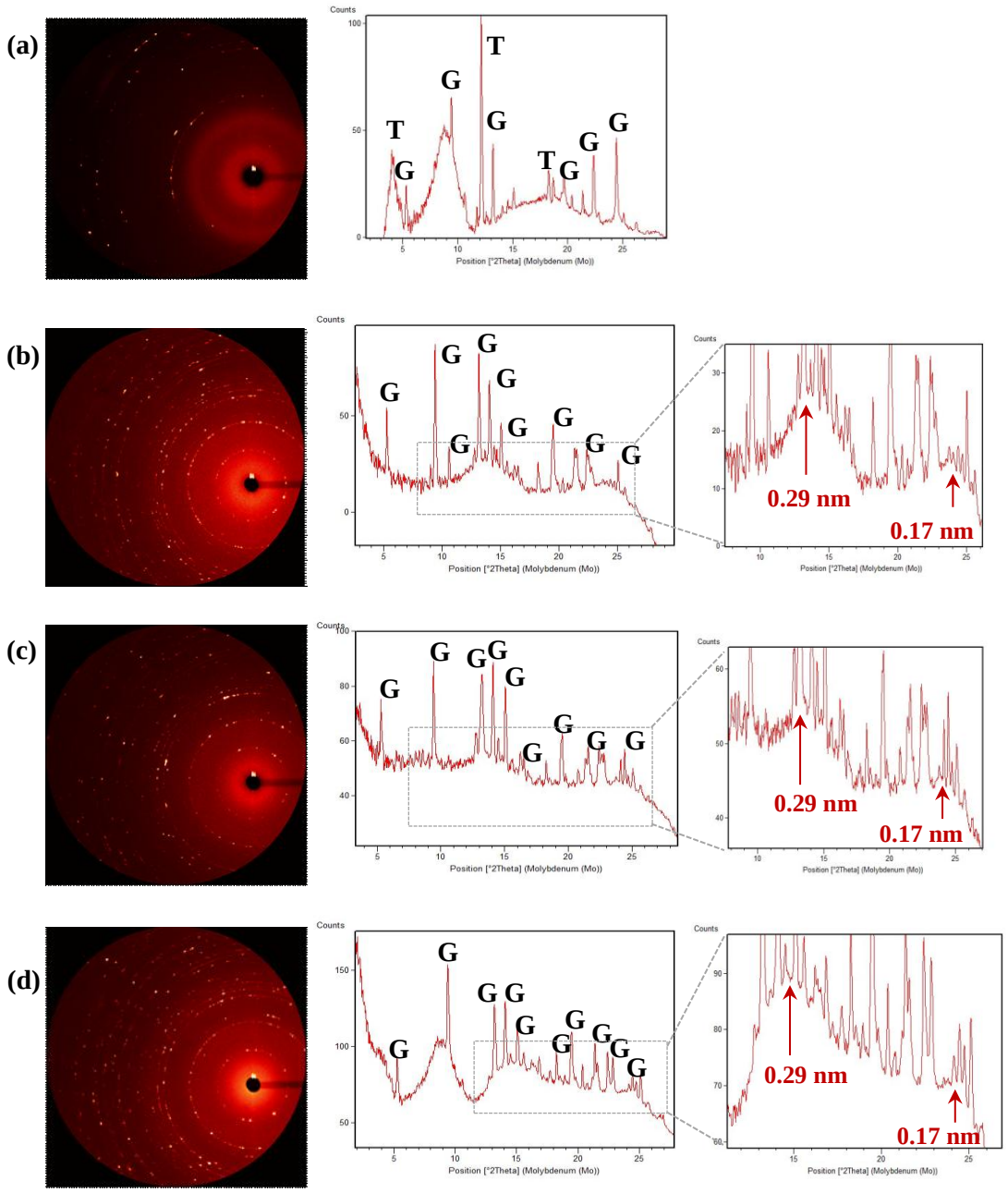

Figure 4.18: 2D μXRD images and integrated μXRD patterns of powder samples of gypsum-bearing tooeleite precipitates formed from solutions of Fe:As=1 at (a) pH 4 (b) pH 6 (c) pH 8 and (d) pH 10 at 25˚C using $Ca(OH)_2$ as the base. The peaks labeled G and T represent gypsum and tooeleite respectively.

4.3.2.3.3. Fe speciation analysis

Iron K-edge μXANES spectra were collected on tooeleite and gypsum-bearing tooeleite powder samples in order to characterize the Fe-bearing phases contained in the precipitates, and to confirm if ferrihydrite was present in the precipitates. The μXANES spectra of the Fe standards have distinct features and can be used to identify the Fe-bearing mineral species in the precipitates. According to Paktunc et al. (2008), ferrihydrite begins to precipitate out of solution in the pH range 2-3. Consequently, ferrihydrite has been suggested as a potential component of the tooeleite and gypsum-bearing precipitates as it may also form in the pH range 2 to 3.5 during the precipitation of tooeleite, particularly at local levels with high concentrations of the base. The normalized Fe μXANES spectra of the standards, tooeleite (NFA127; NFA12760 and NFA12795), and gypsum-bearing tooeleite precipitates (CFA127) are presented in Figure 4.19. NFA127 and CFA127 were formed at pH 2.7 and 25˚C from Fe(III)-As(III) solutions (initial Fe:As =1) using NaOH and $Ca(OH)_2$ as the bases respectively. NFA12760 and NFA12795 were formed under pH 2.7 conditions from Fe(III)-As(III) solutions (initial Fe:As =1) at 60˚C and 95˚C respectively using NaOH as the base. The μXANES spectra of the selected regions in the thin section were fitted with the spectra of standards using linear combination fitting and the results are summarized in Table 4.8.

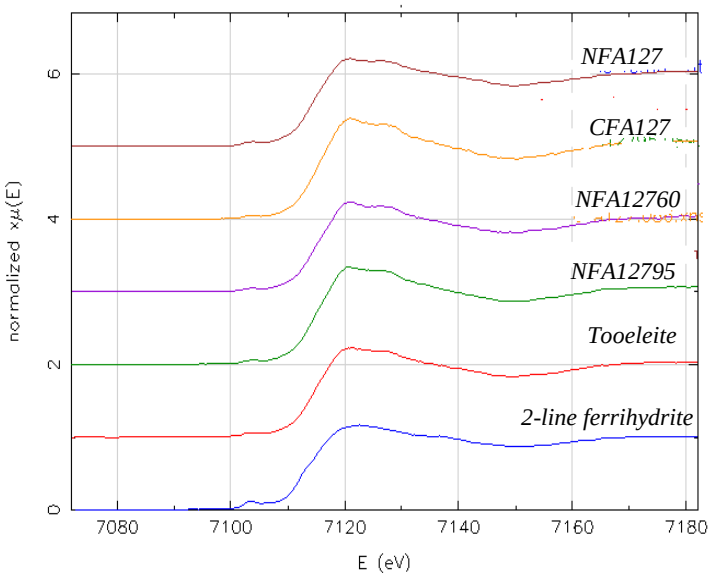

Figure 4.19: Fe K-edge μXANES spectra of Fe bearing standards (2-line ferrihydrite and tooeleite) and (a) tooeleite precipitates 25˚C (NFA127) (b) gypsum-bearing tooeleite precipitates 25˚C (CFA127) (c) tooeleite precipitates 60˚C (d) tooeleite precipitates 95˚C (NFA127)

Table 4.8: Linear combination fitting (LCF) results determined using the Fe K-edge μXANES spectra of 2-line ferrihydrite and tooeleite as the standards

Samples	LCF results (%)	
	Tooeleite	2-line ferrihydrite
NFA127	83.8	16.2
CFA127	100	0
NFA12760	100	0
NFA12795	100	0

Fitted model spectra of less than 5% were considered negligible as they did not improve the fits. Linear combination fitting of the μXANES spectra of the powder samples to those of the standards indicated that tooeleite is the predominant compound in the tooeleite (NFA127; NFA12760; NFA12795) and gypsum-bearing tooeleite precipitates (CFA127). 2-line ferrihydrite was also identified as a component of the tooeleite precipitates (NFA127) formed at 25˚C,

indicating that trace amounts of ferrihydrite were formed during the precipitation of tooeleite at pH 2.7.

4.3.3. Sulphate analysis

Table 4.9 presents the sulphate concentration of solids precipitated from an Fe(III)-As(III) solution (Fe:As molar ratio = 1.0) at pH 2.7, 4, 6 and 8, using NaOH as the base.

Table 4.9: Sulphate concentrations of tooeleite (Fe:As=1)

Sample (precipitates)	Sulphate (wt%)	Phases (μXRD analysis)
pH 2.7 †	10	Tooeleite
pH 4 †	4.6	Tooeleite - partial transformation
pH 6 †	0.7	Ferric arsenite
pH 8 †	0.3	Ferric arsenite

†pH 2.7, pH 4, pH 6, pH 8 represent the precipitates formed from an Fe(III)-As(III) solution (initial Fe:As molar ratio=1) at pH 2.7, 4, 6 and 8 respectively, using NaOH as base.

According to the synchrotron-based μXRD analytical results in Section 4.3.2.3, the pH 2.7 and 4 precipitates consist of tooeleite, while an amorphous phase presumed to be ferric arsenite, was identified in the pH 6 and 8 precipitates. For a comparative study, the sulphate content of the As(III)-bearing ferrihydrite (As(III)-Fh) precipitates formed at pH 4.5 from Fe(III)-As(III) solution (Fe:As molar ratio = 4.0) using NaOH as base was also evaluated. Tooeleite has a ~10% sulphate content, and is only stable in the pH range 2 to 3.5 (Nishimura and Robins, 2008). The results illustrated in Table 4.9 indicate that the sulphate content in the tooeleite precipitates formed at pH 2.7 decreased markedly with increasing pH, suggesting that tooeleite transfoms to an equimolar ferric arsenite at pH>4 with significantly decreasing amounts of sulphate. The As(III)-Fh (Fe:As molar ratio = 4.0) precipitates formed at pH 4.5 had a low sulphate concentration (0.2 wt%).

4.3.4. Tooeleite precipitation at elevated temperature

This study was conducted in order to understand the precipitation mechanism of tooeleite from NaOH neutralized systems with varying initial Fe:As molar ratios (1.0, 1.2 and 1.5) and elevated temperatures (25˚C, 60˚C and 95˚C) at pH 2 and 2.5. The initial solution Fe:As molar ratios of 1.0, 1.2 and 1.5 were used to represent the precipitation of tooeleite from initial solutions of low Fe (Fe:As=1.0); ideal Fe (Fe:As=1.2) and excess Fe (Fe:As =1.5).

Figure 4.20 presents the precipitation of tooeleite from initial solutions of Fe:As=1.0 at elevated temperatures (25˚C, 60˚C and 95˚C) and at pH 2, 2.2 and 2.5. The precipitation of tooeleite from initial solutions of Fe:As=1.2 and Fe:As=1.5 at 25˚C, 60˚C and 95˚C (pH 2 and 2.5) is presented in Appendix A.3. The kinetics results indicate that the As removal efficiency is dependent on the precipitation pH and initial Fe:As molar ratio. A retention time of 1 hour was found to be required for the precipitation of tooeleite from solution and the attainment of quasi-equilibrium. A retention time shorter than 1 hour would result in lower As removal efficiencies, while a longer retention time would marginally improve the As removal efficiencies. At 25˚C, 60˚C and 95˚C, equilibrium was generally achieved after 9 hours for the Fe:As=1.0, 1.2 and 1.5 systems at pH 2 and 2.5. At 25˚C, 60˚C and 95˚C, the maximum As removal efficiency was achieved for solutions with initial Fe:As ratio=1.5 at pH 2.5 (25˚C = ~90%; 60˚C = ~90%; 95˚C = ~84%) due to the presence of excess Fe.

Bulk XRD analysis of the precipitates formed at pH 2 and 2.5 (initial Fe:As ratio=1.0; 25˚C, 60˚C and 95˚C) after retention times of 1 hour and 24 hours, indicated the presence of tooeleite (Figure 4.21). XRD analysis of the precipitates formed at pH 2 and 2.5 after retention

times of 1 hour and 24 hours from initial solutions of Fe:As=1.2 and Fe:As=1.5 at 25˚C, 60˚C and 95˚C is presented in Appendix A.3. The high temperature precipitates (60˚C and 95 ˚C) appeared to be more crystalline than the ambient temperature precipitates. Furthermore, the high temperature precipitates (60˚C and 95 ˚C) had better settling and filtration properties than those formed under ambient conditions, probably due to their crystalline nature.

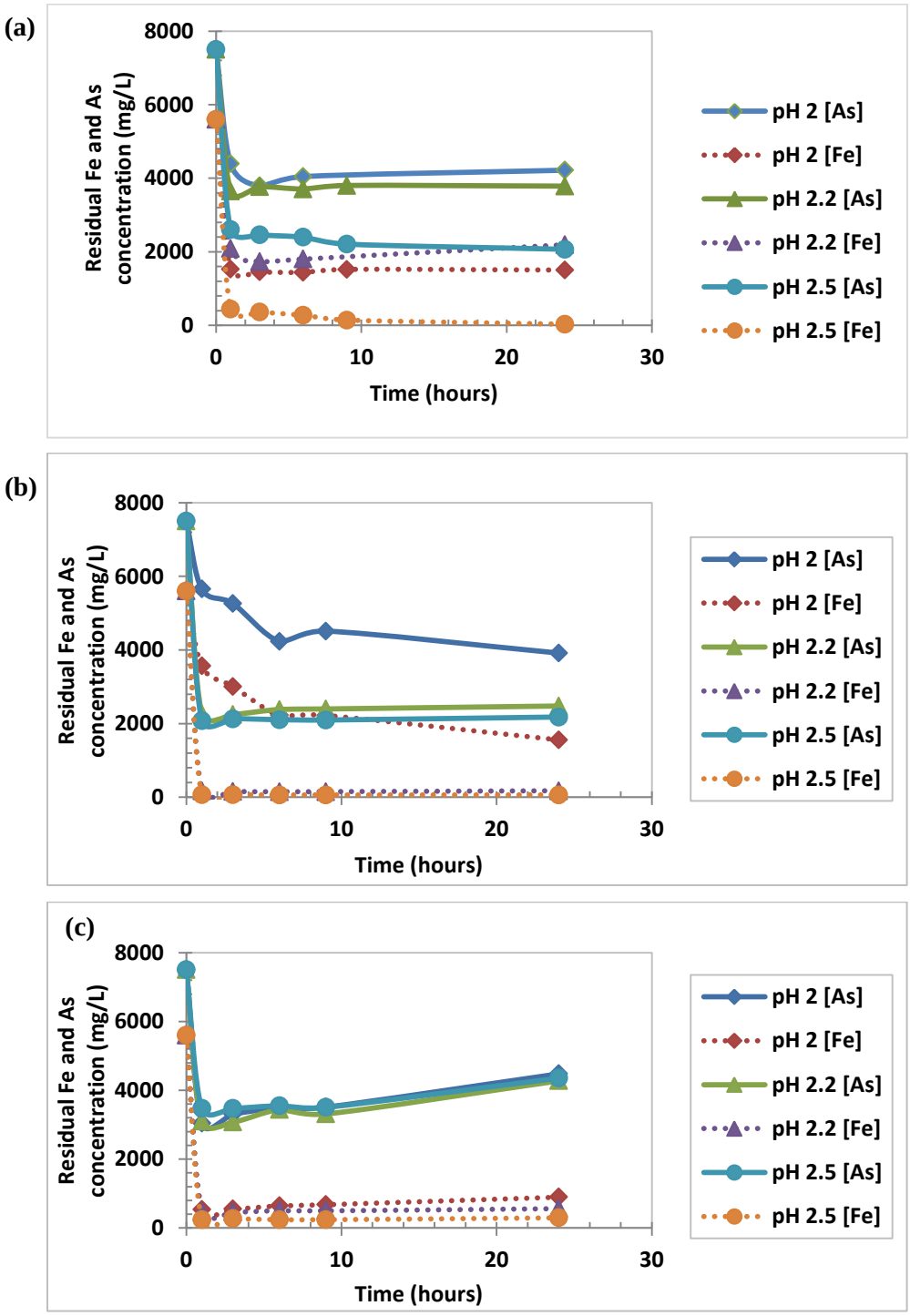

Figure 4.20: Kinetics of As and Fe removal from initial solution Fe:As=1 using NaOH at: (a) 25˚C (b) 60˚C (c) 95˚C (initial As concentration = 7.5 g/L)

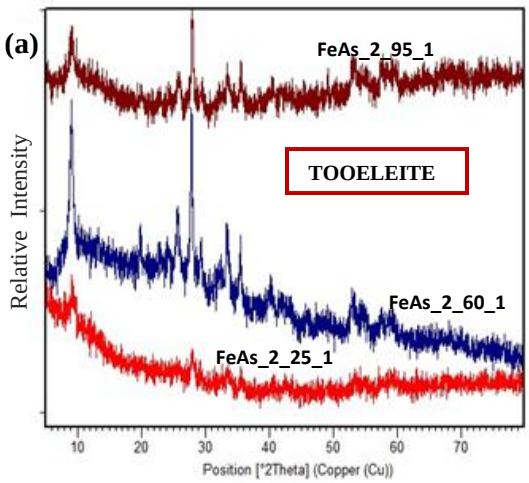

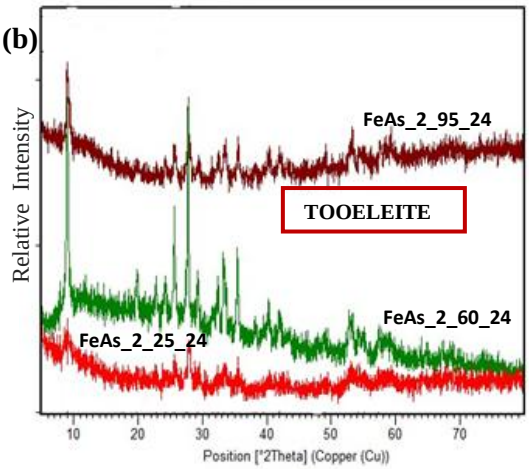

(a) Fe:As=1; pH 2; Equilibration time = 1 hour
*25˚C (FeAs_2_25_1)
*60˚C (FeAs_2_60_1)
*95˚C (FeAs_2_95_1)

(b) Fe:As=1; pH 2; Equilibration time of 24 hours)
*25˚C (FeAs_2_25_24)
*60˚C (FeAs_2_60_24)
*95˚C (FeAs_2_95_24)

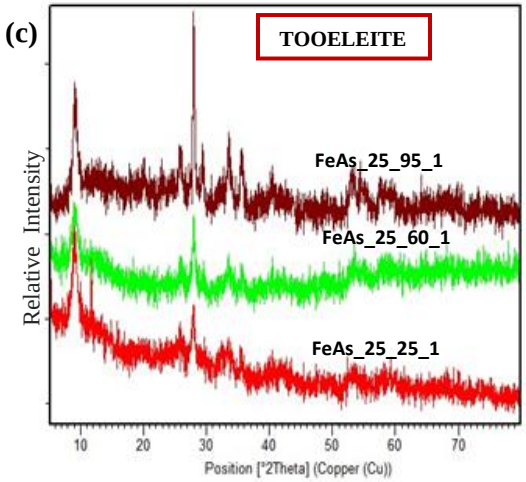

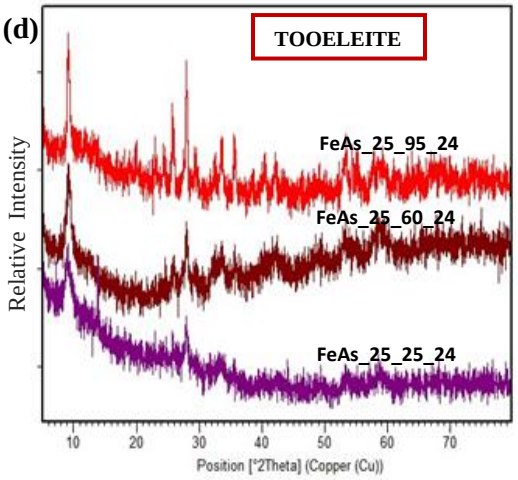

(c) Fe:As=1; pH 2.5; Equilibration time = 1 hour
*25˚C (FeAs_25_25_1)
*60˚C (FeAs_25_60_1)
*95˚C (FeAs_25_95_1)

(d) Fe:As=1; pH 2.5; Equilibration time of 24 hours)
*25˚C (FeAs_25_25_24)
*60˚C (FeAs_25_60_24)
*95˚C (FeAs_25_95_24)

Figure 4.21: XRD patterns of tooeleite precipitates formed at pH 2 (a and b) and pH 2.5 (c and d) (Fe:As=1) using NaOH as the base

4.3.5. Stability experiments

4.3.5.1. Short-term leaching test (US EPA TCLP)

Figure 4.22 presents As leachability of the precipitates formed at pH 2.5, 2.7, 3, 4, 6, 8 and 10 from Fe(III)-As(III) solutions (Fe:As = 1.0, 1.5 and 2.0), at ambient temperature and using NaOH and $Ca(OH)_2$ as the bases. Based on the characterization results in Section 4.3.2., tooeleite was identified in the pH 2.5, 2.7, 3, 4 precipitates. There was probably a minor quantity of ferric arsenite present in the pH 4 precipitates resulting from the partial transformation of tooeleite, although this was not identified by synchrotron-based μXRD analysis. Ferric arsenite, resulting from the transformation of tooeleite, was identified in the pH 6, 8 and 10 precipitates. Gypsum was also identified in the $Ca(OH)_2$ neutralized system precipitates.

A high TCLP As leachability was exhibited by all the precipitates from both the NaOH and $Ca(OH)_2$ neutralized systems. The TCLP As leachability was reduced for the precipitates formed from solutions with higher initial Fe:As molar ratio (Fe:As=2.0), but was higher for precipitates formed at pH>6. The high TCLP As leachability of the pH 2.5, 2.7 and 3 precipitates (Fe:As=1.0) could also be attributed to the presence of minor amounts of arsenolite formed as a result of the high As concentrations and shortage of Fe in solution. The TCLP As leachability of the precipitates formed from initial solutions of Fe:As=1.0, 1.5 and 2.0 exceeded the maximum Canadian MMER (Environment Canada, 1977; Metal Mining Effluent Regulations, 2002) and US EPA TCLP (US EPA, 1992) legislative limits of 0.5 mg/L (monthly mean concentration) and 5 mg/L for mining effluents respectively, and the residues would therefore be classified as hazardous waste. The final pH of the leachates ranged from 4.67 – 7.37.

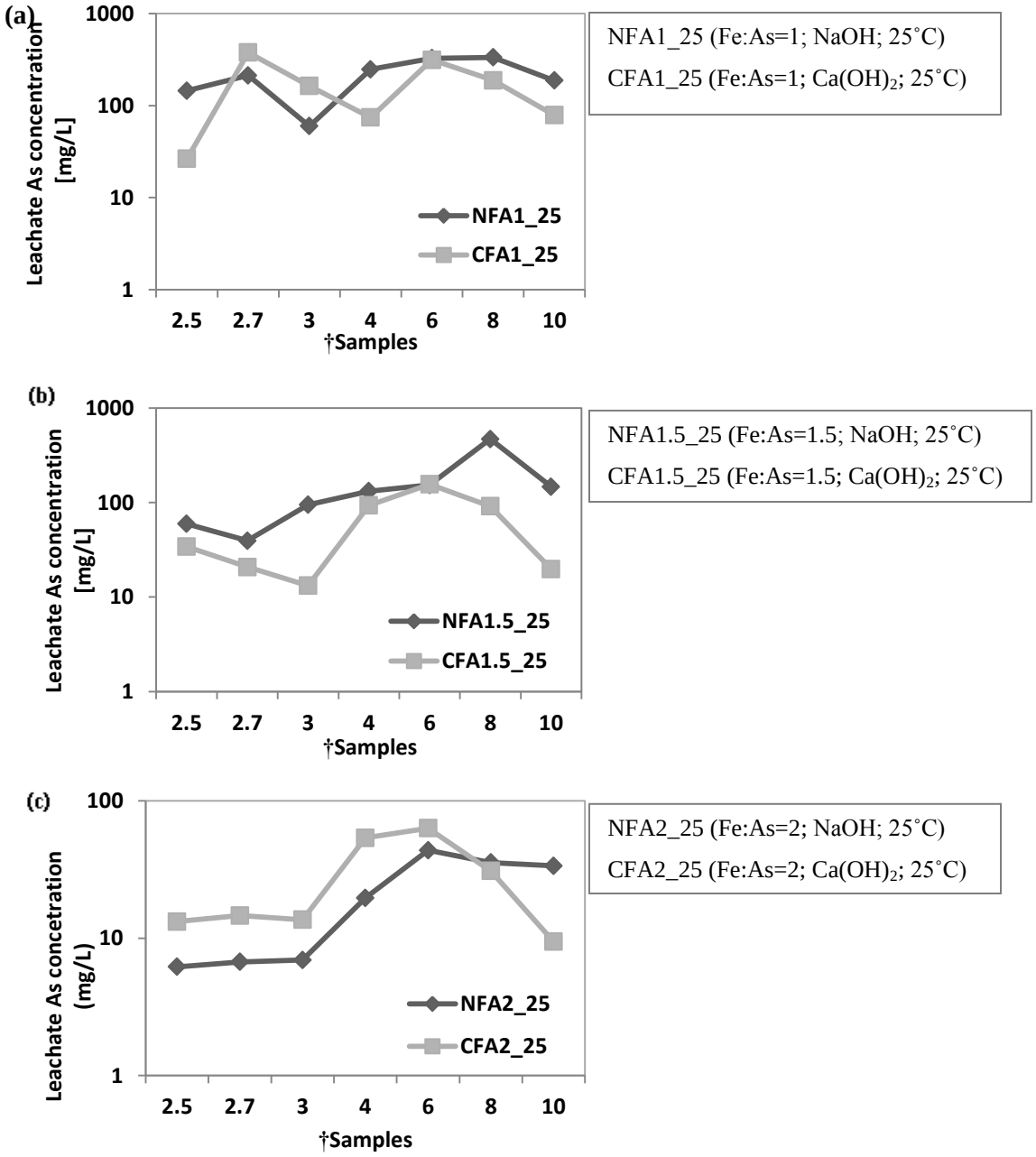

Figure 4.22: As concentration of the leachates for precipitates formed from Fe(III)-As(III) systems at specific pH values of 2.5, 2.7, 3, 4, 6, 8, and 10 using NaOH and $Ca(OH)_2$ as the bases. Fe:As represents the Fe:As molar ratio. †Samples represents the precipitates formed at the specific pH values of of 2.5, 2.7, 3, 4, 6, 8, and 10

4.3.5.2. Long-term leaching tests

The long-term stability of tooeleite and gypsum-bearing tooeleite precipitates was studied under various pH conditions (4, 5, 7, 9) at room temperature and 60˚C. The tooeleite and gypsum-bearing tooeleite precipitates used in these tests were precipitated at pH 2.7 from an initial solution of Fe:As = 1 using NaOH and $Ca(OH)_2$ as bases respectively. Figures 4.23 and 4.24 illustrate the changes of the leachate As concentrations and pH as a function of time at 25˚C for the tooeleite and gypsum-bearing tooeleite precipitates respectively. At the end of the leaching test (after ~30 weeks), the pH 5 leachates of both tooeleite and gypsum-bearing tooeleite had the lowest As concentration of 39.3 mg/L (3.8% As dissolution) and 34.2 mg/L (5.7% As dissolution) respectively, indicating that tooeleite and gypsum-bearing tooeleite precipitates are most stable under pH 5 conditions at 25˚C. The As concentration of the final leachates of tooeleite and gypsum-bearing tooeleite indicate that both phases were least stable under pH 7 conditions. Equilibrium of residual As in solution was not achieved by the end of the leaching test for either the tooeleite or gypsum-bearing tooeleite precipitates. Over the duration of the leaching tests, generally negligible amounts of Fe were released from both tooeleite (<3 mg/L) and gypsum-bearing tooeleite (<6 mg/L) under the various pH leaching conditions (Appendix A.4.). This indicates that the transformation of tooeleite and gypsum-bearing tooeleite occurred at pH>4, and was faster under higher pH conditions, as illustrated in Equation 4.2:

$$\mathbf{6Fe_2O_3.5As_2O_3.2SO_3.12H_2O_{(s)} + 12H_2O_{(l)} = 12FeOOH_{(s)} + 10H_3AsO_{3\,(aq)} + 2H_2SO_{4\,(aq)}} \quad \mathbf{(4.2)}$$

At the start of the tests (after 1 day), the pH of the tooeleite and gypsum-bearing tooeleite leachates decreased to ~pH 2.8 due to the acid generated by the tooeleite transformation at higher pH regimes (Figures 4.23a and 4.24a; Equation 4.2). After 1 day, the pH of the tooeleite and

gypsum-bearing tooeleite leachates fluctuated and gradually increased for 9 weeks, and then remained almost unchanged from 11 to 30 weeks. The final pH of the tooeleite and the gypsum-bearing tooeleite leachates was in the range 5.19-8.76 and 4.65-7.49 respectively.

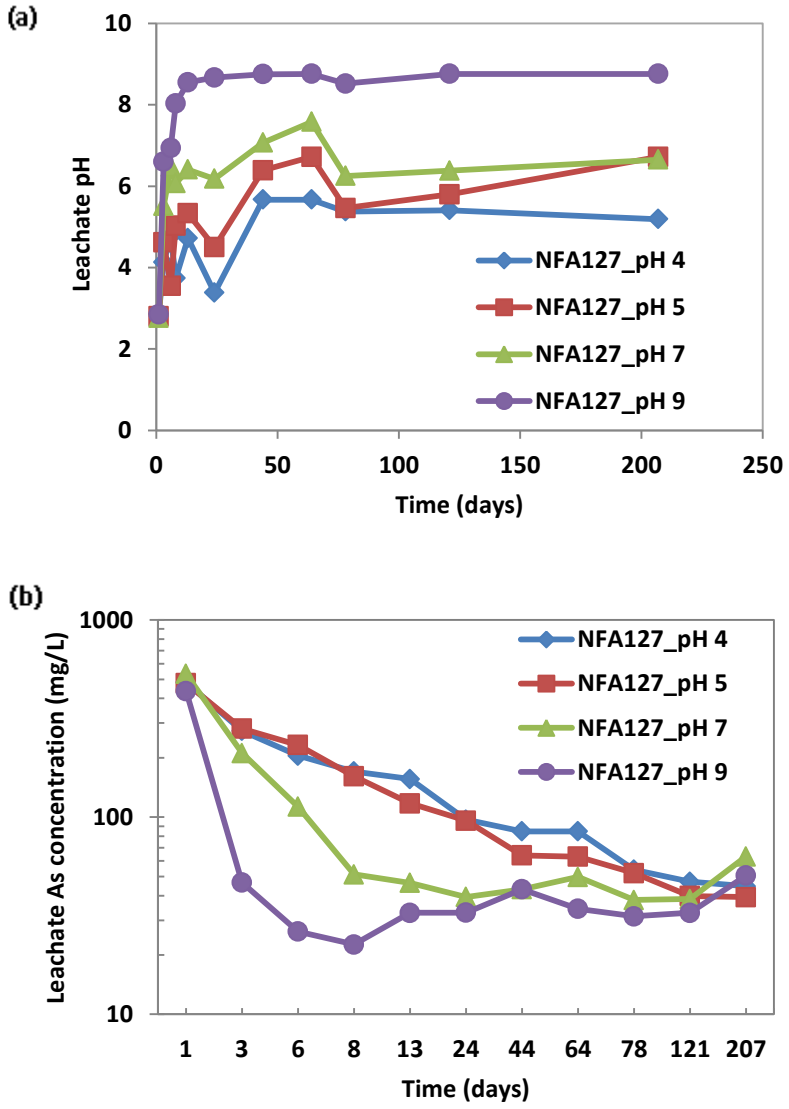

Figure 4.23: Leachate (a) pH and (b) As concentration as a function of time for tooeleite precipitates subjected to long term leaching tests under pH 4, 5, 7 and 9 at 25˚C. NFA127 denotes tooeleite precipitates formed at pH 2.7 with NaOH.

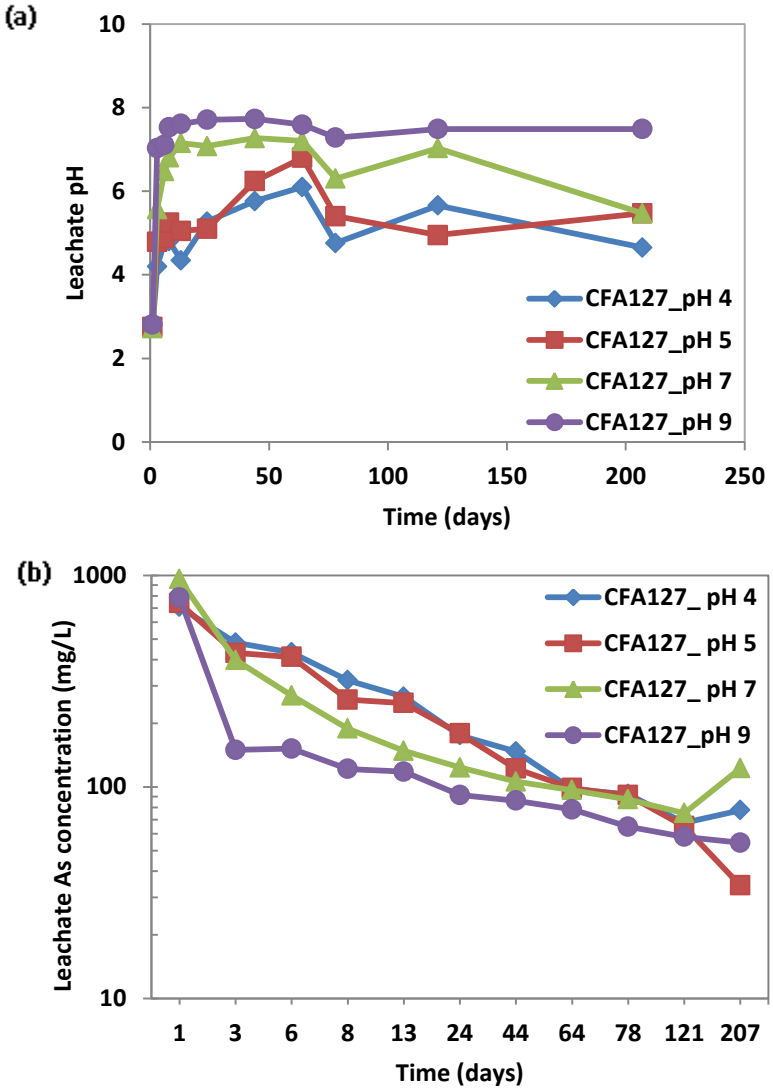

Figure 4.24: Leachate (a) pH and (b) As concentration as a function of time for gypsum-bearing tooeleite subjected to long term leaching tests under pH 4, 5, 7 and 9 at 25˚C. CFA127 denotes gypsum-bearing tooeleite precipitates formed at pH 2.7 with $Ca(OH)_2$ as the base.

The changes in As concentration and pH of the leachates as a function of time for the leaching tests conducted at 60˚C for the tooeleite and gypsum-bearing tooeleite precipitates are presented in Figures 4.25 and 4.26 respectively.

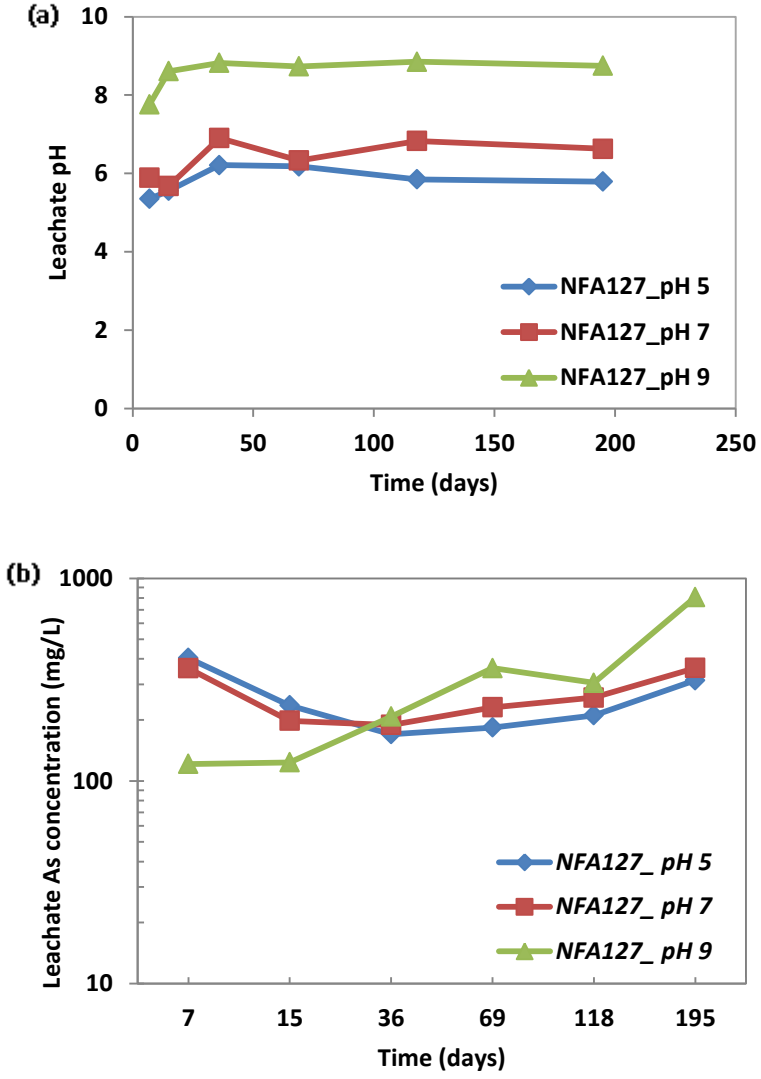

Figure 4.25: Leachate (a) pH and (b) As concentration as a function of time for tooeleite precipitates subjected to long term leaching tests under pH 5, 7 and 9 at 60˚C. NFA127 denotes tooeleite precipitates formed at pH 2.7 with NaOH as the base.

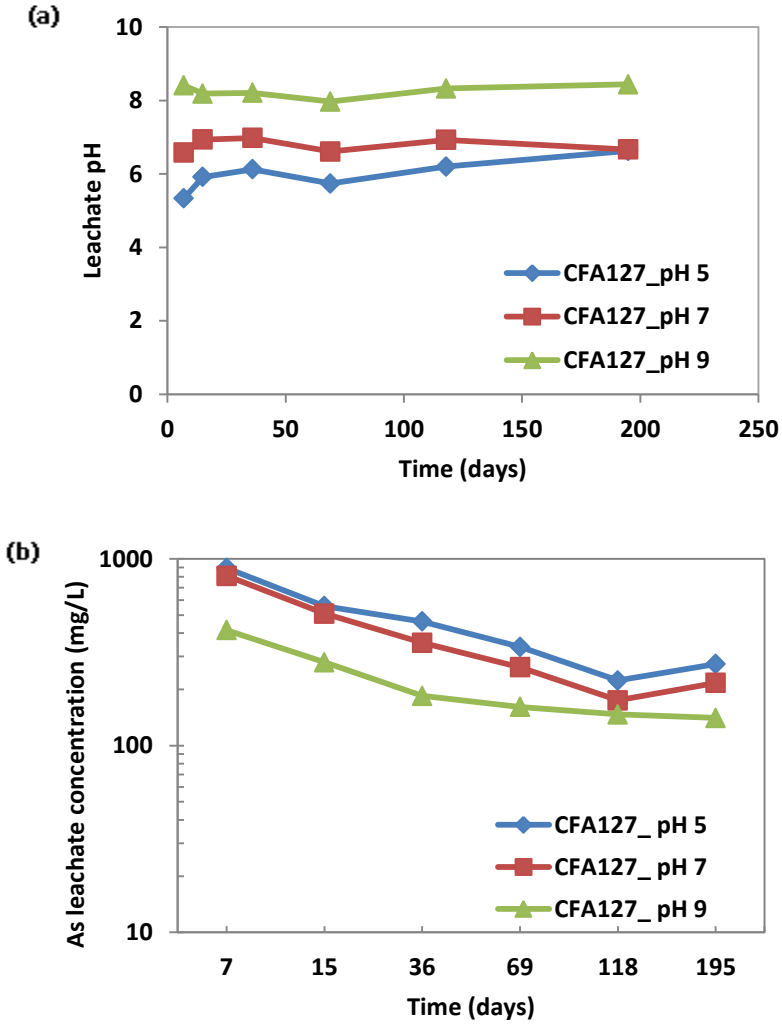

Figure 4.26: Leachate (a) pH and (b) As concentration as a function of time for gypsum-bearing tooeleite precipitates subjected to long term leaching tests under pH 5, 7 and 9 at 60˚C. CFA127 denotes tooeleite precipitates formed at pH 2.7 using $Ca(OH)_2$ as base.

Under accelerated aging at 60˚C for ~30 weeks, tooeleite is most stable under pH 5 conditions (313.8 mg/L; 30% As dissolution) while gypsum-bearing tooeleite is most stable under pH 9 conditions (140.7 mg/L; 23% As dissolution). Equilibrium of residual As in solution was not achieved after the ~30 weeks of leaching of either tooeleite or gypsum-bearing tooeleite.

Generally, negligible amounts of Fe were released from both tooeleite (<3 mg/L) and gypsum-bearing tooeleite (< 6 mg/L) precipitates during the leaching test (Appendix A.4.).

As illustrated in Figures 4.27 and 4.28, characterization of the final solid residues from both the 25˚C and 60˚C leaching tests using XRD analysis identified tooeleite in tooeleite precipitates, and tooeleite and gypsum in the gypsum-bearing tooeleite precipitates. It is proposed that under high temperature conditions (60˚C), tooeleite crystallizes faster than it transforms to ferric arsenite, resulting in the release of As into solution (~25% As release) and the change in Fe:As molar ratio of the tooeleite precipitates from ~1.2 to ~1.5 (with no release of ferric iron into solution). Consequently, the high temperature residues are more crystalline than the ambient temperature residues as indicated by the XRD patterns. However, it is interesting to note that as the pH of the leaching media increased from 5 to 9, the XRD peaks of tooeleite and gypsum in the final solid residues from the respective media increasingly weakened.

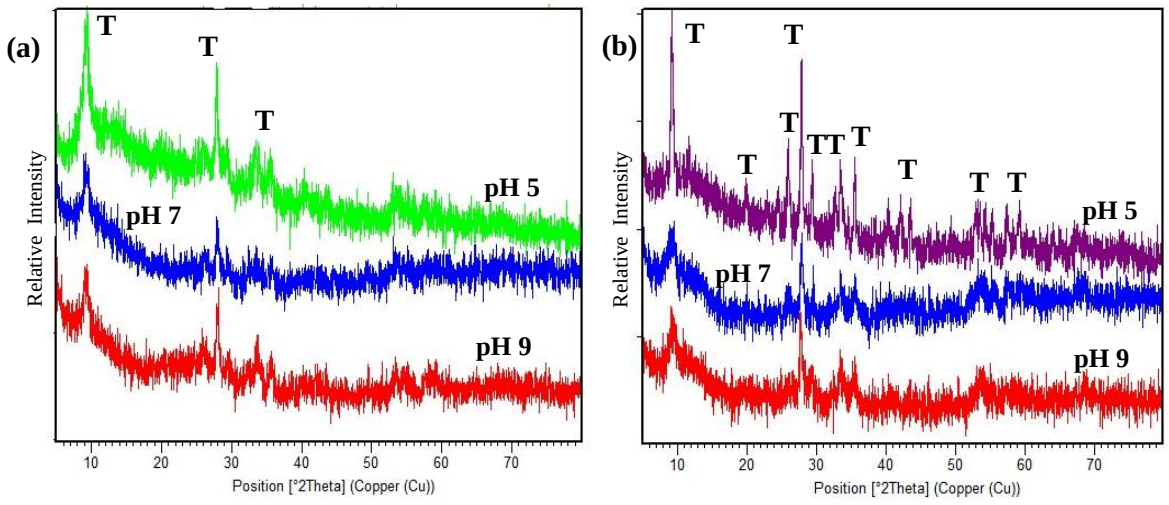

Figure 4.27: XRD patterns of the final solid residues of tooeleite precipitates subjected to long term leaching tests conducted at (a) 25 ˚C (b) 60˚C and pH 5, 7 and 9. T defines tooeleite

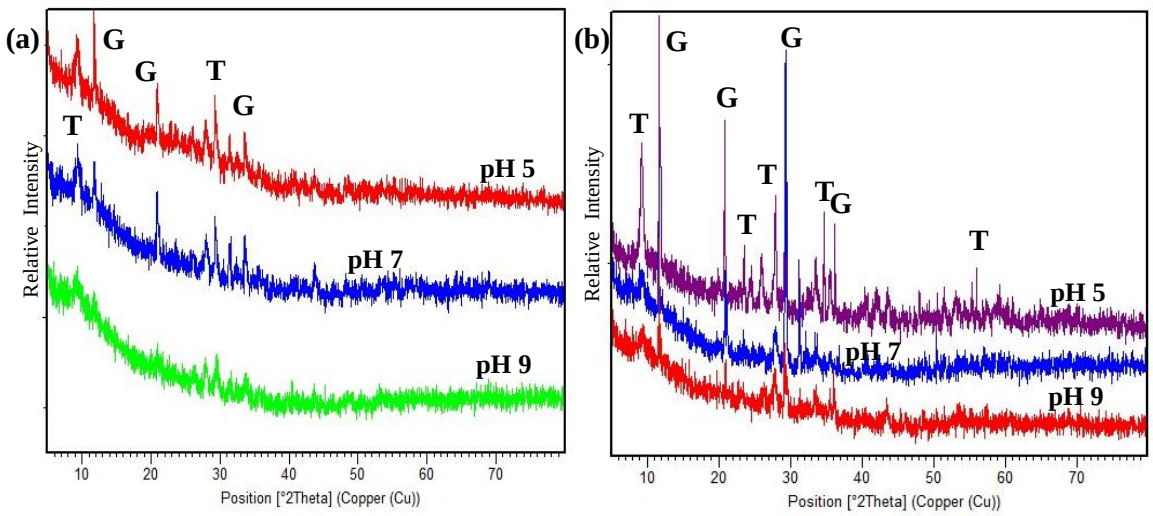

Figure 4.28: XRD patterns of the final solid residues of gypsum-bearing tooeleite precipitates subjected to long-term leaching tests conducted at (a) 25˚C (b) 60˚C under pH 5, 7 and 9 regimes. G and T denote gypsum and tooeleite respectively

4.3.6. High temperature precipitation

4.3.6.1. Effect of precipitation temperature and pH

High temperature precipitation of tooeleite at 60˚C and 95˚C was studied in order to evaluate if high temperature precipitation improved the As removal efficiency, and the stability of the precipitates formed. The precipitation tests were conducted using Fe(III)-As(III) solutions, (initial molar ratio of Fe:As =1), and NaOH and $Ca(OH)_2$ as the bases. The residual As concentration in solution as a function of pH for the precipitation tests conducted at 60˚C and 95˚C is illustrated in Figure 4.29. Increasing the precipitation temperature from 60˚C to 95˚C resulted in lower As uptake in the pH range 3 to 10, for both NaOH and $Ca(OH)_2$ neutralized systems. The employment of $Ca(OH)_2$ as the base led to lower residual As levels compared to NaOH. Figure 4.30 shows a comparison of the arsenic removal efficiency at 25˚C, 60˚C and 95˚C, following the neutralization of Fe(III)-As(III) solutions (Fe:As =1) using NaOH and

$Ca(OH)_2$. The arsenic uptake decreased with increasing temperature, with the highest arsenic removal (99.2% at pH 8) occurring at 25˚C. Higher As removal efficiencies were observed for the $Ca(OH)_2$ neutralized systems compared to the NaOH neutralized systems at all of the three temperatures (25˚C, 60˚C and 95˚C), which may be attributed to the presence of gypsum acting as seed and consequently promoting the efficient removal of As(III) from solution. For both the NaOH and $Ca(OH)_2$ neutralized systems, the As removal efficiency gradually increased with pH in the pH range 2 to 8, at 25˚C, 60˚C and 95˚C. However, in the pH range 8 to10 at 95˚C, the arsenic removal efficiency decreased in the NaOH neutralized system, probably due to the transformation of the As-bearing phase. In the $Ca(OH)_2$ neutralized system, a sudden sharp increase in the As removal efficiency was observed in the pH range 8-10 at 60˚C and 95˚C, which was presumed to be due to the fixation of As in the form of calcium arsenite. However, XRD analysis of the pH 10 precipitates did not identify the presence of calcium arsenite.

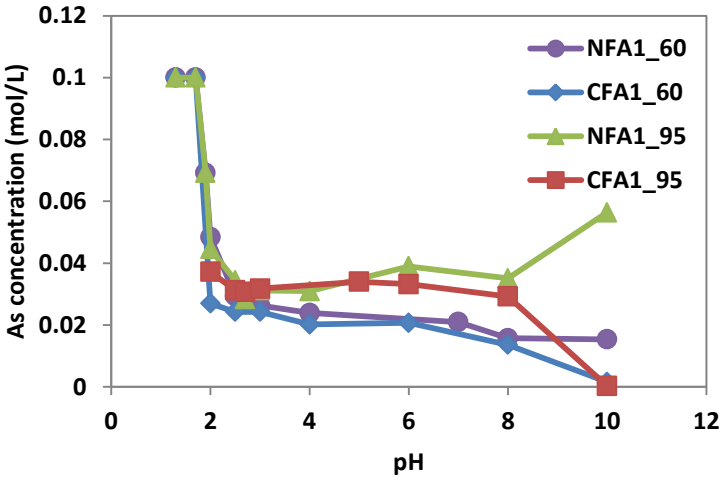

Figure 4.29: Residual As concentration in solution as a function of pH for Fe(III)-As(III) precipitation systems (Fe:As=1) at 25˚C, 60˚C and 95˚C using NaOH and Ca(OH)2 as the bases (Equilibration time = 1 hour). *NFA1_60 and NFA1_95 denote precipitates formed at 60˚C and 95˚C using NaOH as the base. *CFA1_60 and CFA1_95 denote gypsum-bearing precipitates formed at 60˚C and 95˚C, using $Ca(OH)_2$ as the base.

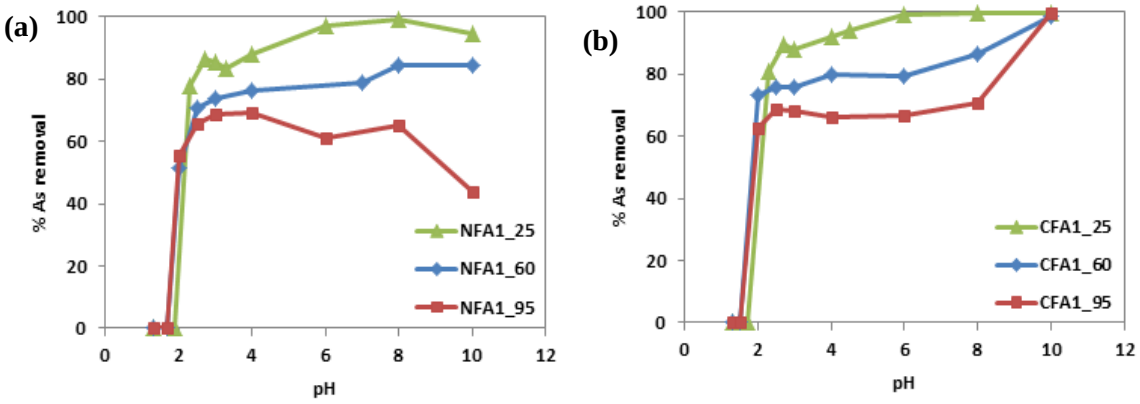

Figure 4.30: As removal efficiency as a function of pH for Fe(III)-As(III) precipitation systems (Fe:As=1) at 25˚C, 60˚C and 95˚C using (a) NaOH (b) $Ca(OH)_2$ as bases (Equilibration time = 1 hour). *NFA1_25, NFA1_60 and NFA1_95 denote precipitates formed at 25˚C, 60˚C and 95˚C using NaOH as the base. *CFA1_25, CFA1_60 and CFA1_95 denote gypsum-bearing precipitates formed at 25˚C, 60˚C and 95˚C using $Ca(OH)_2$ as the base.

Figure 4.31 illustrates the precipitate As:Fe molar ratio and As equilibrium concentration as a function of pH for Fe(III)-As(III) systems (Fe/As = 1.0) neutralized by NaOH at 60˚C and 95˚C. The precipitate As:Fe molar ratio is observed to be higher at 60˚C than at 95˚C. At 60˚C, the precipitate As:Fe molar ratio gradually increased in small increments with increasing pH (~0.73 mole As/mole Fe at pH 2 to ~0.85 mole As/mole Fe at pH 10). However at 95˚C, the initial precipitate As:Fe molar ratio (~0.73 mole As/mole Fe at pH 2) decreased with increasing pH with the precipitate As:Fe molar ratio being obtained at pH 10 (0.44 mole As/mole Fe). These results indicate that the precipitates formed at 95˚C have a lower As:Fe molar ratio than the precipitates formed at 60˚C. At higher pH regimes, the increased As solubility of the precipitates formed at 95˚C, compared to that of the precipitates formed at 60˚C, was probably caused by the transformation of tooeleite at 95˚C to a more crystalline phase, resulting in the change in the

As:Fe molar ratio of the precipitates from ~0.83 (Fe:As = ~1.2) to ~0.67 (Fe:As = ~1.5). The As:Fe molar ratio of ~0.67 (Fe:As = ~1.5) is consistent with the Fe:As molar ratio of crystalline tooeleite (Fe:As=1.5) from the mine waste from Tooele County, Utah that was characterized by Morin et al. (2007).

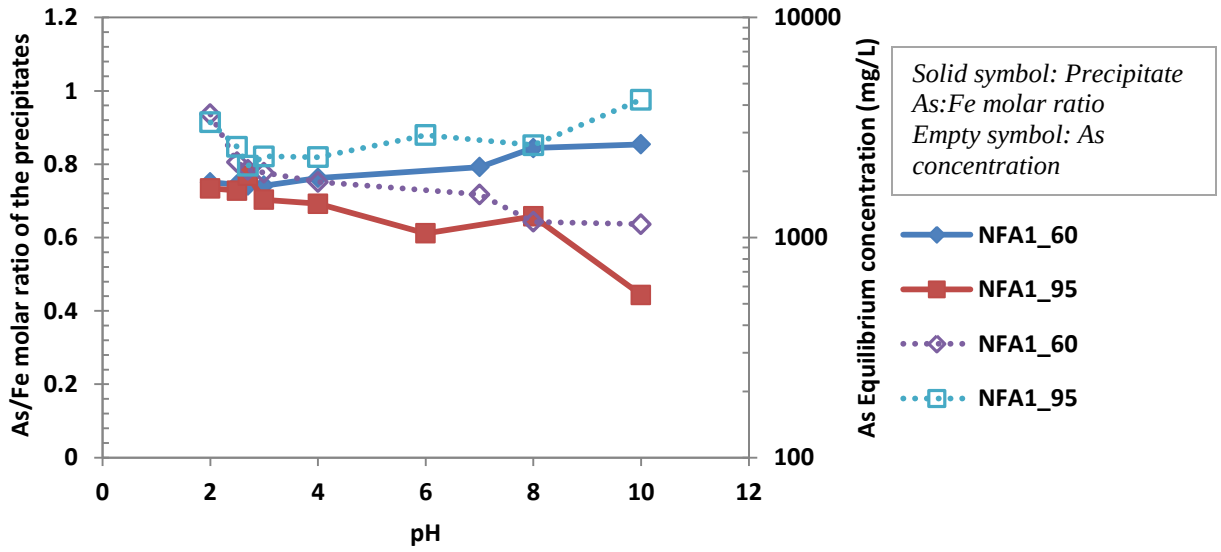

Figure 4.31: Precipitate As:Fe molar ratio and As equilibrium concentration as a function of pH for Fe(III)-As(III) precipitation systems (Fe:As=1) neutralized by NaOH at 60˚C and 95˚C (Equilibration time = 1 hour). *NFA1_60 denotes Fe:As=1 at 60˚C and *NFA1_95 denotes Fe:As=1 at 95˚C.

The precipitate As:Fe molar ratio and As equilibrium concentration as a function of pH for Fe(III)-As(III) systems (Fe/As = 1.0) neutralized by $Ca(OH)_2$ at 60˚C and 95˚C is presented in Figure 4.32. For both systems at 60˚C and 95˚C, the precipitate As:Fe molar ratio is observed to remain relatively stable in the pH range 3 to 8 (~0.8 mole As/mole Fe at 60˚C and ~0.7 mole As/mole Fe at 95˚C), and then to suddenly increase at pH 10 (1 mole As/mole Fe at 60˚C and 95˚C) probably due to the fixation of As in the form of ferric arsenite, as no Fe is released into solution.

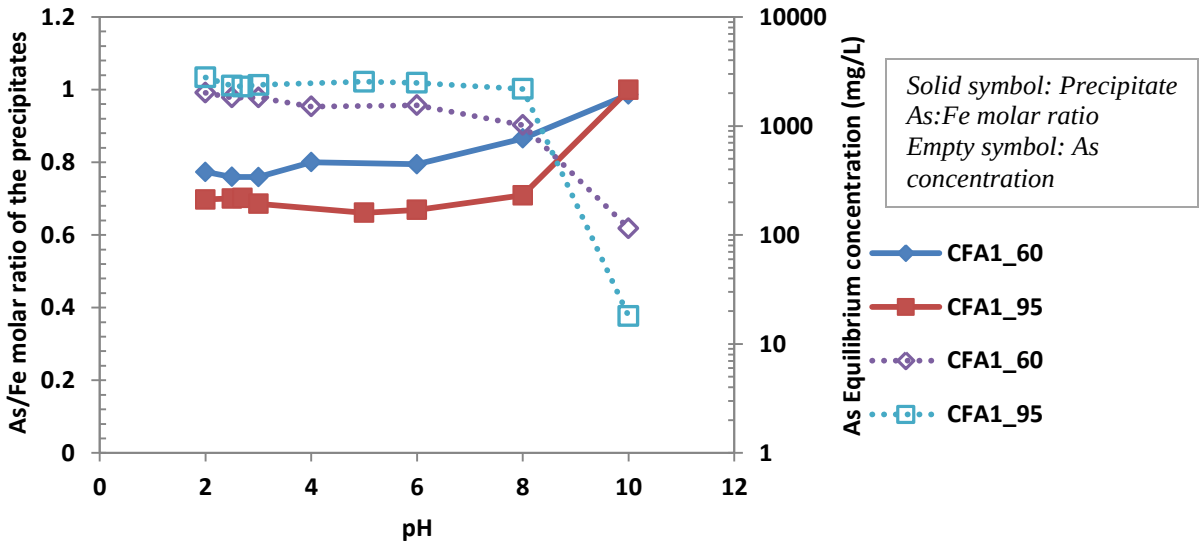

Figure 4.32: Precipitate As:Fe molar ratio and As equilibrium concentration as a function of pH for Fe(III)-As(III) precipitation systems (Fe:As=1) neutralized by $Ca(OH)_2$ at 60˚C and 95˚C (Equilibration = 1 hour). *CFA1_60 denotes Fe:As=1 at 60˚C. *CFA1_95 denotes Fe:As=1 at 95˚C.

4.3.6.2. Phase characterization

Figures 4.33 and 4.34 illustrate the bulk XRD spectra of the high temperature precipitates formed from Fe(III)-As(III) solutions (Fe:As =1) at 60˚C and 95˚C using NaOH and $Ca(OH)_2$ as the bases. XRD analysis identified tooeleite in the precipitates formed from the NaOH neutralized systems in the pH range 2 to 10 at 60˚C and 95˚C. Tooeleite and gypsum were identified in the precipitates obtained from the $Ca(OH)_2$ neutralized systems in the pH range 2 to 10 at 60˚C and 95˚C. The XRD results indicated that tooeleite precipitates, formed at 60˚C and 95˚C, retain their stability with increasing precipitation pH, and do not transform to ferric arsenite at pH >3.5, as was observed to occur in the ambient temperature precipitation system. Furthermore, the XRD spectra indicated that high temperature precipitation enhanced the crystallinity of tooeleite and gypsum-bearing precipitates.

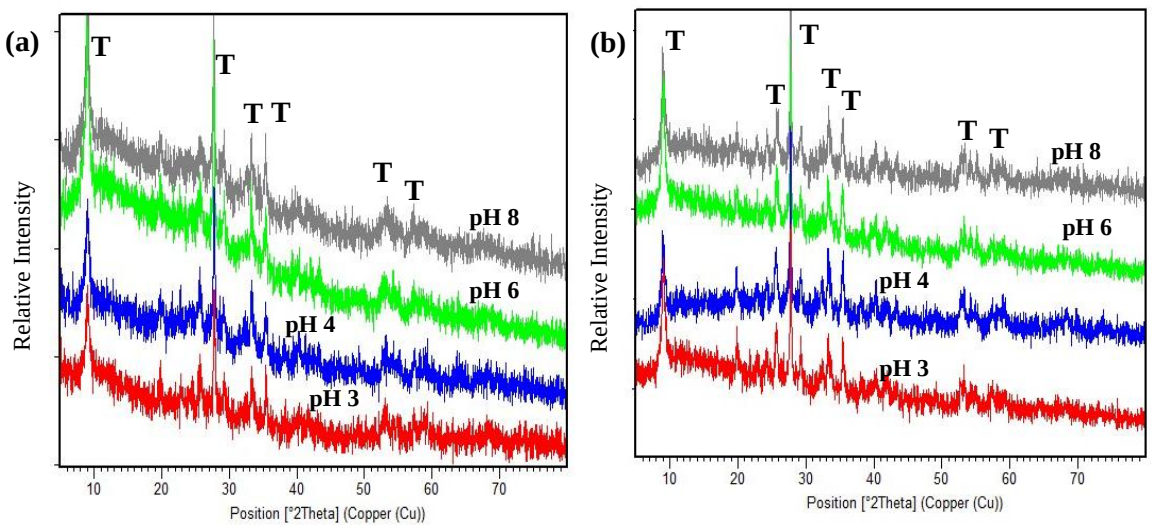

Figure 4.33: XRD patterns of high temperature precipitates formed at (a) 60˚C and (b) 95˚C from solutions of initial Fe:As=1 using NaOH as the base

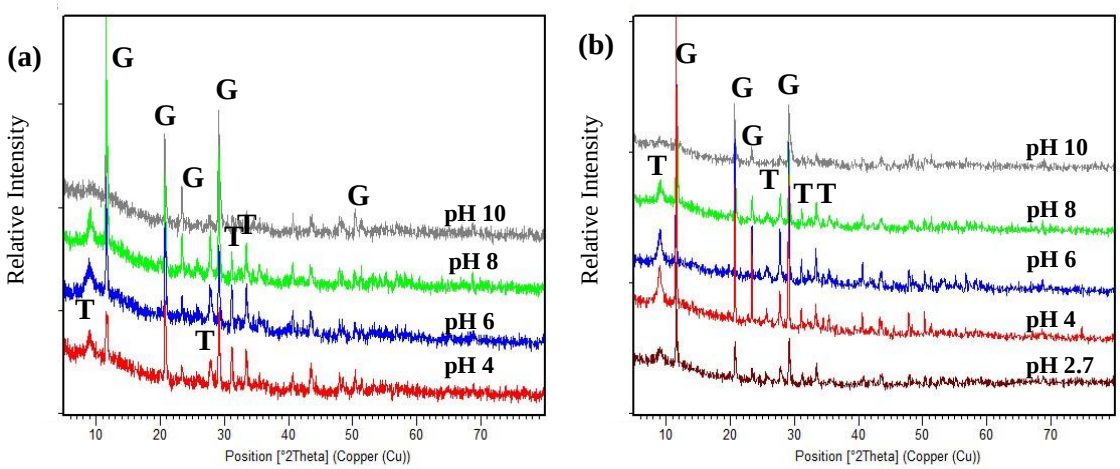

Figure 4.34: XRD patterns of high temperature precipitates formed at (a) 60˚C and (b) 95˚C from solutions of initial Fe:As=1 using Ca $(OH)_2$ as the base

The SEM images indicate that the tooeleite precipitates formed at 60˚C consist of clustered agglomerates of grains with a hairy texture (Figure 4.35A). The images of the tooeleite precipitates formed at 95˚C indicate that the grains become more compact but still retain their

hairy texture (Figure 4.35B). The gypsum-bearing tooeleite precipitates obtained at 60˚C and 95˚C consist of clustered tooeleite solids deposited on needle-like gypsum crystals (>5 µm), as is shown in Figures 4.35C and 4.35D.

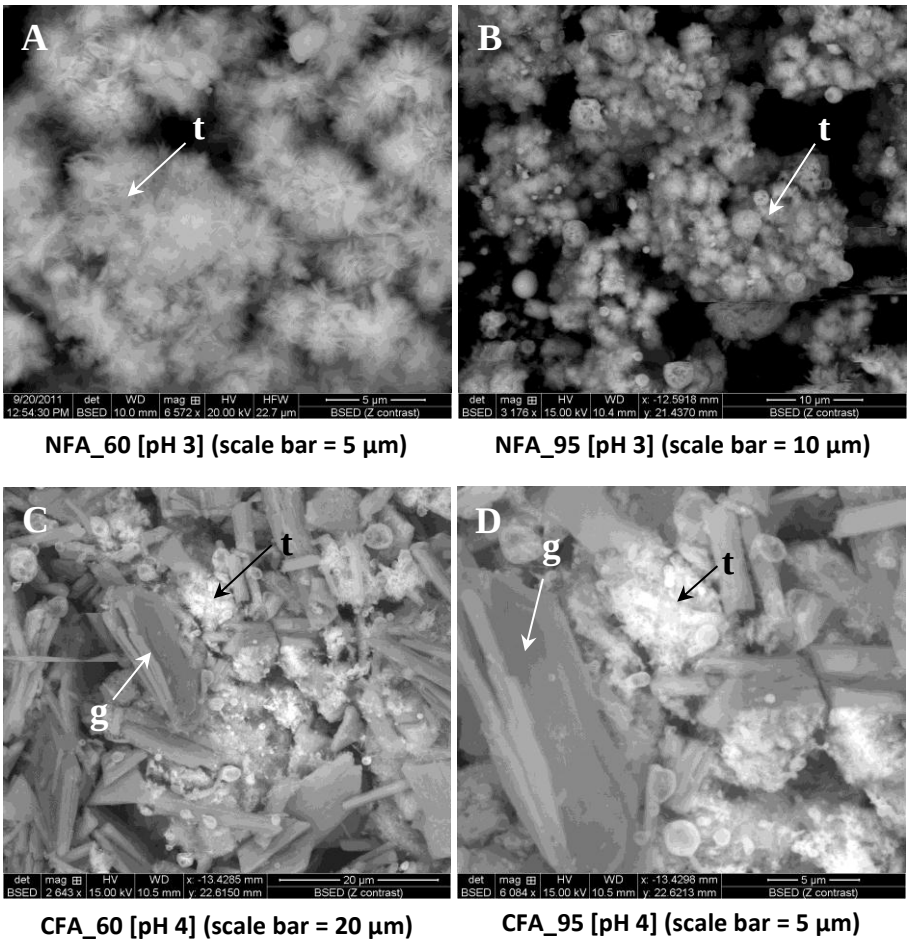

NFA_60 and NFA_95 denote precipitates formed from NaOH neutralized systems at 60˚C and 95˚C respectively.

CFA _60 and CFA_95 denote precipitates formed from $Ca(OH)_2$ neutralized systems at 60˚C and 95˚C respectively.

NFA_60 [pH 3] (scale bar = 5 µm) **NFA_95 [pH 3] (scale bar = 10 µm)**

CFA_60 [pH 4] (scale bar = 20 µm) **CFA_95 [pH 4] (scale bar = 5 µm)**

Figure 4.35: Morphology of high temperature precipitates formed at 60˚C and 95˚C from solutions of initial Fe:As=1 using NaOH and $Ca(OH)_2$ as bases

4.3.6.3. Stability experiments

The TCLP tests were conducted to evaluate the stability of the high temperature tooeleite-bearing precipitates. Figure 4.36 presents the As leachability results of the high temperature precipitates obtained at pH 2.5, 2.7, 3, 4, 6, 8, and 10, using NaOH and $Ca(OH)_2$ as bases.

In the NaOH neutralized system (Figure 4.36a), the most stable precipitates were obtained under pH 2.7 conditions at 60˚C (As leachability 15.5 mg/L) and under pH 2.5 conditions at 95˚C (As leachability 14.1 mg/L). The pH of the leachates ranged from 4.71 to 6.19. In the $Ca(OH)_2$ neutralized system, the most stable precipitates were obtained under pH 2.5 conditions at 60˚C (As leachability 17.9 mg/L) and at 95˚C (As leachability 17.9 mg/L) (Figure 4.36b). The pH of the leachates ranged from 4.9 to 8.3. A comparison of the TCLP results of the precipitates obtained at 25˚C, 60˚C and 95˚C from the $Ca(OH)_2$ neutralized systems is presented in Figure 4.36c. The TCLP results indicate that below pH 6, the 95˚C precipitates are the most stable phase. Above pH 6, the ambient temperature precipitates are more stable than the high temperature precipitates.

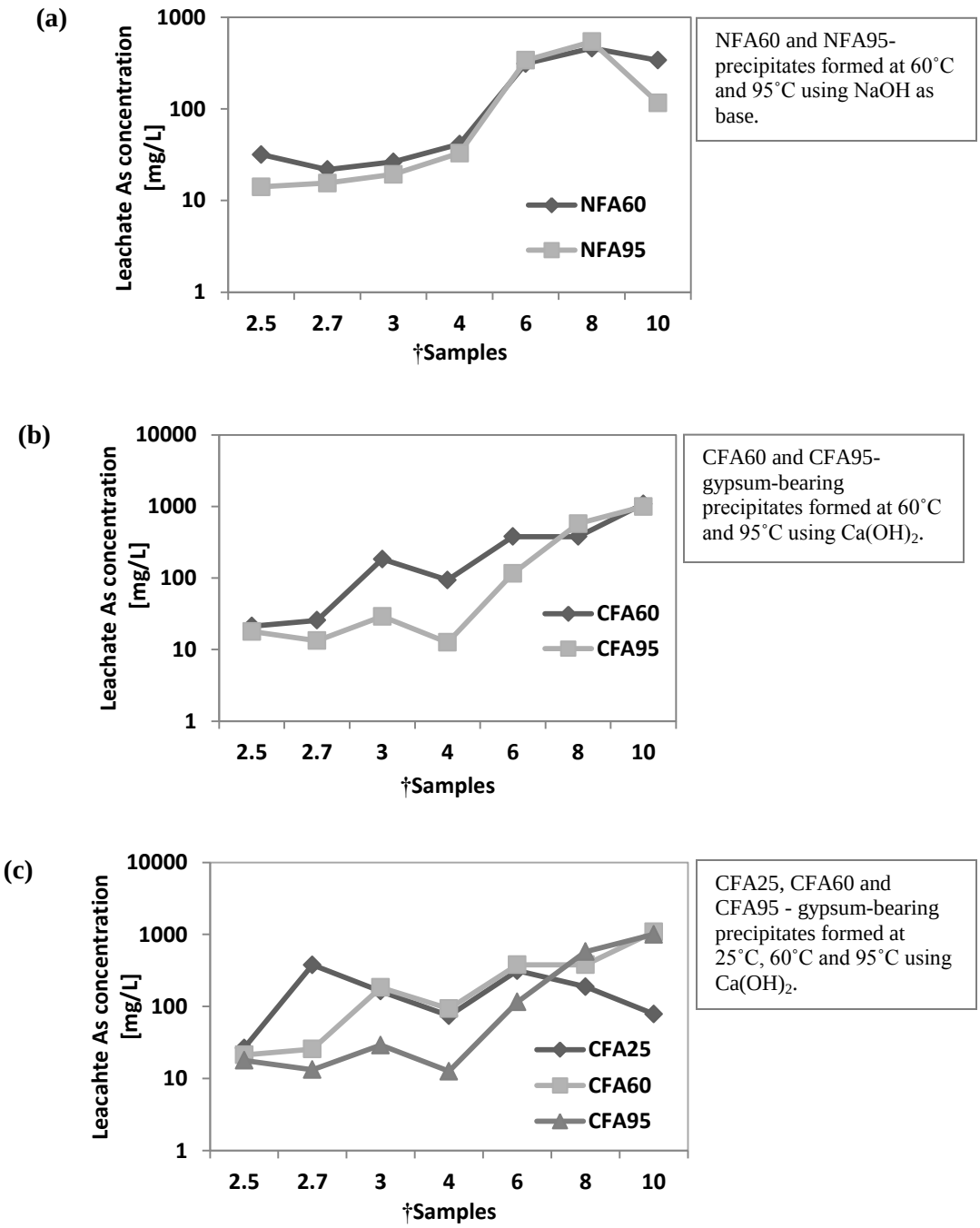

Figure 4.36: As concentration of the TCLP leachates from precipitates formed at the specific pH levels (2.5, 3, 4, 6, 8 and 10) during the neutralization of the Fe(III)-As(III) solutions (Fe:As=1) using NaOH and $Ca(OH)_2$ as the bases respectively. †Samples denote the precipitates formed at the specific pH values of 2.5, 2.7, 3, 4, 6, 8 and 10.

4.4. Conclusions

The effect of initial Fe:As molar ratio and neutralizing agent (NaOH and $Ca(OH)_2$) on the As removal efficiency from Fe(III)-As(III) solutions (Fe:As = 1.0, 1.5 and 2) under ambient conditions was investigated. The effectiveness of As removal was enhanced with increasing Fe:As molar ratio and pH. The use of lime as opposed to sodium hydroxide as a neutralizing agent enhanced the arsenic removal efficiency, with >90% of arsenic being removed at pH>2.7 in the $Ca(OH)_2$ neutralized systems. At pH>4, tooeleite was found to rapidly transform to an equimolar ferric arsenite in both the NaOH and $Ca(OH)_2$ neutralized systems (Fe:As=1).

Bulk XRD analysis of the precipitates formed from the NaOH neutralized systems (Fe:As = 1-2; 25˚C) in the pH range 2 to 4 indicated the presence of tooeleite. However, a poorly crystalline phase was identified in the precipitates formed in the pH range 6 to 10. Bulk XRD analysis of the precipitates formed from the $Ca(OH)_2$ neutralized systems (Fe:As = 1-2; 25˚C) in the pH range 2 to 4 indicated the presence of tooeleite and gypsum. Gypsum was identified in the precipitates formed in the pH range 6 to 10. Synchrotron-based μXRD analysis of the tooeleite precipitates formed from the NaOH neutralized system (Fe:As=1.0; 25˚C) at pH 2 and 4 indicated the presence of tooeleite. A poorly crystalline phase, deemed to be ferric arsenite, was identified in the precipitates formed at pH 6 and 10. μXRD analysis of the precipitates formed from the $Ca(OH)_2$ neutralized system (Fe:As=1; 25˚C) identified tooeleite and gypsum in the precipitates formed at pH 2.5 and 4, while gypsum and a poorly crystalline phase, deemed to be ferric arsenite, were identified in the precipitates formed at pH 6, 8 and 10. Fe K-edge μXANES analysis indicated that tooeleite is the predominant compound in the tooeleite and gypsum-bearing tooeleite precipitates formed at 25˚C, 60˚C and 95˚C from NaOH neutralized systems

(Fe:As=1; pH 2.7). However, 2-line ferrihydrite was also identified as a component of the tooeleite precipitates (Fe:As=1) formed at 25˚C, indicating that trace amounts of ferrihydrite were probably formed during the precipitation of tooeleite at pH 2.7.

An evaluation of the sulphate concentration of solids precipitated from the NaOH neutralized system (Fe:As=1; 25˚C) at pH 2.7, 4, 6 and 8 indicated that the sulphate content of the precipitates decreased with increasing precipitation pH. This was attributed to the presence of tooeleite in the pH 2.7 precipitates, which gradually transformed with increasing pH to form an equimolar ferric arsenite at pH>3.5.

The kinetics of tooeleite precipitation from NaOH neutralized systems with varying initial Fe:As molar ratios (1, 1.2 and 1.5) and precipitation temperatures (25˚C, 60˚C and 95˚C) indicated that the As removal efficiency was enhanced with increasing precipitation pH and initial Fe:As molar ratio. A retention time of 1 hour was found to be required for the precipitation of tooeleite from solution and the attainment of a quasi-equlibrium.

TCLP stability analysis of the precipitates formed from NaOH and $Ca(OH)_2$ neutralized systems (Fe:As=1.0, 1.5, 2.0; 25˚C) indicated that both tooeleite and ferric arsenite have a relatively high As solubility, and the TCLP As leachability decreased with increasing Fe:As molar ratio probably due to the presence of excess ferric iron. The effect of higher Fe:As molar ratios (Fe:As>2) was not studied but data from the Horne (Quebec) and JEB (Northern Saskatchewan) tailings facilities suggest, that under anoxic conditions using Fe:As>3, these precipitates are stable.

The long term stability tests (~30 weeks) conducted on tooeleite and gypsum-bearing tooeleite precipitates (Fe:As=1; pH 2.7; 25˚C) under pH 4, 5, 7 and 9 conditions, indicated that the transformation of tooeleite to ferric arsenite occurred at pH>4, and was faster under higher pH conditions. It is proposed that during the accelerated aging of the tooeleite and gypsum-bearing tooeleite precipitates at 60˚C under pH 5, 7 and 9 conditions, tooeleite crystallizes faster than it transforms to ferric arsenite resulting in the release of As into solution. The As release (~25% As) that occurred during accelerated leaching of these precipitates at 60˚C under the different pH conditions (pH 5, 7 and 9) led to the increase in Fe:As molar ratio of the tooeleite precipitates from ~1.2 to ~1.5.

High temperature precipitation of tooeleite from NaOH and $Ca(OH)_2$ neutralized systems (Fe:As=1 at 60˚C and 95˚C) influenced the crystallinity of the tooeleite precipitates formed at pH<3.5, with higher precipitation temperatures inducing higher crystallinity. Furthermore, high temperature precipitation resulted in the precipitation of tooeleite at pH>4. At pH>4, the increased As solubility of the precipitates formed at higher temperatures compared to ambient temperature conditions was probably due to the transformation of tooeleite to a more crystalline phase resulting in subsequent As release and the increase of the Fe:As molar ratio of the precipitates to ~1.5. The more crystalline tooeleite does not transform to ferric arsenite except after prolonged period at higher temperatures and at >pH 8. High temperature precipitation did not enhance either the As removal efficiency or the TCLP stability of tooeleite compared to that of the ambient temperature precipitation.

The results of this study demonstrate that, although tooeleite or ferric arsenite precipitates at Fe:As molar ratios of 1- 2 have high As and low Fe contents, they would not pass the TCLP test and therefore would have to be disposed of as hazardous waste. The effect of higher Fe:As molar ratios and co-deposition with additional inert solids was not studied but, based on experience at the Horne and JEB tailings facilities, the resulting residues are stable.

Chapter 5

Calcination of tooeleite

5.1. Introduction

Tooeleite has a high As content, high As removal efficiency and low Fe requirements and offers potential for the fixation of As(III) from weak acid effluents. However, tooeleite is only stable in the pH range 2 to 3.5 and would need to be deposited in a lined pond with ongoing monitoring and maintenance of acid conditions, thereby incurring high operating and disposal costs.

The present study investigates the calcination of tooeleite and gypsum-bearing precipitates as a potential approach for enhancing their stability. This approach is used by the Caletones smelter in Chile whereby calcium arsenite is calcined to form a more crystalline calcium arsenate phase. The thermal decomposition of tooeleite was studied in air and nitrogen using thermogravimetry, differential thermal analysis and mass spectrometry (TG/DTA-MS). The effect of excess ferrihydrite in the precipitate and lime additions on the calcination process and the calcine stability were also studied (Opio et al., 2011).

5.2. Materials and methods

5.2.1. Synthesis of tooeleite

Tooeleite was synthesised using the procedure described in Nishimura and Robins, 2008. The batch precipitation of tooeleite was carried out at ambient temperature, using analytical reagent grade chemicals. Tooeleite was sythesized using 0.1 M Fe(III) and 0.1 M As(III) stock solutions. Fe(III) was prepared by dissolving $Fe_2(SO_4)_3.5H_2O$ in distilled water. Arsenious acid (H_3AsO_3) solution was prepared by the dissolution of As_2O_3 in 0.1 M H_2SO_4 at 90˚C. The pH of the Fe(III)-As(III) solution was adjusted to a final pH of 2.7 by the addition of 2 M NaOH solution while being continuously stirred at 350 rpm. The pH was monitored and maintained at a level of 2.7 for 1 hour. At the end of the test, the slurry was vacuum-filtered using a 0.45 µm membrane filter. The filter cake was washed with distilled water and pH 3.6 acidified distilled water (acidified using 0.2 M H_2SO_4), and subsequently oven-dried at 60˚C for 5 hours. Tooeleite precipitates were also synthesized using the same procedure with $Ca(OH)_2$ as the neutralizing agent.

5.2.2. Thermal analysis

Thermogravimetry (TG) and differential thermal analysis (DTA) experiments were performed using TG-DTA/DSC instrument Netzsch STA 449 F3 Jupiter under nitrogen and air atmospheres in order to gain more insight into the thermal behavior of tooeleite. A sample of the tooeleite precipitates (~33 mg) was heated from room temperature to 1250 ˚C at a heating rate of 10˚C /min, under nitrogen and dry air (50 ml/min) atmospheres. The same procedure was repeated using a sample of a mixture of tooeleite precipitates and lime. The lime additions to the tooeleite precipitates were equivalent to 10% by weight of the precipitates. Furthermore, the

thermal decomposition of gypsum-bearing tooeleite precipitates was evaluated under nitrogen and air atmospheres using similar conditions.

5.2.3. Calcination experiments

5.2.3.1. Bulk chemical analysis

Two grams of the tooeleite precipitates were calcined in a laboratory-scale quartz tube furnace at 500 ˚C, 600 ˚C and 870 ˚C in an air stream of 471.95 ml/min for an hour. Calcination runs were carried out under the same experimental conditions using samples of tooeleite precipitates with lime additions (10% by weight of the precipitates). Additional calcination tests were conducted using tooeleite and gypsum-bearing tooeleite at 600˚C, 700˚C and 800˚C. 1M NaOH or $Ca(OH)_2$ solution in an Erlenmeyer flask (250 ml) was used as scrubbing solution to capture the gaseous decomposition products including As_2O_3, SO_2 and SO_3. Chemical analyses of the tooeleite precipitates and calcines were carried out by ICP-OES, subsequent to aqua regia digestion.

5.2.3.2. XRD analysis

The tooeleite and gypsum-bearing tooeleite precipitates as well as their respective calcines were subjected to powder X-Ray Diffraction (XRD) analysis using a Phillips X'Pert Pro MPD diffractometer fitted with an X'Celerator high speed strip detector (X-ray source: Cu Kα radiation (Ni filtered) and operating conditions: 45 KV, 40 MA, 3˚- 80˚ 2θ, step size of 0.02˚, counting time 10 seconds at each step). PanAnalytical HighScore software was used for the identification of phases. The particle-size, morphology and general elemental composition of the tooeleite and gypsum-bearing tooeleite precipitates as well as their respective calcines were

determined by scanning electron microscopy (SEM) and Energy Dispersive X-Ray spectroscopy (EDX) was performed using a MLA Quanta 650 FEG-ESEM machine.

5.2.3.3. Stability tests

In order to assess their stability, the tooeleite precipitates, gypsum-bearing tooeleite precipitates and their respective calcines were subjected to the standard US EPA Method 3111 (Toxicity Characteristic Leaching Procedure – TCLP test) (US EPA, 1996). The modified TCLP test was conducted using an extraction fluid of pH 4.93 ± 0.05 which was prepared using glacial acetic acid and NaOH. The leaching test was conducted by mixing 0.5 g of each sample with the extraction fluid (liquid:solid rato of 20:1) in a 250 ml Erlenmeyer flask. The flasks were placed in an orbital shaker and shaken continuously at 200 rpm for 18 ± 2 hours at room temperature. On completion of the leaching test, the suspensions were vacuum-filtered using 0.45 μm membrane filters. The pH of the leachates was measured before being analyzed for arsenic by ICP-OES.

5.3. Results and discussion

5.3.1. Thermal decomposition of tooeleite

Figure 5.1 shows the thermal behavior of the tooeleite precipitates in the temperature range 30-1250˚C under an atmosphere of nitrogen. A summary of the proposed decomposition stages is presented in Table 5.1. In the first stage (100-270˚C), water is lost. Sulphur dioxide and arsenic trioxide are evolved in the second stage (400-600˚C), and arsenic pentoxide is evolved in the final stage (850-1250˚C). The Thermogravimetric (TG) curve indicates a total weight loss of 55% in the temperature range 100-1250˚C, resulting in hematite and ferric arsenate as the final decomposition products.

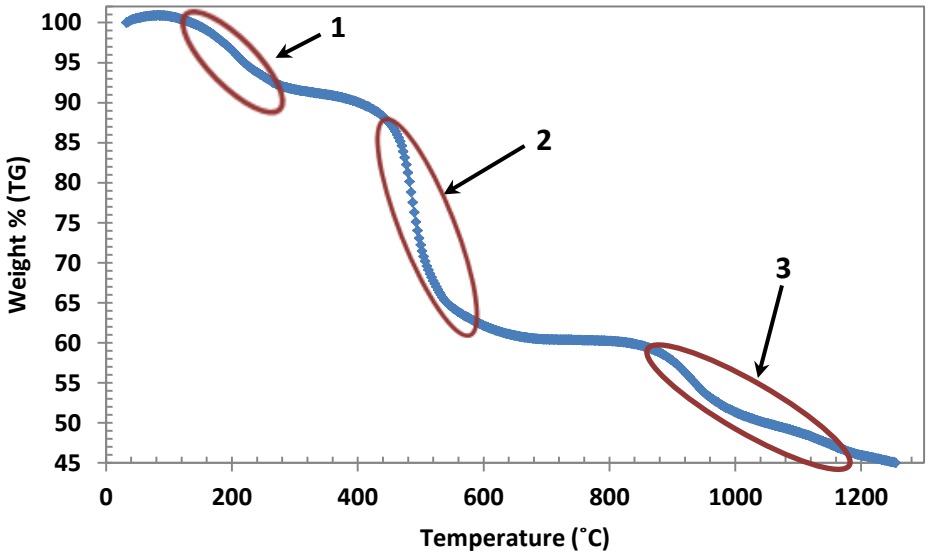

Figure 5.1: The thermal behavior of tooeleite precipitates heated up to 1250˚C in nitrogen at a heating rate of 10˚C /min

Table 5.1: Summary of the decomposition stages of tooeleite precipitates heated up to 1250˚C in nitrogen. Wt loss denotes the weight loss %.

Stages	Wt loss	Temperature (˚C)	Reactions
1	9	100-270	$6Fe_2O_3.5As_2O_3.2SO_3.12H_2O = 6Fe_2O_3.5As_2O_3.2SO_3 + 12H_2O$
2	31	400-600	$6Fe_2O_3.5As_2O_3.2SO_3 = 2FeAsO_4 + 5Fe_2O_3 + 4As_2O_3 + 2SO_2$
3	15	850 - 1250	$2FeAsO_4 + 5Fe_2O_3 = FeAsO_4 + 11/2Fe_2O_3 + 1/2As_2O_5$

Figure 5.2 shows the thermal behavior of the tooeleite precipitates in the temperature range 30-1250˚C under air. The observed thermal behavior is consistent with previous studies by Nishimura and Robins (2008). Table 5.2 presents a summary of the proposed decomposition stages. Water volatilizes at 100-270˚C, followed by sulphur trioxide at 500-800˚C. At 1000-1250˚C, arsenic trioxide is evolved. Nishimura and Robins (2008) suggested that the weight gain observed around 400-600˚C may be due to the oxidation of tooeleite. But as the weight gain was lower than that obtained as a result of complete oxidation, the authors proposed that the weight gain may also partly be due to the sublimation of arsenic trioxide. Volatilization refers to process of evaporation, while sublimation is the direct change from a solid to a gaseous state. The TG curve indicates a total weight loss of 50% in the temperature range 100-1250˚C, resulting in hematite and angelellite as the final decomposition products.

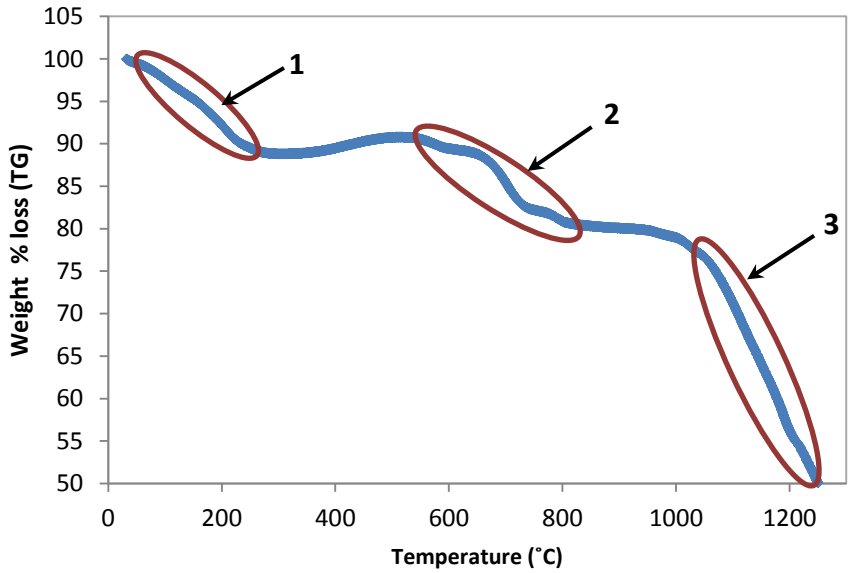

Figure 5.2: The thermal behavior of tooeleite precipitates heated up to 1250˚C in air at a heating rate of 10˚C /min

Table 5.2: Summary of the decomposition stages of tooeleite precipitates heated up to 1250˚C in air. Wt loss denotes the weight loss %.

Stages	Wt loss	Temperature (°C)	Reactions
1	9	100 - 270	$6Fe_2O_3.5As_2O_3.2SO_3.12H_2O = 6Fe_2O_3.5As_2O_3.2SO_3 + 12H_2O$
2	7	500 - 800	$6Fe_2O_3.5As_2O_3.2SO_3 = 6Fe_2O_3.4As_2O_3.2SO_3 + As_2O_3$
			$6Fe_2O_3.4As_2O_3.2SO_3 + 4O_2 = 6Fe_2O_3.4As_2O_5.2SO_3$
			$6Fe_2O_3.4As_2O_5.2SO_3 = 8FeAsO_4 + 2Fe_2O_3 + 2SO_3$
3	30	1000 - 1250	$10FeAsO_4 + Fe_2O_3 = 2Fe_2O_3 + 2Fe_4As_2O_{11} + 3As_2O_5$

5.3.2. Thermal decomposition of tooeleite with addition of lime

Lime (CaO) was added to tooeleite precipitates to investigate its potential to fix the SO_3 gas evolved above 500˚C during the thermal decomposition of tooeleite under air. Figure 5.3 shows the thermal behavior of the tooeleite precipitates heated to 650˚C under air and the proposed decomposition stages are summarized in Table 5.3. The first stage (100 - 220˚C) is associated with the volatilization of water, and the sublimation of As_2O_3 as well as partial oxidation of tooeleite occurs in the second stage (300 - 450˚C) (Nishimura and Robins, 2008).

Sulphur trioxide is evolved in the third stage (580 - 650 ˚C), resulting in ferric arsenate and hematite as the final decomposition products. Figure 5.3 depicts the thermal behavior of a mixture of tooeleite precipitates and lime heated to 650˚C under air and Table 5.4 presents a summary of the proposed decomposition stages. The lime addition was equivalent to 10% by weight of precipitates. Water is evolved in the first stage, and As_2O_3 sublimation as well as partial oxidation of tooeleite occurs in the second stage. In the third stage, the evolved As_2O_3 and a portion of SO_3 are fixed as calcium arsenate and calcium sulphate respectively. The slight weight loss of 3% observed in the third stage is thought to arise from the residual 1 mole of SO_3 that was not fixed by CaO. The final decomposition products include a ferric arsenate phase ($Fe_7As_6O_{24}$), hematite, calcium arsenate and calcium sulphate. Therefore, based on the TG/DTA results, it can be concluded that lime was effective in fixing both the As_2O_3 and SO_3 that was evolved at 500 – 650˚C.

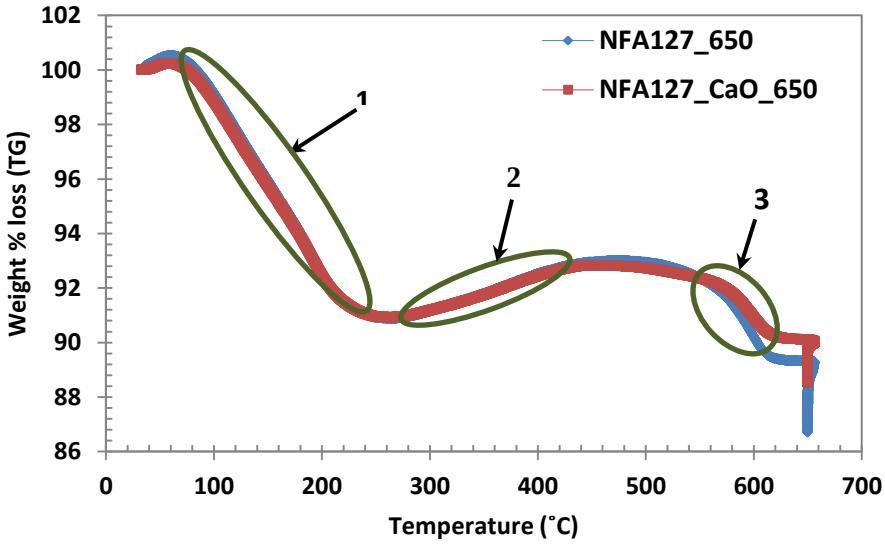

Figure 5.3: The thermal behavior of: (i) tooeleite precipitates (NFA127_650) and (ii) a mixture of tooeleite precipitates and lime (NFA127_CaO_650) heated up to 650˚C, at a heating rate of 10˚C /min in air

Table 5.3: Summary of the decomposition stages of tooeleite precipitates heated up to 650˚C in air. Wt loss denotes the weight loss %.

Stages	Wt loss	Temperature (°C)	Reactions
1	9	100 - 220	$6Fe_2O_3.5As_2O_3.2SO_3.12H_2O = 6Fe_2O_3.5As_2O_3.2SO_3 + 12H_2O$
2	2	300 - 450	$6Fe_2O_3.5As_2O_3.2SO_3 = 6Fe_2O_3.4As_2O_3.2SO_3 + As_2O_3$ $6Fe_2O_3.4As_2O_3.2SO_3 + 4O_2 = 6Fe_2O_3.4As_2O_5.2SO_3$
3	6	580 - 650†	$6Fe_2O_3.4As_2O_5.2SO_3 = 8FeAsO_4 + 2Fe_2O_3 + 2SO_3$

†Heat treated at 650˚C for 1 hour in the TG/DTA.

Table 5.4: Summary of the decomposition stages of a mixture of tooeleite precipitates and lime heated up to 650˚C in air. Wt loss denotes the weight loss %.

Stages	Wt loss	Temperature (°C)	Reactions
1	9	100 - 220	$6Fe_2O_3.5As_2O_3.2SO_3.12H_2O = 6Fe_2O_3.5As_2O_3.2SO_3 + 12H_2O$
2	2	300 - 450	$6Fe_2O_3.5As_2O_3.2SO_3 = 6Fe_2O_3.4As_2O_3.2SO_3 + As_2O_3$ $6Fe_2O_3.4As_2O_3.2SO_3 + 4O_2 = 6Fe_2O_3.4As_2O_5.2SO_3$
3	3	580 - 650†	$6Fe_2O_3.4As_2O_5.2SO_3 + 5/2O_2 = 1/2Fe_7As_6O_{24} + 17/2Fe_2O_3 + 2SO_3 + 7/2As_2O_3$ $6CaO + 2As_2O_3 + O_2 = Ca_3(AsO_4)_2$ $CaO + SO_3 + 0.5O_2 = CaSO_4$ Assumption: 3% weight loss due to one mole of SO_3

†Heat treated at 650˚C for 1 hour in the TG/DTA.

5.3.3. Thermal decomposition of gypsum-bearing tooeleite

Figure 5.4 shows the thermal behavior of gypsum-bearing tooeleite precipitates after heating to 800˚C in a nitrogen atmosphere. The TG curve indicated a total weight loss of 36%, which occurred in three separate stages. Table 5.5 presents a summary of the proposed decomposition stages. In the first stage, water is evolved from both tooeleite and gypsum. In the second stage, water is evolved from gypsum, and the sublimation of As_2O_3 also occurs. In the third stage, As_2O_3 is evolved resulting in angelellite ($Fe_4As_2O_{11}$), hematite (Fe_2O_3) and calcium suphate anhydrite ($CaSO_4$) as the final decomposition products.

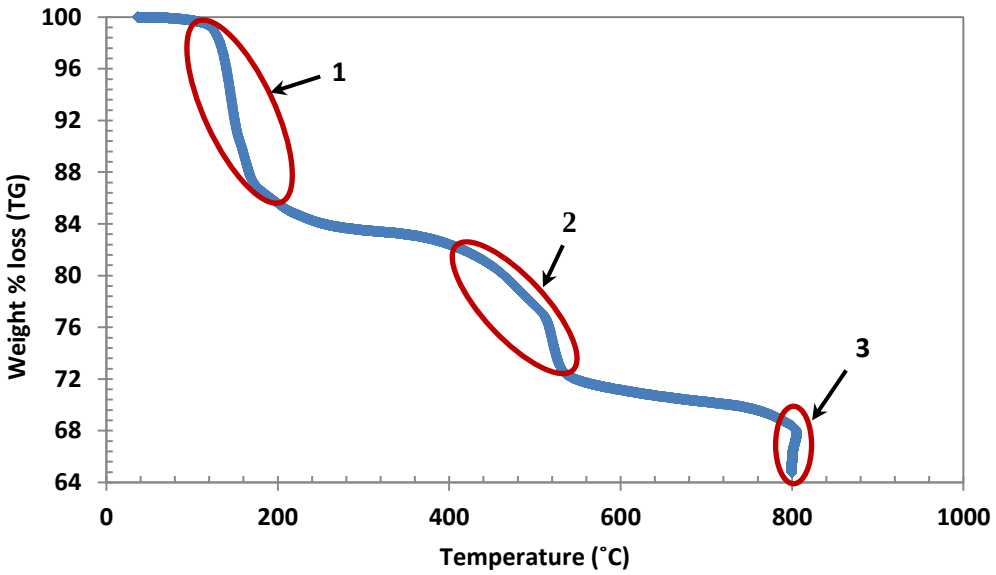

Figure 5.4: The thermal behavior of gypsum-bearing tooeleite precipitates heated up to 800˚C at a heating rate of 10˚C /min in nitrogen. The precipitates are heated at 800˚C for an hour

Table 5.5: Summary of the decomposition stages of gypsum-bearing tooeleite precipitates heated up to 800C in nitrogen. Wt loss denotes the weight loss %.

Stages	Wt loss	Temperature (°C)	Reactions
1	14	100 - 200	$6Fe_2O_3.5As_2O_3.2SO_3.12H_2O = 6Fe_2O_3.5As_2O_3.2SO_3 + 12H_2O$ $CaSO_4.2H_2O = CaSO_4.0.5H_2O + 1.5H_2O$
2	6	400 - 550	$6Fe_2O_3.5As_2O_3.2SO_3 + CaSO_4.0.5H_2O = 1/2Fe_7(AsO_4)_6 +$ $7/2As_2O_3 + 17/2Fe_2O_3 + 2SO_2 + CaSO_4 + 0.5H_2O$
3	4	800†	$Fe_7(AsO_4)_6 + 1/2Fe_2O_3 = 2Fe_4As_2O_{11} + As_2O_3$

†Heat treated at 800˚C for 1 hour in the TG/DTA.

The thermal behavior of gypsum-bearing tooeleite precipitates after heating to 800˚C in air is presented in Figure 5.5 and a summary of the decomposition stages is presented in Table 5.6. The TG curve indicated a total weight loss of 23%. In the first stage, water is volatilized from both tooeleite and gypsum. In the second stage, the sublimation of arsenic trioxide and partial oxidation of tooeleite occurs. In the third stage, As_2O_5, SO_3 and water are evolved, resulting in

angellelite ($Fe_4As_2O_{11}$), hematite (Fe_2O_3) and calcium sulphate anhydrite ($CaSO_4$) as the final products.

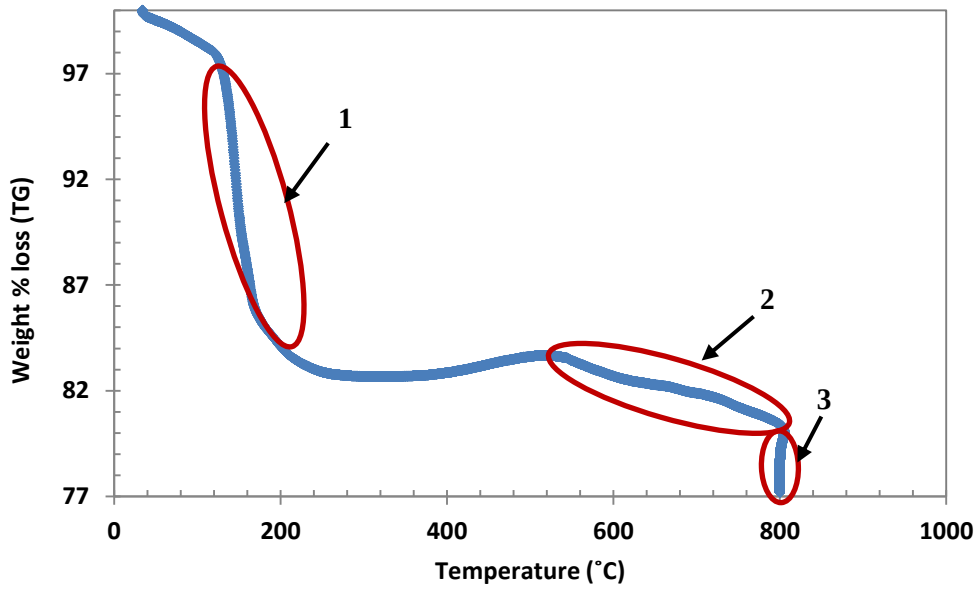

Figure 5.5: The thermal behavior of gypsum-bearing tooeleite precipitates heated up to 800˚C in air

Table 5.6: Summary of the decomposition stages of gypsum-bearing tooeleite precipitates heated up to 800˚C in air. Wt loss denotes the weight loss %.

Stages	Wt loss	Temperature (°C)	Reactions
1	14	100 - 200	$6Fe_2O_3.5As_2O_3.2SO_3.12H_2O = 6Fe_2O_3.5As_2O_3.2SO_3 + 12H_2O$ $CaSO_4.2H_2O = CaSO_4.0.5H_2O + 1.5H_2O$
2	2	400 - 550	$6Fe_2O_3.5As_2O_3.2SO_3 = 6Fe_2O_3.4As_2O_3.2SO_3 + As_2O_3$ $6Fe_2O_3.4As_2O_3.2SO_3 + 4O_2 = 6Fe_2O_3.4As_2O_5.2SO_3$
3	3	550 - 800	$6Fe_2O_3.4As_2O_5.2SO_3 + O_2 + CaSO_4.0.5H_2O = 1/2Fe_7(AsO_4)_6 + 17/2Fe_2O_3 + 5/2As_2O_3 + 2SO_3 + CaSO_4 + 0.5H_2O$
		800†	$Fe_7(AsO_4)_6 + 1/2Fe_2O_3 + 3/2O_2 = 2Fe_4As_2O_{11} + As_2O_5$

†Heat treated at 800˚C for 1 hour in the TG/DTA.

5.3.4. Chemical analysis

The chemical composition of the tooeleite and gypsum-bearing tooeleite precipitates and their respective calcines obtained at 600˚C, 700˚C and 800˚C are presented in Table 5.7. The Fe/As molar ratio of the tooeleite precipitates is slightly higher than the expected actual molar

ratio of 1.2 reported by Nishimura and Robins (2008). The higher Fe/As molar ratio of 1.7 for tooeleite could be attributed to the formation of the mixed species of tooeleite and ferrihydrite during the synthesis of tooeleite at pH 2.7. According to Riveros et al. (2001), As(III)-Fh begins to form at pH 2 to 3.

Table 5.7: Chemical analysis of tooeleite and gypsum-bearing tooeleite and their respective calcines obtained at 600˚C, 700˚C and 800˚C

Sample	Concentration (wt%)				Molar ratio
	Fe	As	S	Ca	Fe/As
Tooeleite	51.1	40.2	8.7	-	1.70
GT†	23.4	24.2	24.6	27.7	1.30
Tooeleite (600˚C)	53.5	43.5	3.1	-	1.65
GT† (600˚C)	23.1	23.8	25.3	27.8	1.30
Tooeleite (700˚C)	63.3	33.7	3	-	2.51
GT† (700˚C)	25.4	20.9	23.9	29.8	1.63
Tooeleite (800˚C)	61.6	37.6	0.7	-	2.19
GT† (800˚C)	27.7	19.3	21.9	31.2	1.92

GT† denotes gypsum-bearing tooeleite

5.3.5. XRD analysis

5.3.5.1. Calcines of tooeleite (with and without lime additions)

The mineral phases identified in the calcines (with and without lime additions) by XRD analysis are presented in Table 5.8. Tooeleite was identified in the precipitates synthesized at 25˚C, but As(III)-Fh was not be detected due to its poorly crystalline nature. In the 500˚C calcines, an iron arsenate phase ($Fe_7(AsO_4)_6$) and an amorphous phase were detected. The amorphous phase could not be identified using the ICCD data files, but based on previous studies by Nishimura and Robins (2008), it is deemed to be ferric arsenate sulphate ($6Fe_2O_3.5As_2O_3.2SO_4$), which formed due to the dehydration of tooeleite. At higher calcination temperatures of 600˚C and 870˚C, crystalline phases were formed from the tooeleite precipitates

with and without lime additions. A crystalline iron arsenate phase ($FeAsO_4$) and hematite were identified in the 600 ˚C calcines. In the 870 ˚C calcines, angellelite ($Fe_4O_3(AsO_4)_2$) and hematite were identified. During the calcination of tooeleite, a white solid residue was deposited on the walls of the glass tube furnace. Analysis of the white solid residue using XRD confirmed that it was arsenic trioxide (Appendix A.6.). The addition of lime resulted in the supplementary formation of calcium arsenate and calcium sulphate in the 600 ˚C calcines, and calcium arsenate in the 870 ˚C calcines.

Table 5.8: Mineral phases identified by XRD analysis of the tooeleite precipitates (with and without lime additions) calcined at different temperatures (500˚C, 600˚C and 870˚C)

Calcine samples	Mineral phases
500 ˚C	Iron arsenate phase, $Fe_7(AsO_4)_6$ (ICDD 55-0128)
600 ˚C	Iron arsenate, $FeAsO_4$ (ICDD 78-1545); Hematite, Fe_2O_3 (ICDD 73-0603)
870 ˚C	Hematite, Fe_2O_3 (ICDD 33-0664) Iron arsenate phase - angelellite, $Fe_4O_3(AsO_4)_2$ (ICDD 83-1554)
600 ˚C (with lime)	Iron arsenate phase, $Fe_7As_6O_{24}$ (ICDD 73-9339); Calcium arsenate, $Ca_3(AsO_4)_2$ (ICDD 39-0010); Calcium sulphate, $CaSO_4$ (ICDD 80-0787)
870 ˚C (with lime)	Angellelite, $Fe_4O_3(AsO_4)_2$ (ICDD 83-1554); Calcium arsenate, $Ca_3(AsO_4)_2$ (ICDD 26-0295); Hematite, Fe_2O_3 (ICDD 33-0664)

5.3.5.2. Calcines of tooeleite and gypsum-bearing tooeleite

The mineral phases identified by XRD analysis of the tooeleite and gypsum-bearing tooeleite precipitates calcined at different temperatures (600˚C, 700˚C, 800˚C) are summarized in Tables 5.9 and 5.10 respectively. Angelellite and hematite were identified in the 800˚C tooeleite calcines (Table 5.9). XRD analysis of gypsum-bearing tooeleite calcines obtained at 600˚C and 700˚C indicated the presence of an iron arsenate phase ($Fe_7As_6O_{24}$) and calcium sulphate (Table

5.10). XRD analysis of the 800˚C calcines detected the presence of angellelite and calcium sulphate (Table 5.10). During the calcination of both tooeleite and gypsum-bearing tooeleite, a white solid residue was deposited on the furnace walls. XRD analysis of the white solid residue indicated the presence of arsenic trioxide (Appendix A.6.). More arsenic trioxide was deposited during the calcination of gypsum-bearing tooeleite compared to that of tooeleite.

Table 5.9: Mineral phases identified by XRD analysis of tooeleite precipitates calcined at different temperatures (600˚C, 700˚C and 800˚C)

Calcine samples	Mineral phases
600 ˚C	Iron arsenate, $FeAsO_4$ (ICDD 78-1545); Hematite, Fe_2O_3 (ICDD 73-0603)
700 ˚C	Iron arsenate, $FeAsO_4$ (ICDD 78-1545); Hematite, Fe_2O_3 (ICDD 73-0603)
800 ˚C	Angellelite, $Fe_4O_3(AsO_4)_2$ (ICDD 83-1554); Hematite, Fe_2O_3 (ICDD 33-0664)

Table 5.10: Mineral phases identified by XRD analysis of gypsum-bearing tooeleite precipitates calcined at different temperatures (600˚C, 700˚C and 800˚C)

Calcine samples	Mineral phases
600 ˚C	Iron arsenate phase, $Fe_7As_6O_{24}$ (ICDD 73-9339); Calcium sulphate (anhydrite), $CaSO_4$ (ICDD 80-0787)
700 ˚C	Iron arsenate phase, $Fe_7As_6O_{24}$ (ICDD 73-9339); Calcium sulphate (anhydrite), $CaSO_4$ (ICDD 80-0787)
800 ˚C	Angellelite, $Fe_4O_3(AsO_4)_2$ (ICDD 83-1554); Calcium sulphate (anhydrite), $CaSO_4$ (ICDD 80-0787)

5.3.6. SEM analysis

Figures 5.6 to 5.10 present the SEM images of the tooeleite calcines (with and without the addition of lime) obtained at 600 ˚C and 870 ˚C. The SEM images indicate that the morphology and particle size of the calcines changed with increasing calcination temperature. The EDX spectra, (a), (b), (c) and (d) correspond to the respective elemental analyses of spots marked a, b, c and d in the SEM images. The SEM image in Figure 5.6 presents the partial transformation of a calcined tooeleite grains (spot b) to form crystalline Fe/As bearing grains

(1 µm to 10 µm) as indicated by the corresponding EDX spectra of spot a. Figure 5.7 shows an image of the calcines at 870 ˚C, which consists of agglomerated small spherical hematite grains (1 µm to 2 µm) on the surface of larger Fe/As/O bearing grains (5 µm to 10 µm). The EDX spectrum indicates the disappearance of sulphur at 870 ˚C (Figures 5.7c and 5.7d). Figure 5.8 shows an image of the tooeleite and lime calcines obtained at 600 ˚C, which consists of agglomerated small Ca/S/As/O bearing grains on the surface of larger Fe/As/O/S bearing grains (20 µm) presumed to be tooeleite. The SEM image of the tooeleite and lime calcines obtained at 870 ˚C indicates the presence of lumpy Ca/As/O bearing grains (~5 µm to 20 µm) (Figure 5.9g) located on the surface of thick mats of particulates, deemed to be hematite based on the EDX compositional analysis (Figures 5.9h and 5.9i). Using SEM, it was observed that the tooeleite calcines obtained at 600˚C and 700˚C (Figures 5.10a and 5.10b) were more crystalline than the gypsum-bearing tooeleite calcines obtained at the same temperatures (Figures 5.10c and 5.10d). Calcination of the gypsum-bearing tooeleite precipitates at 600˚C and 700˚C resulted in the transformation of the crystalline gypsum-bearing tooeleite to lumpy As-bearing aggregates with a lower degree of crystallinity (Figures 5.10c and 5.10d).

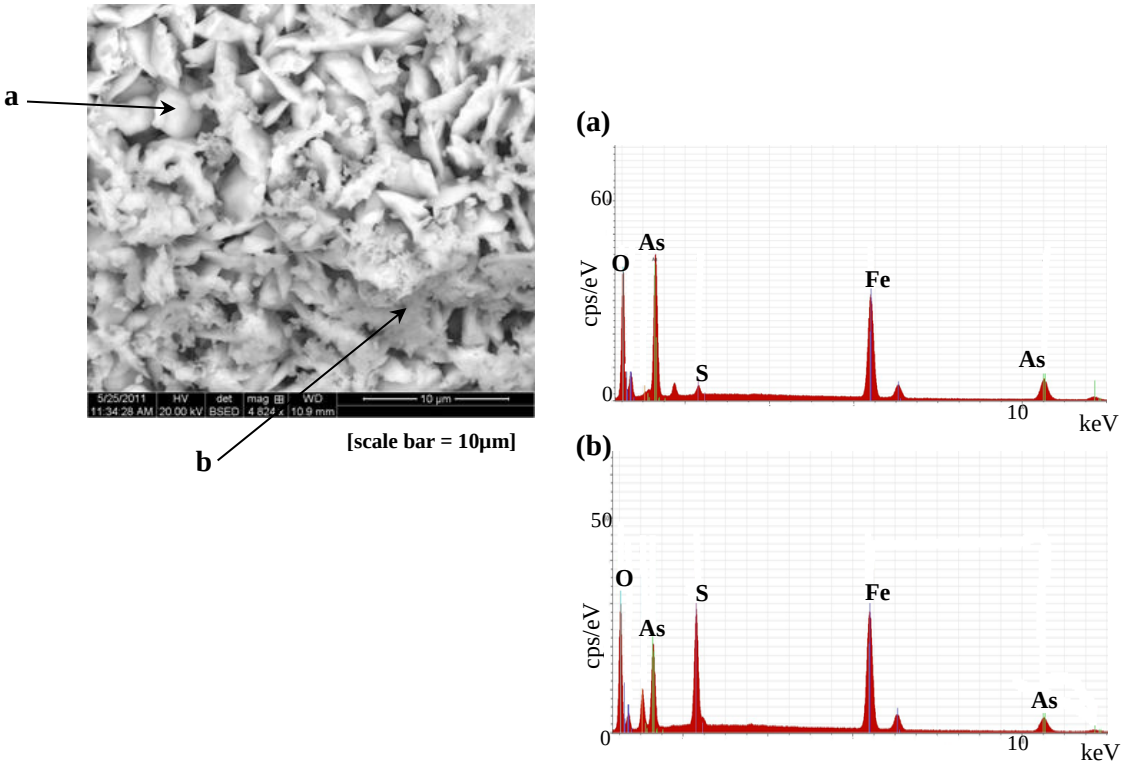

Figure 5.6: SEM images and EDX spectra (x-ray intensity vs energy) of tooeleite calcined at 600˚C

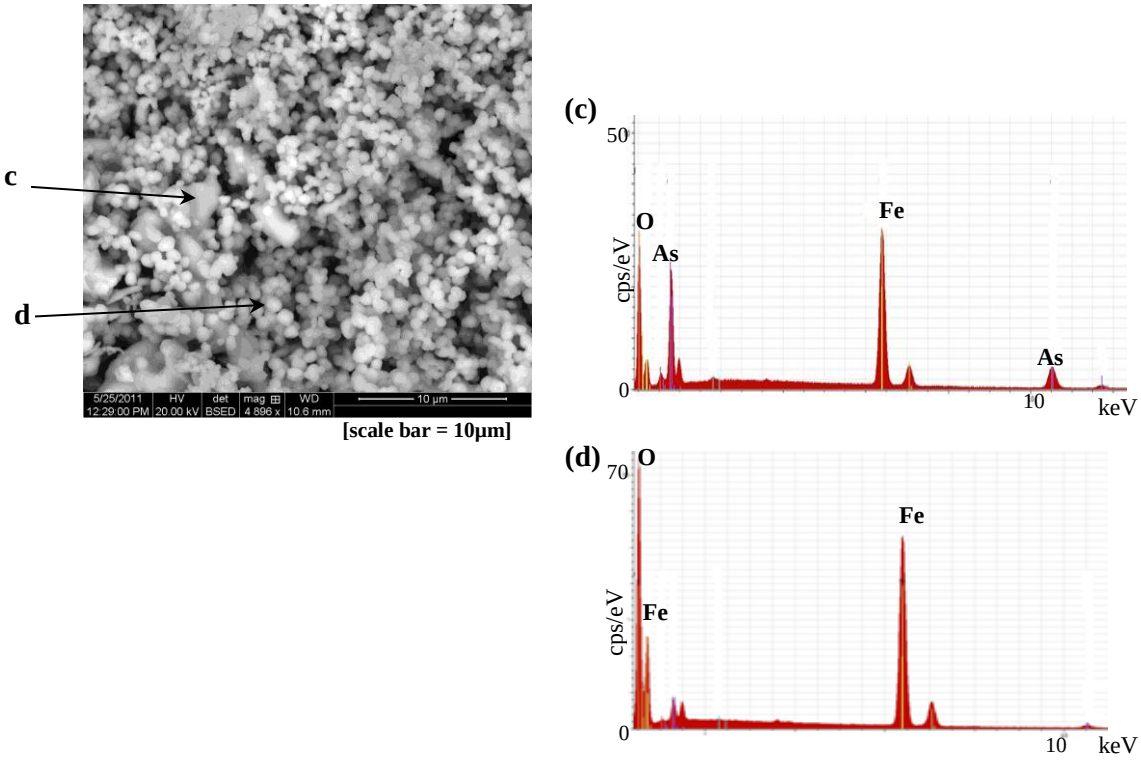

Figure 5.7: SEM image and EDX spectra (x-ray intensity vs energy) of tooeleite calcines at 870˚C

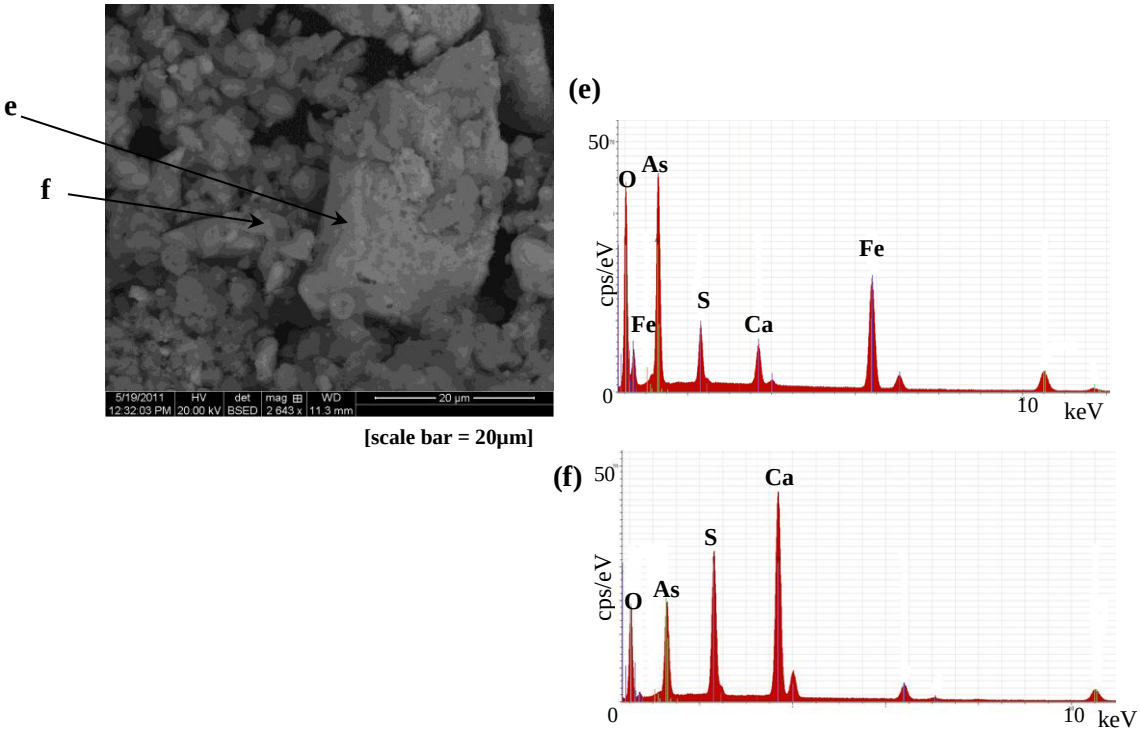

Figure 5.8: SEM image and EDX spectra (x-ray intensity vs energy) of tooeleite and lime calcines at 600˚C

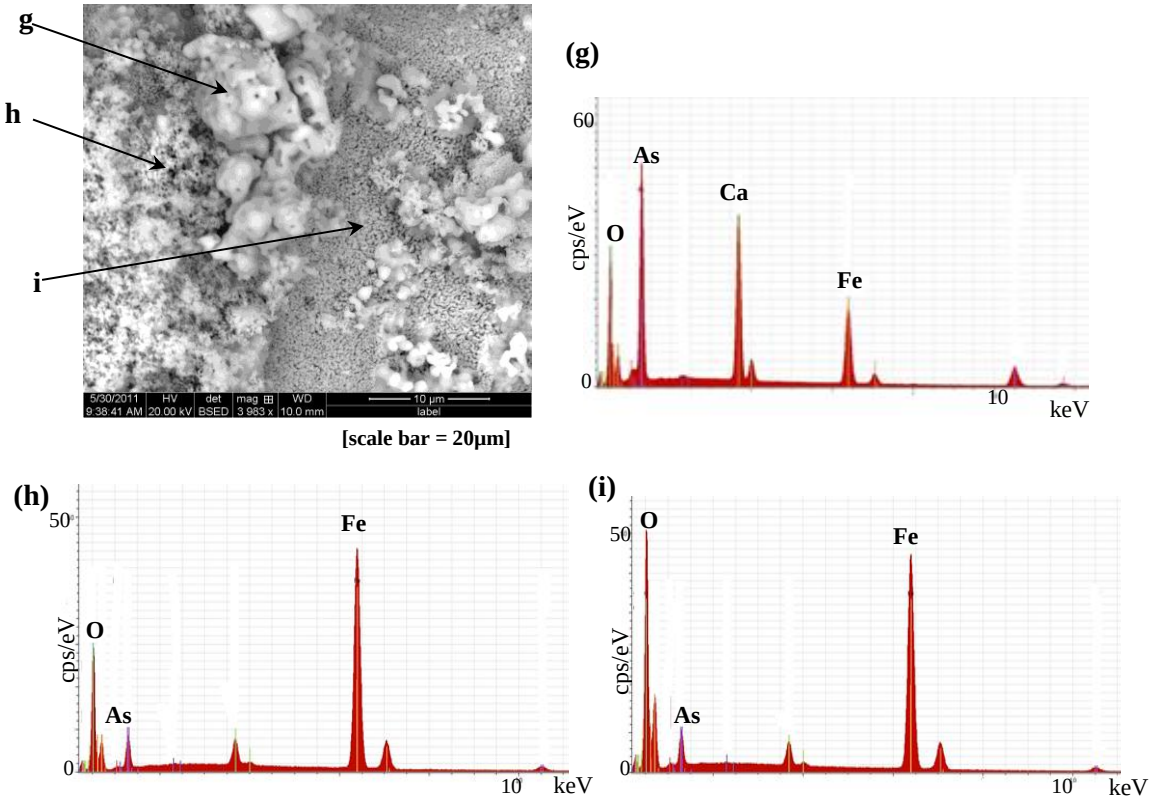

Figure 5.9: SEM image and EDX spectra (x-ray intensity vs energy) of tooeleite and lime calcines at 870˚C

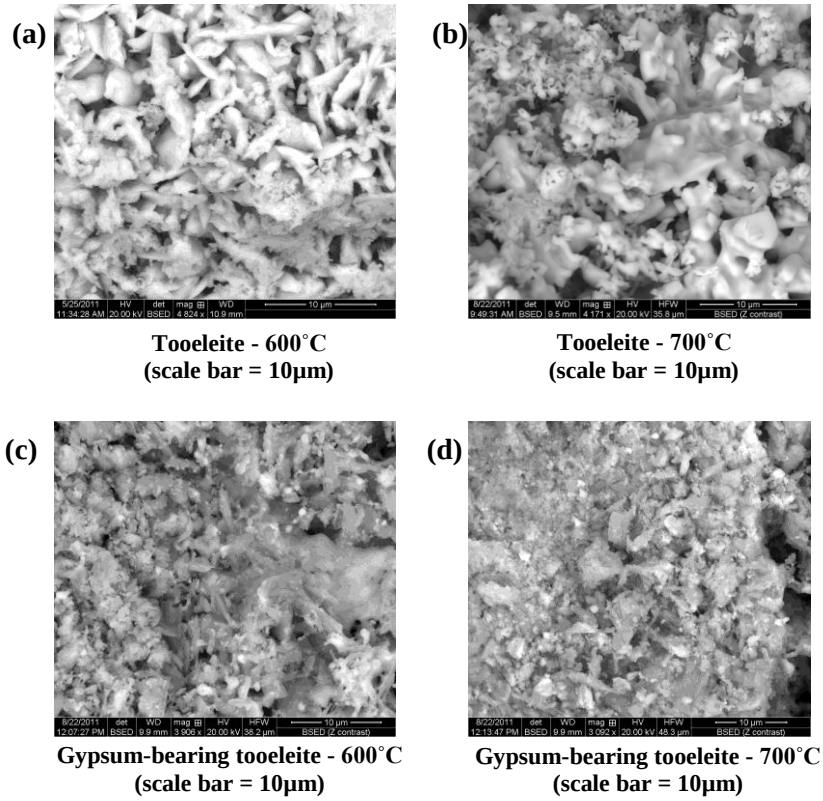

Figure 5.10: SEM images and EDX spectra (x-ray intensity vs energy) of tooeleite and gypsum-bearing calcines at 600˚C and 700˚C respectively

5.3.7. Stability tests

5.3.7.1. Calcines of tooeleite with lime additions

The TCLP leaching test was carried out to predict the stability of the tooeleite precipitates and calcines under specific pH conditions. Figure 5.11 presents the As leachability of the tooeleite precipitates and its respective calcines, as well as the pH of the final leachates after being subjected to the TCLP test. The calcines (without lime addition) obtained at 600 ˚C were the most stable, with an As leachability of 0.49 mg/L. The tooeleite precipitates have a high As leachability as tooeleite is not stable at pH 4.93 of the TCLP test. Tooeleite is stable between pH

2 to 3.5, therefore at pH values above 3.5, tooeleite dissolves incongruently to form arsenical ferrihydrite (As(III)-Fh) (Nishimura and Robins, 2008). Consequently, when subjected to the TCLP test at pH 4.93, the dissolution of tooeleite results in the release of arsenic into solution.

The calcines obtained at 500 ˚C have a low As leachability of 3 mg/L. At 500 ˚C, the TGA studies indicate that the tooeleite precipitates lose their structural water leaving an anhydrous compound which is deemed to be a ferric arsenate sulphate ($6Fe_2O_3.5As_2O_3.2SO_4$) (Nishimura and Robins, 2008). However, XRD analysis detected the presence of trace amounts of ferric arsenate ($Fe_7(AsO_4)_6$), which may also contribute to the stability of the calcines. The TCLP As leachability of the calcines (without lime) obtained at 600 ˚C was very low (0.49 mg/L) indicating that they consist of stable phases. The XRD analytical results indicated the presence of ferric arsenate ($FeAsO_4$) and hematite (Fe_2O_3) phases which contributed to the stability of the calcine. The calcines (without lime) obtained at 870 ˚C leached out slightly higher levels of arsenic when subjected to the TCLP test. These calcines have a higher TCLP As leachability than the calcines obtained at 600 ˚C, which seems to indicate that the angelellite phase ($Fe_4O_3(AsO_4)_2$) formed at 870 ˚C (Pantuzzo, Ciminelli and Brito, 2008) has a higher solubility than the ferric arsenate phase formed at 600 ˚C. Generally, As leachability was reduced by over 90% when the tooeleite precipitates are calcined and subjected to the TCLP test. The pH of the leachates ranged from 4.13 to 5.78.

The addition of lime, to minimise the SO_3 volitalization, decreased the stability of the tooeleite calcines. The calcined products with lime addition were found to be more unstable under the TCLP test compared to the calcines without the lime additive. The high As leachability is

attributed to the calcium arsenate phase ($Ca_3(AsO_4)_2$) which is known to be unstable at low pH (Bothe and Brown, 1999; Monhemius and Swash, 1999; Riveros et al., 2001). The As leachability of the TCLP leachates of the tooeleite precipitates and calcines (with and without lime additions) exceeded the Canadian Metal Mining Effluent Regulations (MMER) arsenic concentration of 0.5 mg/L (maximum monthly mean) (Environment Canada, 1977; Metal Mining Effluent Regulations, 2002) for mining effluents except for the calcines (without lime additions) obtained at 600 ˚C.

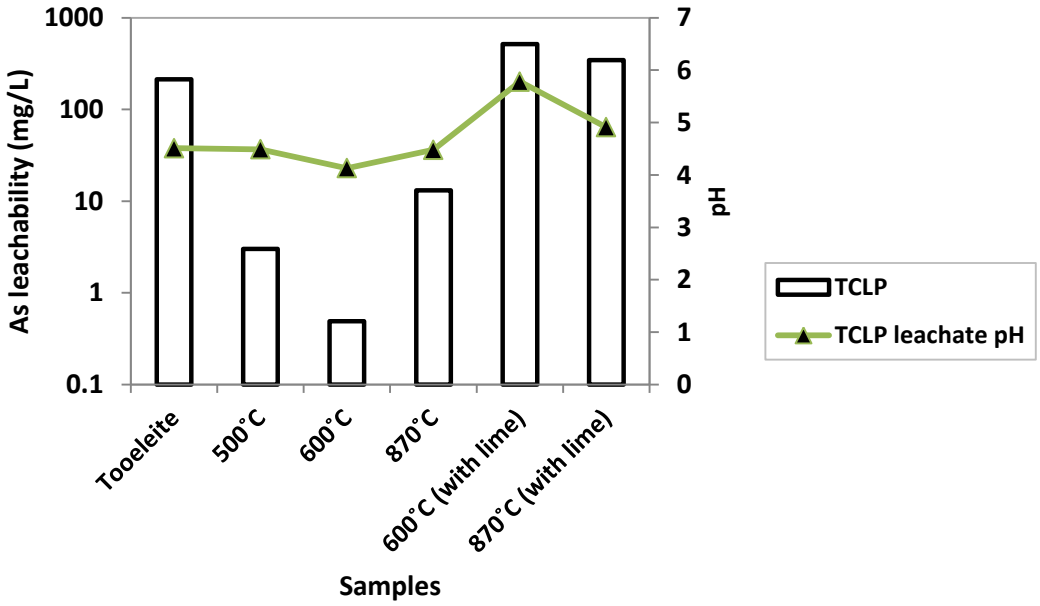

Figure 5.11: As leachability of tooeleite and its corresponding calcines (with and without lime additions) obtained at 500˚C, 600˚C and 870˚C, and their respective TCLP leachate pH

5.3.7.2. Calcines of tooeleite and gypsum-bearing tooeleite

Since lime is the preferred base used for the neutralization and removal of arsenic from copper smelter weak acid effluents due to economical reasons (Riveros et al., 2001; Jia and Demopoulos, 2008), the stability of calcined gypsum-bearing tooeleite precipitates was also investigated. Figure 5.12 presents a comparison of the TCLP leachate results of tooeleite and gypsum-bearing tooeleite, and their respective calcines at 600˚C, 700˚C and 800˚C. The tooeleite calcines obtained at 600 ˚C had the lowest As leachability of 0.49 mg/L. The most stable gypsum-bearing tooeleite calcines were obtained at 600 ˚C, and had an As leachability of 13.1 mg/L. XRD analysis of the gypsum-bearing calcines at 600˚C indicated the presence of an iron arsenate phase ($Fe_7As_6O_{24}$) and calcium sulphate (anhydrite), $CaSO_4$. The gypsum-bearing tooeleite calcines exhibited higher arsenic solubilities compared to the tooeleite calcines. The higher As solubilities of the gypsum-bearing tooeleite calcines could possibly be due to the formation of calcium arsenite/calcium arsenate during calcination, resulting from the arsenic adsorbed by gypsum in the course of the precipitation process. However XRD analysis of the calcines indicated the absence of calcium arsenite/arsenate phases. SEM analysis indicated that the Fe/As grains of the gypsum-bearing tooeleite calcines are less crystalline than the grains of the tooeleite calcines, which could also have attributed to their high As solubilities. Overall, the calcination of gypsum-bearing tooeleite resulted in the reduction of its As leachability by over 92%. The As leachability of the TCLP leachates of the gypsum-bearing tooeleite precipitates and calcines were above the Canadian Metal Mining Effluent Regulations (MMER) arsenic requirement of 0.5 mg/L. The pH of the leachates ranged from 4.51 to 4.90.

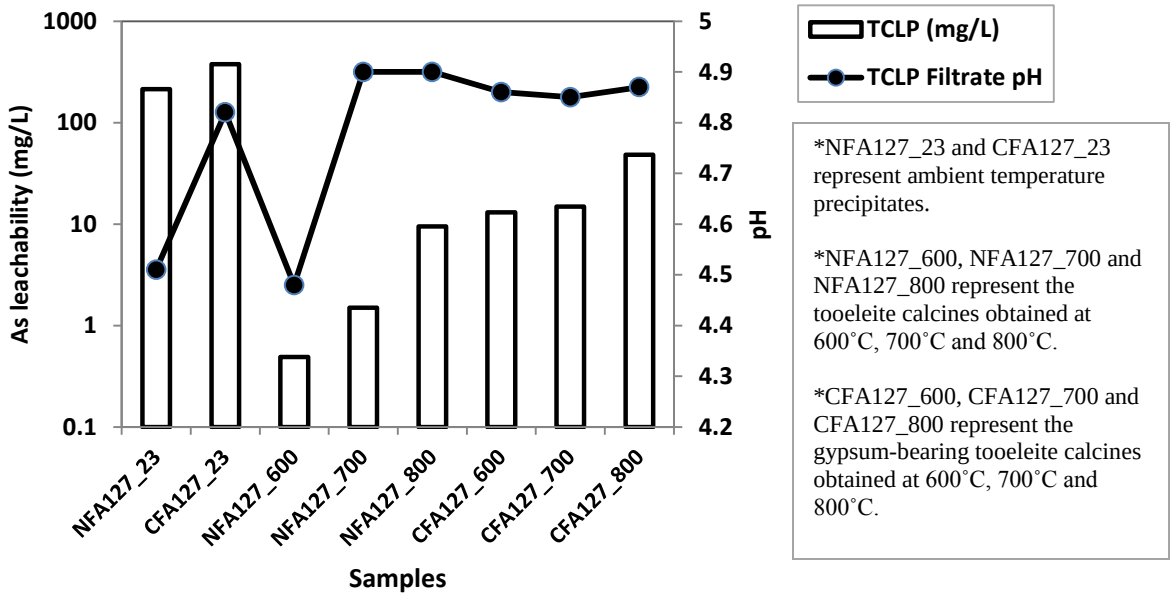

Figure 5.12: As leachability of tooeleite and gypsum-bearing tooeleite precipitates and their calcines (obtained at 600˚C, 700˚C and 800˚C) and their respective leachate pH

5.3.8. Proposed process

Based on the results obtained in this study, a conceptual process flowsheet is proposed for the fixation of As(III) from smelter weak acid effluents. According to the flowsheet illustrated in Figure 5.13, the As-bearing weak acid effluent and recycled As(III)-Fh (Fe:As molar ratio = 4) are pumped to the first vessel of a three-stage precipitation circuit. The As(III)-Fh acts as a source of ferric iron, and is added at an Fe:As molar ratio of 1 to the first vessel. The pH of the mixture is adjusted to pH 2.7- 3, with the addition of lime. Lime is preferred by industry as a neutralizing agent due to its low cost. A retention time of 1 hour is sufficient to remove about 85% of As(III) in the form of tooeleite at <pH 3.

The resulting slurry containing tooeleite and gypsum is subjected to solid-liquid separation. Gypsum-bearing tooeleite precipitates formed at pH 2.7- 3 have low stabilities (typically 378 mg/L As at pH 5) and therefore would need to be disposed of in a lined pond with ongoing monitoring and maintenance. However, calcination of the gypsum-bearing tooeleite precipitates at 600 - 700˚C considerably improves their stability (13.1 to 14.9 mg/L As). Consequently, the gypsum-bearing tooeleite filter cake can either be disposed of in a lined tailings pond or calcined at 600 - 700˚C to form a ferric arsenate calcine of low volume and a relatively high stability that would need to be disposed of in a lined pond.

The filtrate from the first vessel is pumped to the second vessel, and ferric sulphate ($Fe_2(SO_4)_3$) is added to maintain an Fe:As molar ratio of 4 in the second vessel. Lime is added to raise the pH to 5, resulting in the precipitation of any residual As as arsenical ferrihydrite (As(III)-Fh) as well as gypsum. The retention time in the second vessel is an hour. The slurry from the second vessel undergoes solid-liquid separation, and the filter cake (As(III)Fh with an Fe:As molar ratio=4) is recycled back to the first vessel to be used as a source of ferric in the precipitation of tooeleite. The filtrate is pumped to the third vessel. Lime is added to the third vessel to adjust the pH of the filtrate to pH 8-10, thereby resulting in the precipitation of the residual dissolved metals as base metal hydroxides, which are finally sent to the tailings pond for disposal. The retention time in the third vessel is an hour. This process is considered to be economically attractive as As(III) is easily fixed under ambient conditions and has lower iron requirements, resulting in lower precipitation costs.

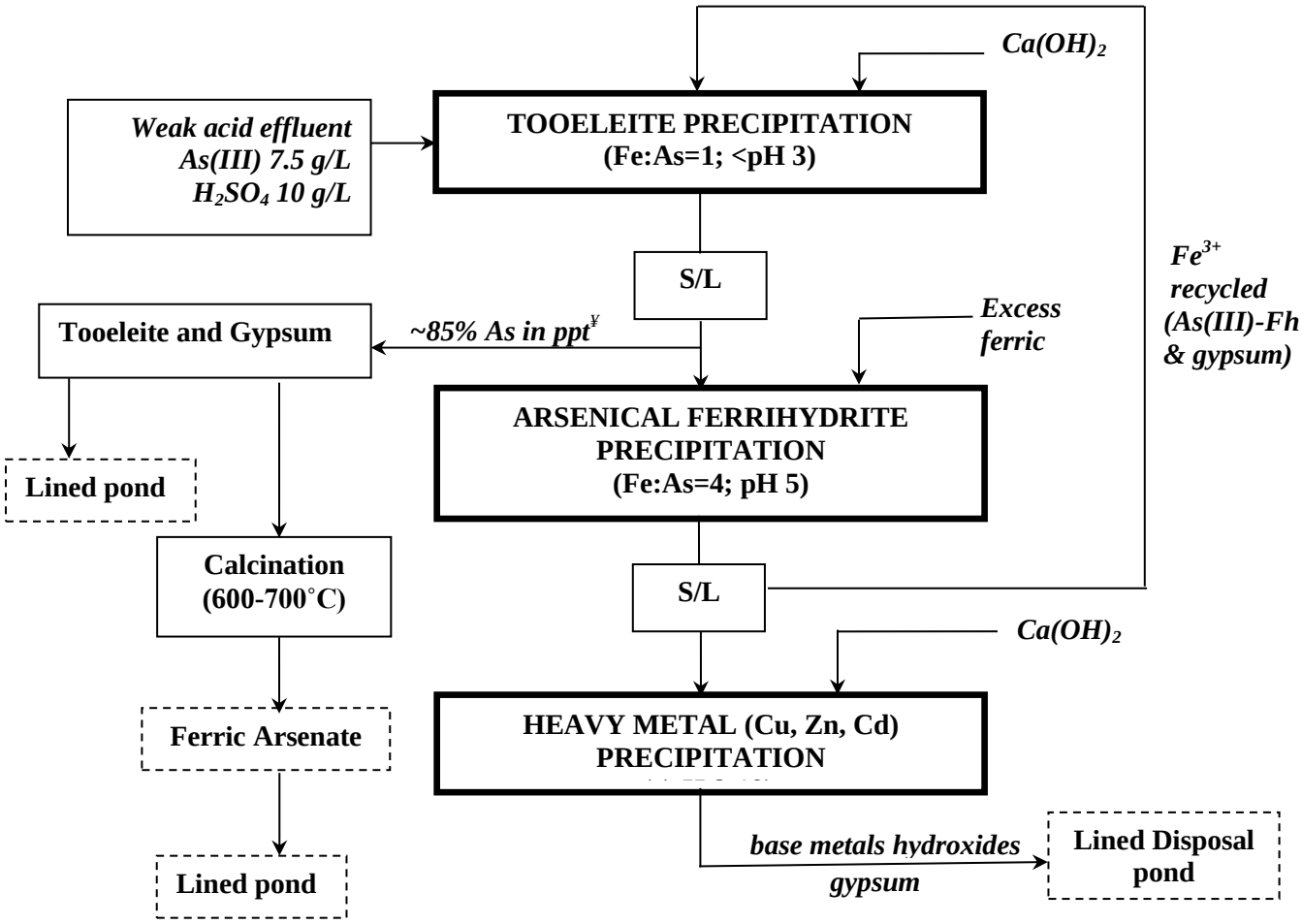

Figure 5.13: A conceptual flowsheet for the fixation of As(III) in a weak acid smelter effluent (As(III) = 7.5 g/L and H_2SO_4 = 10 g/L) to tooeleite and the calcination of tooeleite. ppt¥ denotes precipitates and S/L denotes solid/liquid separation

5.4. Conclusions

Calcination of tooeleite fundamentally improved its stability and the immobilization of As, with the most stable calcines being obtained at 600 ˚C. Calcination of tooeleite reduced the As leachability of the tooeleite residues by >90%. Calcination of tooeleite at 600 ˚C yielded a mixture of hematite and ferric arsenate, as characterized by XRD analysis, which proved to be very stable with an As leachability of 0.49 mg/L when subjected to the TCLP test. Calcination of tooeleite with lime additions was effective in capturing SO_3 evolved in the temperature range of 500 ˚C to 800 ˚C as well as preventing the volatilization of As_2O_3. However, the lime additions reduced the stability of tooeleite calcines generated at both 600 ˚C and 870 ˚C due to the formation of a calcium arsenate phase which is unstable under low pH regimes.

Calcination of gypsum-bearing tooeleite reduced the As leachability of the calcines by >92%. The most stable calcines were obtained at 600˚C, with an As leachability of 13.1 mg/L under TCLP conditions. XRD analysis of the gypsum-bearing calcines (600˚C) indicated the presence of an iron arsenate phase ($Fe_7As_6O_{24}$) and calcium sulphate (anhydrite), $CaSO_4$. The observed higher As solubilities of gypsum-bearing tooeleite and its' calcines compared to those of tooeleite and its' calcines was attributed to arsenic that was adsorbed by gypsum during the precipitation process, probably via As(III)-Fh-Ca(II) association or As(III)-Ca(II) coadsorption by ferrihydrite.

Chapter 6

Conclusions and future work

6.1. Conclusions

6.1.1. Mineralogical characterization of the Horne ETP co-precipitates

Xstrata's Horne Copper Smelter ETP co-precipitates were characterized using synchrotron-based analytical techniques to determine their mineralogy with the aim of understanding the fundamental mechanism of As retention in these residues. In addition, previous literature on As(III)-Fh transformation and stability tests performed on synthetic As(III)-Fh precipitates under simulated disposal conditions were used to try to estimate the long-term stability of the Horne's As-bearing co-precipitates in its disposal pond.

Mineralogical characterization using synchrotron-based analysis indicated that the Horne ETP co-precipitates consisted predominantly of a mixture of gypsum and amorphous ferric arsenate. Other phases that were identified include zinc hydroxide and franklinite (zinc ferrite). Mixed As oxidation states were found to be present in the Horne ETP precipitates, and the predominant species was As(V) which accounted for 49 – 84% of total As in the precipitates. The high As(V) levels detected in the Horne ETP co-precipitates were possibly due to the partial oxidation of the Horne ETP sludge during storage, prior to characterization studies. Based on laboratory tests simulating the Horne ETP, it was previously postulated that during the precipitation in the first stage of the ETP (Fe:As=3; pH 4.5), the As precipitates out as an amorphous equimolar ferric arsenite (Fe:As=1), and most of the excess ferric precipitates as an

amorphous ferrihydrite. It was difficult to explain the puzzling predominance of As(V) in the system. However, based on laboratory precipitation (Mahoney et al., 2007) and synchrotron data (Warner and Rowson, 2007) from the JEB mill ETP (Northern Saskatchewan), it is hypothesized that under the redox conditions in the tailings pond, the nanocrystalline ferric arsenite precipitate is quite rapidly (months) oxidized by excess Fe(III) to As(V) and transformed probably into a Fe(II)-Fe(III)-As(V) phase that is stable at pH 9. It must be noted that the process chemistry of the Horne ETP and JEB ETP and their respective co-contaminants are may be very different, and consequently further work is required to investigate if the gradual oxidation of the As(III) species in Horne ETP co-precipitates by excess Fe(III) to form a Fe(II)-Fe(III)-As(V) phase takes place.

Time series transformation tests performed by evaluating the transformation rate of ferrihydrite in the presence of adsorbed As(III) under simulated in-situ disposal pH 9 conditions existing at the Horne Tailings Facility indicated that increasing quantities of As(III) (high Fe:As ratios) considerably reduced the rate of ferrihydrite transformation and the subsequent As dissolution. Although the findings of these transformation experiments cannot be considered to be representative for the extrapolation of the stability of the Horne precipitates, they suggested that that the Horne ETP co-precipitates will remain stable for thousands of years due to the adsorbed As, along with zinc hydroxide and gypsum that further stabilize and buffer the system.

This research has demonstrated that arsenic removal in the form of As(III) from copper smelter weak acid effluents by lime neutralization and co-precipitation with ferric iron (Fe:As >3) can be equally as effective as As removal, and excess ferric iron is required to ensure the stability of the As-bearing residues.

6.1.2. Tooeleite as a potential disposal option

The investigation of tooeleite as an alternative potential disposal option for the fixation of As from copper smelter weak acid effluents was achieved by investigating the effect of precipitating tooeleite from As(III)-bearing weak acid solutions under varying precipitation conditions (Fe:As molar ratio, pH and neutralizing agent) on the As removal efficiency, and evaluation of the precipitate characteristics and stability. Calcination was also investigated as a potential approach for enhancing the stability of tooeleite for disposal.

The effect of the initial Fe:As molar ratio and neutralizing agent (NaOH and $Ca(OH)_2$) on the As removal efficiency from Fe(III)-As(III) solutions (Fe:As = 1.0, 1.5 and 2) under ambient conditions was investigated. The effectiveness of As removal was enhanced with increasing Fe:As molar ratio and pH. The use of lime as opposed to sodium hydroxide as a neutralizing agent enhanced the arsenic removal efficiency, with >90% of arsenic being removed at pH>4 in the $Ca(OH)_2$ neutralized systems. Tooeleite was found to form in the pH range 2 to 3.5, but rapidly transformed at >pH 4 to form a poorly crystalline equimolar ferric arsenite phase which was stable in the pH range 6 to 8. The poorly crystalline phase deemed to be ferric arsenite was characterized using synchrotron-based μXRD analysis and was found to have two broad peaks at 2.9Å and 1.6Å. Subsequent preliminary studies have indicated that ferric arsenite can also be formed by direct precipitation from an equimolar Fe(III):As(III) weak acid solution at pH 4 to 8. These findings suggest that the neutralization of a Fe(III)-As(III) bearing weak acid solution (Fe:As >3) at pH 4.5 as at the Horne ETP will result in most of the As being precipitated as ferric arsenite together with arsenical ferrihydrite (As(III)-Fh).

TCLP stability analysis of the precipitates formed from NaOH and $Ca(OH)_2$ neutralized systems (Fe:As=1.0, 1.5, 2.0; 25˚C) indicated that both tooeleite and ferric arsenite have a relatively high As solubility at pH 5. Arsenic solubility is still relatively high at higher pH regimes up to pH 10. The effect of higher Fe:As molar ratios and co-deposition with additional inert solids was not studied but data from the Horne (Quebec) and JEB (Northern Saskatchewan) tailings facilities suggest that by using Fe:As>3, the resulting co-precipitates are still stable after up to 20 years under anoxic conditions in their respective tailings disposal areas.

High temperature precipitation of tooeleite at 95˚C resulted in the transformation of tooeleite to a more crystalline phase with the subsequent release of As, suggesting an increase in Fe:As ratio of the precipitates. However, high temperature precipitation did not enhance the As removal efficiency or stability of tooeleite compared to that of the ambient temperature precipitation. Calcination of tooeleite fundamentally improved its TCLP stability, with the most stable calcines being obtained at 600˚C. Calcination of tooeleite precipitates at 600 ˚C yielded a mixture of hematite and ferric arsenate ($FeAsO_4$), as characterized by bulk XRD analysis, which proved to be very stable with a TCLP As leachability of 0.5 mg/L. Calcination of gypsum-bearing tooeleite at 600 ˚C yielded a mixture of an iron arsenate phase ($Fe_7As_6O_{24}$) and calcium sulphate (anhydrite) ($CaSO_4$), but the calcines had a higher TCLP As leachability of 13.1 mg/L possibly due to the formation of calcium arsenite/arsenate from The gypsum-bearing tooeleite calcines exhibited higher arsenic solubilities compared to the tooeleite calcines. SEM analysis indicated that the Fe/As grains of the gypsum-bearing tooeleite calcines were less crystalline than the grains of the tooeleite calcines, which could have attributed to their high As solubilities compared to the tooeleite calcines.

Based on these findings, a new process was proposed for the fixation of As(III) from copper smelter weak acid effluents using tooeleite as a disposal option, which involves the precipitation of As(III) with ferric (Fe:As=1.2) as tooeleite, and the subsequent calcination of tooeleite at 600 – 700˚C to form a ferric arsenate calcine of low volume and a relatively high TCLP stability which is disposed of in a lined tailings pond.

6.2. Recommendations for further research

It is recommended that further research on this work can be undertaken in the following areas:

- It has been postulated, that under actual disposal conditions, the As(III) species in the Horne ETP co-precipitates will gradually be oxidized to As(V) by Fe(III) over time, and concurrently Fe(III) will be reduced to Fe(II) leading to the formation of a Fe(II)-Fe(III)-As(V) phase. Further characterization studies should be carried out using Fe K-edge μXANES analysis to determine if a ferrous arsenate phase is present in the aged Horne ETP co-precipitates. Furthermore, Zn K-edge μXANES analytical studies should be conducted to shed more light on the sorption mechanism of Zn(II) by ferrihydrite.

- Characterization studies using Scanning Electron Microscopy (SEM) and synchrotron-based Extended X-ray Absorption Fine Structure Spectroscopy (EXAFS) in order to determine the morphology of ferric arsenite co-precipitates as well as the molecular structure and the mechanism of As(III) retention in ferric arsenite respectively.

- Further studies are required to determine the transformation of precipitated tooeleite and ferric arsenite at Fe:As molar ratios of 1-1.5 in anoxic and oxic conditions at pH 7-10 (simulating disposal but with little or no excess ferric iron).

- Further precipitation and characterization studies on the high temperature precipitates (60 – 95˚C) of ferric arsenite formed using initial solutions of Fe:As molar ratios of 1-1.5 at pH 6-10.

- Further work on the mechanical structural stability of As-bearing residues disposed of in a tailings management facility.

Bibliography

Alforque, M., 1996. Synthetic Precipitation Leaching Procedure. US EPA (360) 871 – 8748.

Andrade, C.F., Jamieson, H.J., Praharaj, T., Fortin, D., and Kyser, T.K., 2010. Biogeochemical cycling of arsenic in mine-impacted sediments and co-existing pore waters. *Applied Geochemistry* **25**, 199-211.

Ante, A., Bröckl, R., Cabezas, J.A.S. and Schönbrunner, S., 2005. Production of marketable gypsum from weak waste acids – saving disposal volume and costs. *World of Metallurgy – ERZMETALL* **58(2)**, 75-82.

Anthony, J.W., Bideaux, R.A., Bladh, K.W. and Nichols, M.C., 1990. Handbook of Mineralogy, I. Elements, Sulfides, Sulfosalts. Mineral Data Publishing, Tucson, Arizona.

Arai, Y., Lanzarotti, A., Sutton, S.R., Newville, E., Dyer, J., and Sparks, D.L., 2006. Spatial and temporal variability of arsenic solid-state speciation in historically lead arsenate contaminated soils. *Environmental Science and Technology* **40**, 673-679.

Arriagada, F.J. and Osseo-Asare, K., 1984. Gold extraction from refractory ores: Roasting behavior of pyrite and arsenopyrite. In: *Precious Metals: Mining, Extraction and Processing*, Kudryk, V. (ed.), AIME, 367-385.

Bang, S. and Meng, X., 2004. A review of arsenic interactions with anions and iron hydroxides. *Environmental Engineering Research* **9(4)**, 184-192.

Berezowsky, R.M.G.S., Weir, D.R., 1989. Refractory gold: the role of pressure oxidation. In: *Proceedings of World Gold*, AIME, 152-156.

Bluteau, M-C and Demopoulos, G.P., 2007. The incongruent dissolution of scorodite – solubility, kinetics and mechanism. *Hydrometallurgy* **87**, 163-177.

Bothe. J.V. and Brown, P.W., 1999a. Arsenic immobilization by calcium arsenate formation. *Environmental Science and Technology* **33(21)**, 3806-3811.

Bothe, J.V. and Brown, P.W., 1999b. The stabilities of calcium arsenates at 23+/-1 ˚C. *Journal of Hazardous Materials* **B69**, 917-207.

Bowell, 1994. Sorption of arsenic by iron oxides and oxyhydroxides in soils. *Applied Geochemistry* **9(3)**, 279-286.

Boyle, R.W. and Jonasson, I.R., 1973. The geochemistry of arsenic and its use as an indicator element in geochemical prospecting. *Journal of Geochemical Exploration* **2(3)**, 251-296.

Bruckard, W.J., Davey, K.J., Jorgensen, F.R.A., Wright, S., Brew, D.R.M., Haque, N., and Vance, E.R., 2010. Development and evaluation of an early removal process for the beneficiation of arsenic-bearing copper ores. *Minerals Engineering* **23(15)**, 1167-1173.

Carlson, L., Bigham, J.M., Schwertmann, U., Kyek, A. and Wagner, F., 2002. Scavenging of As from acid mine drainage by schwertmannite and ferrihydrite: a comparison with synthetic analogues. *Environmental Science and Technology* **36**, 1712-1719.

Casiot, C., Lebrun, S., Morin, G., Bruneel, O., Personnè, J-C., Elbaz-Pouliche, F., 2005. Sorption and redox processes controlling arsenic fate and transport in a stream impacted by acid mine drainage. *Science of Total Environment* **347**, 122-130.

Casiot, C., Morin, G., Julliot, F., Bruneel, O., Personnè, J-C., Leblanc, M., Duquesne, K., Bonnefoy, V., Elbaz-Pouliche, F., 2003. Bacterial immobilization and oxidation of arsenic in acid mine drainage (Carnoulès creek, France). *Water Research* **37**, 2929-2936.

Celep, O., Alp, I., Deveci, H., and Vicil, M., 2009. Characterization of refractory behaviour of complex gold/silver ore by diagnostic leaching. *Transactions of Nonferrous Metals Society of China* **19**, 707-713.

Cesbron, F.P., Williams, S.A., 1992. Tooeleite, a new mineral from the US Mine, Tooele County, Utah. *Mineraological Magazine* **56**, 71-73.

Cornell, R., Giovanoli, R., Schnidler, P., 1987. Effect of silicate species on the transformation of ferrihydrite into goethite and hematite under alkaline media. *Clays and Clay Minerals* **35(1)**, 21-28.

Cornell, R.M. and Schneider, W., 1989. Formation of goethite from ferrihydrite at physiological pH under the influence of cysteine. *Polyhedron* **8**, 149-155.

Cornell, R.M. and Schwertmann, U., 2003. The iron oxides: structure, properties, reactions, occurrences and uses. 2nd ed. WILEY-VCH GmbH & Co. KGaA. Print.

Cornell, R.M., 1988. The influence of some divalent cations on the transformation of ferrihydrite to more crystalline products. *Clay Minerals* **23(3)**, 329-332.

Cornell, R.M., Giovanoli, R. and Schindler, P.W., 1987. Effect of silicate species on the transformation of ferrihydrite into goethite and hematite in alkaline media. *Clays and Clay Minerals* **38**, 469-476.

Corriveau, M.C., Jamieson, H.E., Parsons, M.B. and Hall, G.E.M., 2011b. Mineralogical characterization of arsenic gold mine tailings from three sites in Nova Scotia. *Geochemistry: Exploration, Environment, Analysis* **11**, 179-192.

Corriveau, M.C., Jamieson, H.E., Parsons, M.B., Campbell, J.L. and Lanzarotti, A., 2011a. Direct characterization of airborne particles associated with arsenic –rich mine tailings: particle size, mineralogy and texture. *Applied Geochemistry* **26**, 1639-1648.

Cudennec, Y. and Lecerf, A., 2006. The transformation of ferrihydrite into goethite or hematite, revisited. *Journal of Solid State Chemistry* **179**, 716-722.

Cummings, D.E., Caccavo, F., Fendorf S., and Rosenzweig, R.F., 1999. Arsenic mobilization by the dissimilatory Fe(III)-reducing bacterium *Shewanella alga* BrY. *Environmental Science and Technology* **33**, 723-729.

Curreli, L., Garbarino, C., Ghiani, M., and Orrù.G, 2009. Arsenic leaching from a gold bearing enargite flotation concentrate. *Hydrometallurgy*, 96 (3), 258-263.

Curreli, L., Ghiani, M., Surracco, M., Orru, G., 2005. Beneficiation of a gold bearing enargite ore by flotation and As leaching with Na-hypochlorite. *Minerals Engineering* **18(8)**, 849-854.

Cutler, J.N., Jiang, D.T., and Remple, G., 2001. Chemical speciation of arsenic in uranium mine tailings by x-ray absorption spectroscopy. *Canadian Journal of Analytical Science and Spectroscopy* **46(4)**, 130-135.

Das, S., Hendry, J.M. and Essilfie-Dughan, J., 2011a. The transformation of two-line ferrihydrite to goethite and hematite as a function of pH and temperature. *Environmental Science & Technology* **45**, 268-275.

Das, S., Hendry, J.M., and Essilfie-Dughan, J., 2011b. Effects of adsorbed arsenate on the rate of transformation of 2-line ferrihydrite at pH 10. *Environmental Science & Technology* **45**, 5557-5563.

Demopolous, G.P, Lagno, F., Wang, Q. and Singhania, S., 2003. The atmospheric scorodite process. In: *Proceedings of Copper 2003–Cobre 2003 Hydrometallurgy of Copper*, The Canadian Institute of Mining, Metallurgy and Petroleum Montreal, Quebec, 597–616.

Demopoulos, G.P., 1994. Options for the immobilization of arsenic as crystalline scorodite. In: Impurity control and disposal in hydrometallurgical processes, G.B. Harris, E. Krause (eds.), Canadian Institute of Mining, Metallurgy and Petroleum, Montreal, 57-69.

Demopoulos, G.P., 1996. Effluent treatment by crystallization. In: *Clean Technology for the Mining Industry*, M.A. Sanchez, F. Vergara, S.H., Castro (eds.), Clean Technology for the Mining Industry, University of Conception, Conception-Chile, 1-12.

Demopoulos, G.P., 2005. On the preparation and stability of scorodite, $FeAsO_4.2H_2O$. In: *Arsenic Metallurgy*, Reddy, R.G., Ramachadran, V. (eds.), TMS (The Minerals, Metals & Materials Society), Warrendale, PA, 7-32.

Demopoulos, G.P., Droppert, D.J., and Van Weert, G., 1995. Precipitation of crystalline scorodite ($FeAsO_4.2H_2O$) from chloride solutions. *Hydrometallurgy* **38**, 245-261.

DeSisto, S.L., Jamieson, H.E. and Parsons, M.B., 2011. Influence of hard pan layers on arsenic mobility in historical gold mine tailings. *Applied Geochemistry* **26**, 2004-2018.

Di Benedetto, F., Pelo, S.D., Caneschi, A., and Lattanzi, P., 2011. Chemical state of arsenic and copper in enargite: evidences from EPR and X-ray absorption spectroscopies, and SQUID magnetometry. *Neues Jahrbuch fur Mineralogie-Abhandlungen* **188(1)**, 11-19(9).

Dixit S. and Hering, J.G., 2003. Comparison of arsenic (V) and arsenic (III) sorption onto iron oxide minerals: Implications for arsenic mobility. *Environmental Science & Technology* **37(8)**, 4182-4189.

Dove, P.M. and Rimstidt, J.D., 1985. The solubility and stability of scorodite, $FeAsO_4.2H_2O$. *American Mineralogist* **70(7-8)**, 838-844.

Droppert, D.J., Demopoulos, G.P., and Harris, G.B., 1996. Ambient pressure production of crystalline scorodite from arsenic-rich metallurgical effluent solutions. In: *Extraction and Processing Division Congress 1996,* The Minerals, Metals and Materials Society, Anaheim, California, U.S.A., 227–239.

Du Pleiss, C.A., Batty, J.D., and Dew, D.W., 2007. Impurities. In: *Biomining*, Rawlings, D.E. and Johnson, B.D. (eds), Springer Publishers, 64-65.

Duquesne, K., Lebrun, S., Casiot. C., Bruneel, O., Personnè, J-C., Leblanc, M., Elbaz-Poulichet, F., Morin, G., and Bonnefoy, V., 2003. Immobilization of arsenite and ferric iron by acidithiobacillus ferrooxidans and its relevance to acid mine drainage. Appiled Environmental Microbiology **69(10)**, 6165-6173.

Dutrizac, J.E. and Jambor, J.L., 1988. The synthesis of crystalline scorodite, $FeAsO_4.2H_2O$. *Hydrometallurgy* **19**, 377-384.

Dutrizac, J.E. and Jambor, J.L., 2007. Characterization of the iron arsenate-sulphate compounds precipitated at elevated temperatures. *Hydrometallurgy* **86**, 146-163.

Dzombak, D.A. and Morel, F.M.M., 1990. Surface complexation modelling, hydrous ferric oxide. Wiley-Interscience: New York, 331.

E. Krause and V.A. Ettel, "Solubilities and Stabilities of Ferric Arsenate Compounds". *Hydrometallurgy* **22**, 311-337.

Egal, M., Casiot, C., Morin G., Parmentier, M., Bruneel, O., Lebrun, S., and Elbaz-Poulichet, F., 2009. Kinetic control on the formation of tooeleite, schwertmannite and jarosite by Acidithibacillus ferrooxidans strains in an As(III)-rich acid mine drainage. *Chemical Geology* **265**, 432 – 441.

Egal, M., Casiot, C., Morin, G., Bruneel, O., and Elbaz-Poulichet, F., 2008. Kinetic controls on iron and arsenic precipitation in acid mine drainage (Carnoules, France). In: *Proceedings, 10th International Mine Water Association Congress*, 267-270.

Emett, M.T. and Khoe, G.H., 1993. Environmental stability of arsenic bearing hydrous iron oxide. G. Warren (Ed.) EPD Congress 1994, TMS, Warrendale, PA, 153-166.

Emett, M.T. and Khoe, G.H., 1994. Environmental stability of arsenic bearing hydrous iron oxide compounds. In: *EPD Congress*, Warren, G.W. (ed), The Minerals, Metals and Materials Society, Warrendale, PA, USA, pp.153-166.

Environment Canada, 1977. Metal Mining Liquid Effluent Regulations and Guidelines (EPS 1-WP-77-1).

Escobar-Gonzalez and Monhemius, A.J., 1988. The mineralogy of arsenates relating to arsenic impurity control. In: *Arsenic Metallurgy Fundamentals and Applications*, Reddy, R.G., Hendrix, J.L., and Queneau, P.B. (eds), The Minerals, Metals and Materials Society, Warrendale, PA, U.S.A., 405-453.

European Synchrotron Radiation Facility, 2012. A Light for Science – web accessed October 2012 http://www.esrf.eu/about/synchrotron-science/synchrotron-light

Fantauzzi, M., Rossi, G., Elsener, B., Loi, G., and Atzei, D., 2009. An XPS analytical approach for elucidating the microbially mediated enargite oxidative dissolution. *Analytical and Bioanalytical Chemistry* **393**, 1931-1941.

Fawcett, S.E. and Jamieson, H.E., 2011. The distinction between ore processing and post-depositional transformation on the speciation of As and Sb in mine waste and sediment. *Chemical Geology* **283**, 109-118.

Ferguson, J.F., and Gavis, J., 1972. A review of the arsenic cycle in natural waters. *Water Research* **6**, 1259-1274.

Filippou, D. and Demopoulos, G.P., 1997. Arsenic immobilization by controlled scorodite precipitate. *Journal of Minerals, Metals and Materials Society* **49(12)**, 52-55.

Filippou, D., St-Germain, P., and Grammatikopoulos, T., 2007. Recovery of metal values from copper-arsenic minerals and other related resources. *Mineral Processing and Extractive Review* **28** (4), 247-298.

Foster, A.L., Brown, G.E., Tingle, T.N., Parks, G.A., 1998. Quantitative arsenic speciation in mine tailings using X-ray absorption spectroscopy. *American Mineralogist* **83**, 553.

Fraser, K.S., Walton, R.H., and Wells, J.A., 1991. Processing of refractory gold ores. *Minerals Engineering* **4 (7-11)**, 1029-1041.

Frost, R.R. and Griffin, R.A., 1977. Effect of pH on adsorption of arsenic and selenium from landfill leachate by clay minerals. *Soil Science Society of America Journal* **41**, 53-57.
Garelick, H., Jones, H., Dybowska, A., and Valsami-Jones, E., 2008. Arsenic pollution sources. *Reviews of Environmental Contamination and Toxicology* **197**, 17-60.

Gautier, J., Grosbois, C., Courtin-Nomade, A., Floc'h, J.P. and Martin, F., 2006. Transformation of natural As-associated ferrihydrite downstream of a remediated mining site. *European Journal of Mineralogy* **18**, 187-195.

Ghosh, A., Mukiibi, M., and Ela, W., 2004. TCLP underestimates leaching of arsenic from soild residuals under landfill conditions. *Environmental Science and Technology* **38**, 4677-4682.

Godbehere, P.W., Pinard, D., and Guimont, J., 1995. Development of a treatment process for an arsenic-bearing weak acid effluent using iron and zinc derived from acid mine drainage and smelter precipitator dust. In: *Copper 95- Cobre 95*, vol. II, A. Casali, G.S. Dobby, M. Molina, and W.J. Thoburn (eds), Canadian Institute of Mining, Metallurgy and Petroleum, Montreal, Canada, 377 – 389.

Goh, K-H. and Lim, T-T., 2005. Arsenic fractionation and influence of various anions on its mobility in the subsurface environment. *Applied Geochemistry* **20**, 229-239.

Goldberg, S. and Johnston, C.T., 2001. Mechanisms of arsenic adsorption on amorphous oxides evaluated using macroscopic measurements, vibrational spectroscopy, and surface complexation modeling. *Journal of Colloid and Interface Science* **234 (1)**, 204-216.

Goldberg, S., 2002. Chemical adsorption of arsenate and arsenite on oxides and clay minerals. *Soil Science Society American Journal* **50**, 1154-1157.

Graeser, S., Schwander, H., Demartin, F., Gramaccioli, C.M., Pilati, T. and Reusser, E., 1994. Fetiasite (Fe^{II},Fe^{III},Ti)$_3O_2As_2O_5$, a new arsenite mineral – its description and structure determination, *American Mineralogist* **79**, 996-1002.

Greenleaf, J.E., Cumbal, L., Staina, I. and Sengupta, A.K., 2003. Abiotic As(III) oxidation by hydrated Fe(III) oxide (HFO) microparticles in a plug flow columnar configuration. *Process Safety and Environmental Protection* **81(2)**, 87-98.

Hammersley, A.P., 1998. FIT2D v10.3 Reference manual v4.0. European Synchrotron Research Facility, Paper ESRF98-HA01T (manual available at http://www.csb.yale.edu/userguides/datamanip/fit2d/fit2d_ref.pdf)

Harris, B., 2003. The removal of arsenic from process solutions: theory and industrial practice. In: *Hydrometallurgy*, volume 2: Electrometallurgy and Environmental Hydrometallurgy. C.A. Young, A.M. Alfantazi, C.G. Anderson, D.B. Dreisinger, B. Harris and A. James (eds), TMS (The Minerals, Metals & Materials Society).

Harris, B., 2003. The removal of arsenic from process solutions: theory and industrial practice. In: *Proceedings of the Fifth International Symposium for Hydrometallurgy*, The Minerals, Metals & Materials Society, Vancouver BC, Canada, 1889–1902.

Harris, G.B. and Krause, E., 1993. The disposal of arsenic from metallurigical processes: its status regarding ferric arsenate. In Reddy, R.G., Weizenbach, R.N. (Eds), Extractive Metallurgy of copper, nickel and cobalt, vol. I. TMS, Warrendale, PA, 1221-1237.

Harris, G.B. and Monette, S., 1988. The stability of arsenic-bearing residues. In: Arsenic Metallurgy: Fundamentals and Applications. Reddy, R.G., Hendrix, J.L., Queneau, P.B. (eds), TMS, Warrendale, PA, 469 – 498.

Hartman, H.L., 1992. Society for Mining, Metallurgy, and Exploration mining engineering handbook, 2nd Edition, vol. 1, 76 .

Harvey, M.C., Schreiber, M.E., Rimstidt, J.D., and Griffith, M.M., 2006. Scorodite dissolution kinetics: implications for arsenic release. *Environmental Science Technology* **40**, 6709-6714.

Hino. J., Kawabata, T., Miyamoto, K., and Yamaki, T., 1995. Removal and recovery of minor elements in copper smelting. In: *Proceedings of Copper-Cobre International Conference*, Vol. III – Electrorefining and Hydrometallurgy of Copper. Cooper, W.C, Dreisinger, D.B., Dutrizac, J.E., Hein, H. and Ugarte, G. (eds). The Metallurgical Society of CIM, 617-627.

Hoffman, J.E., 1993. Remediating copper smelter dusts: the arsenic problem, *JOM Journal of the Minerals, Metals and Materials Society* **45(8)**, 30 - 31.

Hohn, J.W., 2005. Modified ferrihydrite for enhanced removal of arsenic from mine wastewater. M.Sc. Thesis, Department of Metallurgical/Materials Engineering, Montana Tech of the University of Montana, butte, MT.

Huang, H.H., Twidwell, L.G., Young, C.A., Gow, R.N., and McCloskey, J., 2008. Free energies from the solubility of solid compounds using speciation calculations. In: *Hydrometallurgy: Proceedings of the Sixth International Symposium*. C.A.Young, P.R. Taylor, C.G. Anderson, and Y. Choi (eds), Soc. Min. Met. Expl. Littleton, USA, pp. 1123 – 1133.

Hurtado-Jimenez, R. and Gardea-Torresdey, J.L., 2006. Arsenic in drinking water in the Los Altos de Jalisco region of Mexico. *Rev Panam Salud Publica*tion, **20(4)**, 236-247.

Jain, A. and Loeppert, R.H., 2000. Effect of competing anions on the adsorption of arsenate and arsenite by ferrihydrite. *Journal of Environmental Quality* **29(5)**, 1422-1430.

Jain, A., Raven, J.P. and Loeppert, R.H., 1999. Arsenite and arsenate adsorption on ferrihydrite: surface charge reduction and net OH- release stoichiometry, *Environmental Science & Technology* **33(8)**, 1179-1184.

Jambor , J.L. and Dutrizac, J.E.,1998. Occurrence and constitution of natural and synthetic ferrihydrite, a widespread iron oxyhydroxide. *Chemical Reviews* **98**, 2549-2585.

Jamieson, H.E. and Gault, A. Application of synchrotron microanalysis to studies of soilds, sediments, dust and mine waste (in press).

Jamieson, H.E., Walker, S.R., Andrade, C.F., Rasmussen, P., Beauchemin, S., Lanzirotti, A., Parsons, M.B. and Wyre, L.A., 2011. Direct identification of metal compounds in contaminated soil, mine tailings, lake sediments and house dust using synchrotron-based microanalysis. *Human and Ecological Risk Assessment* **17**, 1292-1309.

Jang, J.H. and Dempsey, B.A., 2008. Co-adsorption of arsenic (III) and arsenic (V) onto hydrous ferric oxide: effects on abiotic oxidation of arsenic (III), extraction efficiency, and model accuracy. *Environmental Science& Technology* **42(8)**, 2893-2898.

Jia, Y. and Demopoulos, G.P., 2008. Co-precipitation of arsenate with iron(III) in aqueous sulfate media: Effect of time, lime as base, and co-ions on arsenic retention. *Water Research* **42(3)**, 661–668.

Jia, Y. and Demopoulos, G.P., 2005. Adsorption of arsenate onto ferrihydrite from aqueous solutions: influence of media (sulfate vs nitrate), added gypsum, and pH alteration. *Environmental Science & Technology* **39(24)**, 9523-9527.

Jia, Y., Xu, L., Fang, Z. and Demopoulos, G.P., 2006. Observation of surface precipitation of arsenate on ferrihydrite. *Environmental Science Technology* **40**, 3248-3253.

Jia, Y.F., Demopoulos, G.P., Chen, N., Cutler, J.N. and Jiang, D.T., 2003. Preparation, characterisation and solubilities of adsorbed and co-precipitated iron(III)-arsenate solids. In: *Hydrometallurgy 2003* – Proceedings of the international symposium honouring Professor Ian M. Ritchie, Young, C., Alfantazi, A., Anderson, C., James, A., Dreisinger, D., Harris, B. (eds), vol. 2, TMS, Warrendale, PA, 1923 – 1935.

Johnston, J.H. and Lewis, D.G., 1983. A detailed study of the transformation of ferrihydrite to hematite in aqueous medium at 92˚C. *Geochimica Cosmochimica Acta* **47**, 1823-1831.

Kapaj, S., Peterson, H., Liber, K., and Bhattacharya, P., 2006. Human health effects from chronic arsenic poisoning – A review. *Journal of Environmental Science and Health Part A* **41**, 2399 – 2428.

Karagas, M.R., Le, C.X., Morris, S., Blum, J., Lu, X., and Spate, V., 2001. Markers of low level arsenic exposure for evaluating human cancer risks in the US population. *International Journal of Occupational Medicine and Environmental Health* **14**, 171-175.

Kearns, D.P. and Shields, J.W., 1996. Lowering the threshold for refractory gold deposits with new biooxidation technologies. *MINExpo International*, Las Vegas, NV, September 11, 1996.

Khoe, G.H., Carter, M.T., Emett, E.R. Vance and Zaw, M., 1994. The stability and immobilization of iron arsenate compounds. *Sixth AusIMM Extractive Metallurgy Conference*, The Australian Institute of Mining and Metallurgy, Carlton, Victoria, Australia, 281-286.

Krause, E. and Ettel, V.A., 1989. Solubilities and stabilities of ferric arsenate compounds. *Hydrometallurgy* **2**, 311–337.

Krause, E. and Ettel, V.A., 1985. Ferric arsenate compounds: are they environmentally safe? Solubilities of basic ferric arsenates. In: *Impurity control and disposal*, Proceedings 15th Annual Hydrometallurgical Meeting of CIM, Oliver, A.J. (ed.), Vancouver, August 1985, CIM, Canada.

Krause, E. and Ettel, V.A., 1987. Solubilities and stabilities of ferric arseantes. In: *Crystallization and precipitation*, Proceedings, ISCAP meeting, Starthdee, G.L., Klein, M.O., and Melis, L.A., (eds), Saskatoon, Canada, October 5-7, pp. 195-210.

Kyle, J.H. and Lunt, D., 1991. An investigation of disposal options for arsenic trioxide produced from roasting operations. In: *Fifth AusIMM Extractive Metallurgy Conference*, The Australasian Institute of Mining and Metallurgy, Carlton, Victoria, Australia, 347-353.

Langmuir, D., Mahoney, J. and Rowson, J., 2006. Solubility products of amorphous ferric arsenate and crystalline scorodite ($FeAsO_4.2H_2O$) and their application to arsenic behavior in buried mine tailings. *Geochimica Cosmochimica Acta* **70**, 2942-2956.

Langmuir, D., Mahoney, J., Macdonald, A. and Rowson, J., 1999. Predicting arsenic concentrations in the porewaters of buried uranium mill tailings. *Geochimica Cosmochimica Acta* **63**, 3379-3394.

Lanzirotti, A., Tappero, R., and Schlze, D., 2010. Practical applications of synchrotron-based hard X-ray microprobes in the soil sciences. In: *Advances in understanding soil environments by application of synchrotron-based techniques*, Grafe, M. and Singh, B. (eds.), Elsevier.

Le Berre, J.F., Gauvin, R., and Demopoulos, G.P., 2007. Characterization of poorly-crystalline ferric arsenate precipitated from equimolar Fe(III)-As(V) solutions in the pH range 2 to 8. *Metallurgical and Materials Transactions B* **38(5)**, 751–762.

Lehr, J.H. and Lehr, J.K., 2000. Standard handbook of environmental science, health, and technology. McGraw-Hill Standard Handbook Series (eds) Edition 1, 14-105.

Lenoble, V., Bouras, O., Deluchat, V., Serpaud, B., and Bollinger, J., 2002. Arsenic adsorption onto pillared clays and iron oxides. *Journal of Colloid Interface Science* **255**, 52-58.

Mahoney, J., Langmuir, D., Gosselin, N., and Rowson, J., 2005. Arsenic readily released to pore waters from buried mill tailings. *Applied Geochemistry* **20(35)**, 947-959.

Mahoney, J., Slaughter, M., Langmuir, D. and Rowson, J., 2007. Control of As and Ni releases from a uranium mill tailings neutralization circuit: solution chemistry, mineralogy and geochemical modeling of laboratory study results. *Applied Geochemistry* **22**, 2758-2776.

Manceau, A., Marcus, M.A., and Tamura, N., 2002. Quantitative speciation of heavy metals in soils and sediments by synchrotron x-ray techniques. *Reviews in mineralogy and geochemistry* **49**, 341 – 428.

Mandal, B.K. and Suzuki, K.T., 2002. Arsenic round the world: a review. *Talanta* **58**, 201 – 235.

Manning, B.A., Fendorf, S.E. and Goldberg, S., 1998. Surface structures and stability of As(III) on goethite: Spectroscopic evidence for inner-sphere complexes. *Environmental Science and Technology* **32(16)**, 2383-2388.

Marsden, J., and House, I., 1992. The chemistry of gold extraction. Elis Horwood, New York, pp. 597.

Martinez, C.E. and McBride, M.B., 1998. Co-precipitates of Cd, Cu, Pb and Zn in iron oxides: solid phase transformation and metal solubility after aging and thermal treatment. *Clays and Clay minerals* **46(5)**, 537-545.

Matanitobua, V.P., Noller, B.N., Chiswell, B., Ng, J.C., Bruce, S.L., Huang, D., Riley, M., and Harris, H.H., 2007. Using synchrotron-based absorption spectrometry to identify the arsenic chemical forms in mine waste materials. In: *AIP Conference Proceedings 879*, Ninth International Conference on Synchrotron Radiation Instrumentation, 1845 – 1848.

McCreadie, H., Blowes, D.W., Ptacek, C.J., Jambor, J.L., 2000. Influence of reduction reactions and solid-phase composition on porewater concentrations of arsenic. Environmental Science and Technology **34(15)**, 3159-3166.

McMullen, J. and Thomas, K.G., 2002. Gold roast, autoclaving or bio-oxidation process selection based on bench-scale and pilot plant test workand costs. In: *Mineral Processing Plant, Design, Practice, and Control Proceedings*, Mulnar, A.L., Barratt, D.G. and Halbe, D.N. (eds), Society for Mining Metallurgy and Exploration, vol. 1, 211- 250

Metal Mining Effluent Regulations, 2002. Department of Justice, Canada, SOR/2002-222, Schedule 4. Available: http://laws-lois.justice.gc.ca/eng/regulations/SOR-2002-222/ [Accessed on 13 January 2012].

Meunier, L., Walker, S.R., Koch, I., Wragg, J., Parsons, M.B., Jamieson H.E. and Reimer, K.J., 2010. Effects of soil composition and mineralogy on the bioaccessibility of arsenic from tailings and soil in gold mine districts of Nova Scotia. *Environmental Science and Technology* **44**, 2667-2674.

Moldovan, B.J. and Hendry, M.J., 2005. Characterizing and quantifying controls on arsenic solubility over a pH range 1-11 in a uranium mill-scale. *Environmental Science & Technology* **39(13)**, 4913-4920.

Moldovan, B.J., Jiang, D.T. and Hendry, M.J., 2003. Mineralogical characterization of arsenic in uranium mine tailings precipitated from iron-rich hydrometallurgical solutions. *Environmental Science and Technology* **37**, 873–879.

Monhemius, A.J. and Swash, P.M. (1999) 'Removing and stabilizing As from copper refining circuits by hydrothermal processing. *Journal of Minerals, Metals and Materials Society* **51(9)**, 30–33.

Moore, J.W. and Pearson, R.G., 1981. Kinetics and mechanism (3rd ed), John Wiley & Sons, New York.

Morin, G., Guyot, F., Lebrun, S., Ona-Nguema, G., Baranger, P., Personnes, J.-C. and Bonnefoy, V., 2004. Role of micro-organisms on oxidation state and trapping mechanism of As by iron oxides. (http://ftp.esrf.fr/pub/UserReports/25964_A.pdf).

Morin, G., Juillot, F., Brunneel, O., Personnè, J-C., Elbaz-Poulichet, F., Leblanc, M., Ildefonse, P., Calas, G., 2003. Bacterial formation of tooeleite and mixed As(III)/V-Fe(III) gels in the Carnoules acid mine drainage, France. A XANES, XRD, and SEM study. *Environmental Science and Technology* **37**, 1705-1712.

Morin, G., Ona-Nguema, G., Wang, Y., Menguy, N., Juillot, F., Proux, O., Guyot, F., Calas, G. and Brown, G.E., 2008. Extended x-ray absorption fine structure analysis of arsenite and arsenate adsorption on maghemite. *Environmental, Science & Technology* **42(7)**, 2361-2366.

Morin, G., Rousse, G., and Elkaim, E., 2007. Crystal structure of tooeleite, $Fe_6(AsO_3)4\ SO_4(OH).4H_2O$, a new iron arsenite oxyhydroxy-sulfate mineral relevant to acid mine drainage. *American Mineralogist* **92**, 193-197.

Nelham, N.J., Malatt, K.A., and Vukcevic, S., 2000. The stability of iron phases presently used for disposal from metallurgical systems - A review. *Minerals Engineering* **13(8-9)**, 911-931.
Nickel, E.H. and Nichols, M.C., 1991. Mineral Reference Manual, van Nostrand Reinhold, New York.

Nishimura, T. and Robins, R.G., 1999. A re-evaluation of the solubility and stability regions of calcium arsenites and calcium arsenates in aqueous solution at 25˚C. *Mineral Processing and Extractive Metallurgy Review: An International Journal* **18(3-4)**, 283-308.

Nishimura, T. and Robins, R.G., 2008. Confirmation that tooeleite is a ferric arsenite sulfate hydrate and is relevant to arsenic stabilisation. *Minerals Engineering* **21**, 246 – 251.

Nishimura, T. and Tozawa, K., 1985. Removal from waste water by addition of calcium hydroxide and stabilization of arsenic-bearing precipitates by calcinations. In: *Impurity control*

and disposal, Oliver, A.J. (ed), Canadian Institute of Mining, Metallurgy and Petroleum, Montreal, Canada, 3/1-3/17.

Nishimura, T. and Umetsu, Y, 2000. Chemistry on elimination of arsenic, antimony, and selenium from aqueous solution with iron(III) species. In: *Minor Elements*: Processing and Environmental Aspects of As, Sb, Se, Te, and Bi, Courtney Young (ed.), Society for Mining, Metallurgy, and Exploration, Inc., USA, 2000, 105 – 112.

Nishimura, T., Itoh, C.T. and Tozawa, K.,1991. Equilibria of the Zn(II)-As(III, V)-H_2O system at 25˚C. *Bulletin of Research Institute of Mineral Dressing and Metallurgy Tohuko University* **47(1/2)**, 113-122.

Nishimura, T., Wang, Q., and Umetsu, Y., 1996. Removal of arsenic from process liquors by oxidation of iron(II), arsenic(III) and sulphur(IV) with oxygen. In: *Iron control and disposal*, Dutrizac, J.E. and Harris, G.B. (eds), Canadian Institute of Mining, Metallurgy and Petroleum, Montreal, Canada, 535-548.

Nolan, T.B., 1935. The Gold Hill Mining District, U.S.G.S. *Professional Paper*, 177.

Nordstrom, D.K. and Archer, D.G., 2003. Arsenic thermodynamic data and environmental geochemistry. In: *Arsenic in Groundwater: Geochemistry and Occurrence*, Welch, A.H. and Stollenwerk, K.G. (eds), Kluwer Academic Publishers,1 – 25.

Ona-Nguema, G., Morin, G., Juillot, F., Calas, G. and Brown, G.E., 2005. EXAFS Analysis of arsenite adsorption onto two-line ferrihydrite, hematite, goethite, and lepidocrocite. *Environmental Science Technology* **39(23)**, 9147-9155.

Ona-Nguema, G., Morin, G., Wang, Y., Menguy, N., Juillot, F., Olivi, L., Aquilanti, G., Abdelmouna, M., Ruby, C., Bargar, J.R., Guyot, F., Calas, G. and Brown, G.E. Jr., 2009. Arsenite sequestration at the surface of nano-$Fe(OH)_2$, ferrous-carbonate hydroxide, and green-rust after bioreduction of arsenic-sorbed lepidocrocite by *Shewanella putrefaciens*. *Geochimica et Cosmochimica Acta*, **73(5)**, 1359-1381.

Opio, F., Peacey, J. and Jamieson, H., 2011. Tooeleite, as new possibility for arsenic fixation: thermal decomposition and stabilisation. In: Proceedings of the 2nd International Seminar on Environmental Issues in the Mining Industry, November 2011, Santiago, Chile.

Oscarson, D.W., Huang, P.M., Defosse, C. and Herbillon, A., 1981. Oxidative power of Mn(IV) and Fe(III) oxides with respect to As(III) in terrestrial and aquatic environments. *Nature* **291**, 50-51.

Paige, C.R., Snodgrass, W.J., Nicholson, R.V. and Scharer, J.M., 1996. The crystallization of arsenate-contaminated iron hydroxide solids at high pH. *Water Environment Research* **68**, 981-987.

Paige, C.R., Snodgrass, W.J., Nicholson, R.V. and Scharer, J.M., 1997. An arsenate effect on ferrihydrite dissolution kinetics under acidic oxic conditions. *Water Research* **31**, 2370-2382.
Paktunc, D., Dutrizac, J. and Gertsman, V., 2008. Synthesis and phase transformations involving scorodite, ferric arsenate and arsenical ferrihydrite: Implications for arsenic mobility. *Geochimica et Cosmochimica Acta* **72**, 2649 – 2672.

Paktunc, D., Foster, A., LaFlamme, G., 2003. Speciation and characterization of arsenic in Ketza River mine tailings using X-ray absorption spectroscopy. *Environmental Science and Technology* **37**, 2067-2074.

Paktunc. D. and Bruggerman, K., 2010. Solubility of nanocrystalline scorodite and amorphous ferric arsenate: Implications for stabilization of arsenic in mine wastes. *Applied Geochemistry* **25(5)**, 674-683.

Pantuzzo, F.L. and Ciminelli, V.S.T., 2010. Arsenic association and stability in long-term disposed arsenic residues. *Water Research* **44**, 5631-5640.

Pantuzzo, F.L., Ciminelli, V.S.T., and Brito, W., 2008. New evidences for the role of precipitation and adsorption during Fe(III)-As(V) coprecipitation. In: *Hydrometallurgy–International Symposium*, Phoenix, Arizona, USA, 130–139.

Papangelakis, V.G. and Demopoulos, G.P., 1990. Acid pressure oxidation of arsenopyrite: Part I, Reaction Chemistry. *Canadian Metallurgical Quarterly* **29 (1)**, 1-12.

Papassiopi, N., Vaxevanidou, K., and Paspaliaris, I., 2002. Investigating the use of iron reducing bacteria for the removal of arsenic from contaminated soils. *Water, Air, and Soil Pollution* **3(3)**, 81-90.

Papassiopi, N., Vircikova, E., Nenov, V., Kontopoulos, A., and Monar, L., 1996. Removal and fixation of arsenic in the form of ferric arsenates. Three parallel experimental studies. *Hydrometallurgy* **41**, 243 – 253.

Peacey, J.G., Gupta, M.Z. and Ford, K.J.R., 2010. Review of process options to treat enargite concentrates. In: *Proceedings of Copper, Copper-Cobre 2010*, Hamburg, Germany, 1035 – 1050.

Penderson. H.D., Postma, D., and Jakobsen, R., 2006. Release of arsenic associated with the reduction and transformation of iron oxides. *Geochimica et Cosmochimica Acta* **70 (16)**, 4116-4129.

Pierce, M.L. and Moore, C.B., 1980. Adsorption of arsenite on amorphous iron hydroxide from dilute aqueous solution. *Environmental Science and Technology* **14 (2)**, 214-216.

Pierce, M.L. and Moore, C.B., 1982. Adsorption of amorphous arsenite and arsenate on amorphous iron hydroxide. *Water Research* **16**, 1247-1253.

Piret, N.L., 1999. The removal and safe disposal of arsenic in copper processing. *JOM Journal of the Minerals, Metals and Materials Society* **51(9)**, 16-17.

Pookrod, P., Haller, K.J., and Scamehorn, J.F., 2004. Removal of arsenic anions from water using polyelectrolyte-enhanced ultrafiltration. Separation Science and Technology **39(4)**, 811-831.

Potts, P. J., Bowles, J.F.W., Reed, S.J.B., and Cave, M.R., 1995. Microprobe techniques in the earth sciences. *The Mineralogical Society Series 6*, 163 – 227.

Rancourt, D.G., Fortin, D., Pichler, T., Thibault, P.-J., Lamarche, G., Morris, R.V. and Mercier, P.H.J., 2001. Mineralogy of a natural As-rich hydrous ferric oxide coprecipitate formed by mixing of hydrothermal fluid and seawater: implications regarding surface complexation and color banding in ferrihydrite deposits. *American Mineralogist* **86**, 834-851.

Ravel, B. and Neville, M., 2005. Athena, Artemis, Hephaestus: data analysis for X-ray adsorption spectroscopy using IFEFFIT. *Journal of Synchrotron Radiation* **12(4)**, 537-541.

Raven, K..P., Jain, A., and Loeppert, R.H., 1998. Arsenite and arsenate adsorption on ferrihydrite: kinetics, equilibrium, and adsorption envelopes. *Environmental Science and Technology* **32**, 344-349.

Reddy, K.J., Sullivan, P.J. and Yelton, J.L., 1988. Solubility relationships of zinc associated with acid mine drainage. *Journal of Environmental Quality* **17**, 712-714.

Riveros, P.A. and Dutrizac, J.E., 2008. The leaching of tennantite, tetrahedrite and enargite in acidic sulphate and chloride media. *Canadian Metallurgical Quarterly* **47(3)**, 235-244.

Riveros, P.A., Dutrizac, J.E. and Spencer, P. (2001) 'Arsenic disposal practices in the metallurgical industry. *Canadian Metallurgical Quarterly* **40**, 395–420.

Robins, R.G. and Jayaweera, L.D., 1992. Arsenic in gold processing. *Mineral processing and Extractive Metallurgy Review* **9**, 255-271.

Robins, R.G. and Tozawa, K., 1982. Arsenic removal from gold processing wastewaters: the potential ineffectiveness of lime, *CIM Bulletin* **75(840)**, 171-174.

Robins, R.G., 1981. The solubility of metal arsenates. *Metallurgical Transactions B* **12B**, 103-109.

Robins, R.G., 1983. The stabilities of arsenic (v) and arsenic (III) compounds in aqueous metal extraction systems. In: *Hydrometallurgy: Research, Development and Plant practice*, Osseo-Asare, K. and Miller, J.D. (eds), The Metallurgical; Society of AIME, Warrendale, PA, U.S.A., 291-310.

Robins, R.G., 1985. The aqueous chemistry of arsenic in relation to hydrometallurgical processes. In*: Impurity, control & disposal*, Oliver, A.J. (ed.), CIM, Montreal, pap.1.

Robins, R.G., 1988. Arsenic Hydrometallurgy. In: Arsenic Metallurgy Fundamentals and Applications, Reddy, R.G., Hendrix, J.L., and Queneau, P.B. (eds), *The Minerals, Metals and Materials Society*, Warrendale, PA, U.S.A., 215-247.

Robins, R.G., Huang, J.C.Y., Nishimura, T., Khoe, G.H., 1988. The adsorption of arsenate ion by ferric hydroxide. In: *Arsenic Metallurgy: Fundamentals and Applications*, Reddy, R.G., Hendrix, J.L., Queneau, P.B. (eds.),TMS, Warrendale, PA, 99–112.

Robins, R.G., Nishimura, T., and Singh, P., 2001. Removal of arsenic from drinking water by precipitation, adsorption or cementation. In: *Proceedings of BUET-UNU International Workshop - Technologies for arsenic removal from drinking water*. M.F. Ahmed, M.A. Ali and Z. Adeel (eds), BUET, Dhaka, Bangladesh, May 5 - 7, 59-68.

Robins, R.G., Singh, P. and Das, R.P., 2005. Co-precipitation of arsenic with Fe(III), Al(III) and mixtures of both in a chloride system. In*: Arsenic Metallurgy: Fundamentals and Applications*, Reddy, R.G., Ramachandran, V. (eds), TMS, Warrendale, PA: Minerals, metals and Materials, 113-128.

Robins, R.G., Wong, P.L.M., Nishimura, T., Khoe, G.H. and Huang, J.C.Y., 1991. Basic ferric arsenates – nonexistent In: *EPD Congress 1992*. Hager, J. P. (ed), TMS Warrendale PA, 31-39.

Rochette, E.A., Li, G.C. and Fendorf, S.E., 1998. Stability of arsenate minerals in soil under biotically generated reducing conditions. *Soil Science Society of America Journal* **62**, 1530-1537.

Ruiz, M.C., Vera, M.V., and Padilla, R., 2011. Mechanism of enargite pressure leaching in the presence of pyrite. *Hydrometallurgy* **105(3-4)**, 290-295.

Sadiq, M., 1991. Solubility and speciation of zinc in calcareous soils. In: *Proceedings of International Conference, Metals, Soils, Waters, Plants, Animals*, 57-58, 411-421.

Schwertmann, U. and Taylor, R.M., 1977. In: *Minerals in Soil Environments*, Dixon, J.B. and Weed, S.B. (eds) Soil Science Society of America, Madison, Wiscosin, 145.

Schwertmann, U. and Taylor, R.M., 1989. Iron Oxides. In: *Minerals in Soil Environments*, 2nd edition, Dixon, J.B. and Weed, S.B. (eds) Soil Science Society of America Book series No.1, Madison, Wiscosin, 379-438.

Schwertmann, U., and Murad, E., 1983. Effect of pH on the formation of goethite and hematite from ferrihydrite. *Clays and Clay Minerals* **31**, 277-284.

Schwertmann, U., Stanjek, H., and Becher, H.H., 2004. Long-term in vitro-transformation of 2-line ferrihydrite to goethite/hematite at 4, 10, 15 and 25˚C. *Clay Minerals* **39**, 433-438.

Sherman, D.M. and Randall, S.M., 2003. Surface complexation of arsenic(V) to iron(III) hydroxides: structural mechanism from ab initio molecular geometries and EXAFS spectroscopy. *Geochimica et Cosmochimica Acta* **67(22)**, 4223-4230.

Singh, B., Grafe, M., Kaur, S. and Liese, A., 2010. Applications of synchrotron-based X-ray diffraction and X-ray absorption spectroscopy to the understanding of poorly crystalline and metal-substituted iron oxides. In: *Synchrotron-based techniques in soils and sediments*, Singh, B. and Grafe, M.(eds). Developments in Soil Science, 34, 199-254.

Singhania, S., Wang, Q., Fillipou, D., and Demopoulos, G.P., 2005. Temperature and seeding effects on the precipitation of scorodite from sulphate solutions under atmospheric-pressure conditions. *Metallurgical and Materials B*, Process Metallurgy and Materials Processing Science **36B (3)**, 327-333.

Singhania, S., Wang, Q., Fillipou, D., and Demopoulos, G.P., 2006. Acidity, valency and third-ion effects on the precipitation of scorodite from mixed sulphate solutions under atmospheric-pressure conditions. *Metallurgical and Materials Transactions B* **37B**, 189-197.

Smedley, P.L. and Kinniburgh, D.G., 2002. A review of the source, behaviour, distribution of arsenic in natural waters, *Applied Geochemistry* **17**, 517 – 568.

European Synchrotron Radiation Facility, 2012. A Light for Science – web accessed October 2012 http://www.esrf.eu/about/synchrotron-science/synchrotron-light

Stefanakis, M. and Kontopoulos, A., 1987. Production of environmentally acceptable arsenates-arsenates from solid arsenic trioxide. In: *Arsenic metallurgy fundamentals and applications*, 1988, Reddy, R.G., Hendrix, J.L., and Queneau, P.B. (eds), The Minerals, Metals and Materials Society, Warrendale, PA, U.S.A., 287-304.

Swash, P.M. and Monhemius, A.J., 1994. Hydrothermal precipitation from aqueous solutions containing iron (III) arsenate and sulphate. *Hydrometallurgy 1994*. Chapman and Hall, Cambridge,177-190

Swash, P.M. and Monhemius, A.J., 1995. Synthesis, characterization and solubility testing of solids in the Ca-Fe-AsO_4 system. *Sudbury '95 – Mining and the Environment*, Hynes, T.P. and Blanchette, M.C. (eds), CANMET, Ottawa, Canada, 17-28.

Sun, X. and Doner, H.E., 1998. Adsorption and oxidation of arsenite on goethite. *Soil Science* **163(4)**, 278-287.

Taylor, A., 2010. Gold technology developments and trends. In: *Proceedings of ALTA Gold 2010*, ALTA, Perth, Australia, May 27 – 28.

Tozawa, K. and Nishimura, T., 1984. Oxidation of As(III) to As(V) in aqueous solutions. *Metallurgical Review of MMIJ* (Japan) **1(1)**, 76-87.

Twidwell, L.G., Robins, R.G., and Hohn, J. W., 2005. The removal of arsenic from aqueous solution by coprecipitation with iron(III). In: *Proceedings Arsenic Metallurgy: Fundamentals and Applications.* Reddy, R.G. and Ramachandran,V. (eds) TMS (The Minerals, Metals & Materials Society), 3-24.

Twidwell, L.G. and Leonhard, 2008. Removal of cadmium, copper, nickel, zinc from aqueous solution by adsorption on ferrihydrite and long-term storage stability of the metal leaded product. In: *Proceedings of the Sixth International Symposium, Hydrometallurgy 2008*. Young, C.A., Taylor, P., Anderson, C., Choi, Y. (eds), Phoenix, U.S.A. 149-161.

Twidwell, L.G. and McCloskey, J.W., 2011. Removing arsenic from aqueous solution and long-term product storage. *Journal of the Minerals, Metals and Materials Society* **63(8)**, 94-100.

U.S. Environmental Protection Agency, 1992. Toxicity Chracteristic Leaching Procedure (Method 1311). *In SW-846*: Test methods for evaluating solid waste, physical/chemical methods. Office of Solid Waste, Washington DC.

U.S. EPA 1994. Method 1312 (Synthetic Precipitation Leaching Procedure). US EPA Method 3051 – web accessed November 2009 http://www.sampleprep.duq.edu/dir/3051method.html

US EPA, 1998. Locating and estimating air emissions from sources of arsenic and arsenic compounds. *Office of Air Quality Planning and Standards*, EPA-454-R-98-013, pp. 132.

Valenzuela, A., 2000. Arsenic management in the metallurgical industry, M.Sc. Thesis, University of Laval, Department of Mines and Metallurgy, Quebec, Canada.

Valenzuela, A., Fytas, K., and Sanchez, M., 2000. Arsenic management in pyrometallurgical processes. Part I: *Distribution in smelting/converting, Fifth International Conference on Clean Technologies for the Mining Industry*, vol. II, M.A. Sanchez, F. Vergara and S.H. Castro (eds), University of Concepcion, Chile, 95-105.

Walker, S.R., Jamieson, H.E., Lanzarotti, A., Andrade, C.F. and Hall, G.E.M. 2005. Determining arsenic speciation in iorn oxides: Application of synchrotron micro-XRD and micro-XANES at the grain scale. *The Canadian Mineraologist* **43**, 1205-1224.

Walker, S.R., Parsons. M.B., Jamieson, H.E., and Lanzarotti, A., 2009. Arsenic mineralogy of near-surface tailings and soils: influences on arsenic mobility and bioaccessibility in the Nova Scotia gold mining districts. *The Canadian Mineralogist* **47**, 533-556.

Wang, Q. and Ferron, C.J., 2003. Striving for a sustainable mining industry: Arsenic control through integrated approach. In: *Proceedings of Mining and the Environment III Conference*, Sudbury, Canada, May 26 - 28.

Warner, J. and Rowson, J., 2007. In-situ monitoring and validation of a uranium mill tailings management facility design using X-ray Absorption Near Edge Structure (XANES) spectroscopy. *Synchrotron Radiation News* **20(3)**, 14-17.

Waychunas, G.A., Rea, B.A., Fuller, C.C. and Davis, J.A., 1993. Surface chemistry of ferrihydrite. I. EXAFS studies of geometry of coprecipitated and adsorbed arsenate, *Geochimica et Cosmochimica Acta* **57**, 2251-2269.

Welham, N.J., Malatt, K.A. and Vukcevic, S., 2000. The stability of iron phases presently used for disposal from metallurgical systems – A review. *Minerals Engineering* **13(8-9)**, 911-931.

World Bank, 2007. Environmental, Health and Safety Guidelines – Base metal smelting and refining. International Finance Corporation.

Yee, N., Shaw, S., Benning, L.G., and Nguyen, T.H., 2006. The rate of ferrihydrite transformation to goethite via Fe(II) pathway. *American Mineralogist* **91**, 92-96.

Yusof, A.M., Mahat, M.N., Omar, N., and Wood, A.K.H., 2000. Water quality studies in an aquatic environment of disused tin-mining pools and in drinking water. *Ecological Engineering* **16**, 405-414.

Zhao, Z., Jia Y., Xu, L. and Zhao, S., 2011. Adsorption and heterogeneous oxidation of As(III) on ferrihydrite. *Water Research* **45**, 6496-6504.

Zhu, Y.N., Zhang, X.H., Xie, Q.L., Wang, D.Q. and Cheng, G.W., 2005. Solubility and stability of calcium arsenates at 25˚C. *Water, Air, and Soil Pollution* **169**, 221-238.

Appendix A– Tooeleite precipitation

A.1. Precipitation experiments

(a) Precipitates formed at the various pH levels (pH 2.5, 2.7, 3, 4, 6, 8, 10) from an Fe(III)-As(III) system (initial Fe/As molar ratio of 1.5 and 2.0) at ambient temperature (a) Fe:As=1.5 (NaOH) (b) Fe:As=2 (NaOH) (c) Fe:As=1.5 ($Ca(OH_2)$) (d) Fe:As=2 ($Ca(OH_2)$)

(a)

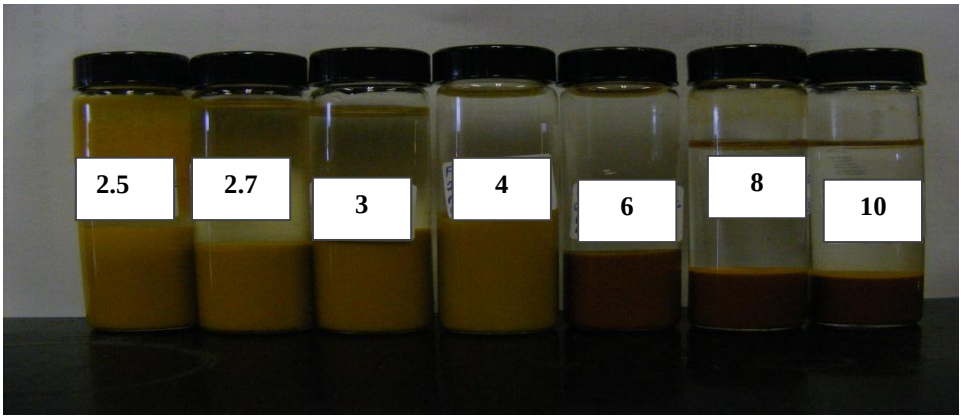

(b)

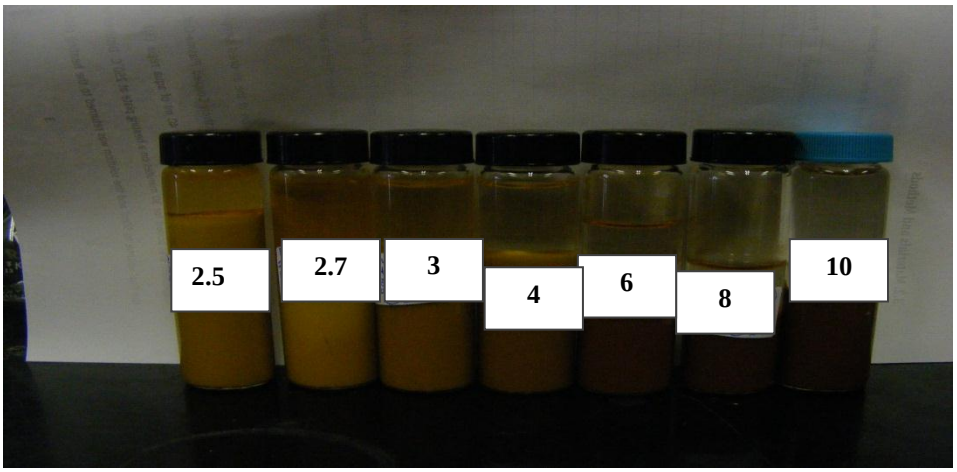

(c)

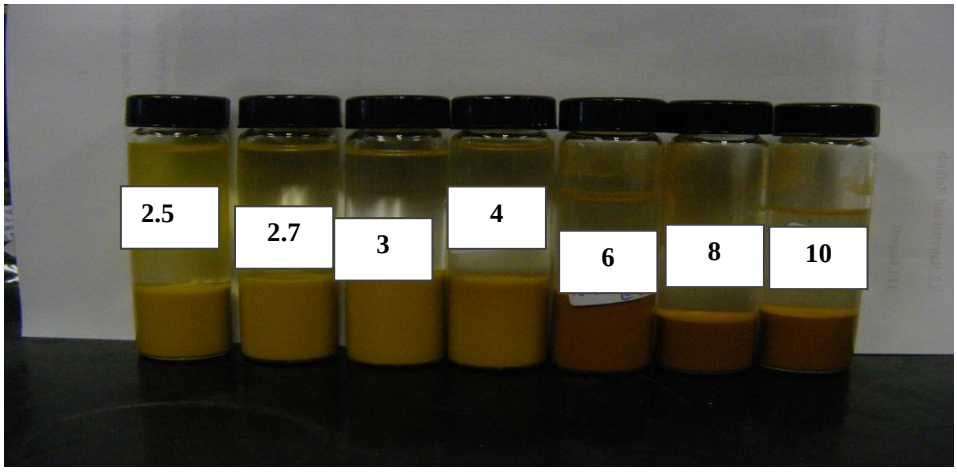

(d)

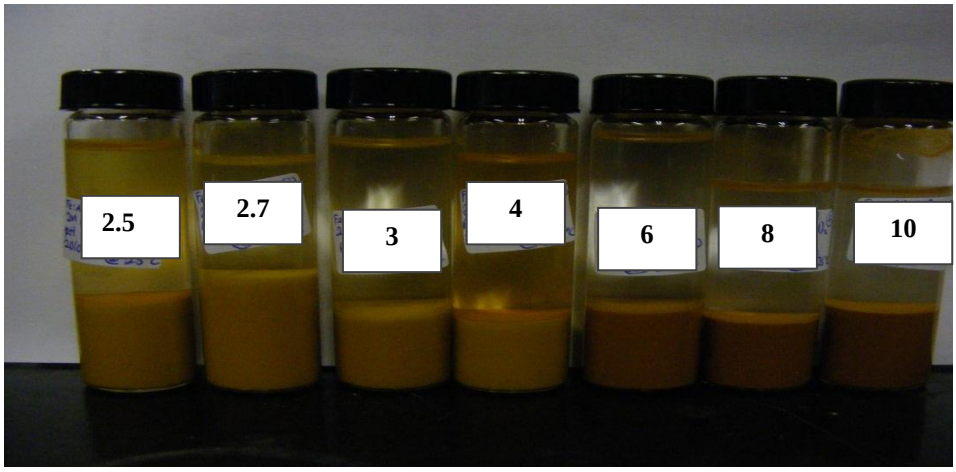

A.2. XRD analysis

(a) XRD spectra of the precipitates formed from Fe(III)-As(III) solutions of initial Fe:As molar ratios of 1.5 and 2: (a) Fe:As=1.5 and (b) Fe:As=2 using NaOH as base (c) Fe:As=1.5 and (d) Fe:As=2 using $Ca(OH)_2$ as base. G and T define gypsum [$CaSO_4$. $2H_2O$] and tooeleite [$Fe_6(AsO_3)_4(SO_4)(OH)_4 \cdot 4H_2O$] respectively.

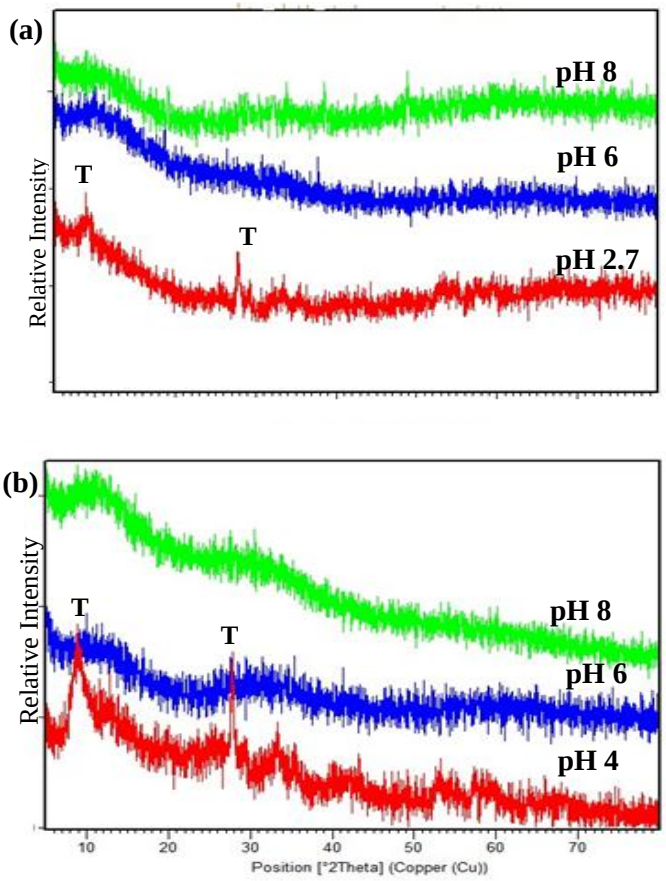

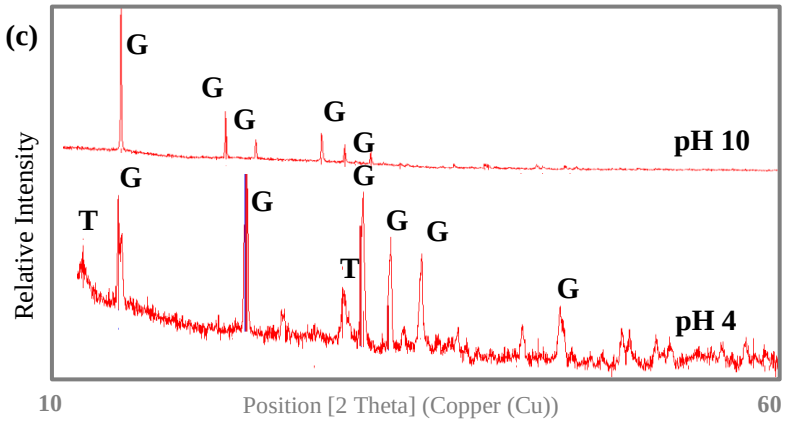
(c)
G
G
G
G
G
pH 10
G
G
T
G
T
G
G
G
pH 4
Relative Intensity
10
Position [2 Theta] (Copper (Cu))
60

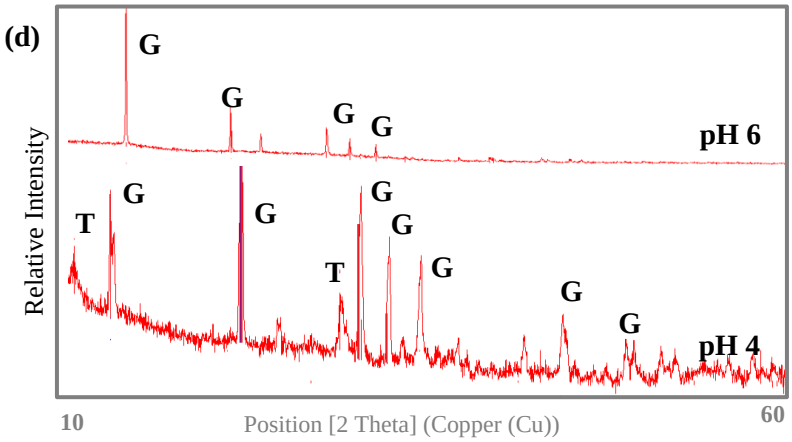
(d)
G
G
G
G
pH 6
G
G
T
G
G
T
G
G
G
pH 4
Relative Intensity
10
Position [2 Theta] (Copper (Cu))
60

A.3. Tooeleite precipitation at elevated temperatures

(a) Kinetics of As and Fe removal from initial solutions of Fe:As molar ratio of 1.2 using NaOH as base at (i) 25˚C (ii) 60˚C (iii) 95˚C (initial As concentration = 7.5 g/L).

(i)

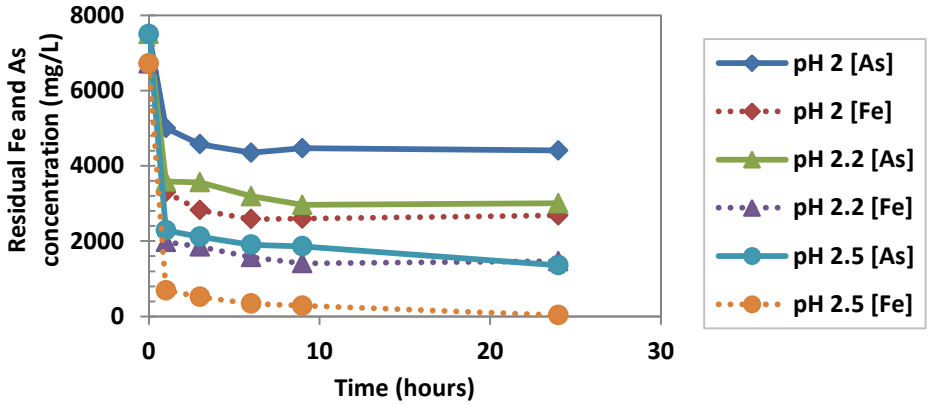

(ii)

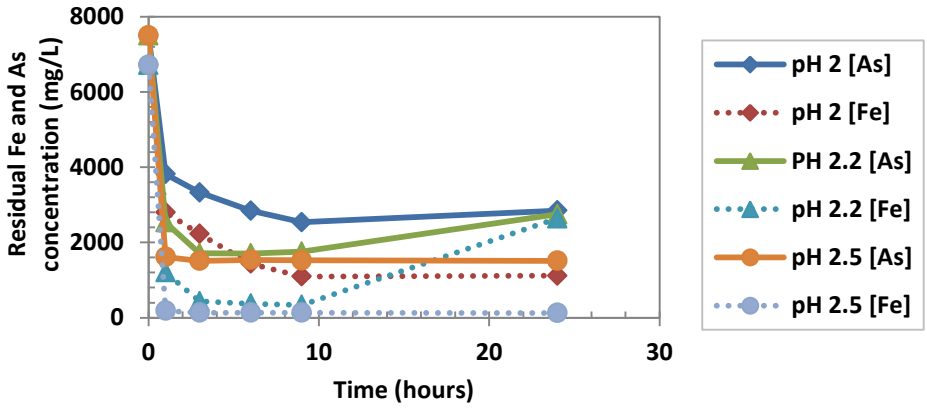

(iii)

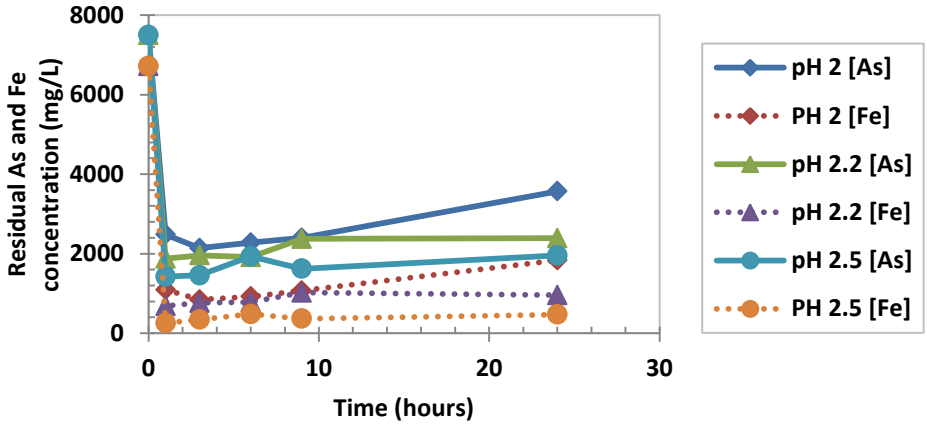

(b) Kinetics of As and Fe removal from initial solutions of Fe:As molar ratio of 1.5 using NaOH as base at (i) 25˚C (ii) 60˚C (iii) 95˚C (initial As concentration = 7.5 g/L).

(i)

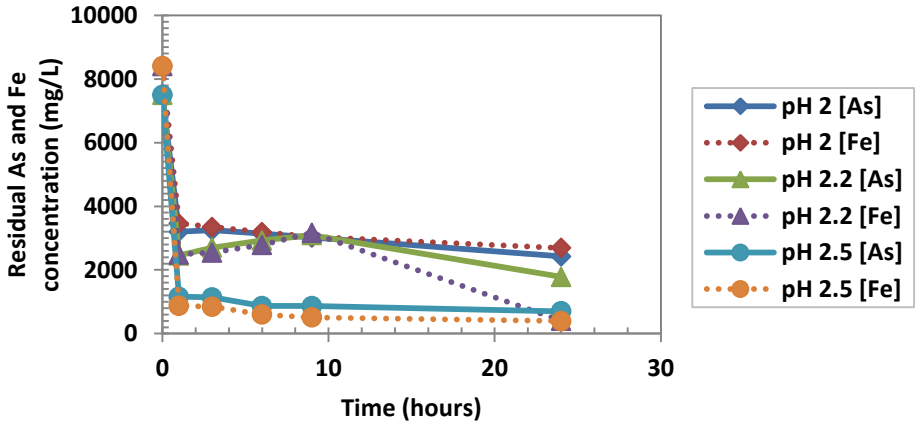

(ii)

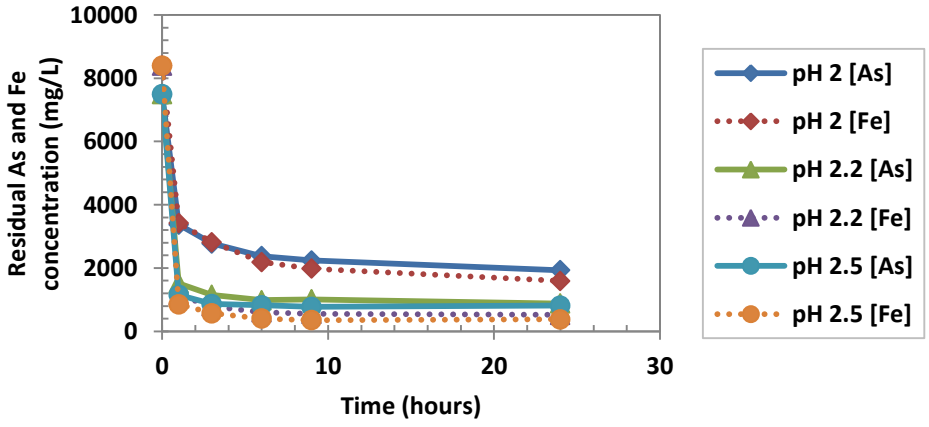

(iii)

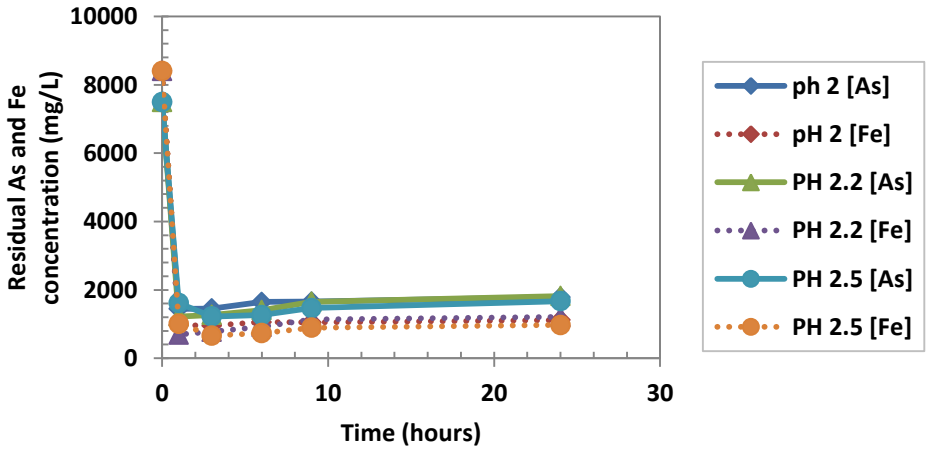

(c) As removal efficiency from initial solutions of Fe:As molar ratio of 1, 1.2 and 1.5 at (i) pH 2 (ii) pH 2.2 (iii) pH 2.5 using NaOH as base at ambient temperature (initial As concentration = 7.5 g/L).

(i)

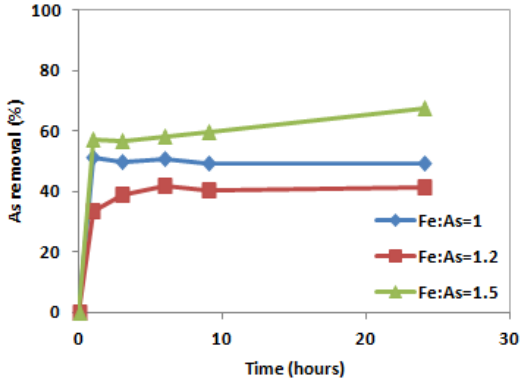

(ii)

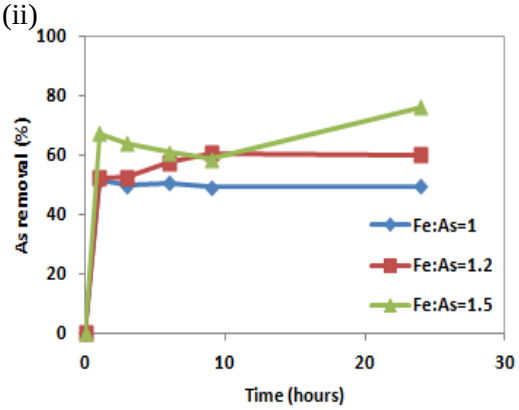

(iii)

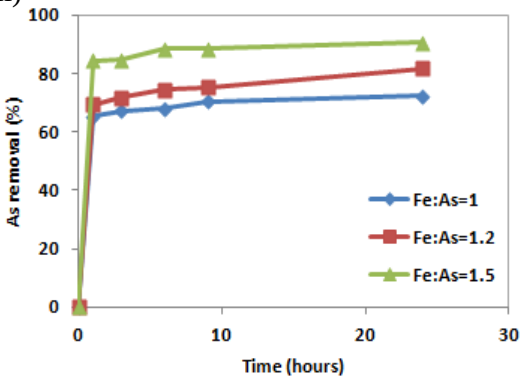

(d) As removal efficiency from initial solutions of Fe:As molar ratio of 1, 1.2 and 1.5 at (i) pH 2 (ii) pH 2.2 (iii) pH 2.5 using NaOH as base at 60˚C (initial As concentration = 7.5 g/L).

(i)

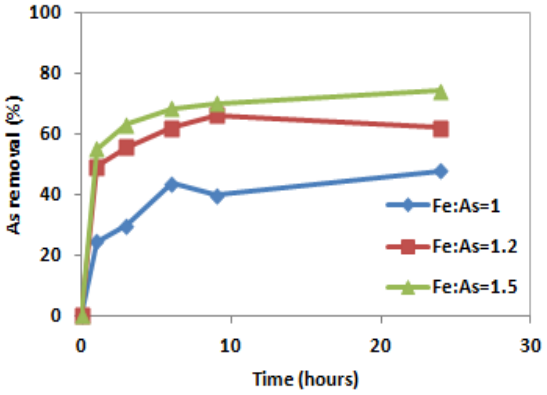

(ii)

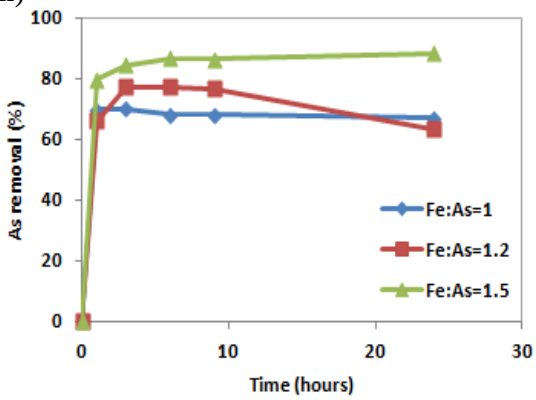

(iii)

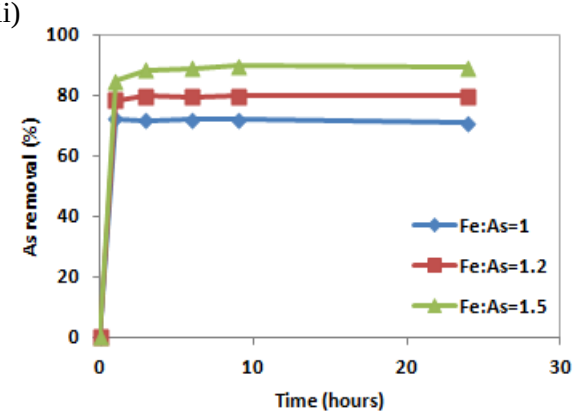

(e) Kinetics of As and Fe removal from initial solutions of (i) Fe:As molar ratio of 1 (ii) Fe:As molar ratio of 1.2 (iii) Fe:As molar ratio of 1.5 using NaOH as base at 95˚C (initial As concentration = 7.5 g/L).

(i)

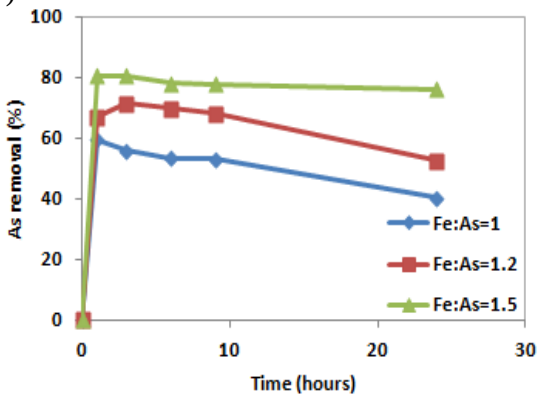

(ii)

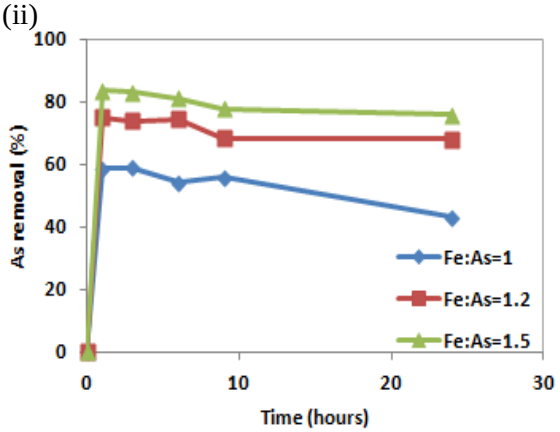

(iii)

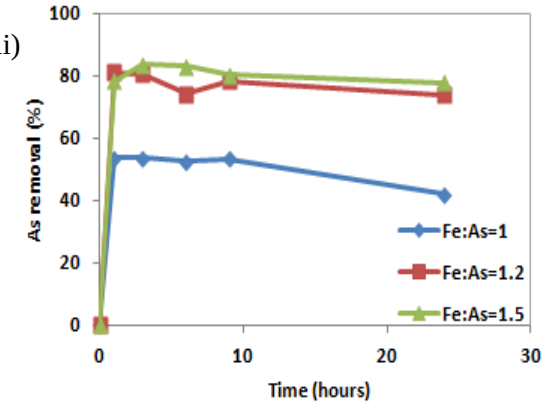

(f) XRD patterns of tooeleite precipitates formed under the conditions of Fe:As molar ratio =1 and pH 2 with NaOH as base: (i) 25˚C (FeAs_2_25_1); 60˚C (FeAs_2_60_1) and 95˚C (FeAs_2_95_1) (equilibration time of 1 hour) (ii) 25˚C (FeAs_2_25_24); 60˚C (FeAs_2_60_24) and 95˚C (FeAs_2_95_24) (equilibration time of 24 hours).

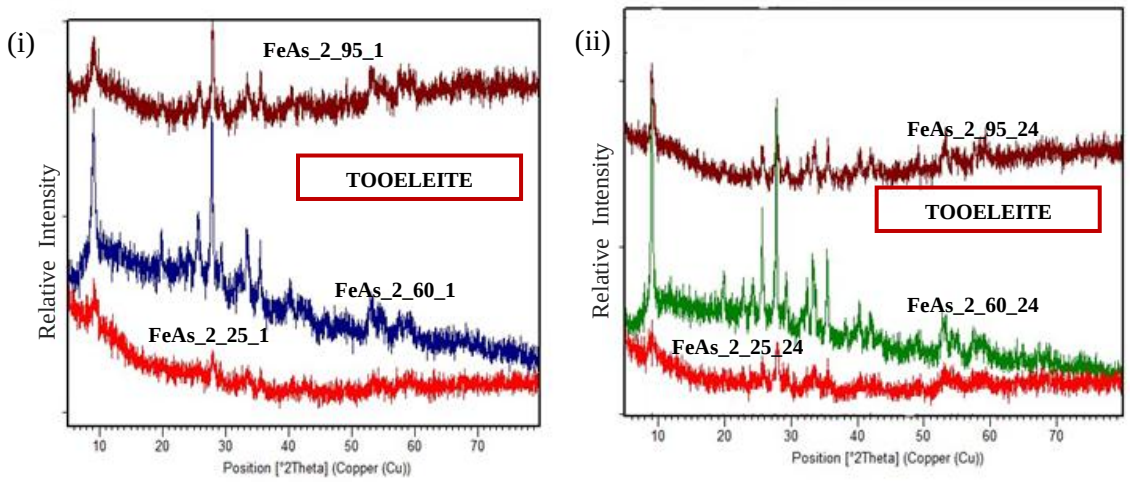

(g) XRD patterns of tooeleite precipitates formed under the conditions of Fe:As molar ratio =1 and pH 2.5 with NaOH as base: (i) 25˚C (FeAs_25_25_1); 60˚C (FeAs_25_60_1) and 95˚C (FeAs_25_95_1) (equilibration time of 1 hour) (ii) 25˚C (FeAs_25_25_24); 60˚C (FeAs_25_60_24) and 95˚C (FeAs_25_95_24) (equilibration time of 24 hours).

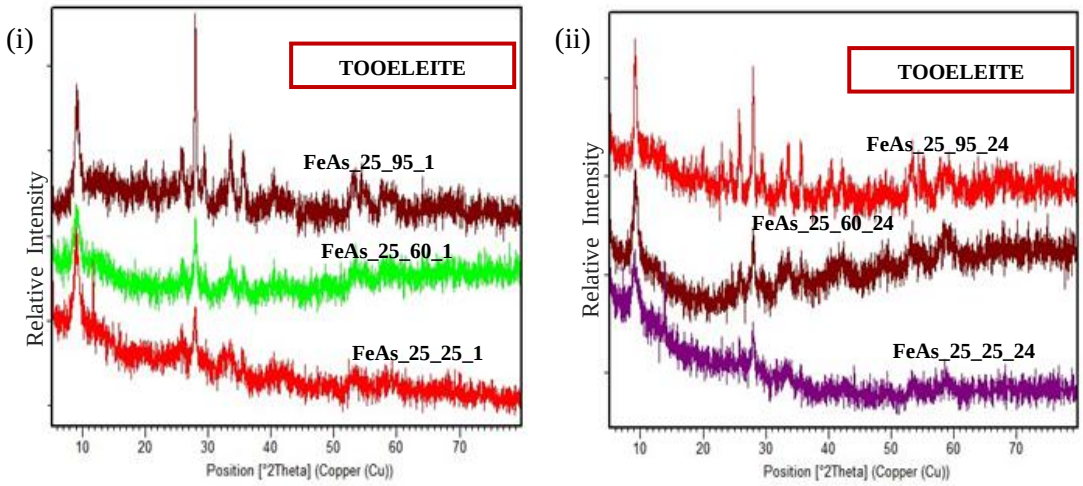

(h) XRD patterns of tooeleite precipitates formed under the conditions of Fe:As molar ratio =1.2 and pH 2 with NaOH as base: (i) 25˚C (FeAs12_2_25_1); 60˚C (FeAs12_2_60_1) and 95˚C (FeAs12_2_95_1) (equilibration time of 1 hour) (ii) 25˚C (FeAs12_2_25_24); 60˚C (FeAs12_2_60_24) and 95˚C (FeAs_2_95_24) (equilibration time of 24 hours).

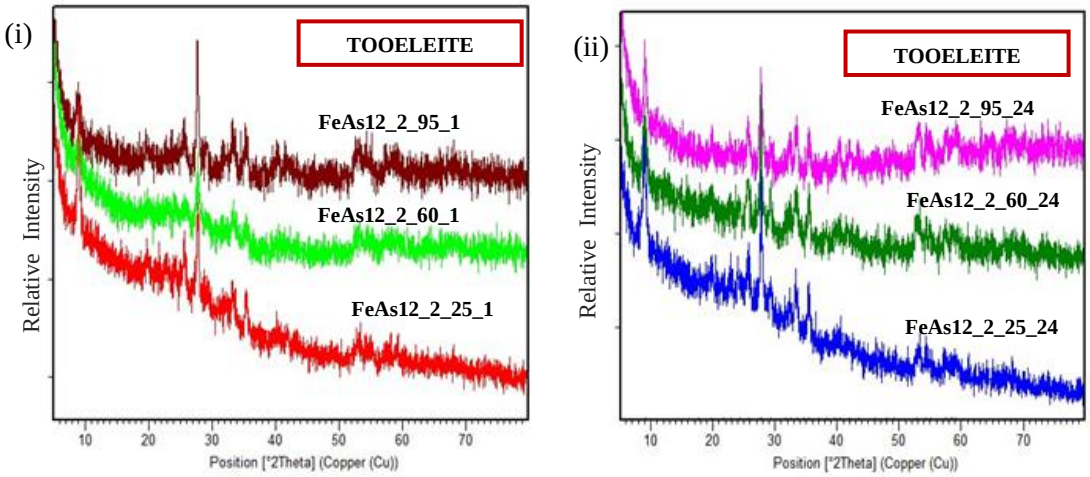

(i) XRD patterns of tooeleite precipitates formed under the conditions of Fe:As molar ratio =1.2 and pH 2.5 with NaOH as base: (i) 25˚C (FeAs12_25_25_1); 60˚C (FeAs12_25_60_1) and 95˚C (FeAs12_25_95_1) (equilibration time of 1 hour) (ii) 25˚C (FeAs12_25_25_24); 60˚C (FeAs12_25_60_24) and 95˚C (FeAs12_25_95_24) (equilibration time of 24 hours).

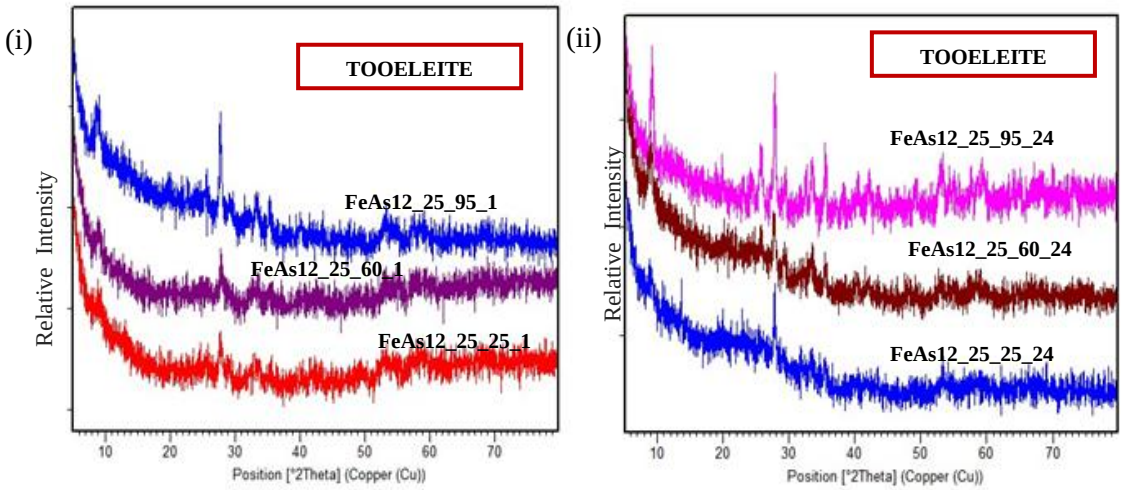

A.4. Stability tests

(a) Final pH of the leachates of the tooeleite and gypsum-bearing tooeleite precipitates subjected to the TCLP test.

Fe:As molar ratio	Base	Precipitates (precipitated at target pH values)						
		pH 2.5	pH 2.7	pH 3	pH 4	pH 6	pH 8	pH 10
Fe:As=1	NaOH	4.67	4.73	4.81	4.88	5.15	5.76	6.37
	$Ca(OH)_2$	4.81	4.80	4.85	4.95	5.54	6.10	7.37
Fe:As=1.5	NaOH	4.79	4.66	4.86	4.77	4.99	5.61	6.84
	$Ca(OH)_2$	4.76	4.79	4.88	4.64	4.88	5.91	7.24
Fe:As=2	NaOH	4.78	4.75	4.74	4.72	5.29	5.90	5.90
	$Ca(OH)_2$	4.71	4.67	4.64	4.75	5.06	5.97	7.37

(b) Leachate pH, and As and Fe concentrations from as a function of time for tooeleite and gypsum-bearing tooeleite subjected to long-term leaching tests under leaching conditions of pH 4, 5, 7 and 9 at 25˚C. NFA127 and CFA127 denote tooeleite precipitates formed at pH 2.7 and 25˚C with NaOH and $Ca(OH)_2$ as the bases respectively.

NFA127_pH

Time Elapsed (days)	1	3	6	8	13	24	44	64	78	121	207
pH changes at initial pH 4	2.86	4.13	4.77	3.74	4.72	3.38	5.67	5.67	5.38	5.41	5.19
pH changes at initial pH 5	2.8	4.62	3.55	5.03	5.33	4.50	6.39	6.72	5.46	5.80	6.72
pH changes at initial pH 7	2.76	5.51	6.47	6.07	6.41	6.18	7.07	7.58	6.25	6.38	6.65
pH changes at initial pH 9	2.85	6.6	6.94	8.03	8.55	8.67	8.75	8.76	8.52	8.76	8.76

NFA127_Fe (mg/L)

Time Elapsed (days)	1	3	6	8	13	24	44	64	78	121	207
Leachates at initial pH 4	14.4	<DL	<DL	5.43	<DL	2.10	1.07	1.13	1.15	<DL	2.7
Leachates at initial pH 5	12.8	<DL	<DL	<DL	<DL	1.39	0.66	0.94	0.68	<DL	<DL
Leachates at initial pH 7	16.3	<DL	<DL	<DL	<DL	0.64	0.62	0.64	0.64	<DL	<DL
Leachates at initial pH 9	12.5	<DL	<DL	<DL	<DL	2.39	5.24	0.72	0.67	<DL	0.1

NFA127_As (mg/L)

Time Elapsed (days)	1	3	6	8	13	24	44	64	78	121	207
Leachates at initial pH 4	483.0	274.1	204.9	170.4	156.0	97.0	84.7	84.7	54.1	47.0	44.6
Leachates at initial pH 5	478.4	281.4	232.2	161.0	117.4	96.0	64.0	63.1	52.0	39.8	39.3
Leachates at initial pH 7	532.7	211.4	113.0	51.2	46.4	39.4	43.1	49.7	38.0	38.4	63.2
Leachates at initial pH 9	436.5	46.6	26.3	22.6	32.7	32.8	43.1	34.3	31.4	32.7	50.6

CFA127_pH

Time Elapsed (days)	1	3	6	8	13	24	44	64	78	121	207
Leachates at initial pH 4	2.78	4.2	4.79	4.8	4.34	5.27	5.76	6.10	4.76	5.66	4.65
Leachates at initial pH 5	2.75	4.79	4.88	5.25	5.05	5.10	6.24	6.80	5.40	4.95	5.47
Leachates at initial pH 7	2.72	5.57	6.48	6.81	7.15	7.08	7.27	7.20	6.30	7.03	5.47
Leachates at initial pH 9	2.81	7.03	7.11	7.53	7.61	7.71	7.73	7.59	7.28	7.49	7.49

CFA127_Fe											
Time Elapsed (days)	**1**	**3**	**6**	**8**	**13**	**24**	**44**	**64**	**78**	**121**	**207**
Leachates at initial pH 4	5.80	<DL	<DL	<DL	2.20	0.63	0.73	0.79	1.14	<DL	5.11
Leachates at initial pH 5	6.21	<DL	<DL	<DL	<DL	0.69	0.63	0.66	0.66	<DL	1.21
Leachates at initial pH 7	9.83	<DL	<DL	<DL	<DL	1.00	0.68	0.66	0.62	<DL	<DL
Leachates at initial pH 9	6.13	<DL	<DL	<DL	6.59	0.69	0.93	0.70	0.63	<DL	<DL

CFA127_As											
Time Elapsed (days)	**1**	**3**	**6**	**8**	**13**	**24**	**44**	**64**	**78**	**121**	**207**
Leachates at initial pH 4	708.0	479.7	431.2	318.6	266.5	175.2	146.8	97.3	92.3	67.7	77.5
Leachates at initial pH 5	737.4	429.6	411.1	258.3	248.8	178.7	121.8	98.5	91.2	65.1	34.2
Leachates at initial pH 7	958.9	397.4	270.1	188.4	147.9	123.4	105.9	96.5	87.3	75.1	122.3
Leachates at initial pH 9	784.6	149.3	151.5	121.4	117.9	91.5	86.0	78.2	64.8	58.0	54.4

(c) Leachate Fe concentrations as a function of time for (i) tooeleite precipitates (ii) gypsum-bearing tooeleite subjected to long-term leaching tests under leaching conditions of pH 4, 5, 7 and 9 at 25˚C. NFA127 and CFA127 denote tooeleite precipitates formed at pH 2.7 and 25˚C with NaOH and $Ca(OH)_2$ as the bases respectively.

(i)

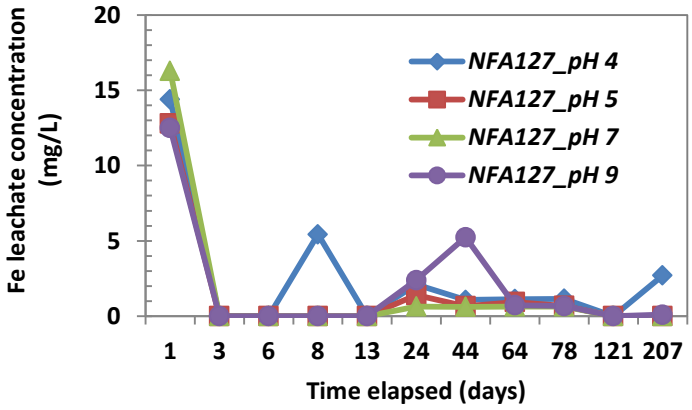

(ii)

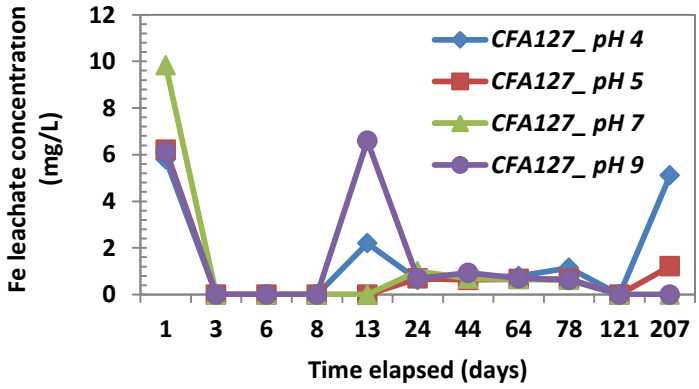

(d) Leachate pH, As and Fe concentrations as a function of time of tooeleite and gypsum-bearing tooeleite precipitates subjected to long-term leaching tests under leaching conditions of pH 5, 7 and 9 at 60˚C. NFA127 and CFA127 denote tooeleite precipitates formed at pH 2.7 and 25˚C using NaOH and $Ca(OH)_2$ as the bases respectively.

NFA127_pH

Time Elapsed (days)	7	15	36	69	118	195
pH changes at initial pH 5	5.35	5.56	6.21	6.18	5.85	5.79
pH changes at initial pH 7	5.89	5.68	6.90	6.33	6.83	6.63
pH changes at initial pH 9	7.76	8.61	8.82	8.73	8.85	8.75

NFA127_Fe

Time Elapsed (days)	7	15	36	69	118	195
Leachates at initial pH 5	<DL	0.85	0.84	0.69	<DL	<DL
Leachates at initial pH 7	<DL	0.67	0.68	0.68	<DL	12.5
Leachates at initial pH 9	<DL	0.68	4.86	14.3	8.17	249.6

NFA127_As

Time Elapsed (days)	7	15	36	69	118	195
Leachates at initial pH 5	403.7	235.6	169.9	183.4	210.7	313.8
Leachates at initial pH 7	359.8	198	189.0	230.9	257.6	361.1
Leachates at initial pH 9	121.1	123.4	207.6	359.9	304.5	808

CFA127_pH

Time Elapsed (days)	7	15	36	69	118	195
pH changes at initial pH 5	5.34	5.92	6.13	5.74	6.20	6.63
pH changes at initial pH 7	6.58	6.94	6.98	6.61	6.93	6.67
pH changes at initial pH 9	8.41	8.19	8.21	7.97	8.33	8.44

CFA127_Fe

Time Elapsed (days)	7	15	36	69	118	195
Leachates at initial pH 5	<DL	0.64	0.66	0.63	<DL	0.12
Leachates at initial pH 7	<DL	0.68	0.63	0.63	<DL	<DL
Leachates at initial pH 9	<DL	0.78	0.82	0.70	<DL	<DL

CFA127_As

Time Elapsed (days)	7	15	36	69	118	195
Leachates at initial pH 5	892.8	557.6	461.7	337.30	223.0	273.4
Leachates at initial pH 7	810.7	508.2	354.9	262.8	174.8	216.6
Leachates at initial pH 9	414.7	279.2	184.5	161.1	146.9	140.7

(e) Leachate Fe concentrations from (i) tooeleite precipitates (ii) gypsum-bearing tooeleite as a function of time at 60˚C under leaching conditions of pH 5, 7 and 9. NFA127 and CFA127 denote tooeleite precipitates formed at pH 2.7 and 25˚C with NaOH and $Ca(OH)_2$ as the bases respectively.

(i)

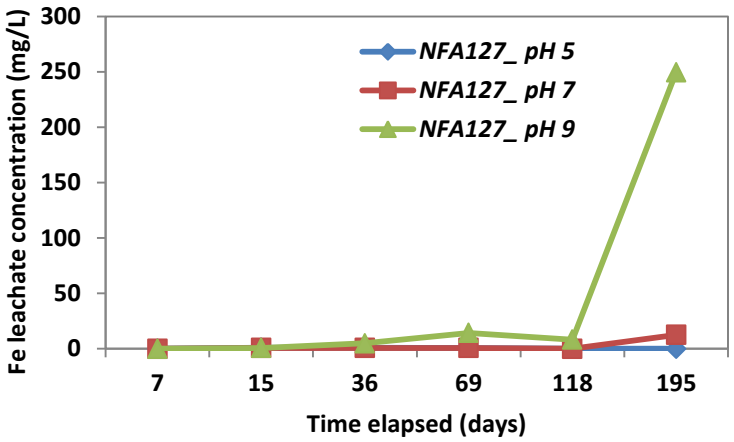

(ii)

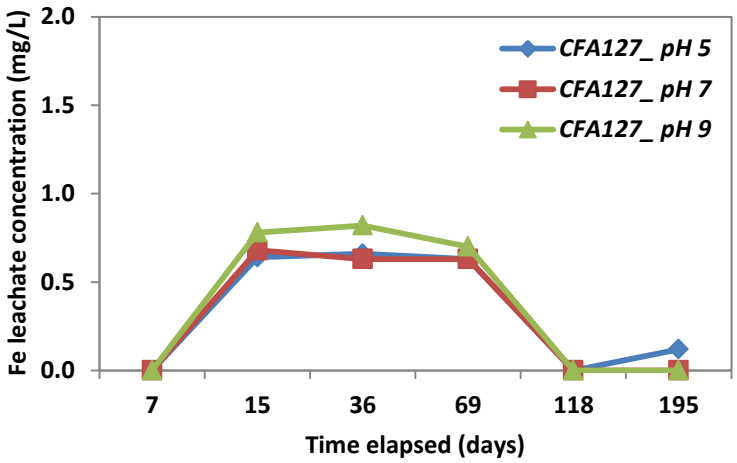

A.5. High temperature precipitation

(a) As and Fe concentrations in solution as a function of pH resulting from the neutralization of Fe(III)-As(III) solutions using 2M NaOH and 2M $Ca(OH)_2$ at (i) 60˚C and (ii) 95˚C.

(i)

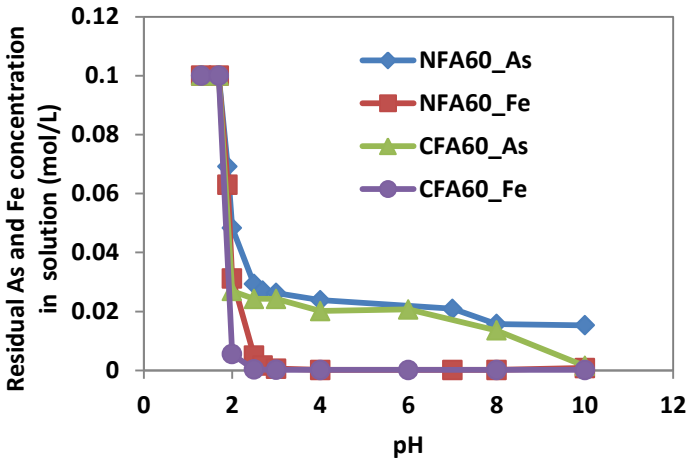

(ii)

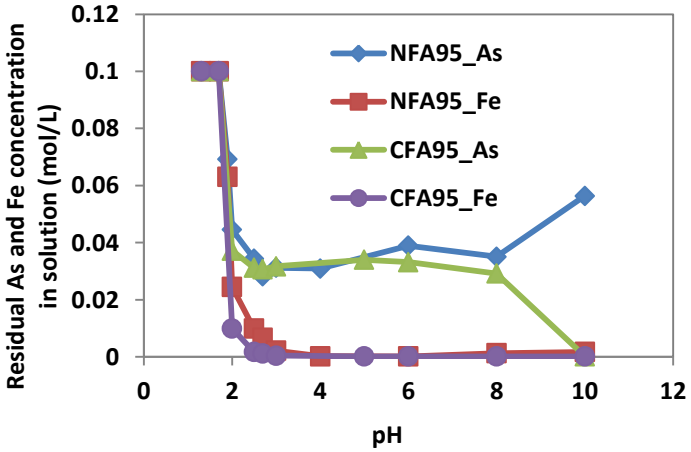

A.6. Tooeleite calcination

(a) XRD patterns of tooeleite precipitates calcined at different temperatures: (i) 500˚C (ii) 600˚C and (iii) 870˚C (iv) 600˚C (with lime) (v) 870˚C (with lime). A, C, Ca and F define angelellite [$Fe_4As_2O_{11}$]; calcium sulphate anhydrite [$CaSO_4$]; calcium arsenate [Ca_3 $(AsO_4)_2$] and ferric arsenate [$Fe_7(AsO_4)_6$] respectively.

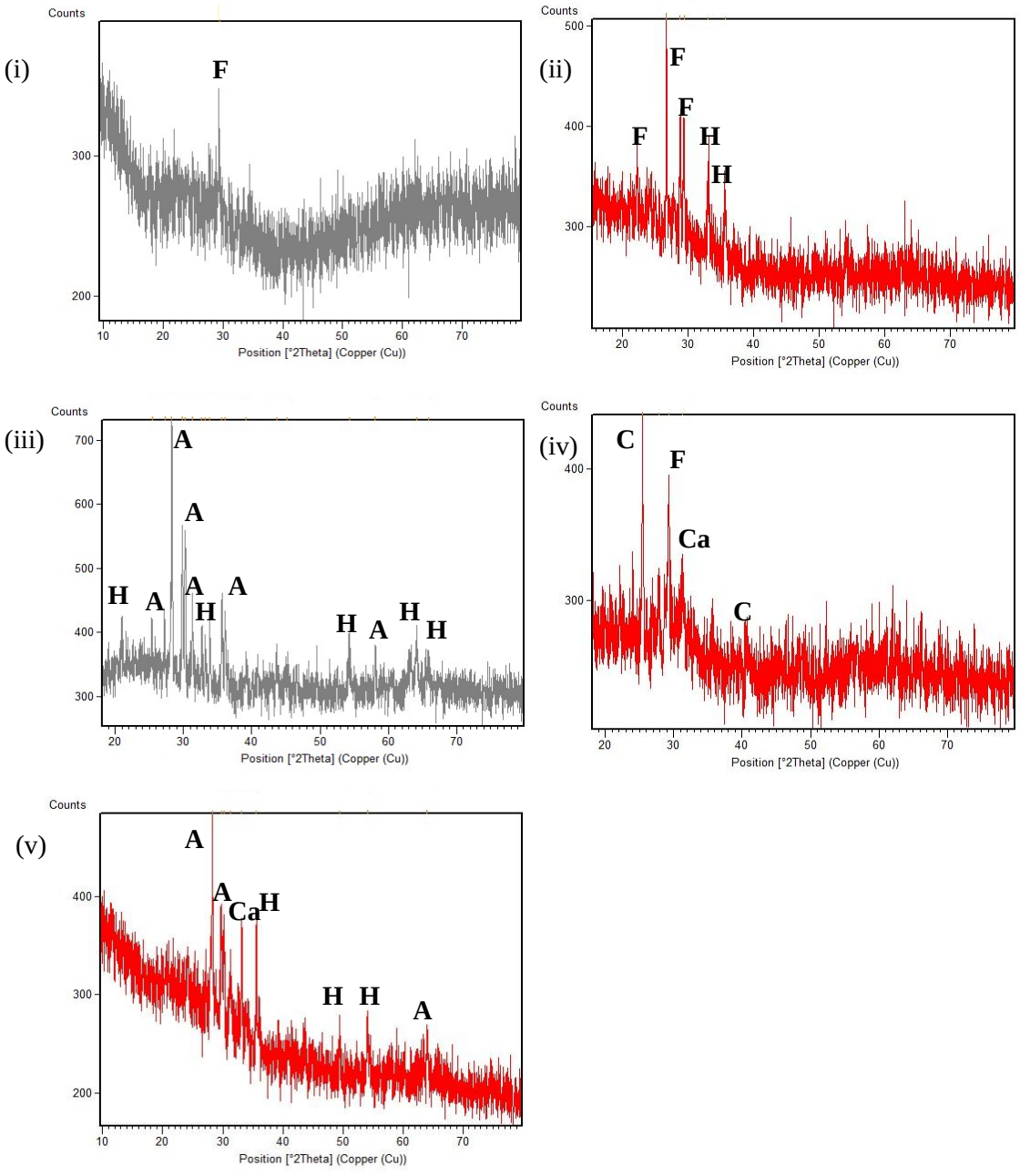

(b) XRD patterns of tooeleite precipitates calcined at different temperatures: (i) 600˚C (ii) 700˚C and (iii) 800˚C. A, F, and H define angelellite [$Fe_4As_2O_{11}$]; ferric arsenate phase [$FeAsO_4$] and hematite [Fe_2O_3] respectively.

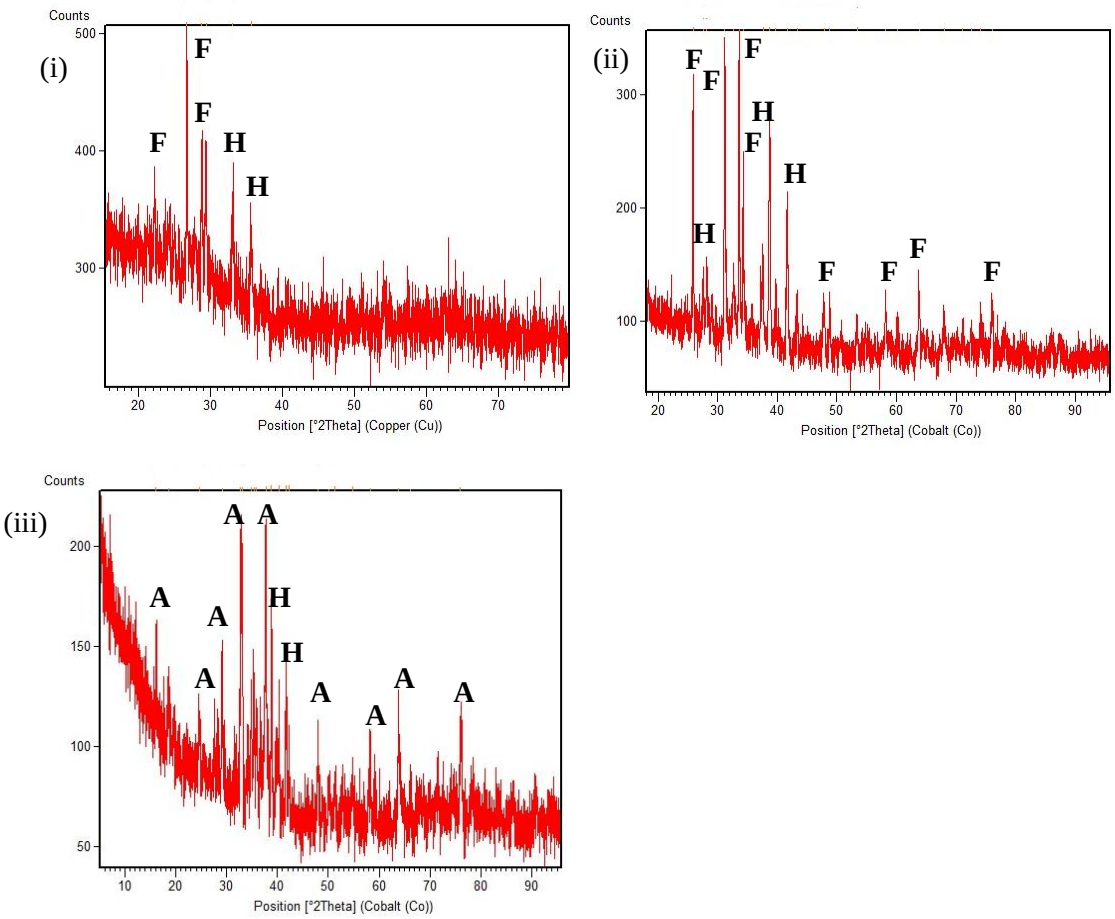

(d) Chemical analysis of the tooeleite residues from the TG/DTAstudies. TN850 denotes tooeleite thermal decomposition under N_2. TA850 & TA1000 denote tooeleite thermal decomposition under air.

Sample	Compounds	Fe:As molar ratio[(1)]	CHEMICAL ANALYSIS			
			Arsenic[(2)]	Iron[(2)]	Sulphur[(2)]	Fe:As molar ratio
			mg/L	mg/L	mg/L	
TN850	$2FeAsO_4$ & $5Fe_2O_3$	**6**	22.4	85.0	<1.0	**5**
TA850	$8FeAsO_4$ & $2Fe_2O_3$	**1.3**	65.0	83.9	1.3	**1.72**
TA1000	$2Fe_4As_2O_{11}$ & $2Fe_2O_3$	**3**	36.9	86.8	<1.0	**3**

(1) Based on thermal decomposition equations in Section 5.3.1. (2) Chemical analysis of TG/DTA residues.

(c) XRD patterns of gypsum-bearing tooeleite precipitates calcined at different temperatures: (i) 600˚C, (ii) 700˚C and (iii) 800˚C. A, C and F define angelellite [$Fe_4As_2O_{11}$]; calcium sulphate anhydrite [$CaSO_4$] and ferric arsenate [$Fe_7(AsO_4)_6$] respectively. (iv) XRD pattern of the white solid residue deposited on the furnace walls during calcination. As defines arsenolite (arsenic trioxide, As_2O_3).

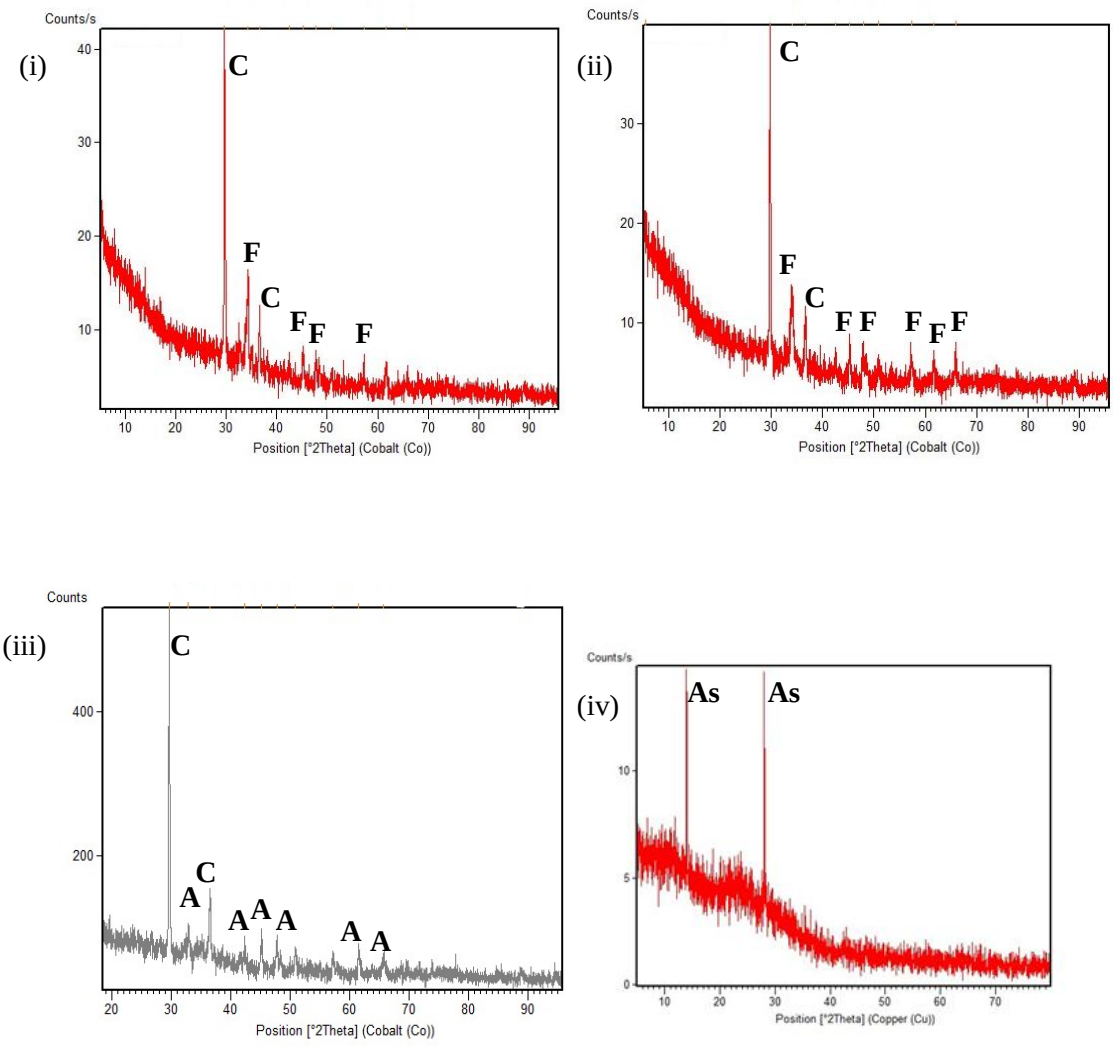

(d) Stability of tooeleite precipitates and calcines as a function of temperature.

	23˚C	500 ˚C	600 ˚C	870 ˚C	600 ˚C (with lime)	870 ˚C (with lime)
TCLP leachate pH	4.49	4.13	4.48	4.91	5.78	5.26
TCLP (As mg/L)	213	3	0.49	13.1	515	344

(e) Stability of tooeleite precipitates and calcines as a function of temperature.

Sample	Temperature (˚C)	TCLP (As mg/L)	TCLP leachate pH
NFA127†	25	213	4.51
CFA127†	25	378	4.82
NFA127	600	0.49	4.48
NFA127	700	1.5	4.90
NFA127	800	9.5	4.90
CFA127	600	13.1	4.86
CFA127	700	14.9	4.85
CFA127	800	48.3	4.87

† NFA and CFA represent tooeleite and gypsum-bearing tooeleite precipitates respectively.

A.6. Error Analysis

(a) Tooeleite Precipitation Experiments: (i) Fe:As=1; NaOH as base at 25˚C (ii) Fe:As=1.5; NaOH as base at 25˚C (iii) Fe:As=2; NaOH as base at 25˚C (iv) Fe:As=1.5; $Ca(OH)_2$ as base at 25˚C . R1, R2, and R3 denote replicate 1, replicate 2 and replicate 3 respectively. S.E. denotes the standard error.

(i)

Sample ID	[As] mg/L			
	R1	R2	R3	S.E.
pH 2.5	1650	1645	1640	2.89
pH 2.7	1020	1035	1030	4.41
pH 3	1075	1080	1060	6.00
pH 4	892	860	870	9.45
pH 6	214	218	225	3.21
pH 8	60	74	81	6.17
pH 10	392	380	365	7.81

(ii)

Sample ID	[As] mg/L			
	R1	R2	R3	S.E.
pH 2.5	1006.00	1020.00	956.00	19.42
pH 2.7	575.50	556.50	584.20	8.18
pH 3	286.60	273.40	275.20	4.13
pH 4	209.50	195.20	183.60	7.49
pH 6	24.52	29.50	17.40	3.51
pH 8	0.97	7.60	4.30	1.91
pH 10	9.78	5.60	8.54	1.24

(iii)

Sample ID	[As] mg/L			
	R1	R2	R3	S.E.
pH 2.5	1006.00	1020.00	956.00	19.42
pH 2.7	575.50	556.50	584.20	8.18
pH 3	286.60	273.40	275.20	4.13
pH 4	209.50	195.20	183.60	7.49
pH 6	24.52	29.50	17.40	3.51
pH 8	0.97	7.60	4.30	1.91
pH 10	9.78	5.60	8.54	1.24

(iv)

Sample ID	[As] mg/L			
	R1	R2	R3	S.E.
pH 2.5	240.80	234.00	226.70	4.07
pH 2.7	180.30	187.60	174.20	3.87
pH 3	186.90	175.80	171.40	4.61
pH 4	38.30	47.00	45.30	2.66
pH 6	10.60	12.70	17.30	1.98
pH 8	1.98	8.90	5.17	2.00
pH 10	6.13	13.20	6.92	2.24

(a) High Temperature Precipitation Experiments: (i) Fe:As=1; NaOH as base at 60˚C (ii) Fe:As=1; NaOH as base at 95˚C (iii) Fe:As=1; $Ca(OH)_2$ as base at 60˚C (iii) Fe:As=1; $Ca(OH)_2$ as base at 95˚C. R1, R2, and R3 denote replicate 1, replicate 2 and replicate 3 respectively. S.E. denotes the standard error

(i)

Sample ID	[As] mg/L			
	R1	R2	R3	S.E.
pH 2.5	2200	2210	2230	8.82
pH 2.7	2030	2020	2060	12.01
pH 4	1790	1830	1810	11.55
pH 6	1570	1545	1560	7.26
pH 8	1180	1170	1140	12.02
pH 10	1150	1135	1145	4.41

(ii)

Sample ID	[As] mg/L			
	R1	R2	R3	S.E.
pH 2.5	2580	2560	2590	8.82
pH 2.7	2120	2170	2130	15.27
pH 3	2340	2320	2350	8.82
pH 4	2320	2310	2330	5.77
pH 6	2920	2930	2890	12.2
pH 8	2630	2610	2580	14.53
pH 10	4230	4200	4235	10.93

(iii)

Sample ID	[As] mg/L			
	R1	R2	R3	S.E.
pH 2.5	1820	1834	1840	5.93
pH 3	1820	1827	1835	4.34
pH 4	1510	1520	1526	4.67
pH 6	1550	1540	1545	2.89
pH 8	1020	1030	1018	3.71
pH 10	115	134	124	5.49

(iv)

Sample ID	[As] mg/L			
	R1	R2	R3	S.E.
pH 2.5	2340	2350	2320	8.82
pH 2.7	2300	2290	2310	5.77
pH 3	2380	2370	2374	2.91
pH 6	2490	2500	2514	6.96
pH 8	2190	2180	2210	8.82
pH 10	18	23.3	27	2.61

(a) TCLP Stability Tests: (i) Fe:As=1; NaOH as base at 25˚C (ii) Fe:As=1.5; NaOH as base at 25˚C (iii) Fe:As=2; NaOH as base at 25˚C (iv) Fe:As=1; $Ca(OH)_2$ as base at 25˚C (v) Fe:As=1.5; $Ca(OH)_2$ as base at 25˚C (vi) Fe:As=2; $Ca(OH)_2$ as base at 25˚C (vii) Fe:As=1; NaOH as base at 60˚C (viii) Fe:As=1; NaOH as base at 95˚C (ix) Fe:As=1; $Ca(OH)_2$ as base at 60˚C (x) Fe:As=2; $Ca(OH)_2$ as base at 95˚C (xi) Calcines [NFA600, NFA700, NFA800 – Fe:As=1; NaOH as base at 600˚C, 700˚C and 800˚C respectively; CFA600, CFA700, CFA800 – Fe:As=1; $Ca(OH)_2$ as base at 600˚C, 700˚C and 800˚C respectively]. R1, R2, and R3 denote replicate 1, replicate 2 and replicate 3 respectively. S.E. denotes the standard error.

(i)

Sample ID	[As] mg/L			
	R1	R2	R3	S.E.
pH 2.7	213	205.6	221.5	7.41
pH 3	60	64.5	55.8	2.51
pH 4	246	234	238	3.53
pH 6	327.1	315.7	324	3.4
pH 8	334	337.7	325	3.61
pH 10	187.4	178	172.6	4.32

(ii)

Sample ID	[As] mg/L			
	R1	R2	R3	S.E.
pH 2.5	59.5	49.2	47.5	3.75
pH 2.7	39.4	20.3	22.6	6.02
pH 3	94.6	91.4	79.2	4.69
pH 4	131.8	135.9	126.4	2.75
pH 6	153.3	159.4	164.1	3.13
pH 8	469.1	470.6	453.1	5.6
pH 10	147.2	162.6	164	5.38

(iii)

Sample ID	[As] mg/L			
	R1	R2	R3	S.E.
pH 2.5	6.18	8.63	16.3	3.05
pH 2.7	6.72	16.3	18.9	3.07
pH 3	6.93	16.6	17	3.29
pH 4	19.6	20.1	18.9	0.35
pH 6	43.6	41.1	47.2	1.66
pH 8	35.5	30.6	25	3.03
pH 10	33.6	35.2	27.8	2.25

(iv)

Sample ID	[As] mg/L			
	R1	R2	R3	S.E.
pH 2.5	26.5	41.7	31.1	4.5
pH 2.7	378	355	363.6	6.71
pH 3	163.3	120.2	124.8	13.66
pH 4	74.3	68.1	65.7	2.56
pH 6	314	325	338.5	7.08
pH 8	188	161.4	159.1	9.27
pH 10	78.8	76.2	65	4.23

(v)

Sample ID	[As] mg/L			
	R1	R2	R3	S.E.
pH 2.5	34.2	15.6	10.2	7.27
pH 2.7	20.8	20.5	8.32	4.11
pH 3	13.2	18.6	8.04	3.05
pH 4	93.3	89.4	85.8	2.17
pH 6	156	149.8	159.5	2.84
pH 8	91.4	96.3	89.7	1.98
pH 10	19.8	21.7	24.1	1.24

(vi)

Sample ID	[As] mg/L			
	R1	R2	R3	S.E.
pH 2.5	13.2	13.5	12.6	0.26
pH 2.7	14.6	12.2	13.8	0.71
pH 3	13.6	15.7	12.1	1.04
pH 4	53.6	13.3	12.1	13.64
pH 6	63.1	62.4	65.3	0.87
pH 8	30.8	26.3	50.5	7.43
pH 10	9.43	14.6	16.4	2.09

(vii)

Sample ID	[As] mg/L			
	R1	R2	R3	S.E.
pH 2.5	31.8	51.8	48	6.13
pH 2.7	21.8	32.4	50	8.22
pH 3	26.5	27.7	35.8	2.92
pH 4	41.3	44.6	56.6	4.65
pH 6	312.3	316.6	325.4	3.86
pH 8	460	471.9	485	7.22
pH 10	339.9	343.9	357	5.16

(viii)

Sample ID	[As] mg/L			
	R1	R2	R3	S.E.
pH 2.5	14.1	17.1	15.6	0.86
pH 2.7	15.5	17.7	33.1	5.54
pH 3	19.3	14.9	28.2	3.91
pH 4	33	20.4	27	3.64
pH 6	340	335	325	4.41
pH 8	542.3	535.6	532.5	2.89
pH 10	116.7	125.4	112.3	3.85

(ix)

Sample ID	[As] mg/L			
	R1	R2	R3	S.E.
pH 2.5	21.3	18.4	19	0.88
pH 2.7	25.7	25.2	24.4	0.44
pH 3	184.1	192.5	183.7	2.87
pH 4	93.5	81.5	71.8	5.22
pH 6	379.1	367.8	374.4	3.28
pH 8	379.7	380.5	395	4.97
pH 10	1084	1072	1075	4.1

(x)

Sample ID	[As] mg/L			
	R1	R2	R3	S.E.
pH 2.5	17.9	12.6	12.5	1.78
pH 2.7	13.3	11.8	10.1	0.92
pH 3	29.1	12.9	27.1	5.1
pH 4	12.6	12.3	11.7	0.26
pH 6	115.6	129.3	123.6	3.97
pH 8	575.7	580.4	568.5	3.46
pH 10	1000	985.4	975.6	7.09

(xi)

Sample ID	[As] mg/L			
	R1	R2	R3	S.E.
NFA600	0.49	2.38	2.14	0.6
NFA700	1.5	2.54	2.75	0.39
NFA800	9.5	6.75	7.64	0.81
CFA600	13.1	11.1	7.51	1.75
CFA700	14.9	16.6	16.1	0.5
CFA800	48.3	41	41	2.43

A.7. Ferric Arsenite precipitation

(i) Direct precipitation of ferric arsenite [pH raised to desired value and stirred continuously for 1 hour at each specific pH regime]: Fe:As=1; NaOH as base; pH 4, pH 6, pH 8

pH	[As] mg/L	Fe:As molar ratio
4	904	1.1
6	289	1.01
8	132	1

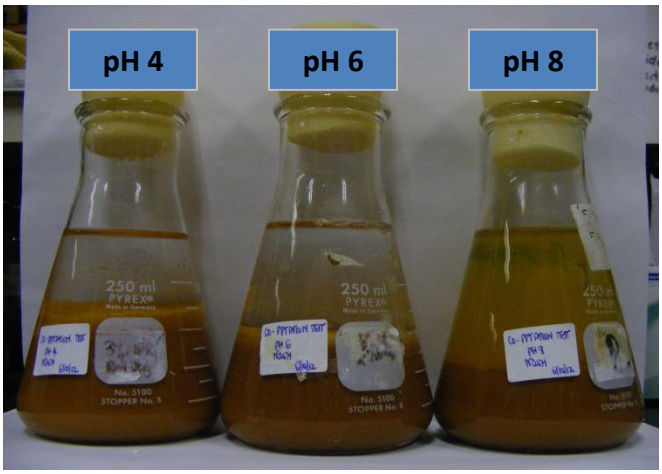

(ii) XRD analysis

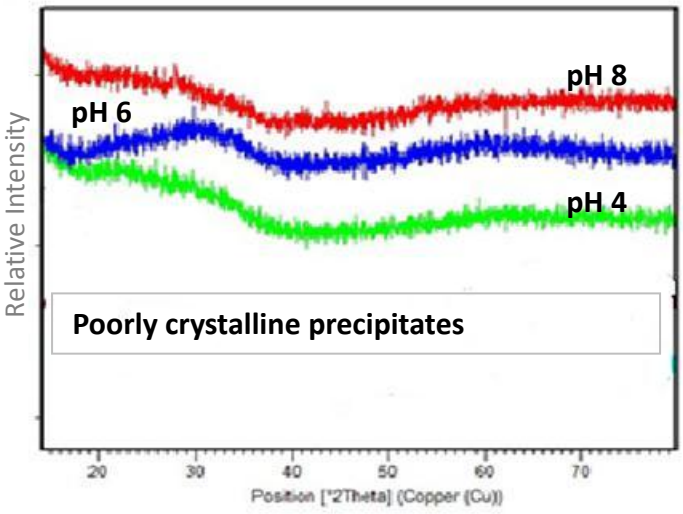

A.8. Chemical analysis

(a) Solid residues from tooeleite long term stability tests

Sample	pH leaching conditions	Fe [ppm]	As [ppm]	Fe:As
Tooeleite 25˚C	5	1430.0	1238.3	1.55
	7	1379.3	1171.0	1.58
	9	1395.5	1238.0	1.51
Tooeleite 60˚C	5	1442.0	1183.3	1.63
	7	1413.5	1175.8	1.61
	9	1310.3	1127.5	1.56

(b) High temperature precipitates (NaOH as the base)

Sample	Precipitation pH	Fe [ppm]	As [ppm]	Fe:As molar ratio	As:Fe molar ratio
Fe:As=1; 60˚C	2	659.5	568.0	1.56	0.64
	4	590.8	536.3	1.48	0.68
	6	649.0	573.5	1.52	0.66
	8	633.8	665.3	1.28	0.78
	10	639.8	615.3	1.39	0.72
Fe:As=1; 95˚C	2	1755.5	1478.8	1.59	0.63
	8	1357.8	1284.0	1.42	0.71
	10	1356.5	1141.8	1.59	0.63

(c) High temperature precipitates ($Ca(OH)_2$ as the base)

Sample	Precipitation pH	Fe [ppm]	As [ppm]	Ca [ppm]	Fe:As molar ratio	Ca:As molar ratio
Fe:As=1; 60˚C	8	252.6	326.0	391.8	1.04	2.25
Fe:As=1; 95˚C	8	206.7	275.5	454.1	1.00	3.09
	10	364.0	357.6	442.8	1.36	2.32

A.9. High Temperature precipitation tests at 60˚C

(a) Direct Precipitation tests at 60˚C - the presence of excess Fe increases the As uptake.

Sample	Precipitation pH	Residual Fe [mg/L]	Residual As [mg/L]
Fe:As=1; 60˚C	6	0.81	360.8
	8	7.10	229.4
Fe:As=1.5; 60˚C	6	0.20	76.7
	8	1.85	41.8

(b) TCLP stability tests – relatively high TCLP As solubility. However, the presence of excess Fe slightly increases the stability of the As-bearing precipitates.

Sample	Precipitation pH	Residual Fe [mg/L]	Residual As [mg/L]
Fe:As=1; 60˚C	6	1.41	515.6
	8	29.8	537.5
Fe:As=1.5; 60˚C	6	<DL	231.9
	8	3.66	135.7